Dynamical twisted mass fermions and baryon spectroscopy

Vincent Drach

THESE

Pour obtenir le grade de

Docteur de l'Université de Grenoble

Spécialité: **Physique Subatomique et Astroparticules**

Prśentée et soutenue publiquement par

Vincent Drach

le 7 juin 2010

Fermions twistés dynamiques et spectroscopie des baryons

Thèse dirigé par M. Jaume Carbonell

JURY

M.	Jaume Carbonell	LPSC - Grenoble	Directeur de thèse
M.	Michael Klasen	LPSC - Grenoble	Président
M.	Laurent Lellouch	CPT - Marseille	Rapporteur
M.	Stephan Narison	LPTA - Montpellier	Examinateur
M.	Janos Polonyi	IPHC - Strasbourg	Examinateur
M.	Giancarlo Rossi	Université Tor Vergata - Rome	Rapporteur

Thèse préparée au Laboratoire de Physique Subatomique et de Cosmologie
dans l'Ecole Doctorale de Physique de Grenoble

Remerciements

Je voudrais tout d'abord remercier mon directeur de thèse, Jaume Carbonell, qui m'a toujours encouragé et soutenu durant ces trois années passées à Grenoble. Je pense que tu as largement influencé ma manière de travailler à l'heure actuelle. Tu m'as beaucoup appris, notamment à "faire de la physique". Je ne peux pas imaginer que ces trois années aient pu mieux se passer, tu as donc été à mes yeux un directeur de thèse exemplaire. Je voudrais aussi remercier Mauro Papinutto. J'ai beaucoup appris grâce à toi et j'ai également passé de très bons moments en ta compagnie. Je tiens aussi à remercier Mariane Mangin-Brinet pour l'aide précieuse qu'elle m'a apporté au début de ma thèse.

Je voudrais remercier les membres de mon jury, à savoir M. Klasen, S. Narison et J. Polony et je tiens à exprimer tout particulièrement ma gratitude à mes deux rapporteurs G. Rossi et L. Lellouch. Laurent et Janos, vous m'avez enseigné beaucoup et j'espère que nous aurons un jour l'occasion de travailler ensemble. Merci encore à Laurent pour avoir patiemment noté toutes tes corrections et commentaires sur mon manuscript, ils m'ont été très utiles.

Je souhaite remercier tous mes collaborateurs de la collaboration "European Twisted Mass" et plus particulièrement la partie française : Benoit Blossier, Philippe Boucaud, Olivier Pène et Pierre Guichon.

Je n'oublie évidemment pas l'ami Pierrot pour les innombrables discussions et les très bons moments passés ensemble autour d'une bière. Je n'oublierai pas de sitôt ces trois années passées en ta compagnie. Bonne chance pour la suite ! Merci aussi à Rémi, cela a toujours été très agréable de discuter et de travailler avec toi. Je salue aussi tous les thésards que j'ai pu rencontrer au laboratoire. Merci Julien pour le Dôme des Ecrins, même si j'ai coulé une bielle je ne suis pas près d'oublier cette aventure. Je remercie également Guillaume et Joe pour les interminables discussions de physique qui m'ont permis de découvrir tant la physique du neutron que la QCD perturbative. Merci aussi à Lauranne pour ce fantastique voyage par-delà le cercle polaire arctique. Merci aussi à Antje et Arnaud pour ces bons moments passés ensemble. Je pense bien sûr ici à toutes ces très bonnes soirées passées au O'Callaghan en votre compagnie.

Pour finir, un petit mot pour les potes de fac. Commençons par cette plus qu'extravagante année de M2 à Marseille. Je pense ici tout particulièrement à Baptiste, Mathieu, et Edouard. On a pas fini de passer de bons moments ensemble et je n'oublie évidemment pas ni ce fantasique voyage au Portugal ni ce séjour au Pouliguen. Nos discussions de physiques sont toujours passionantes et aboutiront je l'espère un jour à des résultats originaux. Je pense aussi "aux lyonnais" Elie, David et Benjamin, cette année à l'ENS fût tout aussi mémorable, et là encore les bons moments passés ensemble témoignent de notre amitié. Merci à Claudia pour m'avoir incité à poursuivre en physique au moment où mon financement se faisait attendre. Enfin je pense aux strasbourgeois Guillaume, Issam, Jérémy et Bruno. J'ai toujours autant de plaisir à vous revoir et c'est en votre compagnie que j'ai lentement commencé à me diriger vers les 170 pages qui suivent...

Préambule

La chromodynamique quantique (QCD de l'anglais "Quantum ChromoDynamics") est la théorie de l'interaction entre les quarks et les gluons. Elle décrit l'une des quatre interactions fondamentales connues et constitue, avec la théorie électrofaible, le modèle standard de la physique des particules. Elle présente les avantages de pouvoir être formulé de manière compacte, de ne dépendre que de sept paramètres —les masses des six quarks et la constante de couplage forte α_s— et de prédire un nombre incalculable d'observables.

Ce succès théorique vient en partie d'une propriété fondamentale de la théorie : *la liberté asymptotique*. Celle-ci prédit que la constante de couplage forte décroît avec l'énergie, rendant les calculs perturbatifs asymptotiquement convergents à haute énergie. Les calculs dans ce régime ont notamment permis d'établir la validité de la théorie dans des accélerateurs, et restent encore aujourd'hui cruciaux pour interpréter avec précision les résultats obtenus dans un grand nombre d'expériences de physique des hautes énergies. A contrario, à basse énergie, les calculs perturbatifs ne décrivent plus les phénomènes observés. La phénoménologie change drastiquement et aucun lien entre la théorie fondamentale n'est évident. On assiste en effet à l'émergence d un grand nombre d'états — stables ou résonnants vis-à-vis de l'interaction forte — qui semblent interagir entre eux sans signature des degrés de liberté fondamentaux que sont les quarks et les gluons. Ceux-ci sont dits *confinés* dans un ensemble d'états apelés *hadrons*. Différentes approches ont été suivies pour décrire la physique hadronique — le but n'est pas d'en donner une liste exhaustive ici — mais force est de constater qu'il est extrêmement difficile de construire des modèles effectifs qui décrivent de manière quantitative l'ensemble des phénomènes observés. L'enigme est d'autant plus stimulante que l'interaction forte résiduelle entre les hadrons est aussi à l'origine de la cohésion des noyaux et de certaines de leur propriétés.

Cette thèse est dédiée à l'étude théorique de la spectroscopie des baryons (composés de trois quarks) en utilisant la seule approche connue à ce jour pour traiter de manière non perturbative la QCD, à savoir *la chromodynamique quantique sur réseau*. Ce document vise à détailler toutes les étapes nécessaires pour extraire l'information physique sur les masses des baryons à partir de la formulation théorique de la QCD.

La QCD sur réseau est une approche numérique basée sur la discrétisation de l'espace quadridimensionel de la formulation Euclidienne de la QCD. Elle fut introduite d'abord comme un outil théorique par K. Wilson en 1974 avant que M. Creutz ne réalise en 1980 la première simulation numérique de théorie quantique des champs sur réseau. La méthode est essentiellement fondée sur l'utilisation de la formulation fonctionnelle de la théorie et consiste à évaluer numériquement l intégrale fonctionnelle en échantillonant, via des méthodes Monte Carlo, l'espace de configurations des champs. Comme nous le verrons, la génération de tels échantillons est de loin la partie la plus coûteuse en terme de puissance de calcul et nécessite l'utilisation des Super Calculteurs les plus perfomants disponibles à l'heure actuelle.
Le premier chapitre retrace brièvement l'avénement de la QCD comme théorie de l interaction forte et résume les principes généraux qui permettent d'effectuer des simulations numériques.

L'accent est mis sur les motivations et les défis qui font de ce champ de recherche un domaine actif. Le second chapitre introduit les fermions utilisés au sein de la collaboration "European Twisted Mass" (ETM). Ceux ci présentent notamment les avantages de permettre la simulation de doublets de quarks (dégénérés ou non), et de garantir que les effets de discrétisation soient d'ordre a^2 (où a est la maille du réseau). En revanche, ils brisent les symétries de parité et d'isospin. Ces symétries ne sont restorées que dans la limite du continu ($a \to 0$) et posent des problèmes propres à ce choix de discrétisation.

Le troisième chapitre est dédié à l'extraction des masses de hadron en QCD sur réseau. On y montre que le comportement à long temps de corrélateurs de la forme $\langle J(x)\bar{J}(0)\rangle$, (où J est un opérateur qui a les nombres quantiques du hadron que l'on cherche à étudier), est exponentiellement décroissant et que le taux de décroissance est donné par la masse du hadron. Les champs interpolants de l'octet de spin 1/2 et du décuplet de spin 3/2 sont ensuite donnés. On démontre ensuite une formule générale qui permet de construire explicitement le corrélateur associé à un champ interpolant (local) de baryon quelconque. Cette formule a été implementée dans un code parallèle et constitue la pierre angulaire dont découle tous les résultats bruts concernant la masse des baryons. Les méthodes d'analyse sont ensuite discutées, l'accent étant mis sur l'estimation des erreurs statistiques.

Le chapitre 4 détaille les algorithmes et les méthodes utilisées pour générer les configurations. Une part importante de mon temps de travail a été dédiée à générer des configurations sur la BG/P de l'IDRIS. Ces configurations sont maintenant activement utilisées dans l'ensemble de notre collaboration et dans divers projets de physique. La problématique principale des calculs sur réseau apparaît clairement dans ce chapitre, en effet, on y explique pourquoi les coûts des simulations à des masses de pion très proches de la masse du pion physique sont prohibitif. Ce chapitre résume également quelques résultats importants obtenus par la collaboration durant ma thèse.

Le chapitre 5 s'attache à décrire les théories effectives dites de pertubations chirales. Elles fournissent de précieux outils pour extrapoler les résultats de nos simulations dans un régime physique. On décrit en particulier les relations obtenues dans le secteur des baryons. Ces formules seront ensuite utilisées dans les chapitres concernant l'étude des résultats réseaux proprement dit. L'interprétation physique des différents termes permet de comprendre les différentes approximations et montre l'incertitude systématique inhérente des résultats. On souligne le fait que la convergence des séries de perturbations chirales dans un régime où la masse du pion est > 300 MeV est fortement discutable.

Le chapitre 6 est consacré à l'analyse des données brutes dans le secteur des baryons légers (Nucléon et Δ) pour les ensembles $N_F = 2$ et $N_F = 2+1+1$. On y étudie les effets systématiques de volumes et de mailles finis. On discute les problèmes liés à l'extrapolation chirale. Le chapitre 7 s'intéresse aux baryons dits étranges.

Dynamical twisted mass fermions and baryon spectroscopy

Abstract

The aim of this work is an ab initio computation of the baryon masses starting from quantum chromodynamics (QCD). This theory describe the interaction between quarks and gluons and has been established at high energy thanks to one of its fundamental properties : the asymptotic freedom. This property predicts that the running coupling constant tends to zero at high energy and thus that perturbative expansions in the coupling constant are justified in this regime. On the contrary the low energy dynamics can only be understood in terms of a non perturbative approach. To date, the only known method that allows the computation of observables in this regime together with a control of its systematic effects is called lattice QCD. It consists in formulating the theory on an Euclidean space-time and to evaluating numerically suitable functional integrals. First chapter is an introduction to the QCD in the continuum and on a discrete space time. The chapter 2 describes the formalism of maximally twisted fermions used in the European Twisted Mass (ETM) collaboration. The chapter 3 deals with the techniques needed to build hadronic correlator starting from gauge configuration. We then discuss how we determine hadron masses and their statistical errors. The numerical estimation of functional integral is explained in chapter 4 . It is stressed that it requires sophisticated algorithm and massive parallel computating on BlueGene type architecture. Gauge configuration production is an important part of the work realized during my Ph.D. Chapter 5 is a critical review on chiral perturbation theory in the baryon sector. The two last chapter are devoted to the analyze in the light and strange baryon sector. Systematics and chiral extrapolation are extensively discussed.

Contents

Chapter 1

Introduction

Contents

As a general introduction, we give a brief presentation of the basic concepts and ideas which lead to the main subject of this thesis. We begin by a short overview of the history of the strong interaction and recall the main ingredients of the Quantum Field Theory (QFT) formalism. This leads to the present formulation of theory of strong interaction, namely the Quantum Chromodynamics (QCD), and to its fundamental properties. We emphasize the important fact that computing observables in this theory is a challenging task for theoritical research. This particular point will naturally motivate the need for a non perturbative formulation of the theory, which is usually only considered from the perturbative point of view. Choosing a discrete space time as a regulator of the theory will provide such a formulation. A number of issues are raised by this approach of quantum field theory and we will briefly discuss them. Finally particular care has been devoted to baryon spectroscopy problems inside a context of an active and promising field of research. Some of the related questions drive theoritical and phenomenological particle physics since decades.

1.1 Early History of the Strong Interaction

In 1919, Rutherford realized that nucleus of all the atoms were composed of hydrogen nuclei. He was the first to understand the fundamental role played by hydrogen nuclei and he called proton this "fundamental particle". Few years after, in 1932, Chadwick [1] realized that the radiation that had been observed by Walther Bothe, Herbert L. Becker, Irène and Frédéric Joliot-Curie was actually due to a neutral particle of about the same mass as the proton, that he called the neutron. These discoveries immediately led theoritical physicists of that time to suggest the existence of a new interaction, stronger that the electromagnetic repulsion, which was able to bind proton and neutron together inside the nucleus. One of the first to propose a theory which explains this interaction between nucleons was Yukawa in 1935 [2] by introducing a new particle, latter called pion. The concept of strong interaction was born.

1.1.1 The Birth of Elementary Particle Physics

During the same period, cosmic rays experiment detecting charged particle trajectories were used to test the Yukawa model. After a complicated story that we will not describe here, the pion was finally found in 1947. Before that, in 1944, Louis Leprince-Ringuet and M. Lhéritier [3] working in a laboratory built on the top of Aiguille du midi (French Alps), measured what is presently known as the first strange particle (kaon) with a mass of about $\sim 500 \pm 10\%$ MeV . After these pioneering experiments, physicists found other neutral and charged particles having masses close to those found by Leprince-Ringuet. They decayed apparently into pions, it was the V^0 particle (the name comes from the shape of the decay) , the θ and the τ. In a modern language, this particles are of course the three kaons (K^+, K^0, K^-), but it took years to establish that θ and τ were two opposite charge states of the same particle and that the V^0 was its neutral counterpart.

In 1947 Rochester and Butler observed the associated production of a pair of unstable particles, and soon after it was proved experimentally that the masses of the two particles of the final state were different, one of them was about 500 MeV, the other greater than that of the nucleon. The heavier one was observed to decay into a pion and a nucleon. These particle were the first hyperons - the so-called Λ^0 and Σs- that we will meet often along this work.

At that time several facts were astonishing physicists and that's why these particle were called "strange particle" : why were they always produced in pairs? why they decayed so 'slowly' (with lifetime typical of weak interaction) although they are produced by a strong interaction process.

In an attempt to answer these questions, Gell-Mann [4] and Nakano & Nishijima [5] , introduced independantly a new additive quantum numbers S, the 'strangeness', which is conserved by strong and electromagnetic interaction but not by weak interaction. Furthermore, a bulk of observation led theoriticians to introduce the concept of baryonic quantum number, which is so far always conserved in all processes observed in Nature, and which allows to explain why a family of particles heavier than the proton always decays into a proton. These states where called baryons. The remaining states involved in strong interaction processes were called mesons. Altogether mesons and baryons constitute the familly of hadrons. It is worthwihe to note that during the fifties and sixties, hundreds of hadrons were found in the first accelerators, leaving the community with a question : "Are all these particles fundamental ?"

1.1.2 Quark Model

During the fifties several theoritical efforts [6] where undertaken to explain such a proliferation of particles. The decisive step in classifing the physical baryons p,n, Λ Σ and Ξ (or Cascade baryons) was realized by Gell-Mann [7] and Ne'eman [8]. The underlying idea was that the strong interaction is symmetric under a symmetry group which can explain that the eight baryons belong to the same multiplet of an irreductible representation. If the symmetry would have been exact, the masses would be degenerate and because the symmetry is only approximate, the masses are splitted. Gell-Mann [9] and Zweig even came one step further : they suggest that hadrons were not elementary particles, but composite objects having an internal structure built up from smaller particle named quarks (taken from a James Joyce's novel *Finnegan's Wake*). It turned out that this approximate symmetry is $SU(3)_f$, the group of unitary transformations acting on a three-dimensional vector space. In the quark model, quarks are in the fundamental representation $\mathbf{3}$ while antiquarks are in the conjugate representation $\bar{\mathbf{3}}$. The three "'flavours" of quarks nowadays known as the 'up' (u), 'down' (d) and 'strange'(s) quarks . In this framework, mesons are bound states of quark-antiquark that can be classified decomposing in irreducible representations the tensor product $\mathbf{3} \otimes \bar{\mathbf{3}} = \mathbf{1} \oplus \mathbf{8}$. The mesons in the $SU(3)_f$ octet are identified with the eight pseudoscalar mesons of negative parity and are represented in Fig. 1.1.

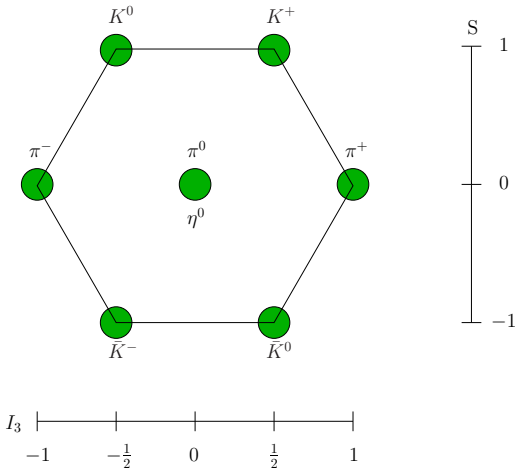

Figure 1.1: Octet of pseudoscalar mesons.

Concerning the baryon they are bound states of three quarks, a similar analysis show that the product $\mathbf{3} \otimes \mathbf{3} \otimes \mathbf{3}$ can be decomposed in $\mathbf{10} \oplus \mathbf{8} \oplus \mathbf{8} \oplus \mathbf{1}$. One of the octet parts constitutes the

spin 1/2 baryons of positive parity shown in Fig. 1.2, while the decuplet are the spin 3/2 baryons of positive parity shown in Fig. 1.3. The decomposition in sum of irreducible representation of the tensor product of fundamental representation of $SU(3)_f$ can be summarized by:

$$\begin{array}{lrcl} \text{Meson} & \mathbf{3} \otimes \bar{\mathbf{3}} & = & \mathbf{8} \oplus \mathbf{1} \\ \text{Baryon} & \mathbf{3} \otimes \mathbf{3} \otimes \mathbf{3} & = & \mathbf{10} \oplus \mathbf{8} \oplus \mathbf{8} \oplus \mathbf{1} \end{array} \tag{1.1}$$

An important assumption of this model is the exactness of the $SU(3)_f$ symmetry between quarks. In Nature it was observed that the masses of the low lying states of mesons and baryons were not degenerate. It appeared that the $SU(3)_f$ was only an approximation and that the $SU(2)_f$ symmetry which relates for instance proton and neutron was a better approximation. From this observation it was deduced that the strange quark had a mass significatively larger than the mass of the up and down quark. Treating the difference of mass between the strange and the two light quarks as a perturbation, Gell-Mann [10] in 1961 and Okubo [11] in 1962 derived relations among masses of the isospin multiplets. More details on the so called Gell-Mann Okubo relation can be found for instance in [12]. They found that for the octet of spin 1/2 baryon the relation

$$\frac{M_\Xi + M_N}{4} = \frac{3M_\Lambda + M_\Sigma}{4} \tag{1.2}$$

which is experimentally very well satisfied. Indeed the left-hand side ≈ 2.23 GeV and the right-hand side ≈ 2.25 GeV.

For the spin 3/2 decuplet of baryons the Gell-Mann Okubo relation predict an equal mass difference among two consecutive ($\Delta S = 1$) isospin multiplets:

$$M_{\Sigma^*} - M_\Delta = M_{\Xi^*} - M_{\Sigma^*} = M_\Omega - M_{\Xi^*} \tag{1.3}$$

Note that the equality Eq. (1.3) was used to predict correctly the Ω^- mass. A third relation exists that connects the octet and decuplet of baryon and reads:

$$3M_\Lambda - M_\Sigma - 2M_N = 2(M_{\Sigma^*} - M_\Delta) \tag{1.4}$$

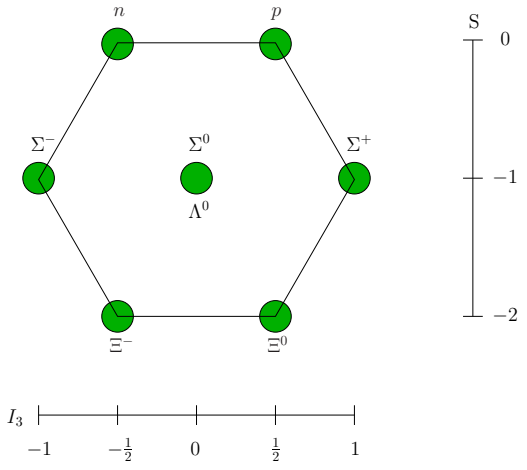

Figure 1.2: Octet of low lying baryon.

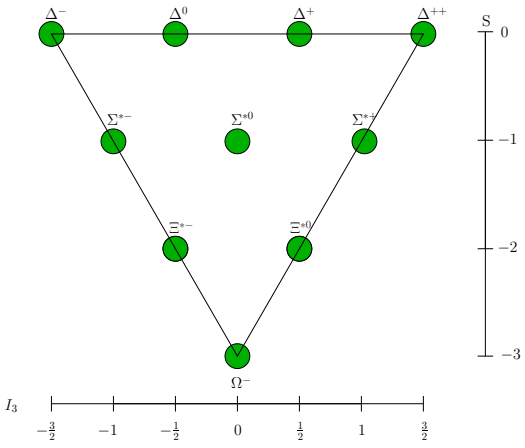

Figure 1.3: Decuplet of low lying baryon.

1.2 Quantum Chromodynamics

The development of Quantum Chromodynamics as a theory of the strong interaction was made possible by tremendous progress on the phenomenological and theoritical side. From the purely theoritical point of view, one of the main steps forward was realized by Yang and Mills in 1954 [13] which generalizes the concept of gauge invariance under abelian $U(1)$ to non-abelian $SU(N)$. At that time, non abelian gauge theories were studied as a curiosity, but together with the sucesses of the quark models in hadron spectroscopy - describing hadrons as bound states of quark - and of the parton model in deep inelastic scattering experiments played a major role in the birth of QCD.

We review here some basic facts about the present formulation of the theory starting from the classical Lagrangian and going through the properties of the quantum field theory.

1.2.1 The QCD Lagrangian and its symmetries

The modern formulation of QCD is given in terms of a relativistic quantum field theory involving quarks and gluons on a four dimensional space-time. The spin 1 gluon field $\mathcal{A}_\mu$ is the Yang-Mills gauge field which takes its values in $\mathfrak{su}(3)$, the Lie algebra of $\mathrm{SU(3)_c}$ generators.

The quarks are described by N_f Dirac fields

$$\psi = \psi_f^{s,c}(x), \quad f = 1 \dots N_f, \quad c = 1, \dots 3, \quad \text{and } s = 1, \dots 4 \tag{1.5}$$

In Nature, six quarks have been discovered so far, and at the classical level the full QCD Lagrangian can be written :

$$\mathcal{L}_{\mathrm{QCD}} = -\frac{1}{2}\mathrm{Tr}\left\{\mathcal{F}_{\mu\nu}\mathcal{F}^{\mu\nu}\right\} + \overline{\psi}(i\not{\mathcal{D}} - M)\psi, \tag{1.6}$$

with $\overline{\psi} = \psi^\dagger\gamma_0$ and the Yang-Mills field tensor

$$\mathcal{F}_{\mu\nu} = \partial_\mu\mathcal{A}_\nu - \partial_\nu\mathcal{A}_\mu + ig[\mathcal{A}_\mu, \mathcal{A}_\nu], \tag{1.7}$$

$\mathcal{A}_\mu$ (and $\mathcal{F}_{\mu\nu}$) can be expanded on the basis formed by the generators of $\mathfrak{su}(3)$, in such way that $\mathcal{A}_\mu = A_\mu^a T^a$ $(a = 1, \dots, 8)$. Properties of this group are listed in A.3. The covariant derivative

$$\mathcal{D}_\mu = \partial_\mu + ig\mathcal{A}_\mu, \tag{1.8}$$

is diagonal in flavor space. The mass matrix M contains the mass of the six quarks on the diagonal, and g is the strong coupling constant. Lagrangian (1.6) has the fundamental property of insuring the invariance of the theory under the local gauge transformation :

$$\begin{aligned} \psi \to \psi' = \Omega\psi, \quad \overline{\psi} \to \overline{\psi}' = \overline{\psi}\Omega^\dagger, \\ \mathcal{A}_\mu \to \mathcal{A}' = \Omega\mathcal{A}_\mu\Omega^\dagger + \frac{1}{g}\Omega\partial\mu\Omega^\dagger, \end{aligned} \tag{1.9}$$

where Ω is an element of the group $\mathrm{SU(3)_c}$ which can be parametrized by a set of real-valued functions $\omega^a(x)$ such that

$$\Omega \equiv \Omega(x) = e^{-i\omega^a(x)T^a} \in \mathrm{SU(3)_c}. \tag{1.10}$$

The classical field theory is then completly defined by the following action :

$$S_{\mathrm{QCD}}[\mathcal{A}, \psi, \overline{\psi}] = \int \mathrm{d}^4x\mathcal{L}_{\mathrm{QCD}}. \tag{1.11}$$

We come now to the question of the symmetries of this action, which play a central role in the current understanding of the theory. The Lagrangian is invariant under Lorentz transformations and phase redefinition of the fermion fields, respectively related to the energy momentum conservation and to the charge conservation. Note that the action is invariant under the discrete symmetries C, P and T which are defined in Appendix C. In principle, relaxing the hypothesis of CP symmetry allows an additional term in the Lagrangian, the so-called θ term, which is very close to zero in experiment. This fine tuning problem is the so-called *strong CP problem*.

Additional symmetries appear in some peculiar limit of QCD parameters. They lead to interesting conclusion in the quantum version of the theory. First of all, for the sake of concretness consider the limit of a mass degenerate doublet of quarks u and d, which is close to be realized in nature. The action is invariant under the transformation :

$$\psi = \begin{pmatrix} u \\ d \end{pmatrix} \to \psi' = U\psi, \quad \overline{\psi} = \begin{pmatrix} \bar{u} & \bar{d} \end{pmatrix} \to \overline{\psi}' = \overline{\psi}U^\dagger, \tag{1.12}$$

where U belongs to $\mathrm{SU}(2)_V$, the set of unitary two by two matrices of determinant one. This symmetry, named *isospin symmetry*, will be of central importance in this work. Furthermore, let us consider the massless limit of the doublet of quark also called the *chiral limit*. The Lagrangian density becomes invariant under two classes of symmetries of special interest. The *axial symmetry* defined by :

$$\psi = \begin{pmatrix} u \\ d \end{pmatrix} \to \psi' = U\psi, \quad \overline{\psi} = \begin{pmatrix} \bar{u} & \bar{d} \end{pmatrix} \to \overline{\psi}' = \overline{\psi}U, \tag{1.13}$$

where U belongs to the set of transformation called $\mathrm{SU}(2)_A$ which can be parametrized by

$$U = e^{i\alpha^a \tau^a \gamma_5}, \quad a = 1, \dots 3 \tag{1.14}$$

where τ^a are the Pauli matrices defined in appendix A, and α^a real numbers. The flavour singlet counterpart of this symmetry is then defined by a phase redefinition of the quark and anti-quark fields as follows :

$$\psi_i \to \psi' = e^{i\alpha\gamma_5}\psi, \quad \overline{\psi} \to \overline{\psi}' = \overline{\psi}e^{i\alpha\gamma_5} \tag{1.15}$$

The last classical symmetry of the theory is the *dilation symmetry* also called *scale invariance*. Scale transformations are defined by

$$\begin{aligned} x &\to x' = e^{-a}x \\ \mathcal{A}_\mu &\to \mathcal{A}'_\mu = e^{ad_\mathcal{A}}\mathcal{A}_\mu \\ \psi &\to \psi' = e^{ad_\psi}\psi(x'), \overline{\psi} \to \overline{\psi}' = e^{ad_\psi}\overline{\psi}(x') \end{aligned} \tag{1.16}$$

where a is a real number, and the canonical dimension of the fields are $d_\mathcal{A} = 1$ and $d_\psi = 3/2$. Scale invariance is related to the fact no dimensionfull parameters appear at the classical level in the massless limit. These last two symmetries are broken at the quantum level by *anomalies* (see for instance [14] and references therein).

1.2.2 Quantization

In this work, we will use the functional integral formalism introduced by Feynman [15], since it provides a way to formulate non perturbatively the theory. Gauge theory quantization is a delicate question and requires additional material that will not be needed in this work. A careful treatment of the gauge symmetry, lead to introduce a new term called the gauge fixing (GF) term $S[\mathcal{A}]_{\mathrm{GF}}$. It breaks gauge invariance but gives a meaning to the formal expression of the path integral. We will see later that this problem is naturally solved for lattice gauge theories when one consider only gauge invariant correlation functions.

It is convenient to define the correlator of a general functional of the field $\mathcal{O}[\mathcal{A},\psi,\overline{\psi}]$ to be:

$$\langle\mathcal{O}[\mathcal{A},\psi,\overline{\psi}]\rangle \equiv \frac{1}{\mathcal{Z}}\int \mathcal{D}\mathcal{A}\mathcal{D}\psi\mathcal{D}\overline{\psi}e^{iS_{\mathrm{QCD}}[\mathcal{A},\psi,\overline{\psi}]+iS_{\mathrm{GF}}[\mathcal{A}]}\mathcal{O}[\mathcal{A},\psi,\overline{\psi}], \tag{1.17}$$

where the partition function $\mathcal{Z}$ defined by :

$$\mathcal{Z} = \int \mathcal{D}\mathcal{A}\mathcal{D}\psi\mathcal{D}\overline{\psi}e^{iS_{\mathrm{QCD}}[\mathcal{A},\psi,\overline{\psi}]+iS_{\mathrm{GF}}[\mathcal{A}]}, \tag{1.18}$$

The correlation function can then be related to the vaccuum expectation value of a T-product of the corresponding operator (denoted with a hat) on the Hilbert space of state as :

$$\langle\mathcal{O}[\mathcal{A},\psi,\overline{\psi}]\rangle = \langle 0|T\mathcal{O}[\hat{\mathcal{A}},\hat{\psi},\hat{\overline{\psi}}]|0\rangle \tag{1.19}$$

The functional integral has to be understood as an integral over all the classical fields configurations of the fields $\mathcal{A},\psi$ and $\overline{\psi}$ over a four dimensional space-time.. Note that in order to give the right statistic to fermions, the classical fermion field in the integral have to be represented by anti-commutting variables. This is realized by representing fields in a *Grassmann algebra*. The integral over such Grassmann valued numbers can be defined, in such a way that we can formally perform the integration analytically :

$$\int \mathcal{D}\psi\mathcal{D}\overline{\psi}e^{i\int \mathrm{d}^4x\overline{\psi}M\psi} \propto \det \mathrm{M} \tag{1.20}$$

Note that this completly defines the theory. This is a consequence of the reconstruction theorem of Wightmann [16, 17], which states that once known all the vaccuum expactation values of the theory the quantum field theory can be fully determined. The path integral formalism is often used in perturbation theory and gives rise to the famous expansion in terms of Feynman diagrams. We will not consider this approach here, because it is not relevant for the physics we are interested in. It is however worthwhile to note that this approach gives spectacular results in its domain of validity, and is at the origin of QCD as a theory of strong interaction (parton model in deep inelastic scattering). It is well known that divergences appear when calculating pertubative expansions of Green functions. This apparently prevents any calculation beyond tree-level, but it was realized by H.A. Kramers [18] that the divergences can systematically be absorbed into a redefintion of parameters according to the *renormalization* techniques(for an historical account see [19]). If this procedure allows to define order by order the perturbative expansion without adding new parameters the theory is said to be renormalizable. Fortunately this is the case of QCD as it was first shown by 't Hooft in [20, 21] using dimensional regularization [22]. As a consequence the physical quantities are no longer parametrized in terms of the parameters entering in the Lagrangian (bare parameters) but rather in terms of renormalized couplings and masses. Furthermore these renormalized parameters loose in general their status of "physical quantities" because they depend on an energy scale μ, unavoidable and inherent of the renormalization procedure[1]. The scale μ is in principle arbitrary, but in practice has to be chosen in such way that the perturbative expansion is valid. The dependence of the renormalized coupling constant (respectively renormalized masses)on the renormalization scale is called the *running of the coupling constant* (respectively *running masses*).

[1]In the so called on shell (OS) scheme, the mass m^{os} satisfies $\mu\frac{dm^{\mathrm{os}}}{d\mu} = 0$ and are thus renormalization group invariant (RGI). This renormalization scheme is particularly convenient for theory without confinement, *i.e* when the fundamental degrees of freedom are asymptotic states of theory. For instance, it is used to define the mass of the electron or of the W and Z bosons. It has the advantage to provide a physical meaning to the mass parameter [23].

1.2.3 Illuminating tools

In this section, we recall two general non perturbative properties of QFT, that relate vaccuum expactation value of T ordered green function to the physical contents of the theory. This can be done through two famous equations. The first one is the so-called Källén-Lehmann representation [24, 25] which provides a method that will be used all along this work. Consider a composite operators $\mathcal{O}$. The spectral representation of the vaccuum expactation value of the two-point function is :

$$\langle 0|T\mathcal{O}(x)\mathcal{O}(y)||0\rangle = \int_0^\infty dM \rho_{\mathcal{O}}(M^2) D_F(x-y;M^2) \tag{1.21}$$

where $D_F(x-y;M^2)$ is the Feynman propagator associated to the state of mass M and $\rho_{\mathcal{O}}(M^2)$ is a positive spectral density function,

$$\rho_{\mathcal{O}}(M^2) = \sum_n (2\pi)\delta(M^2 - m_n^2)|\langle 0|\mathcal{O}(0)|n\rangle|^2 \tag{1.22}$$

The spectrum of the theory can be recovered by studying two-point functions, and by constructing the spectral density. It contains information about single bound states and multiparticle states that have a continuous spectrum.

1.2.4 Perturbation expansion and asymptotic freedom

One of the major reason that led QCD to be a serious candidate as a theory of strong interaction [26,27] is the property of *asymptotic freedom* of non abelian gauge theory discovered in 1973 in a series of seminal paper of Gross and Wilczek and Politzer [26, 28–30]. This property explains the validity of perturbation theory for high energy processes, such as the one observed in colliders. Let us introduce one more important concept which is believed to belong to the small set of "beyond the perturbative level tools" : *the renormalization group*. It was first discussed in [31, 32] .

In order to apply renormalization techniques, one has to regularize the theory, and to identify the divergences of Green functions by introducing a scale Λ. Then, to renormalize, one absorbs into a parameter redefinition the divergent part of the function at one scale μ_0. A renormalized Green function and the renormalized parameters g_r and m_r depend therefore on the substraction point μ_0. We could have chosen another renormalization point μ, and it would have led to other value of the renormalized parameters. For a renormalizable theory, both Green function are related by a finite multiplicative renormalization which depends of μ and μ_0. For a general Green's function in momentum space one can write :

$$G_r(p, g_r(\mu), m_r(\mu), \mu) = \mathcal{R}(\mu, \mu_0)\ G_r(p, g_r(\mu_0), m_r(\mu_0), \mu_0) \tag{1.23}$$

To be consistent, the functions $\mathcal{R}(\mu, \mu_0)$ have to form an abelian group called the renormalization group. Note that, by definition, physical observables are quantity that are invariant under such transformation.

The renormalization group equation implement that the un-renormalized Green's function does not depend on the renormalization scale μ if all parameters called here g_0, m_0 and Λ are fixed.

$$0 = \mu \frac{d}{d\mu} G(p, g_0, m_0, \Lambda) \tag{1.24}$$

Assuming that G renormalized multiplicatively :

$$G_{\mathrm{r}}(p, g_r, m_r, \mu) = Z_{\mathrm{G}}(g_0, \frac{\mu}{\Lambda}, \frac{m_0}{\Lambda}) G_0(p, g_0, m_0, \Lambda), \tag{1.25}$$

we deduce the following relation

$$\left(\mu\frac{\partial}{\partial\mu}+\beta\frac{\partial}{\partial g_r}-\gamma+m_r\gamma_m\frac{\partial}{\partial m_r}\right)G_r=0 \tag{1.26}$$

where

$$\beta\left(g_{\rm r},\frac{m_{\rm r}}{\mu}\right) = \mu\frac{dg_{\rm r}}{d\mu} \tag{1.27a}$$

$$\gamma_m\left(g_{\rm r},\frac{m_{\rm r}}{\mu}\right) = \frac{\mu}{m_{\rm r}}\frac{dm_{\rm r}}{d\mu} \tag{1.27b}$$

$$\gamma\left(g_{\rm r},\frac{m_{\rm r}}{\mu}\right) = \mu\frac{d\ln Z_G}{d\mu} \tag{1.27c}$$

We can choose a mass-independent renormalization scheme and the renormalization group functions do not depend of $m_{\rm r}$. We can write explicit solutions of the renormalization group equation Eqs. (1.27). In particular we have

$$\frac{m(\mu)}{m(\mu_0)}=\exp\left\{\int_{g_{\rm r}(\mu_0)}^{g_{\rm r}(\mu)}dh\frac{\gamma_m(h)}{\beta(h)}\right\} \tag{1.28}$$

$$\frac{\mu}{\mu_0}=\exp\left\{\int_{g_{\rm r}(\mu_0)}^{g_{\rm r}(\mu)}\frac{dh}{\beta(h)}\right\} \tag{1.29}$$

The Eqs. (1.28) and (1.29) gives the running of the renormalized parameters in terms of the renormalization group functions. Unfortunately, only a finite number of terms in the perturbation series of the renormalization functions are known. For example in the QCD case, the β function expansion can be written in the following way :

$$\beta=-\sum_{n\geq 0}\beta_n g_{\rm r}^{n+3} \tag{1.30}$$

with $\beta_0>0$. Expanding β to its first order in Eq. (1.28), we obtain

$$g_{\rm r}(\mu)=\frac{g_{\rm r}(\mu_0)}{1+\beta_0 g_{\rm r}(\mu_0)\ln\left(\frac{\mu}{\mu_0}\right)} \tag{1.31}$$

While $g_{\rm r}(\mu_0)$ and $g_{\rm r}(\mu)$ are small, this equation gives us a good approximation of the running coupling constant. Note that one has $g_{\rm r}(\mu)\to 0$ for $\mu\to\infty$. This is the asymptotic freedom property. It explains why, in QCD, pertubative expansions can be used at large momentum. Conversely, at low energy, the coupling constant increase, and non pertubative phenomena occur.

1.2.5 QCD in Euclidean space-time

The phase in the functional integral Eq. (1.17) is difficult to estimate numerically. To circumvent this problem, one performs an analytical continuation of the time component of the 4-vectors to purely imaginary values. This is the Wick rotation. This rotation of the time coordinate $x^0\to -ix^0$ leads to a Euclidean 4-vector norm :

$$x^2=\left(x^0\right)^2-|\vec{x}|^2 \quad\to\quad -x_{\rm E}^2=-\left(x^0\right)^2-|\vec{x}|^2 \tag{1.32}$$

It was shown by Osterwalder and Schrader [33] that under certain conditions one can recontruct the whole quantum field theory in Minkovski space from Euclidean field theory. The most important condition is the so called *Osterwalder-Schrader positivity* or *reflection positivity*, which replace Hilbert space positivity and the spectral condition of the Minkowskian formulation.

The Euclidean QCD action then reads

$$S_{\mathrm{E}}[\mathcal{A},\psi,\overline{\psi}] = -\frac{1}{2}\mathrm{Tr}\left\{\mathcal{F}_{\mu\nu}\mathcal{F}^{\mu\nu}\right\} + \overline{\psi}(\not{\mathcal{D}} + M)\psi \tag{1.33}$$

and the correlation functions are obtained formally by integrating over the whole space of configurations. In general one has:

$$\langle \mathcal{O}[\mathcal{A},\psi,\overline{\psi}]\rangle = \frac{1}{\mathcal{Z}_{\mathrm{E}}}\int \mathcal{D}\mathcal{A}\mathcal{D}\psi\mathcal{D}\overline{\psi}e^{-S_{\mathrm{E}}[\mathcal{A},\psi,\overline{\psi}]}\mathcal{O}[\mathcal{A},\psi,\overline{\psi}], \tag{1.34}$$

using the notation introduced in 1.2.1 and where $\mathcal{O}[\mathcal{A},\psi,\overline{\psi}]$ is a generic functional of the fields. The partition function is

$$\mathcal{Z}_{\mathrm{E}} = \int \mathcal{D}\mathcal{A}\mathcal{D}\psi\mathcal{D}\overline{\psi}e^{-S_{\mathrm{E}}[\mathcal{A},\psi,\overline{\psi}]} \tag{1.35}$$

1.3 QCD on the Lattice

In the numerical simulations of QCD that we are going to present we restricted ourselves to a degenerate doublet of light quarks $m_u = m_d$ (isospin limit). We will consider two ensembles of simulations corresponding to $N_f = 2$ and to $N_f = 2+1+1$ flavor dynamical quarks. The $1+1$ sector refers to the non degenerate heavy doublet of the strange and charm quarks with a mass denoted by m_s and m_c.

These two simplified versions of QCD are sufficiently accurate for our purpose.On one hand because we will never consider observables involving correlation function which contains bottom or top quarks and on the other hand because the loop corrections due to these quarks are negligible in the observables we aim to compute. This is the decoupling theorem which states that if we want to compute Green's functions in multiple scale models, we can neglect masses much heavier than the energy of proceses that we are considering. From this point of view, the $N_f = 2$ case is a particular version of the $N_f = 2+1+1$ one in the formal limit $m_s, m_c \to \infty$.

1.3.1 Lattice regularization

In order to simulate QCD numerically, we need to give a precise meaning to Eq. (1.34). The lattice formulation of QCD in a Euclidean space is a non perturbative regularization of the theory. The idea is to replace the continuum variable x_μ by a discrete coordinate on a four dimensional hypercube with a lattice spacing a :

$$x_\mu \longrightarrow n_\mu a, \quad n \in [\![0, L-1]\!]^3 \times [\![0, T-1]\!], \tag{1.36}$$

and with volume $V = L^3 \times T$. The boundary conditions are chosen to be periodic for the gauge field . The quark fields are periodic in space direction and anti-periodic in time.

The finite lattice spacing introduces an ultraviolet cutoff and the finite volume introduces an infrared cutoff. All the divergences are then regularized.

Note that the momenta allowed in the spatial directions are :

$$\vec{k} = \pm\frac{2\pi\vec{n}}{aL}, \text{with} \;\; n_i = 1, \ldots, L/2. \tag{1.37}$$

In the next section, we show how the Yang-Mills part of the action can be written on a discretized space-time, and how the integral over the gauge field is defined.

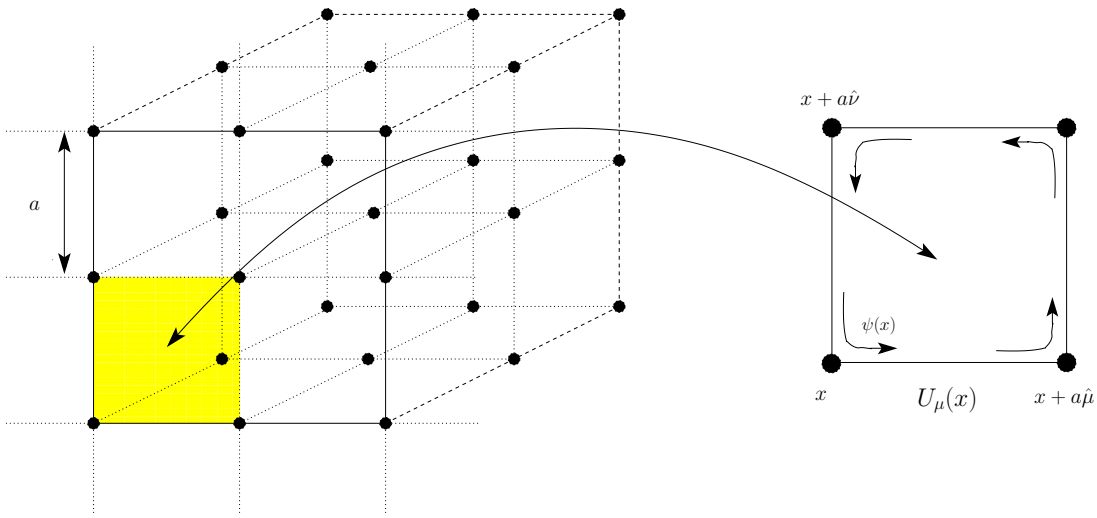

Figure 1.4: A lattice

1.3.2 Lattice gauge theory

The first step in formulating the $\mathrm{SU(3)_c}$ Yang Mills theory on a lattice is to find a discrete lattice action which tends to the continuun Yang-Mills action at the classical level when the lattice spacing vanishes. The Wilson gauge action [34] has this property. It is constructed from an elementary field $U_\mu(x)$ living on the links of the lattice and which belong to the $\mathrm{SU(3)_c}$ group.

Defining the so-called plaquette variable

$$U_{\mu\nu}(x) = U_\mu(x)U_\nu(x+\hat{\mu})U_\mu^\dagger(x+\hat{\nu})U_\nu^\dagger(x) \tag{1.38}$$

the Wilson gauge action then reads :

$$S_{\mathrm{G}}^{(W)}[U] = \beta \sum_x \sum_{\mu<\nu} \left(1 - \frac{1}{3}\mathrm{Re\ Tr}\left\{\mathrm{U}_{\mu\nu}(\mathrm{x})\right\}\right) \tag{1.39}$$

where

$$\beta = \frac{6}{g^2} \tag{1.40}$$

is the unique parameter of the action and it is reated to bare coupling g. The Yang Mills continuum action can be recovered up to $\mathcal{O}(a^2)$ terms by setting :

$$U_\mu = e^{iag\mathcal{A}_\mu} \tag{1.41}$$

and expanding in powers of a. The gauge transformation 1.9 for the $\mathcal{A}_\mu$ becomes for the link variables U_μ :

$$U_\mu(x) \longrightarrow U'_\mu(x) = \Omega(x)U_\mu(x)\Omega^{-1}(x+\mu) \tag{1.42}$$

It follows from this property that the Wilson gauge action preserves gauge invariance.

We can now define properly the measure of the functionnal integral over the gauge field:

$$\int \mathcal{D}\mathcal{A} = \int \prod_{x,\mu} \mathrm{d}U_\mu(x) \tag{1.43}$$

where the product is over all lattice points x and directions μ. Unlike in the continuum the lattice gauge fields belongs to the compact group SU(3) and are thus bounded. Therefore we can use the standard definition of group integration measure, like the invariant *Haar measure* [35]. The number of variables of integration is finite and the path integrals free from any divergences. The set of all the link variable $U = \{U_\mu(x), \forall x, \forall \mu\}$ is called *gauge field configuration*.

1.3.3 Fermions on the lattice and the doubling problem

The lattice formulation of fermionic fields appears to be a more delicate issue. As Wilson first noticed in [34], the naive discretization of the free field theory involving fermions gives rise to $2^4 = 16$ fermions excitation rather than one even in the continuum. This problem is called the *doubling problem*. In order to overcome it one introduces additional terms in the action which vanishes in the continuum limit.

Unfortunately, even if there is a priori an infinite choice of such terms, they often break relevant symmetries of the continuum action, like chiral invariance. This fact was summarized by the Nielsen Ninomiya no-go theorem in [36–38] which states that a massless Dirac operator D cannot fulfill at one the following properties :

- $D(x)$ is a local operator (bounded by $e^{-\gamma|x|}$)
- the Fourier transform of $D(x)$ has the right continuum limit up to $\mathcal{O}(ap^2)$ for $p \ll \pi/a$
- $\tilde{D}(p)$ is invertible for $p \neq 0$
- The action is invariant under chiral transformation, i.e $\{\gamma_5, D\} = 0$

The so-called Wilson action breaks this last point by adding an operator of dimension 5 proportional to some unphysical parameter r. In the continuum limit the Wilson term vanishes. However the explicit breaking of chiral symmetry at finite lattice spacing, leads to many theoritical and practical problems which continue to motivate physicists to find new actions having better chiral properties.
To write the Wilson action one need to define the forward covariant difference operator

$$\nabla_\mu \psi(x) = \frac{1}{a}\left[U_\mu(x)\psi(x + a\hat{\mu}) - \psi(x)\right] \tag{1.44}$$

and the backward covariant difference operator

$$\nabla^*_\mu \psi(x) = \frac{1}{a}\left[\psi(x) - U^{-1}_\mu(x - a\hat{\mu})\psi(x - a\hat{\mu})\right]. \tag{1.45}$$

The massless *Dirac-Wilson operator* in a given background gauge field then reads :

$$D_W[U] = \sum_\mu \frac{1}{2}\left[\gamma_\mu\left(\nabla_\mu + \nabla^*_\mu\right) - ar\nabla^*_\mu\nabla_\mu\right], \tag{1.46}$$

where the Wilson parameter r can be chosen in $-1 \leq r \leq 1$. The corresponding action for a massive quark is

$$S^{(W)}_{\mathrm{F}}[\psi, \overline{\psi}, U] = a^4 \sum_x \overline{\psi}(x)\left(D_{\mathrm{W}}[U] + m_0\right)\psi(x). \tag{1.47}$$

In order to have dimensionless quantities, we re-scale the field introducing the *hopping parameter* κ as follow :

$$\psi \to \frac{\sqrt{2\kappa}}{a^{3/2}}\psi, \quad \overline{\psi} \to \frac{\sqrt{2\kappa}}{a^{3/2}}\overline{\psi}, \quad \kappa = \frac{1}{2am_0 + 8r} \tag{1.48}$$

which leads to the *hopping parameter representation* of the Dirac-Wilson action :

$$S_{\mathrm{F}}^{(W)}[\psi,\overline{\psi},U] = \sum_x \Bigg\{ \overline{\psi}(x)\psi(x) - \kappa\overline{\psi}(x) \sum_{\mu=0}^{3} \Big[U_\mu(x)(r+\gamma_\mu)\psi(x+a\hat{\mu}) + U_\mu^\dagger(x-a\hat{\mu})(r-\gamma_\mu)\psi(x-a\hat{\mu}) \Big] \Bigg\} \tag{1.49}$$

1.3.4 Monte Carlo Integration

Putting together the results of the last two sections we can now write the correlation functions of QCD regularized on a lattice. After integrating over the Grassmann variables we obtain:

$$\langle \mathcal{O}[\psi,\overline{\psi},U] \rangle = \frac{1}{\mathcal{Z}_{\mathrm{E}}} \int \prod_{x,\mu} \mathrm{d}U_\mu(x)\ \det\ (\mathrm{D_W[U]} + \mathrm{m_0})\, \mathrm{e}^{-\mathrm{S_G^{(W)}[U]}} \tilde{\mathcal{O}}[\mathrm{U}] \tag{1.50}$$

Where $\tilde{\mathcal{O}}[U]$ can be computed in terms of the inverse Wilson-Dirac operator summing over all Wick contractions. The problem is to perform $\mathcal{O}(V)$ integrals over the gauge group. Since we are interested in V as large as possible, the standard numerical integration fail. The solution comes from Monte Carlo integration techniques which consist in generating a sample of a finite number N of independant gauge configurations $U^{(i)}$ with a probability distribution given by

$$P[U] = \ \det\ (\mathrm{D_W[U]} + \mathrm{m_0})\, \mathrm{e}^{-\mathrm{S_G^{(W)}[U]}}, \tag{1.51}$$

Correlators are then estimated by

$$\langle \mathcal{O}[\psi,\overline{\psi},U] \rangle = \bar{\mathcal{O}} + \mathcal{O}(\frac{1}{\sqrt{N}}), \text{with} \quad \bar{\mathcal{O}} = \frac{1}{\mathrm{N}} \sum_{\mathrm{i}=1}^{\mathrm{N}} \tilde{\mathcal{O}}[\mathrm{U^{(i)}}] \tag{1.52}$$

Generating such an ensemble of configuration is highly non trivial due to the presence of the determinant of the Dirac operator and requires the development of sophisticated hybrid Monte Carlo algorithms (HMC) running on supercomputers, and using massive parallelism. The computation of the fermion determinant is by far the most time consuming part of the simulation. More details will be given on this subject in Chapter 4.

1.3.5 Continuum limit

Quantities computed at finite lattice have to be extrapolated to the continuum. To be concrete let us begin with one flavour QCD. The corresponding regularization on an infinite lattice depends on two bare parameters (am_0, g_0). Introducing the correlation length $\xi(am_0, g_0)$, which governs the exponential decay of the correlation functions, the continuum limit is the ensemble of points in the two parameters space (am_0, g_0), where the correlation length ξ become infinite. By using the statistical mechanics language, it correspond to look for a second order phase transition in the phase diagram. In this regime, long range phenomena occurs that are no more sensitive to microscopic details of the discretized action. This definition is reasonable since the correlation length correspond to the inverse of a mass in lattice units denoted by am and according to the criteria that, $\xi \to \infty$ in the continuum, we expect $am \to 0$. In that case, while $a \to 0$ we can have a a finite mass m.

In fact asymptotic freedom guarantees that this limit is achieved when the coupling constant $g_0(a)$ vanishes or conversely when $\beta(a) \to \infty$ (see for instance [35]).

In practice, we have to work with a lattice a finite size and two strategies can be followed. Either we have to take the limit $\beta \to \infty$ keeping fix the physical size of the box. This can be done

in practice by fixing first mL, and then taking $\beta \to \infty$. This correspond to computing physical observables in a continuum box of a finite size. Or, we can first extrapolate lattice data in the infinite volume limit and then take the limit $\beta \to \infty$. The two limits are expected to commute.

Considering for instance ratio of masses, we expect them to be independent of β in the vicinity of the continuum limit since for large β. However the dependence as a function of β depend on the discretized version of the theory. This is illustrated in Fig. 1.5, where the behaviour close to the continuum associated to two different discretized action S_1 and S_2 is shown as a function of the lattice spacing. The approach to the continuum of observables, will be refered to as the scaling behaviour. The continuum limit is expected to be universal while the scaling behaviour is not.

Several efforts and progress have been made in the lattice QCD community to improve the scaling behaviour of discretized actions, in order to obtain a better control on this important systematic effects of lattice calculations.

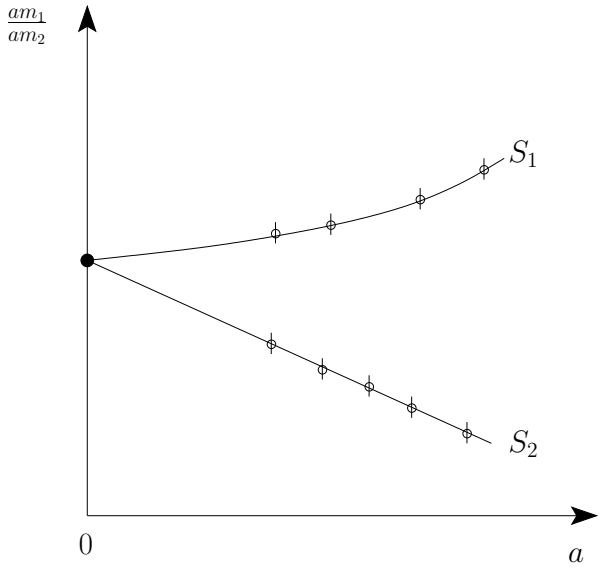

Figure 1.5: Scaling properties of two discretized actions S_1 and S_2. The ratio of two typical hadronic mass in lattice units is shown as a function of the lattice spacing. The continuum limit is universal while the scaling properties are not.

1.4 Octet and Decuplet of baryon : Presentation

Let us close this chapter by summarizing the current knowledge about the properties of the baryon octet and decuplet. Tables 1.1 and 1.2 list the quantum numbers, the masses, the width or lifetime as well as the main decay mode of the low lying states.

The proton is the only state stable on all the known interactions. All the other members of the octet decay mainly through the weak interaction, involving the CKM matrix element $V_{\rm us}$. The main decay channels thus violate strangeness conservation. The only exception is the Σ^0 which decays via electromagnetic interactions to the Λ.
Concerning the decuplet, with the only exception of the Ω^-, they are strong resonances of spin 3/2 with the following hierarchy of widths $\Gamma_\Delta > \Gamma_{\Sigma^*} > \Gamma_{\Xi^*}$. They decay with a typical strong interaction life time of $\sim 10^{-23}$ seconds to their $\Delta S = 0$ octet partner emiting a pion. The Ω^-

Particle	$I(J^P)$	Mass (MeV)	Mean life (s)	Main Decay Modes
p	$\frac{1}{2}(\frac{1}{2}^+)$	938.272029 ± 0.000080	$> 2.1 \times 10^{29}$	stable
n	$\frac{1}{2}(\frac{1}{2}^+)$	939.565360 ± 0.000081	885.7 ± 0.8	$pe^-\bar{\nu}_e$ (100)%
Λ	$0(\frac{1}{2}^+)$	1115.683 ± 0.006	$2.631 \pm 0.02 \cdot 10^{-10}$	$p\pi^-(63.9 \pm 0.58),\ n\pi^0(35.8 \pm 0.5)$
Σ^+	$1(\frac{1}{2}^+)$	1189.37 ± 0.07	$0.8018 \pm 0.0026 \cdot 10^{-10}$	$p\pi^0(51.57 \pm 0.30),\ n\pi^+(48.31 \pm 0.30)$
Σ^0	$1(\frac{1}{2}^+)$	1192.642 ± 0.024	$7.4 \pm 0.7 \cdot 10^{-20}$	$\Lambda\gamma(100)$%
Σ^-	$1(\frac{1}{2}^+)$	1197.449 ± 0.030	$1.479 \pm 0.011 \cdot 10^{-10}$	$n\pi^-(99.848 \pm 0.005)$%
Ξ^0	$\frac{1}{2}(\frac{1}{2}^+)$	1314.83 ± 0.20	$2.90 \pm 0.09 \cdot 10^{-10}$	$\Lambda\pi^0(99.523 \pm 0.013)$%
Ξ^-	$\frac{1}{2}(\frac{1}{2}^+)$	1321.13 ± 0.20	$1.639 \pm 0.015 \cdot 10^{-10}$	$\Lambda\pi^-(99.887 \pm 0.035)$%

Table 1.1: Octet properties taken from [39]

Particle	$I(J^P)$	Mass (MeV)	Width (MeV)	Mean life (s)
Δ^{++}	$\frac{3}{2}(\frac{3}{2}^+)$	1231.88 ± 0.29	109.07 ± 0.48	
Δ^+	$\frac{3}{2}(\frac{3}{2}^+)$	1231.6	111.2	
Δ^0	$\frac{3}{2}(\frac{3}{2}^+)$	1234.35	117.58 ± 1.16	
Δ^-	$\frac{3}{2}(\frac{3}{2}^+)$			
Σ^{*+}	$1(\frac{3}{2}^+)$	1382.8 ± 0.4	35.8 ± 0.8	
Σ^{*0}	$1(\frac{3}{2}^+)$	1383.7 ± 1.0	36 ± 5	
Σ^{*-}	$1(\frac{3}{2}^+)$	1387.2 ± 0.5	39.4 ± 2.1	
Ξ^{*0}	$\frac{1}{2}(\frac{3}{2}^+)$	1531.80 ± 0.32	9.1 ± 0.5	
Ξ^{*-}	$\frac{1}{2}(\frac{3}{2}^+)$	1535.0 ± 0.6	9.9 ± 1.9	
Ω^-	$0(\frac{3}{2}^+)$	1672.45 ± 0.29		$0.821 \pm 0.011 \cdot 10^{-10}$

Table 1.2: Decuplet properties taken from [39]

decays through the weak interaction to the Ξ (no states of spin 1/2 have three s quarks).
The question of the mass splitting between the different isospin multiplet commponent is far from trivial. It comes both from the isospin symmetry breaking ($m_u \neq m_d$) and from the different charge of the u ($+\frac{2}{3}$) and d($-\frac{1}{3}$) quarks. This question will not be raised in this work since all our investigations are performed in the isospin limit and without electromgnetic interaction. In this approximation one could expect an exact mass degeneracy in the multiplet. We will see however that it is case only up to $\mathcal{O}(a^2)$.

1.5 Aim of this work - Motivations

In this work all the steps going from the generation of gauge configurations to the computation of correlators and their analysis have been covered. Our final analysis is devoted to the study of the baryon spectrum which offers a rich variety of observables, without increasing the number of parameters with respect to the predictions.

In Chapter 2 we will present the fermionic part of the action used in our simulations, namely the twisted mass fermions. They can be used to simulate degenerate or non-degenerate quarks and the two approaches will be described. The advantage and the drawbacks of this type of fermions will be discussed in order to justify the analysis strategy followed in this work.

In Chapter 3, the theoritical framework to extract masses from suitable two-point correlators

is explained. A general formula that allows to measure any baryonic two-point function is derived. This constitutes an essential part of this work. Smearing techniques as well as the analysis procedure are set up in the light of Chapter 2.

In Chapter 4, we explain the gauge configuration production. This step is the most expensive from a numerical point of view and is exclusively performed on supercomputers like BlueGene. An important part of my Ph.D time has been devoted to manage, control and participate in this task. In particular by measuring and tuning quantities of primary importance to understand the physical parameters of the simulations.

In Chapter 5, we develop the essential aspects of chiral perturbation theory in the baryon sector, which are an important tool to understand our lattice data.

The main results of this work are presented in Chapters 6 and 7. The raw baryon masses computed in our lattice simulations are given. We analyze the artefacts due to our discretization procedure (finite volume, finite lattice spacing effects), and compare with experiment.

All this work has been done in the framework of European Twisted Mass Collaboration (ETMC) which involves about fourty member and eight European countries:

- Cyprus: Nicosia
- Germany : Berlin, Hamburg, Münster
- Italy: Rome, Trento
- Netherlands: Groningen
- Spain : Valencia
- Switzerland: Bern
- United-Kingdom: Liverpool
- France: Paris, Grenoble

This allow to share the computational resources and human ability to compute a large number of physical observables.

Chapter 2

Twisted Fermions

Contents

Wilson twisted mass QCD [40, 41] is a lattice regularization that allows automatic $\mathcal{O}(a)$ improvement [42]. One of the historical reasons why a twisted mass term was was introduced to solve the so called problem of exceptional configurations. The Wilson-Dirac operator is not protected against zero modes, whereas the twisted mass wilson operator is protected against them. Interesting review are [43–45]

2.1 Continuum theory at the classical level

2.1.1 Degenerate fermions

The twisted mass (tm) fermion action in the continuum for a 2 flavour fermion field χ:

$$S_{\mathrm{tm}}[\chi,\overline{\chi},U]_{(m_0,\mu)} = \int \mathrm{d}^4x\overline{\chi}\left(\not{\mathcal{D}} + m_0 + i\mu\gamma_5\tau^3\right)\chi \tag{2.1}$$

where $\mathcal{D}_\mu$ is the covariant derivative, m_0 the usual mass term and μ an additional parameter of this model called the twisted mass. Note that the Pauli matrice τ^3 in the twisted mass term of eq. 2.1 acts in flavour space. The isospin doublet field χ is said to be in the *twisted basis*, and the reason for that will become clear later. The standard Dirac action is recovered in the limit $\mu \to 0$

Let us start by considering the properties of the twisted mass action at the classical level. Under the axial transformations in flavour space with a real parameter ω_l

$$\begin{aligned}\chi &\to e^{i\frac{\omega_l}{2}\gamma_5\tau^3}\chi \\ \overline{\chi} &\to \overline{\chi}e^{i\frac{\omega_l}{2}\gamma_5\tau^3}\end{aligned} \tag{2.2}$$

the form of the action is left unchanged, with the replacement

$$\begin{aligned}m_0 &\to m_0' = m_0\cos\omega_l + \mu\sin\omega_l \\ \mu &\to \mu' = -m_0\sin\omega_l + \mu\cos\omega_l\end{aligned} \tag{2.3}$$

Let us consider the particular case of the twisted mass action 2.1 with $m_0 = 0$ refered hereafter as the maximally twisted mass (mtm) action:

$$S_{\mathrm{mtm}}[\chi,\overline{\chi},U] = S_{\mathrm{tm}}[\chi,\overline{\chi},U]_{(0,\mu)} = \int \mathrm{d}^4x\overline{\chi}\left(\not{\mathcal{D}} + i\mu\gamma_5\tau^3\right)\chi \tag{2.4}$$

Performing an axial rotation 2.3 with $\omega_l = \frac{\pi}{2}$, we find:

$$S_{\mathrm{tm}}[\chi,\overline{\chi},U]_{(0,\mu)} \to S_{\mathrm{tm}}[\chi,\overline{\chi},U]_{(\mu,0)} = S_{\mathrm{Dirac}}[\chi,\overline{\chi},U] \tag{2.5}$$

We see that the maximally twisted fermions are completly equivalent to the Dirac fermions at the classical level and constitute an alternative formulation of "classical" QCD.

Our strategy for the numerical simulation of QCD will be the following: we will use the twisted mass action at maximal twist angle and rotate back our correlators to the *physical basis* ψ defined by

$$\psi = e^{i\frac{\pi}{4}\gamma_5\tau^3}\chi, \qquad \overline{\psi} = \overline{\chi}e^{i\frac{\pi}{4}\gamma_5\tau^3} \tag{2.6}$$

From the classical field theory point of view, all the symmetry of the Dirac action are preserved in the maximally twisted mass action. They can however have a misleading form in the twisted basis. For instance the axial transformation in the physical basis becomes the vector transformation in the twisted one. This statement can be generalized at the classical level for an arbitrary twist angle case showing that the two classical field theory are completly equivalent.

In practice, the quantization of twisted mass formulation allows to avoid numbers of problem raised by other regularizations, as we will see in section 2.2.

2.1.2 Non-degenerate fermions

We will present now the generalization of this theory to the case of non-degenerate flavour doublet, in order to simulate a theory closer to the real world and containing strange and charm quarks in the sea. The aim is to build and action which, after a chiral rotation, gives the standard Dirac action for two non degenerate flavours.

In this section we will concentrate on the so-called heavy sector. Consider a field χ which has two flavour components with the action

$$S_{\rm tm}^{(1+1)}[\chi,\overline{\chi},U]_{(m_0,\mu_\sigma,\mu_\delta)} = \int \mathrm{d}^4x\overline{\chi}\left(\not{\mathcal{D}} + m_0 + i\mu_\sigma\gamma_5\tau^1 + \mu_\delta\tau^3\right)\chi \tag{2.7}$$

with μ_σ and μ_δ positive. Performing a chiral rotation of the form :

$$\chi \to e^{i\frac{\omega_h}{2}\gamma_5\tau^1}\chi, \qquad \overline{\chi} \to \overline{\chi}e^{i\frac{\omega_h}{2}\gamma_5\tau^1} \tag{2.8}$$

the action is left unchanged, with the replacement

$$\begin{aligned} m_0 &\to m_0' = m_0\cos\omega_h + \mu\sin\omega_h \\ \mu_\sigma &\to \mu_\sigma' = -m_0\sin\omega_h + \mu\cos\omega_h \\ \mu_\delta &\to \mu_\delta' = \mu_\delta \end{aligned} \tag{2.9}$$

We define the maximal twist as in the degenerate case setting $m_0 = 0$ in eq. 2.7

$$S_{\rm mtm}^{(1+1)}[\chi,\overline{\chi},U] = \int \mathrm{d}^4x\overline{\chi}\left(\not{\mathcal{D}} + i\mu_\sigma\gamma_5\tau^1 + \mu_\delta\tau^3\right)\chi, \tag{2.10}$$

By performing a rotation of angle $\omega_h = \frac{\pi}{2}$, we find that :

$$S_{\rm mtm}^{(1+1)}[\chi,\overline{\chi},U] \to S_{\rm Dirac}^{(1+1)} = S_{\rm tm}[\chi,\overline{\chi},U]_{(\mu_\sigma,\mu_\delta)} = \int \mathrm{d}^4x\overline{\chi}\left(\not{\mathcal{D}} + \mu_\sigma + \mu_\delta\tau^3\right)\chi \tag{2.11}$$

This suggest to identify the strange (m_s) and charm quark (m_c) mass to be :

$$\begin{aligned} m_s &= \mu_\sigma - \mu_\delta \\ m_c &= \mu_\sigma + \mu_\delta \end{aligned} \tag{2.12}$$

As in the degenerate case the twisted mass action with non degenerate fermions is equivalent to the standard Dirac action.

Note that in the twisted basis, the fields are coupled by non vanishing off diagonal terms in flavour space. Its inversion is no longer factorized in flavour but requires to deal with a matrix which is twice as big.

$$\mathcal{D}_{light} = \begin{pmatrix} D_+ & 0 \\ 0 & D_- \end{pmatrix} \qquad \mathcal{D}_{heavy} = \begin{pmatrix} D_{ss} & D_{sc} \\ D_{cs} & D_{cc} \end{pmatrix} \tag{2.13}$$

2.2 Twisted fermions on the lattice

We present in this section the discretized version of the twisted fermions as well as the main properties of the underlying quantum field theory. We will restrict ourselves to the two degenerate flavours case, even if the fundamental properties can be generalized in the case $N_f = 2+1+1$ of a field theory containing a doublet of degenerate quarks and a doublet of non-degenerate quarks.

2.2.1 Lattice action

The twisted mass formulation term does not prevent the doubling problem. To solve it, we will combine it with a Wilson-Dirac operator. This is not the unique solution, and in principle any other discretization of the Dirac operator removing the doubling problem can be used. The bare discretized action for the light sector we will use in this work reads

$$S_{\mathrm{F}}^{(N_f=2)}[\chi,\overline{\chi},U] = a^4 \sum_{x,\mu} \overline{\chi}(x) \left(D_{\mathrm{W}}[U] + m_0 + i\mu\gamma_5\tau^3\right) \chi(x) \tag{2.14}$$

where D_{W} refers to the massless Wilson-Dirac operator defined in Eq. (1.46), m_0 and μ are bare mass parameters whose physical meaning will be clarified latter. This action can be rewritten in terms of the hopping parameter (1.49) in the form:

$$S_{\mathrm{F}}^{(N_f=2)}[\chi,\overline{\chi},U] = \sum_x \Bigg\{ \overline{\chi}(x)(1+2i\kappa\mu\gamma_5\tau^3)\chi(x) - \kappa\overline{\chi}(x) \sum_{\mu=0}^{3} \Big[U_\mu(x)(r+\gamma_\mu)\chi(x+a\hat{\mu}) + U_\mu^\dagger(x-a\hat{\mu})(r-\gamma_\mu)\chi(x-a\hat{\mu}) \Big] \Bigg\} \tag{2.15}$$

which is implemented in our code.

2.2.2 Tuning to maximal twist

The main interest of using twisted mass regularization is automatic $\mathcal{O}(a)$ improvement achieved at maximal twist angle. We will see in this section how this is realized in practice.

Our starting point is the bare discretized action :

$$S_{\mathrm{F}}^{(N_f=2)}[\psi,\overline{\psi},U] = a^4 \sum_{x,\mu} \overline{\chi}(x) \left(D_{\mathrm{W}}[U] + m_0 + i\mu\gamma_5\tau^3\right) \chi(x) \tag{2.16}$$

A natural generalization of the maximal twist condition $m_0 = 0$ at the classical level is to impose $m_R = 0$. Wilson fermions in the massless limit explicitly breaks the chiral symmetry at finite lattice spacing. One important consequence is that the quark mass is no longer multiplicatively renormalizable but acquires an additive renormalization term m_{c}, i.e

$$m_R = Z_m m_0 \longrightarrow m_R = Z_m(m_0 - m_{\mathrm{c}}) \tag{2.17}$$

where Z_m is the renormalization constant. This is why, at the quantum level, to set the bare quark mass $m_0 = 0$ is not equivalent to tune the action to maximal twist.

To define properly maximally twisted QCD, one has to define the renormalized quark mass. In order to do this, we give without proof that the partially conserved current relation obtained at finite lattice spacing by performing a transformation of the form :

$$\chi \to e^{i\alpha\gamma_5\tau^a}\chi, \qquad \overline{\chi} \to \overline{\chi}e^{i\alpha\gamma_5\tau^a}, \quad a = 1,2 \tag{2.18}$$

is

$$\langle 0|\partial_\mu \mathcal{A}_\mu^a(x)\mathcal{O}|0\rangle = 2im_0\langle 0|\mathcal{P}^a(x)\mathcal{O}|0\rangle + ira\langle 0|\overline{\chi}(x)\nabla_\mu\nabla_\mu^*\chi(x)\mathcal{O}|0\rangle \tag{2.19}$$

$\mathcal{A}_\mu^a$ and $\mathcal{P}^a$ are referred as the axial and pseudoscalar bilinear operator defined by:

$$\begin{aligned} \mathcal{A}_\mu^a &= \overline{\chi}\tau^a\gamma_\mu\gamma_5\chi \\ \mathcal{P}^a &= \overline{\chi}\tau^a\gamma_5\chi \end{aligned} \tag{2.20}$$

The two terms on the right hand side of Eq. (2.19) are due to the fact that the mass and the Wilson term are not invariant under (2.18). Note that this identity holds at finite lattice spacing and that the second term on the right hand side contributes to the renormalization of the mass and of the operator $\mathcal{A}_\mu^a$.

The renormalized fermionic action can be written as :

$$S_{\rm mtQCD}^{N_f=2} = \int \mathrm{d}^4x \overline{\chi}(x) \left[\not{\mathcal{D}} + m_R + i\mu_R\gamma_5\tau^3\right] \tag{2.21}$$

Applying the transformation (2.18), one finds at the level of the renormalized correlation functions that

$$\langle 0|\partial_\mu \mathcal{A}_{\mu,R}^a(x)\mathcal{O}|0\rangle = 2im_R\langle 0|\mathcal{P}_{\mu,R}^a(x)\mathcal{O}|0\rangle \tag{2.22}$$

Using the fact that the bilinear operators are multiplicatively renormalizable, we can deduce the relation between the PCAC mass and the renormalized mass m_R. To this purpose, let us introduce Z_A and Z_P, the renormalization constant of the axial and pseudoscalar bilinear, in the following way

$$\begin{aligned} \mathcal{A}_{\mu,R}^a &= Z_A\mathcal{A}_\mu^a, \quad a=1,2 \\ \mathcal{P}_R^a &= Z_P\mathcal{P}^a, \quad a=1,2 \end{aligned} \tag{2.23}$$

Defining the so-called PCAC mass $m_{\rm PCAC}$, to be

$$m_{\rm PCAC} = \frac{\sum_{\vec{x}}\langle 0|\partial_\mu \mathcal{A}_\mu^a(x)\mathcal{O}|0\rangle}{2\sum_{\vec{x}}\langle 0|\mathcal{P}_\mu^a(x)\mathcal{O}|0\rangle} \tag{2.24}$$

we conclude that the following relation must hold :

$$m_R = Z_P^{-1}Z_A m_{\rm PCAC} \tag{2.25}$$

Recalling that our aim is to tune the action to maximal twist, namely to fulfill

$$m_R = 0 \tag{2.26}$$

we deduce that this is satisfied by imposing that the PCAC mass vanishes.

We define the *critical mass* by the following equation:

$$m_{\rm PCAC}(\beta, m_0 = m_{\rm c}, \mu) = \mathcal{O}(a\mu) \tag{2.27}$$

This defines by the same the so called *critical line* in the parameter space (β, m_0, μ) on which maximal twist is achieved.

To summarize, in our numerical simulation the action depends on the three bare parameters (β, m_0, μ) in the $N_F = 2$ case and five $(\beta, m_0, \mu, \mu_\sigma, \mu_\delta)$ in the $N_F = 2+1+1$ case.

As we have already explained in chapter 1, β controls the lattice spacing and the continuum limit is reached at $\beta \to \infty$.

Concerning the bare twisted mass μ, on can show by performing the rotation to the physical basis (2.6), that it controls the physical light quark mass and consequently the pion mass. Its denomination is thus somehow misleading since, the physical quark mass is not controlled by m_0 but by the twisted quark mass μ. The same happens in the non degenerate sector, where (μ_σ, μ_δ) control, according to Eq. (2.12), the strange and charm quark masses.

As discussed above the mass parameter m_0 is tuned in order to make the PCAC mass (2.24) vanish and to reach maximal twist. This has to be done for each set of $(\beta, \mu, \mu_\sigma, \mu_\delta)$ parameters.

The following remarks are in order.

A careful theoritical study of maximally twisted fermions show that the criterium (2.27) is not unique and suffers from $\mathcal{O}(a)$ ambiguities. A detailed discussion of this particular fact can be found in [46–48] .

In practice we will follow two different strategies depending on the N_f value. In the $N_f = 2$ case, m_0 is tuned to maximal twist only for the lightest quark mass μ. In the $N_f = 2 + 1 + 1$ case, the PCAC mass is tuned to zero for each value of μ. This choice is more expensive from a numerical point of view.

It is worth noticing that m_0 together with the Wilson term are responsible for an isospin and parity breaking in the physical basis. This fact has important consequences at finite lattice spacing. For instance, the splitting of the π^0 and $\pi^{\pm}$, which decreases with a, appears to be large, although difficult to estimate precisely, in the current numerical simulations. A careful theoritical study using the Symanzik expansion shows that this artefact is anomalously large in the pion sector. A special effort has been devoted all along this work to study empirically the isospin breaking in the computation of baryonic masses as we will see in chapter 6 and 7.

2.2.3 Symanzik expansion - $\mathcal{O}(a)$ improvement

The Symanzik expansion, is a powerful theoritical tool to analyze the cutoff dependence in lattice QFT. It has been proved that the cutoff effects can be modeled by writting the effective discrete action on the form :

$$S_{\text{eff}} = S_0 + aS_1 + a^2 S_2 + \dots, \tag{2.28}$$

where S_0 is the continuum action :

$$S_0 = \int \mathrm{d}^4 x \overline{\chi}(\not{\mathcal{D}} + i\mu\gamma_5\tau^3)\chi, \tag{2.29}$$

and $S_k = \int \mathrm{d}x^4 \mathcal{L}_k$ are corrective terms that describe the finite lattice spacing effects. Dimensional analysis shows that S_k has a mass dimension k or equivalently that the Lagrangians $\mathcal{L}_k$ has a dimension $4 + k$. Following the well known rule of Weinberg which states that $\mathcal{L}_k$ is obtained by listing exhaustively all the composite local operators of dimension $4 + k$ that are authorized by the lattice symmetries. It can be shown in particular that S_1 reduces to a unique term:

$$S_1 = \int \mathrm{d}^4 x \; c_{\text{SW}} \overline{\chi} \frac{i}{4} \sigma_{\mu\nu} F_{\mu\nu} \chi \tag{2.30}$$

The action is however not the only source of lattice artefacts. In order to consistently describe the cutoff effects we have to expand the operator of interest as :

$$\mathcal{O}_{\text{eff}}[\psi, \overline{\psi}] = \mathcal{O}_0[\psi, \overline{\psi}] + a\delta\mathcal{O}[\psi, \overline{\psi}] + \dots \tag{2.31}$$

Here $\mathcal{O}_0$ is the continuum operator and $\mathcal{O}_1$ is a linear combination of local fields.

The Green's function on the lattice, can then be expressed as an expansion in terms of continuum expectation values:

$$\langle \mathcal{O}_{\text{eff}}[\psi, \overline{\psi}] \rangle = \langle \mathcal{O}_0[\psi, \overline{\psi}] \rangle^{\text{cont}} - a \int \mathrm{d}^4 y \; \langle \mathcal{O}_0 \mathcal{L}_1 \rangle^{\text{cont}} + a \langle \delta\mathcal{O} \rangle^{\text{cont}} + \mathcal{O}(a^2) \tag{2.32}$$

Defining the $\mathcal{R}_5$ transformation to be

$$\chi \to i\gamma_5\tau^1\chi, \quad \overline{\chi} \to i\gamma_5\tau^1 \tag{2.33}$$

one can show that S_0 and S_1 transform under $\mathcal{R}_5$ as:

$$S_0 \to S_0, \quad S_1 \to -S_1 \tag{2.34}$$

Equivalently, given an operator $\mathcal{O}$ with a definite $\mathcal{R}_5$ parity, one can show that $\delta\mathcal{O}$ has the opposite $\mathcal{R}_5$ parity. This statement can be summarize by :

$$\mathcal{O} \to \pm\mathcal{O}, \quad \delta\mathcal{O} \to \mp\delta\mathcal{O} \tag{2.35}$$

Since in the physical basis and in the continuum, $\mathcal{R}_5$ is a an exact symmetry that interchanges the two flavours, all observables are even under this transformation. Thus all continuum expectation values odd under $\mathcal{R}_5$ are exactly zero. Therefore if $\mathcal{O}$ is an $\mathcal{R}_5$ even operator one obtains that

$$\langle \mathcal{O}_{\text{eff}}[\psi, \overline{\psi}] \rangle = \langle \mathcal{O}_0[\psi, \overline{\psi}] \rangle^{\text{cont}} + \mathcal{O}(a^2) \tag{2.36}$$

and if $\mathcal{O}$ is $\mathcal{R}_5$ odd :

$$\langle \mathcal{O}_{\text{eff}}[\psi, \overline{\psi}] \rangle = -a \int \mathrm{d}^4 y \ \langle \mathcal{O}_0 \mathcal{L}_1 \rangle^{\text{cont}} + a \langle \delta\mathcal{O} \rangle^{\text{cont}} + \mathcal{O}(a^2) \tag{2.37}$$

We conclude that, in the mtmQCD case, all physical observables are automaticly $\mathcal{O}(a)$ improved. This fundamental property of maximally twisted mass fermions allows to have better scaling properties than in the Wilson regularization. This formulation is thus a way to realize the improvement of the Wilson regularization for all the physical observables avoiding the delicate task of improving the action and each operator.

Chapter 3

Spectroscopy in Lattice QCD

Contents

Reproducing the experimentally observed spectrum of hadronic particles is one of the strongest tests that QCD is the correct theory to describe energy at low energy. The first works on QCD spectroscopy using lattice QCD go back to the very beginning of lattice simulations. The first quenched studies were performed in 1981-1982 in [49–53].

First we derive the fact that the exponential decay of hadronic correlation functions is related to hadron masses. Then we explains how to build the baryonic interpolating field and derive a general formula that allow to evaluate any two-point baryonic function as a function of the invert Dirac operator. We show in 3.4 how the overlap of creation and annihilation operators with the ground state of the hadron can be improved by using extended source and sink operators. Sections 3.5 and 3.6 we discuss the technical issues related to the analysis and to the error estimation of the lattice results. Finally we introduce the σ-term that controls the dependence of the hadron masses as a function of the quark masses.

3.1 Spectral representation of 2-point correlation functions

In this section we will explain how to extract physical quantities, like masses, from two-point functions, in a generic case, as well as the main sources of statistical and systematical uncertainties.

We will assume that the Hilbert space of states of QCD is well defined and we will choose a basis of eigenstates of the full interacting Hamiltonian, H. Since the momentum operator $\vec{P}$ commutes with H, the theory is invariant under translation, we can diagonalize them simultaneously, and denote the common eigenstates by $\{|n, \vec{q}\rangle\}$. Because this is a fundamental point in lattice QCD it is important to define clearly the completness relation :

$$\mathbf{1} = \sum_n \int \frac{\mathrm{d}^3\vec{q}}{(2\pi)^3 2E_n(\vec{q})} |n, \vec{q}\rangle\langle n, \vec{q}| \tag{3.1}$$

the integration is over all the total three momenta that can have the state n, which can be a multiparticle states. It immediatly lead to the question of *unstable particles* or *resonances* which by definition never appear in asymptotic states.

We have already seen in Eq. (1.19) that in the infinite time extension limit, the correlation functions are the vaccuum expectation value of a $\mathcal{T}$-product of operator. However since we are interested in working in finite volume with periodic boundary conditions, one can show that:

$$\langle \mathcal{O}[\mathcal{A}, \psi, \overline{\psi}]\rangle = \frac{\mathrm{Tr}\Big[\mathcal{T}\ \mathrm{e}^{-\mathrm{iHT}}\hat{\mathcal{O}}[\mathcal{A}, \psi, \overline{\psi}]\Big]}{\mathrm{Tr}\Big[\mathcal{T}\ \mathrm{e}^{-\mathrm{iHT}}\Big]} \tag{3.2}$$

where the trace is over all the Hilbert space of states, H is the Hamiltonian and T is time extent of the lattice.

Consider the following euclidean two-point function :

$$C(t, \vec{p}) = \sum_{\vec{x}} e^{ipx} \langle J_1(x) J_2^\dagger(0)\rangle \tag{3.3}$$

where J_1 and J_2 are for concretness two mesonic color singlet operators, and $x = (t, \vec{x})$is a space-time coordinate. J_1 and J_2 are called *interpolating fields* for reasons that will become clear in a few lines.

Note that in Minkowski space this operator belongs to an irreducible representation of the Lorentz group and can thus be written in terms of the translation operator P_μ as

$$J_1(x) = e^{iPx} J_1(0) e^{-iPx} \tag{3.4}$$

Expliciting the trace in Eq. (3.2), and insterting the complete set of states defined previously, we get :

$$\langle J_1(x)J_2^\dagger(0)\rangle = \frac{\sum_{n,\vec{q}_n;m,\vec{p}_m} e^{-iE_n(\vec{q}_n)T}e^{-i(q_n-p_m)x}\langle n,\vec{q}_n|\hat{J}_1(0)|m,\vec{p}_m\rangle\langle m,\vec{p}_m|\hat{J}_2^\dagger(0)|n,\vec{q}_n\rangle}{\sum_{n,\vec{q}_n} e^{-iE_nT}} \tag{3.5}$$

where p_n and q_n are 4-momenta satisfying :

$$p_n = \begin{pmatrix} E_n(\vec{p}_n) \\ \vec{p}_n \end{pmatrix}, \quad q_n = \begin{pmatrix} E_n(\vec{q}_n) \\ \vec{q}_n \end{pmatrix} \tag{3.6}$$

Performing the Wick rotation, we get in Euclidean space and for large T and τ :

$$C(\tau,\vec{p}) \xrightarrow{T,\tau\to\infty} \frac{e^{-E_1(\vec{p})\tau}}{2E_1(\vec{p})} Z_1 Z_2^\dagger + \frac{e^{-E_1(\vec{p})(T-\tau)}}{2E_1(\vec{p})} Z_1^\dagger Z_2 \tag{3.7}$$

with

$$\begin{aligned} Z_1 &= \langle 0|J_1(0)|1,\vec{p}\rangle \\ Z_2 &= \langle 0|J_2(0)|1,\vec{p}\rangle \end{aligned} \tag{3.8}$$

Note that the energy E_0 of the vaccuum state $|0\rangle$ drops out and can thus be assume to vanish. E_1 is the state of the lowest energy. At finite time subdominant contributions appears but on a finite lattice they are exponentially suppressed, since the energy spectrum is discrete.

In the special case of $J_2 = J_1$, the coefficient in front of the forward moving and backward moving state becomes equal and real and Eq. (3.7) becomes:

$$C(\tau,\vec{p}) \xrightarrow{T,\tau\to\infty} \frac{2|Z_1|^2 e^{-\frac{T}{2}E_1(\vec{p})}}{2E_1(\vec{p})} \cosh\Big[E_1(\vec{p})\Big(\frac{T}{2}-\tau\Big)\Big] \tag{3.9}$$

This is the general rule: two-point correlation functions are dominated for large time by the smallest mass of states which have a non vanishing overlap with the two operators J_1 and J_2.

The natural question to answer now is how to construct operators that have a maximal overlap with the baryonic states that we are interested in.

3.2 Baryonic correlators

In order to specify the most general interpolating field which have an overlap with a given member of the octet and decuplet, we have to find the most general operator which belongs to an isospin multiplet with a given I^2 and I_z, a given strangeness S and a given spin s.

To fix ideas, we give in tables 3.2 and 3.3 an exhaustive list of the quantum numbers of the members of the baryon octet and decuplet. Then we construct the interpolating field, studying the transformation under Lorentz and isospin symmetry.

3.2.1 Interpolating fields

As mentionned in section 1.1.2, the baryon interpolating field has to transform under the representation $\mathbf{3}\otimes\mathbf{3}\otimes\mathbf{3}$ of $\mathrm{SU}(3)_\mathrm{f}$. It must have the general following form:

$$\mathcal{O}_{\mathrm{ABC}}^{abc,ijk} = \psi_{\mathrm{A}}^{a,i}\psi_{\mathrm{B}}^{b,j}\psi_{\mathrm{C}}^{c,k} \tag{3.10}$$

where $a, b, c = 1, 2, 3$ are the color indices, $i, j, k = 1, 2, 3, 4$ are the spinor indices and $A, B, C = u, d, s$ are the flavour indice. Because the state has to be a singlet under $\mathrm{SU(3)_c}$ transformation, the only way to construct a such object is to contract the operator with the completly antisymmetric tensor of Levi-Civita :

$$\mathcal{O}^{ijk}_{\mathrm{ABC}} = \epsilon^{abc} \psi^{a,i}_{\mathrm{A}} \psi^{b,j}_{\mathrm{B}} \psi^{c,k}_{\mathrm{C}} \tag{3.11}$$

We have listed in 3.1 the possible isospin states of the three quarks depending of their strangeness $S = 0, -1, -2$.

S	Isospin content
0	$\mathbf{\frac{1}{2}} \oplus \mathbf{\frac{1}{2}} \oplus \mathbf{\frac{3}{2}}$
-1	$\mathbf{0} \oplus \mathbf{1}$
-2	$\mathbf{\frac{1}{2}}$
-3	$\mathbf{0}$

Table 3.1: Isospin content of the possible three quark states for different values of S

Concerning the Lorentz transformation of O_{ABC} the most general way to construct a baryonic interpolating field with defined quantum numbers (S,J,I) is to contract the first pair of quark fields, and couple the resulting intermediate state to the third quark. The general spin structure is:

$$O^{\Gamma\Lambda}_{\mathrm{ABC}} = \epsilon^{abc} \left(\psi^{Ta}_{\mathrm{A}} C\Gamma \psi^{b}_{\mathrm{B}}\right) \Lambda \psi^{c}_{\mathrm{C}} \tag{3.12}$$

where Γ and Λ stands for an arbitrary Dirac matrices in the set $\{1, \gamma_5, \gamma_\mu, \gamma_5\gamma_\mu, \sigma_{\mu\nu}\}$ and the charge conjugation $C = i\gamma_0\gamma_2$ matrice has been explicitly factorized for convenience. The relevant properties of C can be found in Appendix A.1. Notice that the Dirac indices of the intermediate state $\left(\psi^{Ta}_{\mathrm{A}} C\Gamma \psi^{b}_{\mathrm{B}}\right)$ are implictly summed and the spinor indices of the baryon interpolating field is carried by $\Lambda\psi^{c}_{C}$.

The interest of factorizing C in eq. 3.12 becomes clear considering the behaviour of the interpolating field under a Lorentz transform Λ. A Dirac spinor belonging to the representations $(\frac{1}{2}, \frac{1}{2})$ transform as :

$$\psi(x) \to \Lambda_{\frac{1}{2}} \psi(\Lambda^{-1}x), \quad \overline{\psi} \longleftarrow \overline{\psi}\Lambda^{-1}_{\frac{1}{2}}, \quad \Lambda_{\frac{1}{2}} = e^{-\frac{i}{4}\omega_{\mu\nu}\sigma^{\mu\nu}} \tag{3.13}$$

where $\sigma^{\mu\nu} = \frac{i}{2}[\gamma^\mu, \gamma^\nu]$ and $\omega_{\mu\nu}$ are the parameters of the transformation. Using the property

$$\Lambda^{-1}_{\frac{1}{2}} \gamma^\mu \Lambda_{\frac{1}{2}} = \Lambda^\mu_\nu \gamma^\nu \tag{3.14}$$

it is straightforward to show that

$$\psi^T \longleftarrow \psi^T \Lambda^T_{\frac{1}{2}} \tag{3.15}$$

and to obtain:

$$\Lambda^T_{\frac{1}{2}} = C\Lambda^{-1}_{\frac{1}{2}} \tag{3.16}$$

This give us to find the transformation law of $O^{\Gamma\Lambda}_{\mathrm{ABC}}$ which reads:

$$O^{\Gamma\Lambda}_{\mathrm{ABC}} \to \epsilon^{abc} \left(\psi^{Ta}_{\mathrm{A}} C\Lambda^{-1}_{\frac{1}{2}} \Gamma \Lambda_{\frac{1}{2}} \psi^{b}_{\mathrm{B}}\right) \Lambda\Lambda_{\frac{1}{2}} \psi^{c}_{\mathrm{C}} \tag{3.17}$$

One can see from this equation that $\psi^T C\Gamma\psi$ transforms as $\overline{\psi}\Gamma\psi$, which has well known transformation properties.

Strangeness	Baryon	Interpolating field	I	I_z
$S=0$	p	$\chi^p = \epsilon_{abc}(u_a^T C\gamma_5 d_b)u_c$	$1/2$	$+1/2$
	n	$\chi^n = \epsilon_{abc}(d_a^T C\gamma_5 u_b)d_c$	$1/2$	$-1/2$
$S=1$	Λ	$\chi^{\Lambda^8} = \frac{1}{\sqrt{6}}\epsilon_{abc}\{2(u_a^T C\gamma_5 d_b)s_c + (u_a^T C\gamma_5 s_b)d_c - (d_a^T C\gamma_5 s_b)u_c\}$	0	0
	Σ^+	$\chi^{\Sigma^+} = \epsilon_{abc}(u_a^T C\gamma_5 s_b)u_c$	1	$+1$
	Σ^0	$\chi^{\Sigma^0} = \frac{1}{\sqrt{2}}\epsilon_{abc}\{(u_a^T C\gamma_5 s_b)d_c + (d_a^T C\gamma_5 s_b)u_c\}$	1	$+0$
	Σ^-	$\chi^{\Sigma^-} = \epsilon_{abc}(d_a^T C\gamma_5 s_b)d_c$	1	-1
$S=2$	Ξ^0	$\chi^{\Xi^0} = \epsilon_{abc}(s_a^T C\gamma_5 u_b)s_c$	$1/2$	$+1/2$
	Ξ^-	$\chi^{\Xi^-} = \epsilon_{abc}(s_a^T C\gamma_5 d_b)s_c$	$1/2$	$-1/2$

Table 3.2: Interpolating fields and quantum numbers for the baryons in the octet representation.

Strangeness	Baryon	Interpolating field	I	I_z
$S=0$	Δ^{++}	$\chi_\mu^{\Delta^{++}} = \epsilon_{abc}(u_a^T C\gamma_\mu u_b)u_c$	$3/2$	$+3/2$
	Δ^+	$\chi_\mu^{\Delta^+} = \frac{1}{\sqrt{3}}\epsilon_{abc}\{2(u_a^T C\gamma_\mu d_b)u_c + (u_a^T C\gamma_\mu u_b)d_c\}$	$3/2$	$+1/2$
	Δ^0	$\chi_\mu^{\Delta^0} = \frac{1}{\sqrt{3}}\epsilon_{abc}\{2(d_a^T C\gamma_\mu u_b)d_c + (d_a^T C\gamma_\mu d_b)u_c\}$	$3/2$	$-1/2$
	Δ^-	$\chi_\mu^{\Delta^-} = \epsilon_{abc}(d_a^T C\gamma_\mu d_b)d_c$	$3/2$	$-3/2$
$S=1$	Σ^{*+}	$\chi_\mu^{\Sigma^{*+}} = \sqrt{\frac{2}{3}}\epsilon^{abc}\{(u^{Ta}C\gamma_\mu u^b)s^c + (u^{Ta}C\gamma_\mu s^b)u^c + (s^{Ta}C\gamma_\mu u^b)u^c\}$	1	$+1$
	Σ^{*0}	$\chi_\mu^{\Sigma^{*0}} = \sqrt{\frac{2}{3}}\epsilon^{abc}\{(u^{Ta}C\gamma_\mu d^b)s^c + (d^{Ta}C\gamma_\mu s^b)u^c + (s^{Ta}C\gamma_\mu u^b)d^c\}$	1	$+0$
	Σ^{*-}	$\chi_\mu^{\Sigma^{*-}} = \sqrt{\frac{2}{3}}\epsilon^{abc}\{(d^{Ta}C\gamma_\mu d^b)s^c + (d^{Ta}C\gamma_\mu s^b)d^c + (s^{Ta}C\gamma_\mu d^b)d^c\}$	1	-1
$S=2$	Ξ^{*0}	$\chi_\mu^{\Xi^{*0}} = \epsilon_{abc}(s_a^T C\gamma_\mu u_b)s_c$	$1/2$	$+1/2$
	Ξ^{*-}	$\chi_\mu^{\Xi^{*-}} = \epsilon_{abc}(s_a^T C\gamma_\mu d_b)s_c$	$1/2$	$-1/2$
$S=3$	Ω^-	$\chi_\mu^{\Omega^-} = \epsilon_{abc}(s_a^T C\gamma_\mu s_b)s_c$	0	$+0$

Table 3.3: Interpolating fields and quantum numbers for baryons in the decuplet representation.

The usual interpolating fields for the baryon octet and decuplet are listed in Table 3.2 and 3.3. They have been used in other works as for instance in [54–56].

It is worth noticing that this choice is not unique. For instance, in the nucleon case, it is also possible to consider the following interpolating field:

$$\chi_2^p = \epsilon^{abc}(u_a^T C d_b)\gamma_5 u_c \tag{3.18}$$

or some linear combination of them [57–59]. A systematic study of the various interpolating field should allow to improve mass determination.

The basic object to consider is thus the baryon two-point functions,

$$C(t,\vec{p}) = \sum_{\vec{x}} e^{ipx}\langle O_{\mathrm{ABC}}^{\Gamma\Lambda}(x)\bar{O}_{\mathrm{ABC}}^{\Gamma\Lambda}(0)\rangle \tag{3.19}$$

which generalizes the mesonic case Eq. (3.7).

In the case of twisted mass QCD, one has to evaluate this correlator in the physical base defined in Chapter 2 Eq. (2.6). The interpolating fields given in Tables 3.2 and 3.3 do not have a defined parity. One can project on physical states by means of the projector on positive or negative parity:

$$P^{\pm} = \frac{1 \pm \gamma_0}{2} \tag{3.20}$$

the projected correlators are denoted by

$$C^{\pm}(t, \vec{p}) = \mathrm{Tr}\left\{P^{\pm} C(t, \vec{p})\right\}. \tag{3.21}$$

They are dominated for large Euclidean time by the ground state energy of a particle which has the quantum numbers of $O^{\Gamma\Lambda}$ and a three momentum $\vec{p}$.

3.3 Evaluation of correlators

The basic ingredient we need to compute correlators is the quark propagator for a given background gauge field defined by

$$\sum_z \mathcal{D}_{\mathrm{A}}^{ab,rs}(x,z)\mathcal{S}_{\mathrm{A}}^{bc,st}[U](z,y) = \delta^4(x-y)\delta^{ac}\delta^{rt} \tag{3.22}$$

where $\mathcal{D}_{\mathrm{A}}$ is the Dirac operator of quark of flavour A, b, c are colour indices, and s, t are spinor indices.

In the twisted mass case the Dirac operator depends of the flavour index A so we have to do one inversion for each flavour (contrary to the pure Wilson case) .

Wick's Theorem allows to perform the integration on fermion field and express any correlation functions as an average over the gauge ensemble in terms of quark propagators on a fixed background. The goal of this section is to obtain an explicit form of the general two-point correlator.

3.3.1 Mesons two-point functions

Let us consider the mesonic two-point function of two interpolating fields of the form:

$$J^1 = \bar{\psi}_{\mathrm{A}}\Gamma^1\psi_{\mathrm{B}}, \quad J^2 = \bar{\psi}_{\mathrm{A}}\Gamma^2\psi_{\mathrm{B}} \tag{3.23}$$

where the tensorial indices of Dirac matrices are implicit.

The straightforward application of Wick's theorem gives

$$\langle J^1(x)J^{2\dagger}(0)\rangle = \langle \delta_{\mathrm{AB}}\mathrm{Tr}\left\{S_{\mathrm{A}}^{rr}(0,0)\Gamma^1\right\}\mathrm{Tr}\left\{S_{\mathrm{A}}^{ss}(x,x)\tilde{\Gamma}^2\right\} - \mathrm{Tr}\left\{S_{\mathrm{B}}^{rs}(0,x)\tilde{\Gamma}^2 S_{\mathrm{A}}^{sr}(x,0)\Gamma^1\right\}\rangle \tag{3.24}$$

with

$$\tilde{\Gamma}^2 = \gamma_0\Gamma^{2\dagger}\gamma_0 \tag{3.25}$$

Note that for twisted mass fermions, we have

$$S_{\mathrm{A}}(0,x) = \gamma_5 S_{\tilde{\mathrm{A}}}^{\dagger}(x,0)\gamma_5 \tag{3.26}$$

where $\tilde{A}$ is the flavour index partner of flavour A in the twisted mass doublet. One has for instance,

$$S_u(0,x) = \gamma_5 S_d^{\dagger}(x,0)\gamma_5 \tag{3.27}$$

Equation 3.24 becomes thus:

$$\begin{aligned}\langle 0|J^1(x)J^{2\dagger}(0)|0\rangle =&\langle \delta_{\mathrm{AB}}\mathrm{Tr}\left\{S^{rr}_{\mathrm{A}}(0,0)\Gamma^1\right\}\mathrm{Tr}\left\{S^{ss}_{\mathrm{A}}(x,x)\tilde{\Gamma}^2\right\}\\ &-\mathrm{Tr}\left\{\gamma_5 S^{\dagger rs}_{\tilde{\mathrm{B}}}(x,0)\gamma_5\tilde{\Gamma}^2 S^{sr}_{\mathrm{A}}(x,0)\Gamma^1\right\}\rangle\end{aligned} \tag{3.28}$$

The evaluation of disconnected contributions requires to compute the propagator $S^{ss}_{\mathrm{A}}(x,x)$. As we will see at the end of Chapter 4, evaluation of such diagrams is extremely noisy and responsible for large statistical errors.

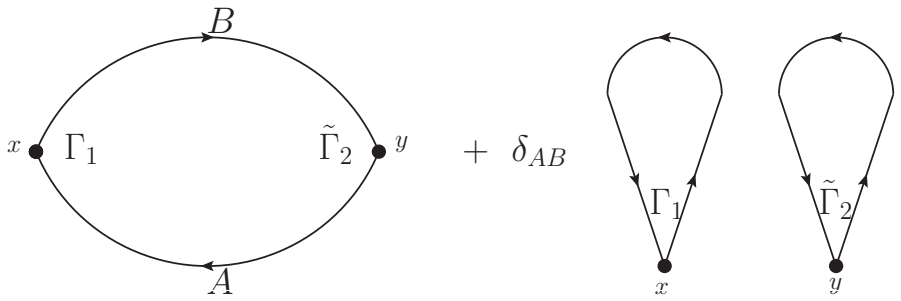

Figure 3.1: Contraction of a general mesonic correlation function.

3.3.2 Baryons

Let us now consider the contractions for a baryonic two-point function with interpolating fields of the general form:

$$J_{\mu\nu} = \epsilon^{abc}\sum_i \lambda_i\left(\psi^{aT}_{\tilde{A}_i}\Gamma^i_\mu\psi^b_{\tilde{B}_i}\right)\Lambda^i_\nu\psi^c_{\tilde{C}_i},\quad \bar{J}_{\mu\nu} = -\epsilon^{abc}\sum_i \lambda^*_i\bar{\psi}^a_{\tilde{C}_i}\tilde{\Lambda}^i_\nu\left(\bar{\psi}^b_{\tilde{B}_i}\tilde{\Gamma}^i_\mu\bar{\psi}^{cT}_{\tilde{A}_i}\right) \tag{3.29}$$

where:

$$\begin{cases}\tilde{\Lambda}^i_\nu = \gamma_0\Lambda^{i\dagger}_\nu\gamma_0\\ \tilde{\Gamma}^i_\mu = \gamma_0\Gamma^{i\dagger}_\mu\gamma_0\end{cases} \tag{3.30}$$

As for the mesonic correlator we can work out the Wick contractions and obtain :

$$\begin{aligned}\langle J_{\mu\nu}(x)\bar{J}_{\rho\sigma}(0)\rangle = \Bigg\langle \sum_{i,j}\epsilon^{abc}\epsilon^{a'b'c'}\lambda_i\lambda^*_j\Lambda^i_\nu\Big\{&\delta_{\tilde{\mathrm{A}}_\mathrm{i}\tilde{\mathrm{C}}_\mathrm{j}}\Big[\delta_{\tilde{\mathrm{B}}_\mathrm{i}\tilde{\mathrm{B}}_\mathrm{j}}\delta_{\tilde{\mathrm{C}}_\mathrm{i}\tilde{\mathrm{A}}_\mathrm{j}}\mathcal{S}^{cc'}_{\tilde{\mathrm{C}}_\mathrm{i}}\left(\Gamma^i_\mu\mathcal{S}^{bb'}_{\tilde{\mathrm{B}}_\mathrm{i}}\tilde{\Gamma}^j_\rho\right)^T\Big)^T\\ &-\delta_{\tilde{\mathrm{A}}_\mathrm{j}\tilde{\mathrm{B}}_\mathrm{i}}\delta_{\tilde{\mathrm{C}}_\mathrm{i}\tilde{\mathrm{B}}_\mathrm{j}}\mathcal{S}^{cb'}_{\tilde{\mathrm{C}}_\mathrm{i}}\left(\Gamma^i_\mu\mathcal{S}^{bc'}_{\tilde{\mathrm{B}}_\mathrm{i}}\tilde{\Gamma}^{jT}_\rho\right]\mathcal{S}^{aa'}_{\tilde{\mathrm{A}}_\mathrm{i}}\\ &+\delta_{\tilde{\mathrm{A}}_\mathrm{i}\tilde{\mathrm{B}}_\mathrm{j}}\Big[\mathcal{S}^{ca'}_{\tilde{\mathrm{C}}_\mathrm{i}}\delta_{\tilde{\mathrm{B}}_\mathrm{i}\tilde{\mathrm{A}}_\mathrm{j}}\delta_{\tilde{\mathrm{C}}_\mathrm{i}\tilde{\mathrm{C}}_\mathrm{j}}\mathrm{Tr}\left\{\mathcal{S}^{ab'}_{\tilde{\mathrm{A}}_\mathrm{i}}\left(\Gamma^i_\mu\mathcal{S}^{bc'}_{\tilde{\mathrm{B}}_\mathrm{i}}\tilde{\Gamma}^{jT}_\rho\right)^T\right\}\\ &-\delta_{\tilde{\mathrm{B}}_\mathrm{i}\tilde{\mathrm{C}}_\mathrm{j}}\delta_{\tilde{\mathrm{C}}_\mathrm{i}\tilde{\mathrm{A}}_\mathrm{j}}\mathcal{S}^{cc'}_{\tilde{\mathrm{C}}_\mathrm{i}}\left(\Gamma^{iT}_\mu\mathcal{S}^{ab'}_{\tilde{\mathrm{A}}_\mathrm{i}}\tilde{\Gamma}^j_\rho\right)^T\mathcal{S}^{ba'}_{\tilde{\mathrm{B}}_\mathrm{i}}\Big]\\ &+\delta_{\tilde{\mathrm{A}}_\mathrm{i}\tilde{\mathrm{A}}_\mathrm{j}}\Big[\delta_{\tilde{\mathrm{B}}_\mathrm{i}\tilde{\mathrm{C}}_\mathrm{j}}\delta_{\tilde{\mathrm{C}}_\mathrm{i}\tilde{\mathrm{B}}_\mathrm{j}}\mathcal{S}^{cb'}_{\tilde{\mathrm{C}}_\mathrm{i}}\left(\Gamma^{iT}_\mu\mathcal{S}^{ac'}_{\tilde{\mathrm{A}}_\mathrm{i}}\tilde{\Gamma}^{jT}_\rho\right)^T\mathcal{S}^{ba'}_{\tilde{\mathrm{B}}_\mathrm{i}}\\ &-\delta_{\tilde{\mathrm{B}}_\mathrm{i}\tilde{\mathrm{B}}_\mathrm{j}}\delta_{\tilde{\mathrm{C}}_\mathrm{i}\tilde{\mathrm{C}}_\mathrm{j}}\mathcal{S}^{ca'}_{\tilde{\mathrm{C}}_\mathrm{i}}\mathrm{Tr}\left\{\mathcal{S}^{ac'}_{\tilde{\mathrm{A}}_\mathrm{i}}\left(\Gamma^i_\mu\mathcal{S}^{bb'}_{\tilde{\mathrm{B}}_\mathrm{i}}\tilde{\Gamma}^j_\rho\right)^T\right\}\Big]\Big\}\tilde{\Lambda}^j_\sigma\Bigg\rangle\end{aligned} \tag{3.31}$$

Some comments are in order:

- The matrices Λ and $\tilde{\Lambda}$ do not play any role in the contractions. They are simply factorized out to the left and right
- Contrary to the meson case, there are no disconnected terms nor changes of flavour in the propagators.

3.3.3 Some particular cases.

We now treat some special interesting cases of two-point function, writting them explictly in terms of the quark propagators and structure Dirac matrices Γ and Λ. We will show that the particular form of the latter allows for substantial simplifications.

Let us begin with the nucleon correlators which will be the building blocks of of the analysis in this work.

Nucleon

A direct application of the formula Eq. (3.31) to the nucleon interpolating field given in Table 3.2 gives:

$$\langle \chi^p(x)\bar{\chi}^p(0)\rangle = -\epsilon^{abc}\epsilon^{a'b'c'}\left\langle \left\{ \mathcal{S}_u^{cc'}\left(\Gamma_\mu \mathcal{S}_d^{bb'}\tilde{\Gamma}_\mu\right)^T \mathcal{S}_u^{aa'} - \mathcal{S}_u^{ca'}\mathrm{Tr}\left\{\mathcal{S}_u^{ac'}\left(\Gamma_\mu \mathcal{S}_d^{bb'}\tilde{\Gamma}_\mu\right)^T\right\}\right\}\right\rangle \quad (3.32)$$

with $\Gamma = C\gamma_5 = -\tilde{\Gamma}$. The two terms are reprensented graphically in Fig. 3.2. The gray blob reprensent the structure $\psi^T\Gamma\psi$. When the contractions involve only these parts of the interpolating field, a trace appears in the contraction. The term containing the trace is thus depicted by the first diagram.

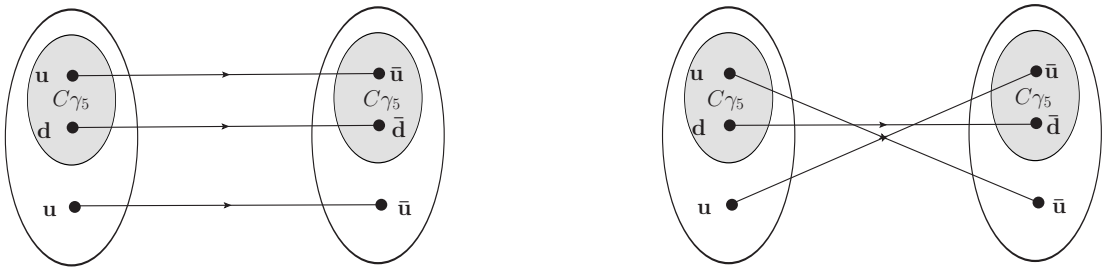

Figure 3.2: Contraction of the two-point nucleon correlation function.

Delta

In that case we have

$$\Gamma_\mu = C\gamma_\mu \quad (3.33)$$

Using that $C\gamma_\mu C^{-1} = -\gamma_\mu^T$, it is straightforward to show the relation

$$\Gamma_\mu^T = \Gamma_\mu, \quad \tilde{\Gamma}_\mu^T = \tilde{\Gamma}_\mu \quad (3.34)$$

The formula Eq. (3.31) then gives :

$$\langle \chi_\mu^{\Delta^{++}}(x)\bar{\chi}_\mu^{\Delta^{++}}(0)\rangle = -2\epsilon^{abc}\epsilon^{a'b'c'}\left\langle \Big\{ -2\mathcal{S}^{cc'}\left(\Gamma_\mu \mathcal{S}^{bb'}\tilde{\Gamma}_\mu\right)^T\mathcal{S}^{aa'} + \mathcal{S}^{ca'}\mathrm{Tr}\left\{\mathcal{S}^{ac'}\left(\Gamma_\mu\mathcal{S}^{bb'}\tilde{\Gamma}_\mu\right)^T\right\}\Big\}\right\rangle \tag{3.35}$$

It is an interesting point to compare it to the two-point function of the Δ^+ since in the continuum limit, the two correlators should be stricly equal. We get, using Eq. (3.31) that

$$\begin{aligned}\langle \chi_\mu^{\Delta^{+}}(x)\bar{\chi}_\nu^{\Delta^{+}}(0)\rangle = -\frac{2}{3}\epsilon^{abc}\epsilon^{a'b'c'}\Big\langle &\Big\{2\mathcal{S}_{\tilde{u}}^{ca'}\mathrm{Tr}\left\{\mathcal{S}_{\tilde{u}}^{ac'}\tilde{\Gamma}_\nu\mathcal{S}_d^{Tbb'}\Gamma_\mu\right\} - 2\mathcal{S}_u^{cc'}\tilde{\Gamma}_\nu\mathcal{S}_d^{Tbb'}\Gamma_\mu\mathcal{S}_u^{aa'}\\ &+\mathcal{S}_u^{cc'}\tilde{\Gamma}_\nu\mathcal{S}_u^{Tab'}\Gamma_\mu\mathcal{S}_d^{ba'} - \mathcal{S}_u^{cb'}\tilde{\Gamma}_\nu\mathcal{S}_u^{Tac'}\Gamma_\mu\mathcal{S}_d^{ba'}\\ &+\mathcal{S}_d^{cb'}\tilde{\Gamma}_\nu\mathcal{S}_u^{Tbc'}\Gamma_\mu\mathcal{S}_u^{aa'} - \mathcal{S}_d^{cb'}\tilde{\Gamma}_\nu\mathcal{S}_u^{Tac'}\Gamma_\mu\mathcal{S}_u^{ba'}\\ &+\mathcal{S}_{\tilde{d}}^{ca'}\mathrm{Tr}\left\{\mathcal{S}_{\tilde{u}}^{ac'}\tilde{\Gamma}_\nu\mathcal{S}_u^{Tbb'}\Gamma_\mu\right\}\Big\}\Big\rangle\end{aligned} \tag{3.36}$$

Now in the continuum limit $S_u = S_d = S$, and we obtain the following expression :

$$\langle \chi_\mu^{\Delta^{+}}(x)\bar{\chi}_\nu^{\Delta^{+}}(0)\rangle = -2\epsilon^{abc}\epsilon^{a'b'c'}\left\langle \left\{S^{ca'}\mathrm{Tr}\left\{S^{ac'}\tilde{\Gamma}_\nu S^{Tbb'}\Gamma_\mu\right\} - 2S^{cc'}\tilde{\Gamma}_\nu S^{Tbb'}\Gamma_\mu S^{aa'}\right\}\right\rangle \tag{3.37}$$

We find that in the continuum, the two-point functions of the Δ^{++} and of the Δ^+ are degenerate, as expected. Note that at finite lattice spacing the expression of the two-point functions in terms of the quark propagators differs. The difference between the two-point functions is an $\mathcal{O}(a^2)$ effect due to the breaking of the isospin symmetry by the twisted fermions.

3.4 Extended source and sink operators

In order to improve the overlap between the hadronic interpolating field and the desired state, one can make use of extended quark fields. To implement this in practice we use the so-called *smearing* techniques. The idea is to build a non local interpolating field, which has defined quantum numbers and preserves gauge invariance. To this aim, one builds an effective extended quark field iteratively, in the following way:

$$\tilde{\psi}^{(1)}(\vec{x},t)_a^r = \sum_{\vec{y}} F(\vec{x},\vec{y},t)^{rs}\psi(\vec{y},t)_a^s \tag{3.38}$$

where

$$F(\vec{x},\vec{y},t)^{rs} = \frac{1}{1+6\alpha}\Big(\delta^{rs}\delta(\vec{x}-\vec{y}) + \alpha H(\vec{x},\vec{y},t)^{rs}\Big) \tag{3.39}$$

with

$$H(\vec{x},\vec{y},t) = \sum_{i=1}^{3}\Big(U_i(\vec{x},t)\delta_{\vec{x},\vec{y}-i} + U_i^\dagger(\vec{x}-i,t)\delta_{\vec{x},\vec{y}+i}\Big) \tag{3.40}$$

This is the Gaussian smearing.

The gauge links entering in F are highly fluctuating quantities. One can smooth them by replacing each gauge link by an average over its neighboors. This procedure can be implemented in various ways. We use here the so-called *3D APE smearing*, which is also defined iteratively. For one iteration we have :

$$U_\mu \longrightarrow \tilde{U}_\mu = \mathcal{P}_{\mathrm{SU}(3)}\Big(U_\mu + \alpha \sum_{\nu\neq\mu\neq 0} S_{\mu,\nu}(x) + S_{\mu,-\nu}(x)\Big) \tag{3.41}$$

Where $S_{\mu,\nu}(x)$ is the forward staple:

$$S_{\mu,\nu}(x) = U_\nu(x)U_\mu(x+\nu)U_\nu^\dagger(x+\mu) \tag{3.42}$$

and $S_{\mu,-\nu}(x)$ is the backward:

$$S_{\mu,-\nu}(x) = U_\nu^\dagger(x-\nu)U_\mu(x-\nu)U_\nu(x-\nu+\mu) \tag{3.43}$$

We average the links only in the spatial directions, i.e $\mu = 1, 2, 3$. $\mathcal{P}_{\mathrm{SU}(3)}$ maps an arbitrary 3×3 matrix to the gauge group SU(3). This "projection" is however not unique.

Our choice consists in two steps. The first step is based on the polar decomposition which states that an arbitrary matrix M can be written in a unique way in the form

$$M = HU \tag{3.44}$$

with H hermitiean and positive definite given by $H^2 = M^\dagger M$ and

$$U = \frac{H}{H^\dagger H} \tag{3.45}$$

unitary. The second step consists in "projecting" U in SU(3) dividing by the third root of its determinant. One finally has:

$$M_{proj} = \mathcal{P}_{\mathrm{SU}(3)}\Big(M\Big) = \frac{U}{\det{}^{1/3}\, U} \tag{3.46}$$

Note that the third root is defined in the complex plane with a branch cut, we choose the first determination which has the minimal Schur norm.

One can show that the Wick contraction obtained with the extended quarks keep the same structure than the one obtained with local field, provided the quark propagator is replaced by an effective quark propagator associated to the extended source. This leads to the following definitions:

$$\begin{aligned}
\overrightarrow{\mathcal{S}}^{\,st}_{ab}(y,z,U(t_z)) =& \langle \psi_a^s(y)\tilde{\bar{\psi}}_b^t(\vec{z},t_z)\rangle \\
\overleftarrow{\mathcal{S}}^{\,st}_{ab}(y,z,U(t_z)) =& \langle \tilde{\psi}_a^s(y)\bar{\psi}_b^t(\vec{z},t_z)\rangle \\
\overleftrightarrow{\mathcal{S}}^{\,st}_{ab}(y,z,U(t_z)) =& \langle \tilde{\psi}_a^s(y)\tilde{\bar{\psi}}_b^t(\vec{z},t_z)\rangle
\end{aligned} \tag{3.47}$$

They are named the smeared-local SL ($\overleftarrow{\mathcal{S}}$), local-smeared LS ($\overrightarrow{\mathcal{S}}$) and the smeared-smeared SS ($\overleftrightarrow{\mathcal{S}}$) propagators. These propagators together with Eq. (3.28) and Eq. (3.31) are the building blocks to compute hadronic correlators with smeared quarks.

We will detail in what follows how to compute them in practice. One can show that the local-smeared propagator is the solution of the equation

$$\sum_y D^{rs}_{ab}(x,y)\overrightarrow{\mathcal{S}}^{\,st}_{bc}(y,z,t_z) = \mathcal{C}^{(n)rt}_{ac}(x,z) \tag{3.48}$$

which is the equivalent to Eq. (**??**) with an inhomogeus source term $\mathcal{C}^{(n)}$ defined by the recursion formula:

$$\mathcal{C}^{(n)rt}_{ac}(x,z) = \sum_{\vec{z}\,'} F(\vec{z},\vec{z}\,',t_z)^{tt'}\mathcal{C}^{(n-1)rt'}_{ac}(x,[\vec{z}\,',t_z]) \tag{3.49}$$

where

$$\mathcal{C}_{ac}^{(1)rt}(x,z) = F(\vec{z},\vec{x},t_z)^{tr}\delta_{ac}\delta_{t_x,,t_z} \tag{3.50}$$

and n stands for the iteration number of Gaussian smearing. Equivalently one can show that the smeared-local propagator, is related to the local-local propagator by the relation

$$\overleftarrow{\mathcal{S}}_{ab}^{st}(y,z,U(t_z)) = \sum_{\vec{z}} F(\vec{x},\vec{z},t_y)^{rt}\mathcal{S}_{ab}^{ts}([\vec{z},t_x],y) \tag{3.51}$$

The smeared-smeared propagator is obtained by replacing in Eq. (3.51) the local-local propagator by the local-smeared one:

$$\overleftrightarrow{\mathcal{S}}_{ab}^{st}(y,z,U(t_z)) = \sum_{\vec{z}} F(\vec{x},\vec{z},t_y)^{rt}\overrightarrow{\mathcal{S}}_{ab}^{ts}([\vec{z},t_x],y) \tag{3.52}$$

Note that to smear a quark field at the sink, does not require additional inversion since we can apply directly the smearing to the propagator.

3.5 Resampling methods for statistical error estimates

The numerical estimation of any correlation function, in particular the hadron correlator introduced in the last section, requires a sum over a finite number of gauge configuration according to Eq. (1.52).

Several methods exist to evaluate statistical errors on quantities that are estimated via finite samples of N measurements. This vast subject is very important in our case since a careful estimate of statistical errors is needed to make reliable predictions. One additional difficulty in the statistical analysis of the lattice data is due to the inherent correlation between different configurations, between different timeslices for a given configuration, or generally between measurements due to the HMC algorithm used to generate the gauge configurations.

In this section, we present the most common methods that are useful in this context : the so-called *Jackknife*, the *Bootstrap*, and finally the Γ-*method*. The first two methods use the concept of resampling, which consist in building virtual ensembles of data from the original one. In order to introduce them we consider a random variable X, and a set of measurements of X : $\{X_i, i = 1,\ldots,N\}$. We note :

$$\bar{X} = \frac{1}{N}\sum_{i=1}^{N} X_i \tag{3.53}$$

the estimator of the mean.

3.5.1 Jackknife

Let us divide the ensemble of N measurements of X into N_{bin} subsets obtained by retrieving p elements from the initial set. The standard case correspond to $N_{\text{bin}} = N$ and $p = 1$. Averaging on each subset provide N_{bin} estimates of the average $\bar{X}$ from which we can deduce the Jackknife estimation of the variance σ_X. One way to implement it is to define the average on each Jackknife set by:

$$\bar{X}_k = \bar{X} - \frac{1}{p}\sum_{i=k}^{p+k} X_i \tag{3.54}$$

The Jackknife estimation of the variance is then :

$$\sigma_X^2 = \frac{N_{\text{bin}}-1}{N_{\text{bin}}}\sum_k (\bar{X}_k - \bar{X})^2 \tag{3.55}$$

This method can be generalized to secondary observables which are either a function of the primary variable or a more complicated relation denoted by $Y = f(X)$. We build a set of N_{bin} estimates of $\bar{Y}$ for each sample k:

$$Y_k = f(\bar{X}_k) \tag{3.56}$$

The variance of Y can then be estimated using as in the primary observable case the relation

$$\sigma_Y^2 = \frac{N_{\text{bin}} - 1}{N_{\text{bin}}} \sum_k (Y_k - \bar{Y})^2 \tag{3.57}$$

The number of bins is the only parameter of the method. It has to be chosen carefully. Indeed, if it is large one obtain small errors, but they are underestimated because of the correlation between measurements. If one decrease the number of bins, correlation between the bins is small but the dispersion will be large and the variance will be overestimated.

3.5.2 Bootstrap

The bootstrap method has some similarities to the jackknife method. It makes a random selection to build a new set with M values, so it is possible that the new set has repetitions. In fact we could even have $M > N$. The statistical analysis is then performed on the bootstrap sample. This process is repeated a large number of times N_{boot} and one can construct an estimator of the variance using the distribution of the variance on each bootstrap sample.

3.5.3 Γ Method

This third method is not based on resampling our data set but rather on a careful study of the variance of a correlated set of measurements. One of the main advantages of this method is that it allows to estimate the integrated autocorrelation time of secondary quantities. In particular the Γ-method will be extensively used in chapter 4 to analyse integrated autocorrelation times of plaquette variables, pseudoscalar masses, or PCAC masses. For a detailed discussion of this method see [60].

To illustrate this techniques let us first consider the case where X is a primary variable. One can show that an estimator of the ensemble variance σ_X is

$$\sigma_X^2 = \frac{1}{N} \sum_{n=-W}^{W} \Gamma_X(n), \tag{3.58}$$

where $\Gamma_X(n)$ is the estimator of the autocorrelation function defined by:

$$\Gamma_X(n) = \frac{1}{N - |n|} \sum_{i}^{N-|n|} (X^i - \bar{X})(X^{i+|n|} - \bar{X}). \tag{3.59}$$

and W is a parameter that refers to the number of consecutive measurements satisfying $2W+1 \ll N$. Note that $\Gamma_X(0) = \bar{\sigma}_X^2$ is the naive estimator of the variance. The integrated autocorrelation time is defined for an infinite set of measurements by

$$\tau_{\text{int}}(X) = \frac{1}{2} + \sum_{n=1}^{\infty} \frac{\Gamma_X(n)}{\Gamma_X(0)}, \tag{3.60}$$

and an estimator of it is given by

$$\tau_{\text{int}}(X) = \frac{1}{2\Gamma_X(0)} \sum_{n=-W}^{W} \Gamma_X(n) = \frac{N\sigma_X^2}{2\bar{\sigma}_X^2}. \tag{3.61}$$

One of the central interests of the Γ-method is its generalization to secondary observables. We have in mind for instance the case of correlators, effective masses or ratios of correlators. To this aim, let us consider a non-linear function of several primary observable $F[X]$ where X stands for a set of primary random variable $X \equiv \{X_1, \dots\}$. Each element X_j is realized by a set of measurement $\{X_j^i, \imath = 1, \dots N\}$. In the particular case of a correlator analysis C is the ensemble of primary random variables $\{C(t_1), \dots, C(\tau), \dots, C(t_2)\}$ with $t_1 < \tau < t_2$ and where t_1 and t_2 fix the fit window. The main idea in generalizing the Γ-method to secondary observables is to estimate the deviation from the true value, by expanding $F(\bar{X})$ arround $F(X)$. Defining

$$\bar{X}_f = \sum_i \frac{\partial F[X]}{\partial X_i} \bar{X}_i \tag{3.62}$$

the deviation σ_F^2 is estimated using 3.61 with:

$$\Gamma_{\bar{X}_f}(n) = \frac{1}{N-|n|} \sum_{i=1}^{N-|n|} (X_f^i - \bar{X}_f)(X^{i+|n|} - \bar{X}_f) \tag{3.63}$$

3.6 Correlator analysis

3.6.1 Two-point correlators

To extract baryon masses in the rest frame, we generalize Eq. (3.9) to fermions. The picture is a bit more involved in this case, indeed in general the simplest operators used for the description of baryons are coupled to both parities. The asymptotic behaviour of the correlator contains contributions of both parities.

Let us define a correlation function between two generic fermionic interpolating field J_1 and J_2.

$$C(\tau, \vec{p}) = \sum_{\vec{x}} \langle J_1(x) \bar{J}_2(0) \rangle \tag{3.64}$$

One can show the following equation, in the case of antiperiodic boundary conditions of the quark fields

$$\begin{aligned} C(\tau, \vec{p}) \xrightarrow{T,\tau\to\infty} \mathcal{P}_+ \Big[Z_1^{(+)} Z_2^{(+)} e^{-E_1^{(+)}(\vec{p})\tau} - Z_1^{(-)} Z_2^{(-)} e^{-E_1^{(-)}(\vec{p})(T-\tau)} \Big] \\ + \mathcal{P}_- \Big[Z_1^{(-)} Z_2^{(-)} e^{-E_1^{(-)}(\vec{p})\tau} - Z_1^{(+)} Z_2^{(+)} e^{-E_1^{(+)}(\vec{p})(T-\tau)} \Big] \end{aligned} \tag{3.65}$$

with the following definition:

$$\begin{aligned} Z_1^{(+)} &= \langle 0 | J_1(0) | 1, +, \vec{p} \rangle \\ Z_1^{(-)} &= \langle 1, -, \vec{p} | J_1(0) | 0 \rangle \\ Z_2^{(+)} &= \langle 1, +, \vec{p} | \bar{J}_2(0) | 0 \rangle \\ Z_2^{(-)} &= \langle 0 | \bar{J}_2(0) | 1, -, \vec{p} \rangle \end{aligned} \tag{3.66}$$

and

$$\mathcal{P} = \frac{1 \pm \gamma_0}{2} \tag{3.67}$$

We are thus lead to the following definition of the parity projected correlators at zero momentum $C_X^{\pm}(t)$ for large Euclidean time with $\vec{p} = \vec{0}$

$$C_X^{\pm}(t) = C_X^{\pm}(t, \vec{p} = \vec{0}) = \frac{1}{2} \mathrm{Tr}(1 \pm \gamma_0) \sum_{\mathbf{x}_{\mathrm{sink}}} \langle J_X(\mathbf{x}_{\mathrm{sink}}, t_{\mathrm{sink}}) \bar{J}_X(\mathbf{x}_{\mathrm{source}}, t_{\mathrm{source}}) \rangle, \qquad t = t_{\mathrm{sink}} - t_{\mathrm{source}} \tag{3.68}$$

Space-time reflection symmetries of the action and the anti-periodic boundary conditions in the temporal direction for the quark fields imply, for zero three-momentum correlators, that $C_X^+(t) = -C_X^-(T-t)$. In order to increase statistics we average correlators in the forward and backward direction and define:

$$C_X(t) = C_X^+(t) - C_X^-(T-t)\,. \tag{3.69}$$

To minimize correlations between measurements, we choose randomly on the whole lattice the source location x_{source} for each configuration.

All the computed correlators presented in this work have been obtained following the above described procedure.

3.6.2 Effective Mass

The effective mass of a given hadronic state X is defined by

$$m_{\text{eff}}^X(t) = -\log(C_X(t)/C_X(t-1)) \tag{3.70}$$

Assuming a correlator of the form

$$C(t) = \sum_n c_n e^{-m_n t} \tag{3.71}$$

one has

$$m_{\text{eff}}^X(t) = m_X + \log\left(\frac{1+\sum_{i=1}^{\infty} c_i e^{\Delta_i t}}{1+\sum_{i=1}^{\infty} c_i e^{\Delta_i (t-1)}}\right) \underset{t\to\infty}{\longrightarrow} m_X \quad , \tag{3.72}$$

where $\Delta_i = m_i - m_X$ is the mass difference of the excited state i with respect to the ground state mass m_X. The effective mass exhibits a plateau for large time that has to be fitted in order to extract the mass. This is illustrated in Fig. 3.3 by the nucleon effective mass computed on a $L = 24$ for $\beta = 3.9$ and $\mu = 0.0085$ with 1817 measurements. The errors are estimated using the Jackknife method.

It is worthwhile to note that the error on the effective mass increases exponentially with the time as shown in Fig. 3.4. A careful theoritical analysis of the two-point function variance show that such is the general behaviour. One can estimate that in the case of the nucleon the error behaves

$$\Delta m(t) \sim e^{-(m_n - \frac{3}{2}m_\pi)t} \tag{3.73}$$

This result constitutes a severe limitation in computing baryon masses. Indeed, on one hand, and in order to suppress excited contribution, the mass has to be measured at large euclidean times. On the other hand, the signal to noise ratio grows exponentially and thus sully the interesting region with error bars. This is a serious drawback known as the *signal to noise ratio problem*.

As a further check of our statistical error calculation, we can test the dependence of the effective mass relative error computed at a fixed time as a function of the number of measurements N. In Fig. 3.5 we show that the error decrease like $1/\sqrt{N}$ as expected from Eq. (1.52). One can also estimate from this figure the size of the error on the correlator we can expect in our simulation: a $\sim 1\%$ error is obtained with ~ 1500 configurations.

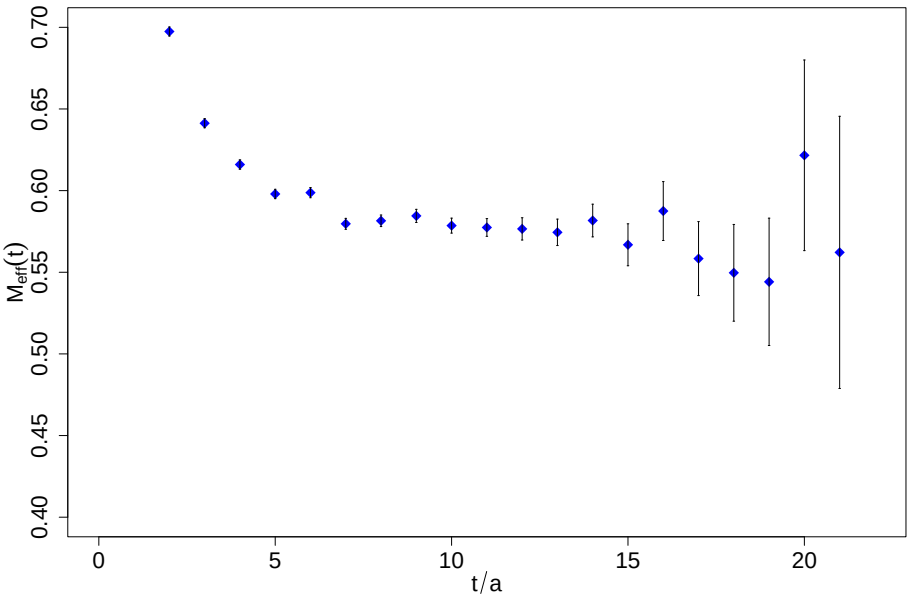

Figure 3.3: Nucleon effective mass as a function of the time in lattice units on a $24^3 \times 48$ lattice with $\beta = 3.9$ $\mu = 0.0085$ and 1817 measurements.

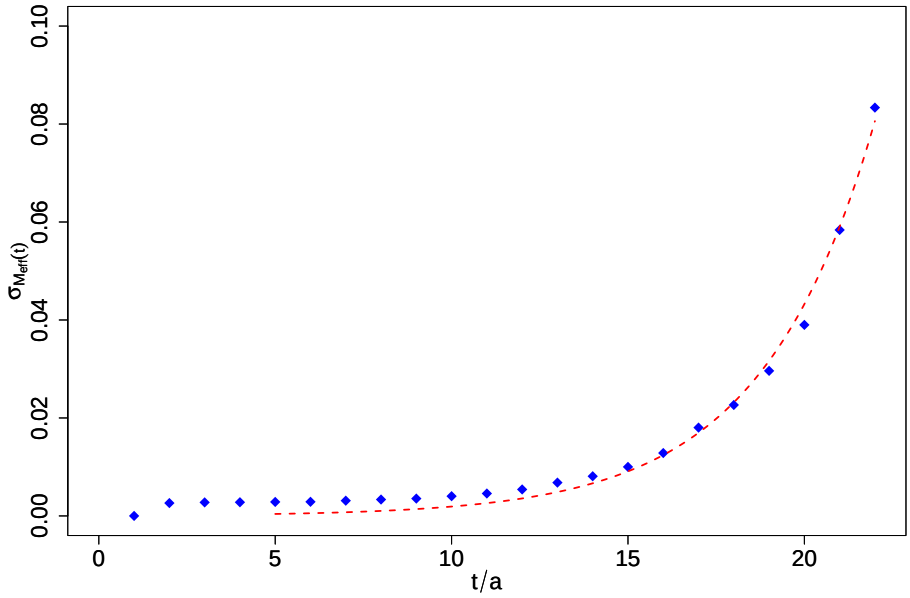

Figure 3.4: Error on the nucleon effective mass as a function of the time in lattice units on a $24^3 \times 48$ lattice with $\beta = 3.9$ $\mu = 0.0085$ and 1817 measurements. An empirical fit of the form $\sigma_{M_{eff}(t)} = Ae^{+B\frac{t}{a}}$ gives $A \sim 0.0004$ and $B \sim 0.311$. The dotted red curve show the best fit to the data.

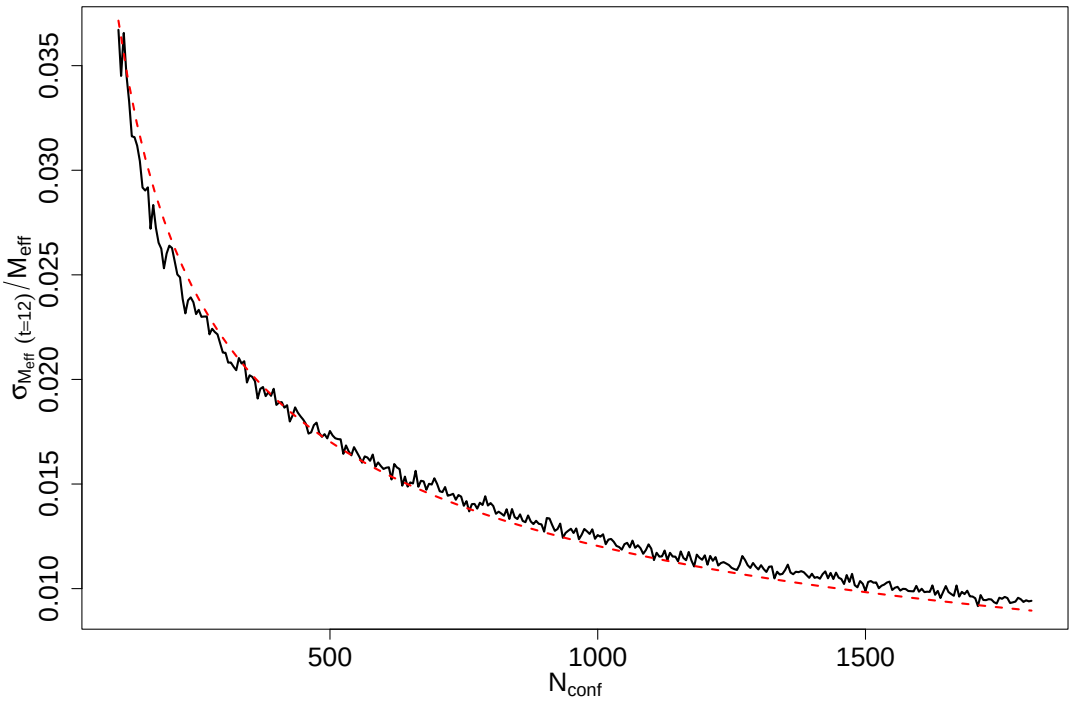

Figure 3.5: Scaling of the error on the effective mass at $t/a = 12$ measured on $L = 24$ lattice with $\beta = 3.9$ and $\mu = 0.0085$. The red dotted curve show a fit of the form $\sigma_{M_{eff}}(t) = \frac{A}{\sqrt{N}}$, the best fit value of A is ~ 0.3807

3.6.3 Automatic Fitting Procedure

One of the problems in extracting the physical mass m_X from the computed effective mass $m_{eff}(t)$ is to determine an approximate plateau region. This is achieved by optimizing a constant fit between two timeslices t_1 and $t_2 > t_1$.

The determination of the optimal plateau range is a delicate issue, since we are faced with an exponential decrease of the excited states contribution, which is responsible for the non-flatness of the signal, and to an exponential increase of the signal to noise ratio. On one hand we want to start to fit with a time t_1 as large as possible, on the other hand the statistical error dramatically increase with the lattice time. To determine an optimal value of the interval $[t_1, t_2]$, we must find a compromise between statistical error and excitation contribution. The excitated states contribute to the signal according to Eq. (3.72) and a pertinent criterium to neglect them is to see wheter or not they are smaller than statistical noise.

To illustrate the behaviour of the plateau fit, we plot as a function of t_1 the mass extracted in Fig. 3.6 and this for several values of t_2.

We first observe that the results (central value as well as the error bar) do not depend on t_2. This is due to the fact that the statistical weight of the effective mass at large times is small (large error bars). A first conclusion is that the difficult part of the problem is to fix the starting fit point t_1.

A second remark is that the measured mass decreases as t_1 becomes larger. As already

mentioned this is due to the excited states contamination that introduce a bias which decrease with time. One can conclude that whatever the plateau region is, the asymptotic mass will be overestimated.

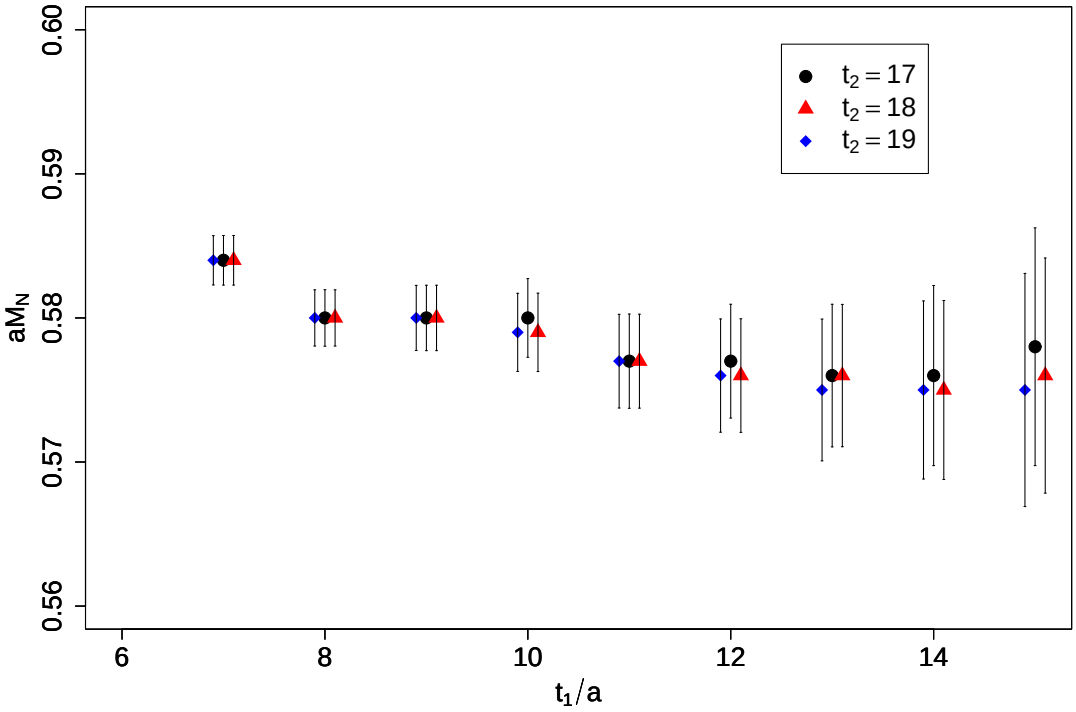

Figure 3.6: Nucleon as a function of the starting point of fit t_1/a for several values of t_2/a. We choose $t_2/a = 17, 18$ and 19. Gauge ensemble with $\beta = 3.9$ $\mu = 0.0085$ and 1817 measurements on a $24^3 \times 48$ lattice

We are now ready to define a criterium to fix the plateau. Denoting $M(t_1, t_2)$ the fitted mass for a plateau range $[t_1, t_2]$, an systematic criterium to determine an optimal value of t_1 is by choosing the smaller value such that

$$\frac{dM(t_1, t_2)}{dt_1} \approx 0 \tag{3.74}$$

where $\approx$ means here compatible within the Jackknife computed error bars. The value of t_2 is chosen as large as possible since the result does not depend strongly on it.

For instance, we show in Fig. 3.7 the derivative with respect to t_1 of the fitted mass. The statistical error bars are computed using th Jackknife method. In that case, the optimal value found is $t_1 = 8$ as indicated by a dotted line on the plot.

This criterium has the advantage to take into account the statistical error on the effective mass and implement the idea that excited state contributions have to be smaller than the statistical error. As a consequence, when the number of measurements increases, the statistical errors will decreases, the condition Eq. (3.74) will become more stringent and the starting point t_1 will increase.

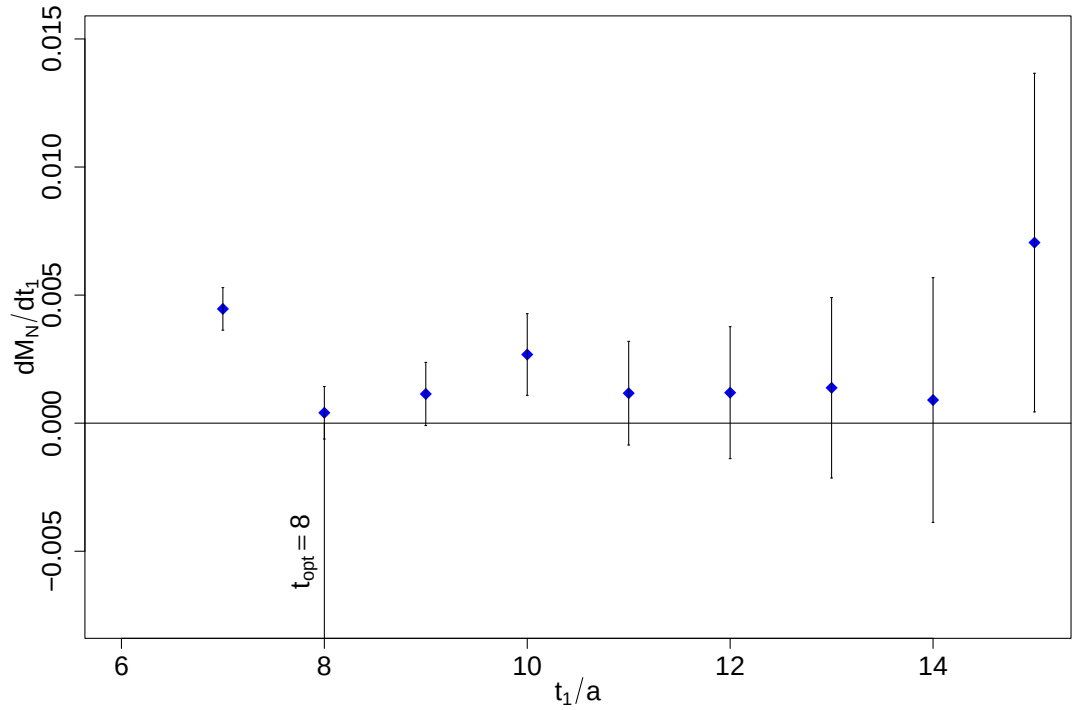

Figure 3.7: dM_N/dt_1 as a function of the t_1. Gauge ensemble $\beta = 3.9$ $\mu = 0.0085$ $L = 24$ and 1817 measurements.

Another appreciated advantage is that our criterium works in practice even if the signal is not very clear. This way of choosing t_1 appears to be convenient to fit a large number of plateau on a large number of gauge ensemble without any biased introduced "by eyes". In practice we obtain with this method a χ^2/d.o.f always close to one.

One of its drawbacks is that the correlations between timeslices tend to diminish the variation of the effective mass between neighbooring timeslices. One can thus expect that the value of t_1 obtained with could be too small. A conservative solution would have been to fit one or two timeslice after the criterium is satisfied. However this strategy has not been chosen in this work.

We have illustrated in Fig. 3.8 the possible bias introduced by this method by plotting the value of the relative error on the fitted mass as a function of t_1. The relative error σ_{M_N}/M_N denoted by blue points increases rapidly as expected due to the exponential signa-to-noise ratio problem. A double exponential fit of the correlator allows to estimate the excited states contribution relative to the fitted ground state mass. This systematic bias becomes smaller than the statistical error for $t_1 > 9$. We have filled in gray the t_1 region where excited states dominate. Note however two important things. On one hand, the statistics is very large in this example, and the relative error on the mass is thus of $\sim 5‰$. On the other hand the excited states contributions do not depend on the statistics.

Furthermore, the determination of the double exponential fit parameters is even a more challenging task, not only because it introduces additional parameters but also because their values depend strongly on the starting point of the fit. This resutls into large error bars which make uncertain estimation of the excited states contribution.

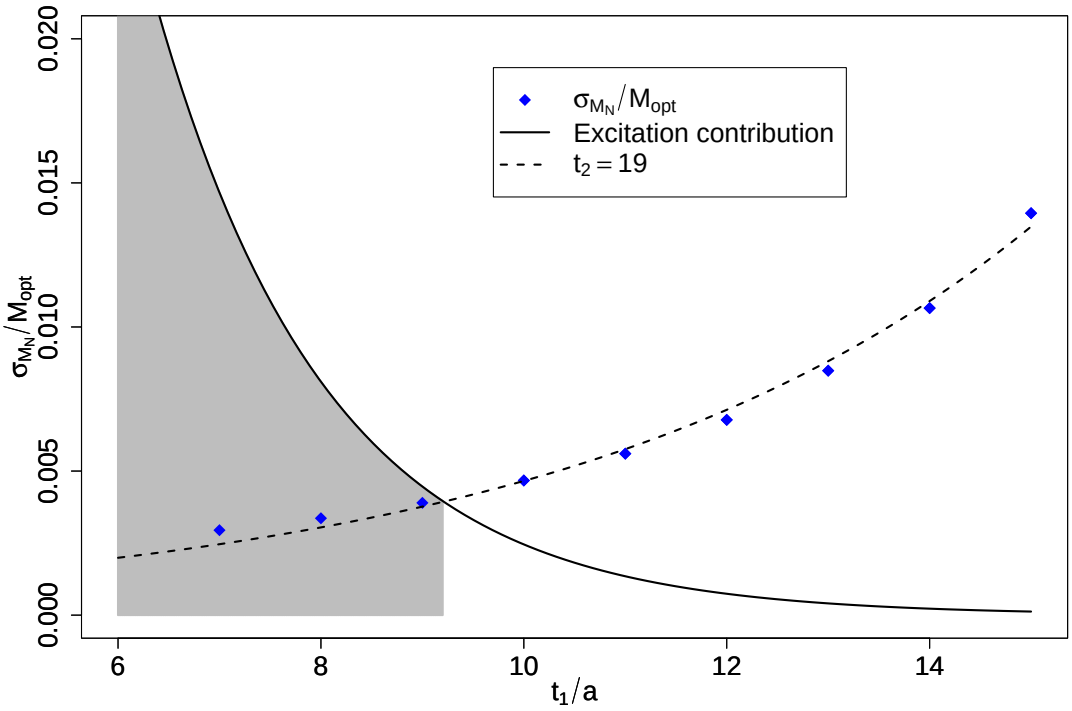

Figure 3.8: Relative error on the nucleon mass as a function of the fitting window. Gauge ensemble $\beta = 3.9$ $\mu = 0.0085$ $L = 24$ and 1817 measurements. The region where excited state contributions is bigger than statistical error is filled in gray. It has been estimated using a double exponential fit to the correlator.

3.7 Quark mass dependence of hadron masses

We introduce in this section the concept of *the sea quark mass* and *the valence quark mass*. The sea quark mass refers to the bare quark mass that enters in the gauge configuration production through the determinant of the Dirac operator.

On a given set of configurations, one can however perform the contraction using a propagator defined as the inverse of the Dirac operator with another mass value, this is the valence quark mass.

In a lattice simulations - unlike experiment - it is possible to vary the sea and valence quark mass independently. This technique allows to simulate for instance a strange quark on $N_F = 2$ gauge ensembles. The strange quark contribution being neglected in the generation of the gauge configurations, this approximation of QCD is named partially quenched. We will use this approximation in chapter 7.

Another important information, provided by studying independently sea and valence quark contributions, is to investigate the QCD matrix elements that control the dependence of hadron masses in quark mass parameters. The idea is to take formally the derivative with respect to the bare quark mass of suitable correlators (see for instance [61]). Equivalently this method has been used to study dependence of correlation functions with respect to β, see for instance [62].

See also [63, 64].

One can deduce from this analysis that the derivative with respect to the bare quark mass of a hadron is determined by the scalar form factor at zero momentum transfer. This result was first obtained by generalizing the Feynman Hellman theorem [65] in QFT . To summarize one has

$$\sigma_h = m_R \frac{\partial M_h}{\partial m_R} \tag{3.75}$$

with

$$\sigma_h = \sigma(t=0) = m_R \langle h, \vec{0} | \bar{u}u(0) + \bar{d}d(0) | h, \vec{0} \rangle \tag{3.76}$$

In our analysis of the baryon spectrum, the σ will be obtained as a by product of our analysis. This an important quantity which is not well known experimentally. Lattice simulation should improve the situation in the next years. In the case of the nucleon, the σ_N term can be related to various quantities as the strangeness of the nucleon, the quark mass ratio, the $\pi - N$ scattering amplitude. This is also an important quantity in the framework of dark matter direct detection [66].

Chapter 4

Gauge Configuration Generation

Contents

In this chapter we present some aspects of the gauge configuration generation which is the main building block of our Euclidean QCD simulations as well as the more expensive numerical task. The problem is to estimate the high dimensional (real dimension $= 4 \times 8 \times V$) integral over the gauge field (1.50). The hope is that, most of the contribution to this integral comes from a small ensemble in the enormous functional space. Empirically it seems to be the case and stochastic integration with *importance sampling* is an effective method to perform such integrals.

The main goal is to build an ensemble of configuration $\aleph = \{U^{(1)}, \ldots, U^{(i)}, \cdots\}$ that has the property to sample the space of all configuration with a probability density given by

$$p[U] = \frac{1}{\mathcal{Z}} \text{ det } \mathrm{D_{tmQCD}[U]e^{-S_G[U]}} \tag{4.1}$$

where S_G is the gauge action, and $D_{\mathrm{tmQCD}}[U]$ the twisted mass Dirac operator on the flavour space, either in the $N_f = 2$ or $N_f = 2 + 1 + 1$ case. This gauge ensemble is such that any correlation function on the lattice denoted symbolically by :

$$\langle O \rangle = \int \mathcal{D}U p[U] O[U] \tag{4.2}$$

can be approximated by

$$\bar{O} = \frac{1}{N} \sum_{i=1}^{N} O[U^{(pi)}] = \langle O \rangle + \mathcal{O}(\frac{1}{\sqrt{N}}) \tag{4.3}$$

where N is the number of measurements performed on a subset of $\aleph$ and p an integer parameter chosen to decrease the correlation between two configurations.

To generate $\aleph$ one needs a stochastic process providing a dynamics in the configurations space with a transition probability $T(U^{(i)} \to U^{(i+1)})$ between two configurations $U^{(i)}$ and $U^{(i+1)}$ such that Eq. (4.1) is fulfilled. The sequence of configuration thus generated is called a *Markov chain*. It is fully determined by $U^{(1)}$ and the transition probability $T(U^{(i)} \to U^{(i+1)})$.

In this work two gauge actions are used : the so-called *tree level-Symanzik Improved action* [67] and the *Iwasaki action* [68]. The tree level-Symanzik Improved action includes besides the plaquette term $U^{1\times1}_{x,\mu,\nu}$, also rectangular (1×2) Wilson loops $U^{1\times2}_{x,\mu,\nu}$:

$$S_g^{\mathrm{tlSym}} = \frac{\beta}{3} \sum_x \left(b_0 \sum_{\substack{\mu,\nu=1 \\ 1\le\mu<\nu}}^{4} \left\{ 1 - \mathfrak{Re}\mathrm{Tr}\left\{ U^{1\times1}_{x,\mu,\nu} \right\} \right\} + b_1 \sum_{\substack{\mu,\nu=1 \\ \mu\neq\nu}}^{4} \left\{ 1 - \mathfrak{Re}\mathrm{Tr}\left\{ U^{1\times2}_{x,\mu,\nu} \right\} \right\} \right) \tag{4.4}$$

with $b_1 = -1/12$ and the normalization condition $b_0 = 1 - 8b_1$. Note that at $b_1 = 0$ this action becomes the usual Wilson plaquette gauge action.

The Iwasaki action has the same form with $b_1 = 0.331$.

The algorithm introduced in 1953 by Metropolis [69], was the first algorithm adapted to simulate QFT on a lattice in 1980 [70, 71]. However this algorithm becomes inefficient in the case of dynamical simulations, and nowadays the most common algorithms used are based on the *Hybrid Monte Carlo Algorithm* (HMC) [72]. A lot of progress has been made during the last years to accelerate this algorithm. The goal is not to give a detailed review of them, but rather to introduce the basic concepts of HMC.

4.1 Skectch of the HMC algorithm

In order to introduce the algorithm, we will restrict ourself to the case of Wilson's twisted mass formulation of lattice QCD with one doublet of mass degenerate quarks ($N_f = 2$). In this case we have the following property :

$$\text{det } \mathrm{D[U]_{tmQCD}} = \text{ det } \mathrm{Q^\dagger Q} \tag{4.5}$$

with

$$Q = D_{\mathrm{W}}[U] + m_0 + i\mu\gamma_5 \tag{4.6}$$

Note that Q does not act on flavour space, and that $Q^\dagger Q$ is positive definite and protected against zero eigenvalues by μ^2.

Using a complex *pseudo fermion field* representation for the determinant we get :

$$\det \mathrm{Q}^2 \propto \int \mathcal{D}\phi\mathcal{D}\phi^\dagger \mathrm{e}^{-\mathrm{S_{PF}[U,\phi,\phi^\dagger]}} \tag{4.7}$$

where

$$S_{\mathrm{PF}}[U,\phi,\phi^\dagger] = \sum_x \phi^\dagger(x)\left(Q^\dagger Q\right)^{-1}\phi(x) \tag{4.8}$$

is the so-called *pseudo fermion action*. Let us introduce the tracceless Hermitian field $\Pi_\mu(x)$ as conjugate of the gauge fields $U_\mu(x)$ and define the molecular dynamics Hamiltonian:

$$\mathcal{H}[P,U,\phi,\phi^\dagger] = \frac{1}{2}\sum_{x,\mu}\Pi_\mu^2(x) + S_G[U] + S_{\mathrm{PF}}[U,\phi,\phi^\dagger] \tag{4.9}$$

The underlying dynamical system evolves in a phase space of real dimension $64 \times V$. The corresponding trajectories of the gauge fields are integrated by the computational function called *Molecular Dynamics update*. The HMC algorithm then performs an accept/reject step with respect to $\Delta\mathcal{H} = \mathcal{H}[U',\Pi'] - \mathcal{H}[U,\Pi]$ using the acceptance probability

$$P_{\mathrm{ac}} = \min\left(1, \mathrm{e}^{\Delta\mathcal{H}}\right) \tag{4.10}$$

The momenta Π are generated randomly from a gaussian distribution at the beginning of the molecular dynamics evolution. The pseudo fermion fields are not evolved during the trajectory and is obtained from a random gaussian field R by $\phi = QR$.

The integration of the equations of motion are a crucial point of the algorithm. One can show indeed that the HMC algorithm is exact if the integration scheme is reversible and area preserving.

4.1.1 Molecular Dynamics

Introducing the so-called *Monte Carlo time* t, the Hamilton equations of motion read:

$$\begin{aligned} \dot{U}(t) =& \frac{d\mathcal{H}}{dP} = P \\ \dot{\Pi}(t) =& -\frac{dH}{dU} = -F[U] \end{aligned} \tag{4.11}$$

where the forces are

$$\begin{aligned} F[U] &= F_G[U] + F_{\mathrm{PF}}[U] \\ F_G[U] &= \frac{dS_G}{dU}[U] \\ F_{\mathrm{PF}}[U] &= \frac{dS_{\mathrm{PF}}}{dU}[U] \end{aligned} \tag{4.12}$$

The easiest way to integrate these equations over a Monte Carlo time step ϵ is to use the *leap frog (or Verlet) algorithm*:

$$\begin{aligned} \mathcal{T}_U(\epsilon) &: \quad U_t \longrightarrow U_{t+\epsilon} = e^{\epsilon\Pi_t}U_t \\ \mathcal{T}_\Pi(\epsilon) &: \quad \Pi_t \longrightarrow \Pi_{t+\epsilon} = \Pi_t - \epsilon F_t \end{aligned} \tag{4.13}$$

noticing that:

$$\mathcal{T}_\Pi(\frac{\epsilon}{2})\mathcal{T}_\Pi(\epsilon)\mathcal{T}_\Pi(\frac{\epsilon}{2}) \quad : \quad (\Pi_t, U_t) \longrightarrow (\Pi_{t+\epsilon}, U_{t+\epsilon}) + \mathcal{O}(\epsilon^3) \tag{4.14}$$

Despite its simplicity, we use in our numerical simulation a more elaborated version of the algorithm, which adapts the time step ϵ to the intensity of the force.

4.1.2 Heavy sector

Let us denote by $D_h[U]$ the twisted mass Dirac operator in the non degenerate case and define

$$Q_h = \gamma_5 D_h[U] \tag{4.15}$$

Note that one has $\det \mathrm{D_h[U]} = \det \mathrm{Q_h[U]}$. Contrary to the light sector action, the fermionic determinant in the heavy sector is evaluated using a pseudo fermions field doublet Φ_h

$$\det \mathrm{Q_h[U]} \propto \int \mathcal{D}\Phi_\mathrm{h} \mathrm{e}^{-\Phi_\mathrm{h}^\dagger \left(\mathrm{QQ}^\dagger\right)^{-1/2} \Phi_\mathrm{h}} \tag{4.16}$$

We evaluate $\left(Q_h Q_h^\dagger\right)^{-1/2}$ using a polynomial approximation of the inverse square root: this is the so-called *Polynomial HMC*(PHMC) [73]

$$\left(Q_h Q_h^\dagger\right)^{-1/2} = P_{n,\epsilon}\left(Q_h Q_h^\dagger\right) \tag{4.17}$$

which uses a Chebysheff polynomial $P_{n,\epsilon}$ of degree n, to approximate the function $\frac{1}{\sqrt{X}}$ on the intervall $[\epsilon, 1]$. It is constructed to ensure a desired overall precision $R_{n,\epsilon}$ on the interval $[\epsilon, 1]$:

$$P_{n,\epsilon}(X) = \frac{1}{\sqrt{X}}\{1 + R_{n,\epsilon}\} \tag{4.18}$$

In our HMC code, the polynomial is used in its factorized form

$$P_{n,\epsilon}(X) = c\left[\prod_i^n (X - z_i)\right] \tag{4.19}$$

where z_i are the complex root of P, and c is a normalization constant.

Note that in practice, in the HMC algorithm nothing prevents us from using different polynomial in the molecular dynamics and in the metropolis test. We take advantage of this property to use a polynomial of small degree (~ 100) in the molecular dynamics update and a polynomial of high degree $\tilde{P}$ (~ 1800) for the acceptance test. Manipulating polynomial of such degree is challeging and requires some once and for all care. First, the roots and normalization constant of $\tilde{P}$ are computed and stored once at all before the production runs start. Second, they have to be computed with a very high precision. We use a library called CLN[1] which allows to manage and use numbers with arbitrary precision. We also use the *Clenshaw algorithm* which keep rounding errors at a tolerable level [74]. To give an idea the roots are computed with ~ 1600 decimals.

For a given ϵ, the degree of the polynomial has to be tuned in order to estimate correctly the inverse of the square root for all the configurations that will be produced during the run. This improbable estimation, which is only a small part of the PHMC *savoir-faire*, is crucial in order to guarantee the exactness of the HMC algorithm. This is a posteriori achieved by checking online that the lowest and highest eigenvalues of $Q_h Q_h^\dagger$, suitably normalized, are always contained in the range $[\epsilon, 1]$. The degree of the polynomial has to be chosen in order to offer a good compromise between time of computation and acceptance rate.

[1] Class Library for Numbers

4.1.3 Practical implementation

The practical implementation of the HMC algorithm is summarized in Fig. 4.1.

The code starts by initializing a configuration U. Several choices are possible between a randomly chosen U (hot start), a constant background $U = 1$, or by reading an existing configuration from another run. Then the code generates the momentum Π_μ according to a gaussian distribution. Light and heavy pseudofermion fields are also generated from a gaussian distribution to which is applied the operator Q or $Q_h^{1/2}$.

The molecular dynamics begins by computing the forces and uses an integrator to evolve the system to an infinitesimal step. This process is repeated until Monte Carlo time $\tau = 1$. Note that during the compuations of the forces, the estimation of heavy quark contributions is done using the polynomial P which is not the most accurate.

At the end of the trajectory an acceptance test is performed, and the hamiltonian of the new configuration is evaluated using the precise polynomial $\tilde{P}$. After this test the new configuration is either the initial one or the new one, and the trajectory number is increased by one. Informations on the configuration are then written in *output.data* and *phmc.data* (informative relative to the heavy sector). The configuration is written on the harddisk. According to the frequency of the online measurements, light correlators are compute or not. Note that every $\sim 40 - 50$ trajectory a reversibilty check is also performed by reversing the Monte Carlo time. This test allows to check that no problem occurs on the machine, and is important since reversibility of the HMC algorithm is a crucial criterium to guarantee its exactness.

The whole process is then started again, until the desired number of trajectories is achieved.

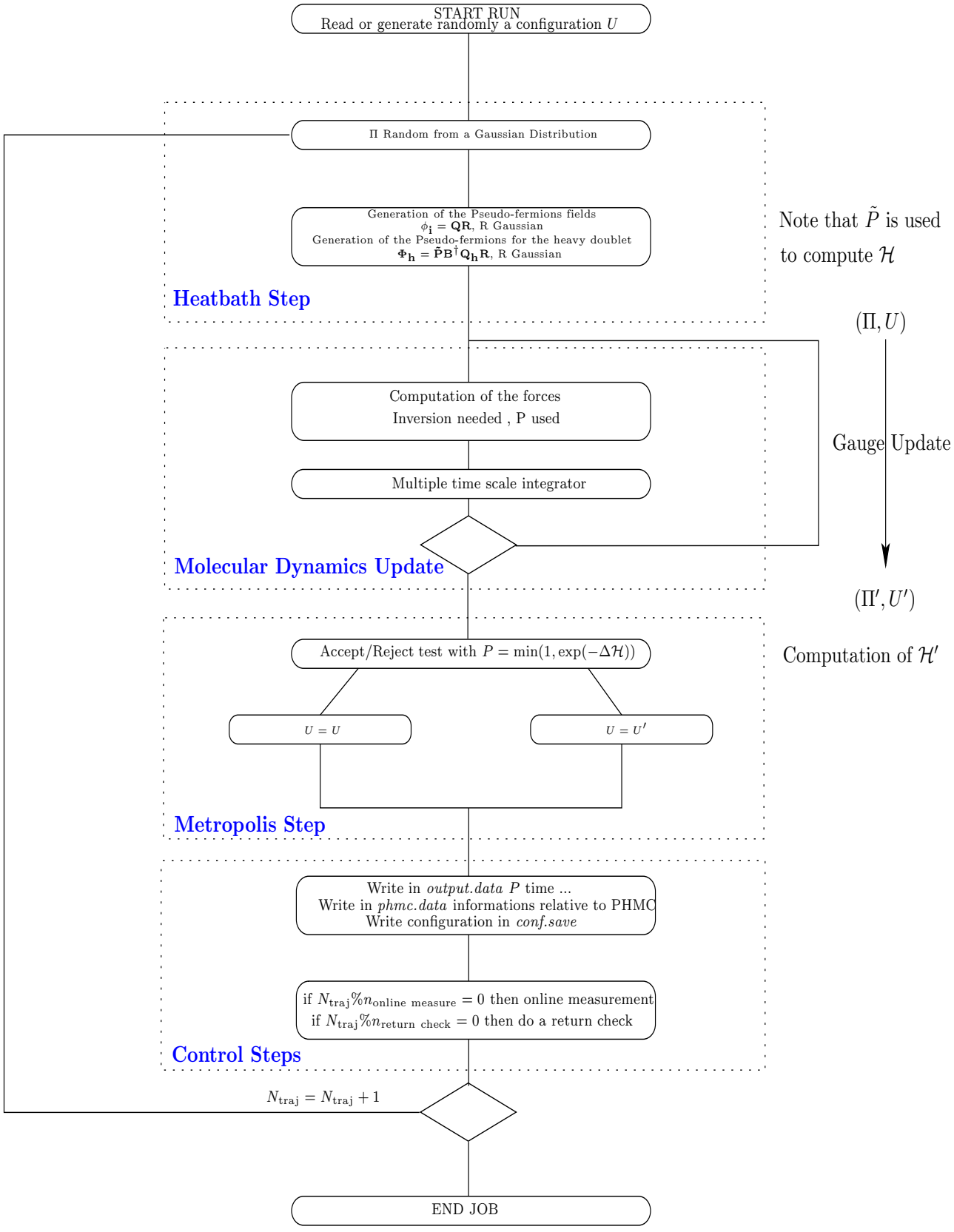

Figure 4.1: HMC algorithm

4.2 Characterizing a run

In order to control that the evolution of the run goes smoothly online information is required. The most common observables are the plaquette and $\Delta\mathcal{H}$ measurements, and a logical variable to control whether the configuration has been accepted or not. There is also informations on the minimal and maximal eigenvalue of the heavy sector Dirac operator to check the consistency of PHMC. We present in this section some of these results in the case of $N_f = 2 + 1 + 1$ runs.

In a second part we present the analysis of the online measurement of correlators. These measurements allow to tune the Wilson quark mass (m_0) to its critical value, in order to be at maximal twist. Other interesting quantities to measure online are the pseudoscalar mass and decay constant.

4.2.1 Algorithm control

The first check to perform during the gauge configuration production is the *thermalization* of observables. Indeed, starting from an existing configuration produced with another set of parameters, the first elements of the Markov chain have a memory of the initial state, and are therefore irrelevant. The question is to estimate the number of configurations to be rejected i.e the Monte Carlo time required for thermalization. Note that this characteristic time depends on the observable chosen and on the parameters of the run. Moreover we have no idea a priori of its value. The common criteria to decide that the observable is thermalized is to wait much longer than the typically measured characteristic times. We show in Fig. 4.2 the example of plaquette thermalization for a $L = 32$, $T = 64$ run with $N_f = 2 + 1 + 1$ flavours at $\beta = 2.0$. The light quark mass is of $a\mu = 0.0025$ and the heavy doublet mass $a\mu_\sigma = 0.13$ and $a\mu_\delta = 0.16$.

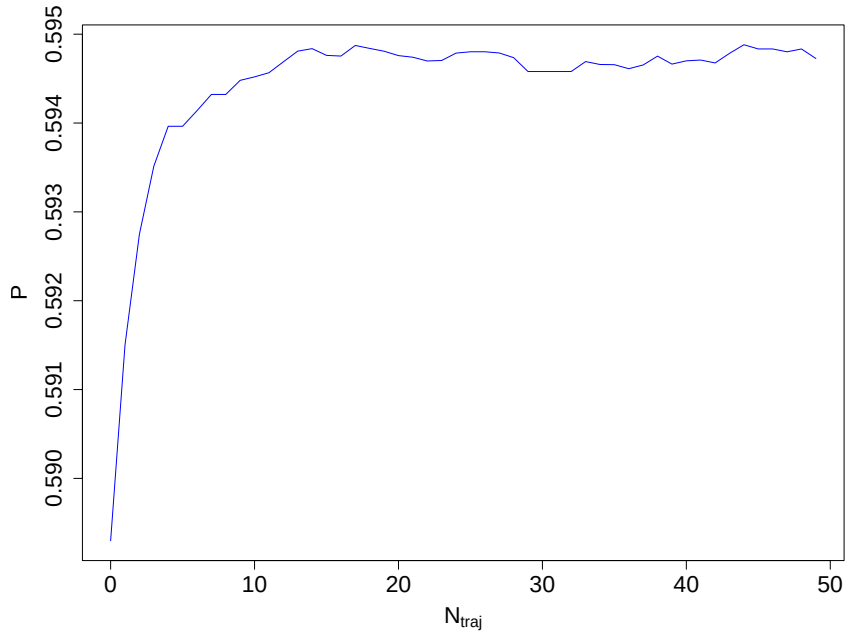

Figure 4.2: Thermalization of the plaquette variable for a $32^3 \times 64$ lattice $\beta = 2.0$, $a\mu = 0.0025$, $a\mu_\sigma = 0.13$, $a\mu_\delta = 0.16$

As can be seen in this figure, the typical number of trajectories needed to reach a plateau region is ~ 20. Such an estimation should be repeated in principle for each observable and lattice action. In practice this is rarely done. We compensate this thoughtlessness by taking an extremely conservative criterium: we drop out the first one thousand trajectories before starting any physical analysis on a run, and we safely declare that the run is thermalized.

We show in Fig. 4.3 a history of the plaquette measurements for nearly ~ 7000 $\beta = 1.95$ thermalized trajectories, following our previous criterium. The light quark mass is $a\mu = 0.0025$ and the heavy doublet masses are $a\mu_\sigma = 0.135$ and $a\mu_\delta = 0.17$

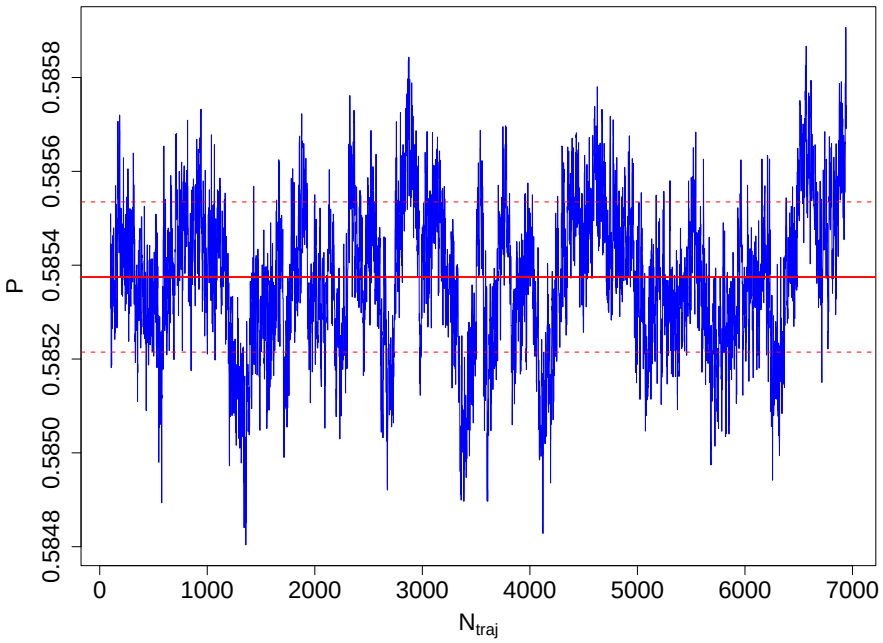

Figure 4.3: Plaquette history for a $L = 32$, $T = 64$ run at $\beta = 1.95$, with $a\mu = 0.0025$, $a\mu_\sigma = 0.135$ and $a\mu_\delta = 0.17$

The corresponding histogram, displayed in Fig. 4.4 gives us access to the variance of the plaquette. Note however that the naive variance does not provide an estimation of the statistical error due to the correlations between measurements. A precise estimation of this error would require using the methods described in chapter 3. The effective statistics is in fact $N_{meas}/2\tau_{int}$ where τ_{int} is the integrated autocorrelation time defined in Eq. (3.61).

The gaussian distribution of the plaquette measurement is a necessary conditions for the absence of a complicated phase structure of the statistical field theory.

Another important information directly related to the acceptance of the algorithm is the quantity $e^{-\Delta\mathcal{H}}$. As we have seen in Eq. (4.10), if this quantity is smaller than one, it gives the probability to accept the configuration or to reject it. Of course the aim is to accept as many configurations as possible provided the price to pay is not too high. Indeed, if the integrator was exact, the energy would be exactly conserved, and the acceptance rate would be one. However the numerical cost will never compensate the number of configuration saved. A compromise is thus needed. In practice, it is obtained when $\sim 80\%$ of the configurations are accepted. We show in Fig. 4.5 $e^{-\Delta\mathcal{H}}$ as a function of the Monte-Carlo time for the same run parameters than in Fig. 4.3.

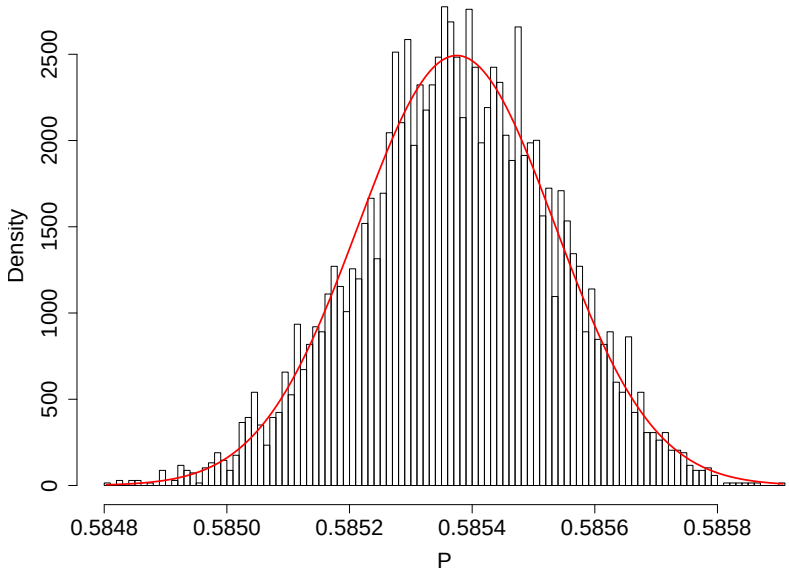

Figure 4.4: Distribution of the plaquette measurement for the same run as used in Fig. 4.3

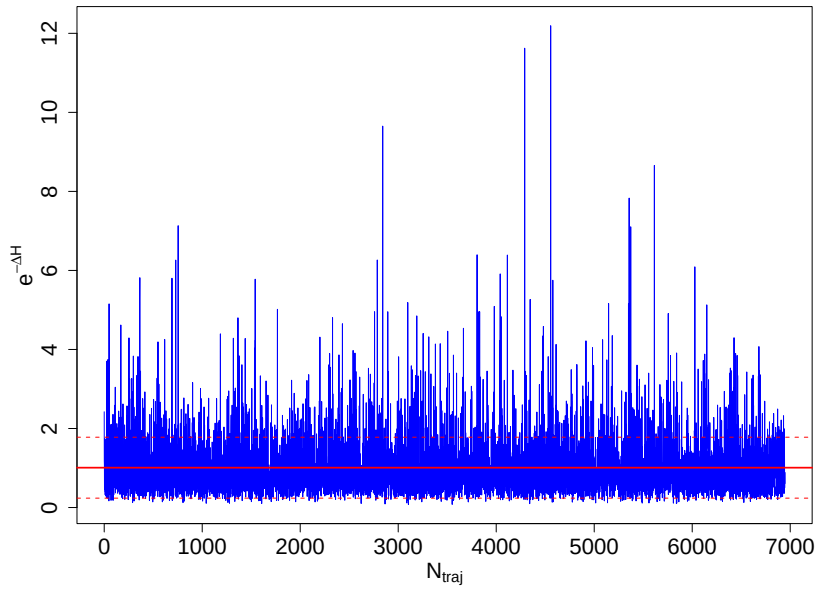

Figure 4.5: $e^{-\Delta\mathcal{H}}$ history for the $L = 32$, $T = 64$ run at $\beta = 1.95$, with $a\mu = 0.0025$,$a\mu_\sigma = 0.135$ and $a\mu_\delta = 0.17$

The acceptance rate for this run turns to be 74%. We observe that some configurations are automatically accepted by the algorithm ($e^{-\Delta\mathcal{H}} \leq 1$). The computed average is very close to one (red lines on the figure) which guarantees the exactness of the algorithm.

As we mentioned before, the eigenvalue of the Dirac operator in the heavy sector, has to be computed during a PHMC run, in order to be sure that the polynomial expansion of inverse of the square root has the required precision. We checked along the run that a suitably normalized operator has its eigenvalues in the interval $[\epsilon, 1]$. Keeping the same run as in Fig. 4.3 and with $\epsilon = 2.10^{-5}$, we illustrate in Fig. 4.6 and 4.7 the fluctuation of the minimal and maximal eigenvalues as a function of the Monte-Carlo time.

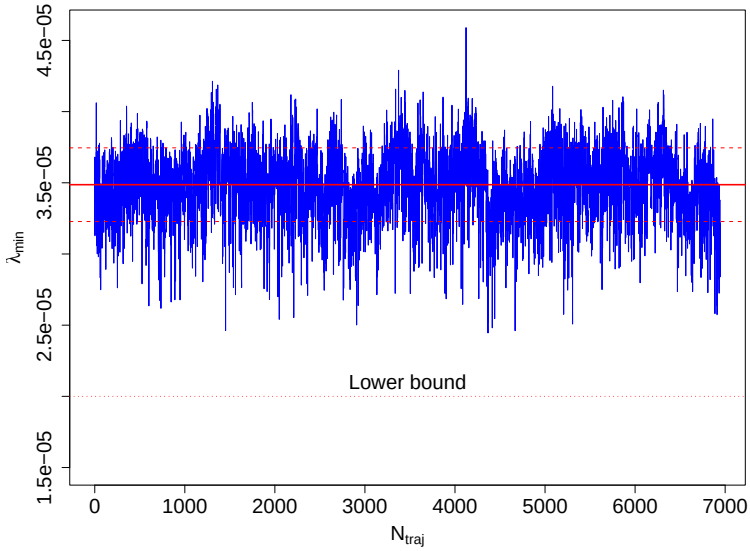

Figure 4.6: Minimal eigenvalue history for the run used in Fig. 4.3

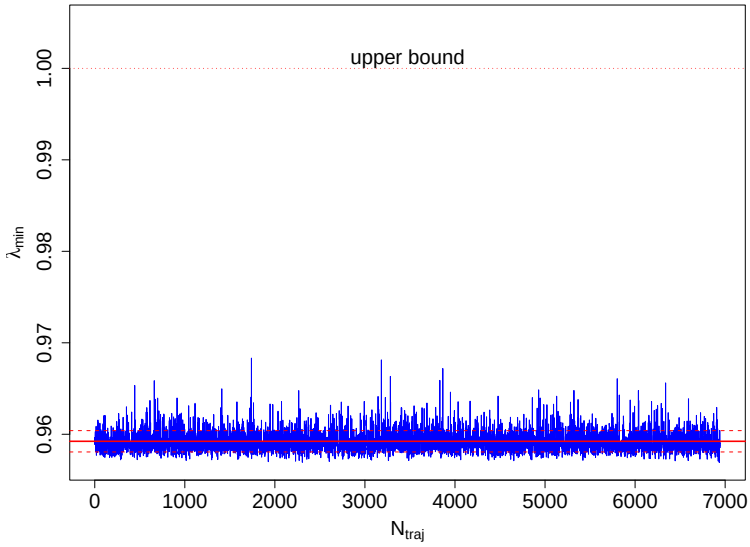

Figure 4.7: Maximal eigenvalue history for the run used in Fig. 4.3

We clearly see the fluctuations of the lowest eigenvalue, which stays above ϵ. Conversely, the highest eigenvalue remains smaller than 1 as needed, and we can safely use this ensemble without suspecting a failure in the convergence of the algorithm.

4.2.2 Dependance on the light quark mass

We cannot close this part without showing the qualitative behaviour of some observables as a function of the light quark mass. Actually, this will face us with one of the major problems of lattice QCD when trying to compute physical observable at the physical pion mass. This issue is of central importance since, as we will see in chapter 6 and 7, the extrapolation procedure used to reach this point is the most important source of systematic error in lattice QCD.

We will summarise this, by showing only two results which already give us a feeling of what is happening when the light quark mass decreases. First of all we compare the time distribution on a BlueGene/P needed to generate one configuration at maximal twist in Fig. 4.8 for two different value of the light quark mass. Keeping the same physical volume and the same local volume on each processor of the computer (in this case one rack of BlueGene namely 4096 CPUs), we observe that when dividing the quark mass by a factor three, the computation time increases by 30%. The order of magnitude of the physical time needed to generate 5000 trajectories is of 55 consecutive days of numerical computation on one BG/P rack. Note that we neglect here the time needed to tune $\kappa_{\rm cr}$ to maximal twist, although is was far from negligible !

In this case the lightest quark mass corresponds to a pion mass of ~ 270 MeV which is still two times heavier than the physical value. In this regime, the HMC algorithm scales slowly as a function of μ. When approaching the physical value the time needed to produce one trajectory increases dramatically.

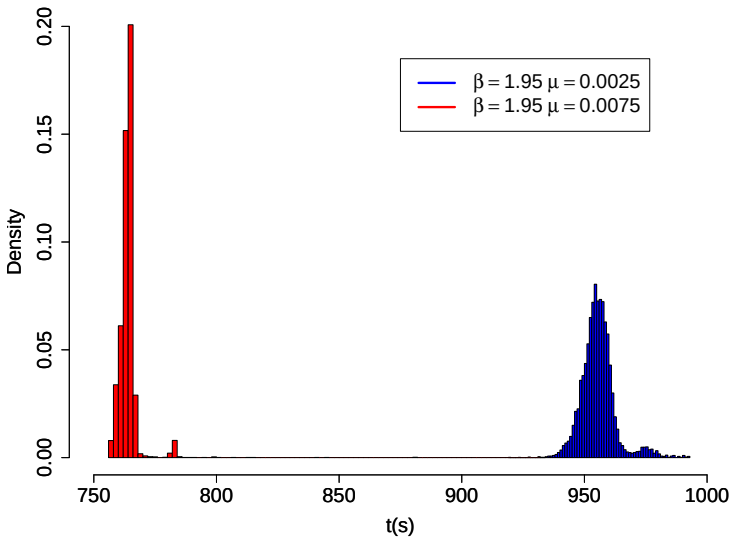

Figure 4.8: Distribution of the time needed to produce one trajectory for two runs, $L = 32$, $T = 64$ run at $\beta = 1.95$, $a\mu_\sigma = 0.135$ and $a\mu_\delta = 0.17$, the light quark masses are $\mu = 0.0025$ (blue) and $\mu = 0.0075$ (red).

We display in Fig. 4.9 the Monte Carlo history and the distribution of the plaquette for the same runs than for the previous figure. We observe that fluctuations increase when the light quark mass is decreased. The (normalized) plaquette distributions are also shown, and confirm that dispersion of the results is larger for the light quark mass. The history also shows longer

wavelength fluctuations over the Monte Carlo time for the smallest μ value. This generates large autocorrelation times which makes difficult the analysis and increases the statistical errors. For some particular physical parameters one can even suspect that the HMC algorithm failed to explore the whole configuration space because of the very large autocorrelation time. The statistical errors are then underestimated, and it is therefore impossible in a reasonable amount of time to perform physical measurements.

This effect can be quantified by estimating the integrated autocorrelation time for several observable as the pseudoscalar mass is decreased.

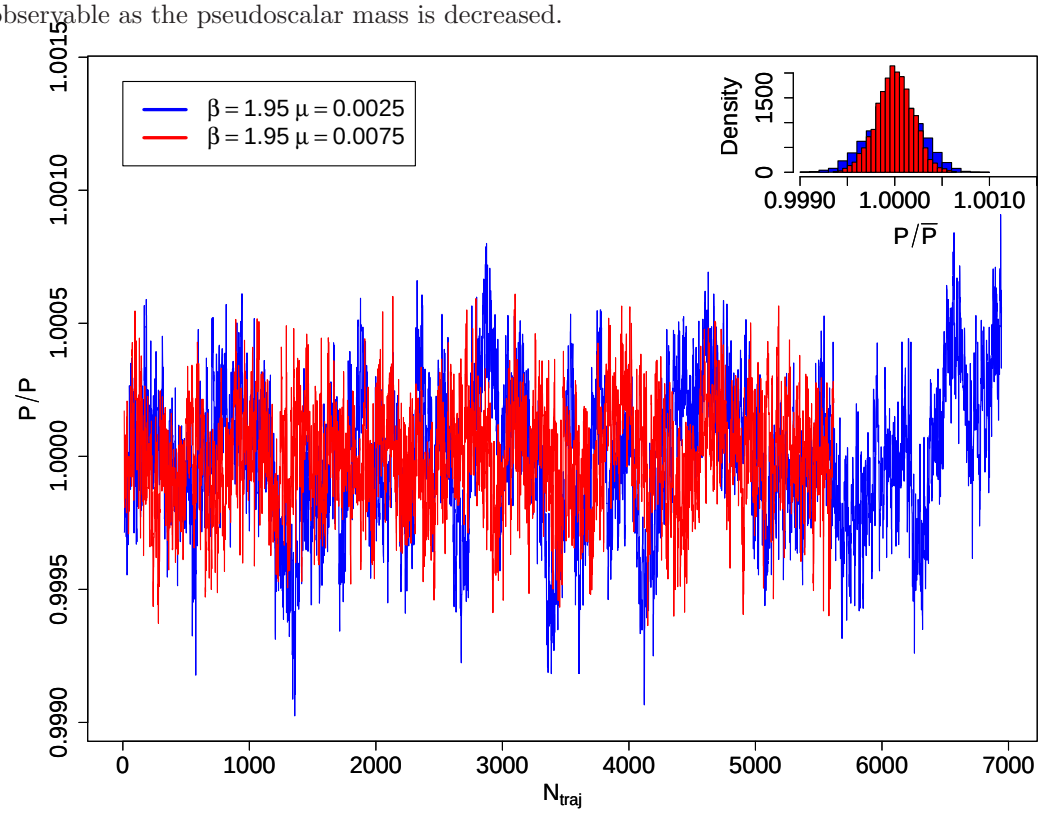

Figure 4.9: Comparison of the plaquette history and of the distribution of the measurement for the two runs used in Fig. 4.8

The explosion of the computation time for light quark mass is due to a QCD property often refered as the *critical slowing down*. Note, however, that substantial and encouraging efforts are done in the community to improve the algorithm, and that the improvement realized during the last years already yield significative progress. Note that first simulations "at the physical point" have been performed during my Ph.D by the collaboration PACS-CS [75] and BMW [76].

4.3 Tuning and online measurements

Additional informations are provided by online measurements that compute significant correlators during the run. They are performed with a frequency that can be changed, but in general every two trajectories. They involve one extra inversion of one stochastic source [77] (see [78] for a review). Using the one-end-trick [78, 79] one can reconstruct three correlators of the light

sector, namely $\langle PP \rangle$, $\langle PA \rangle$ and $\langle PV \rangle$ with

$$\begin{aligned} P^a &= \overline{\chi}\gamma_5 \frac{\tau^a}{2}\chi \\ V^a_\mu &= \overline{\chi}\gamma_\mu \frac{\tau^a}{2}\chi \\ A^a_\mu &= \overline{\chi}\gamma_5\gamma_\mu \frac{\tau^a}{2}\chi \end{aligned} \tag{4.20}$$

From $\langle PP \rangle$ we can obtain the pseudoscalar mass together with the pseudo scalar decay constant in the twisted mass case. From $\langle PP \rangle$ and $\langle PA \rangle$ we can measure the fundamental quantity that allow to tune a run at maximal twist, namely the PCAC quark mass. Finally in the correlator $\langle PV \rangle$ we can extract the renormalization constant Z_V. Further details are given in [80].

These correlators are analysed using the Γ-Method analysis, and the bootstrap is used to cross check results.

Choosing the strategy to tune m_{PCAC} to zero at each value of the light quark mass insures us that we are at maximal twist. The tuning is done using several hundreds of trajectory for different value of the Wilson quark mass (m_0) until the criterium

$$m_{\mathrm{PCAC}} = 0 \pm 0.1\mu \tag{4.21}$$

is satisfied.

We show in Fig. 4.10, the maximal twist tuning plot for the $32^3 \times 64$ run at $\beta = 2.0$, $\mu = 0.0025$, $\mu_\sigma = 0.15$ and $\mu_\delta = 0.16$. The two dotted lines correspond to the bound of Eq. (4.21). We show the lattice results (empty circles) for four values of κ and we indicate by a star the linearly interpolated value of the optimal κ_{cr}. We see that our last trial gives a satisfactory well tuned value and corresponds to $\kappa = 0.159441$. Note that the three other points have cost ~ 1500 trajectories which cannot be used to produce physics results. However the last value is well tuned at maximal twist and guarantee automatic $\mathcal{O}(a)$ improvement.

Before closing this section, we show in Fig. 4.11 the PP correlator for a $32^3 \times 64$ run at $\beta = 1.95$ and $\mu = 0.0025$. A hyperbolic cosine fit allows to extract the pseudoscalar mass together with the pseudoscalar decay constant (see Eq. (3.9)). Note that in practice, mesonic two-points correlators are usually extremely precise. Their accuracy can be even improved by using stochastic techniques that decrease the variance of the measurement.

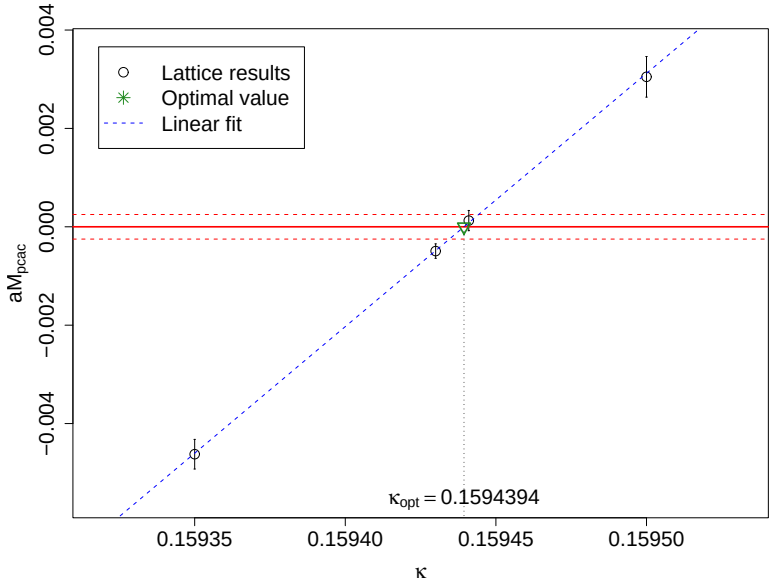

Figure 4.10: Tuning κ for $\beta = 2.0$ and $a\mu_l = 0.0025$ on a $32^3 \times 64$ lattice. We show am_{PCAC} as a function of κ for 4 values of κ (empty circle). We indicate by a star the linearly interpolated value of the optimal κ_{cr}.

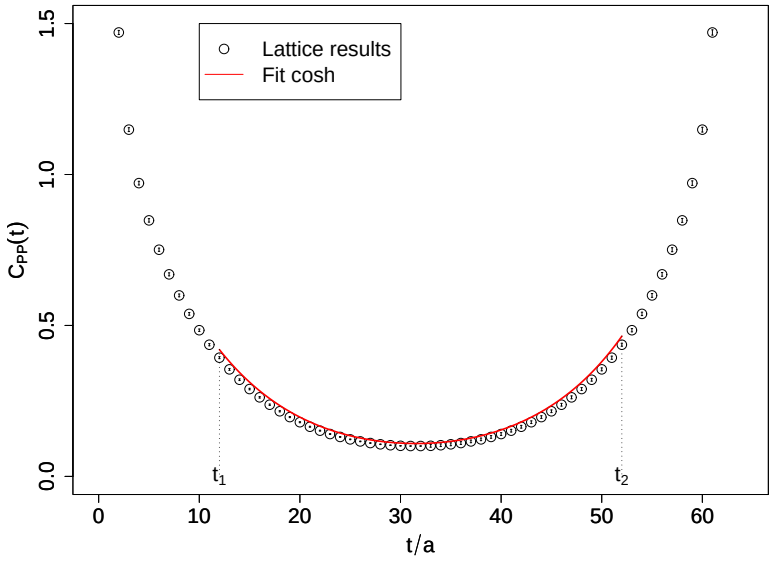

Figure 4.11: Pseudoscalar correlator as a function of t/a obtained with online measurements on a $32^3 \times 64$ lattice at $\beta = 1.95$, $a\mu_l = 0.0025$. A hyperbolic cosine fit is shown in the range $[11, 51]$ to guide the eyes.

4.4 $N_f = 2$ simulations

We present in this chapter the $N_f = 2$ gauge ensembles together with some selected physical results that will be useful in my baryon analysis. Most of them are taken from [81].

4.4.1 Gauge configurations

In Table 4.1 we summarize the $N_f = 2$ gauge configuration ensembles generated by the ETM collaboration. Simulations are performed at the four values $\beta = 3.8$, $\beta = 3.9$, $\beta = 4.05$ and $\beta = 4.2$. The lattice spacing is fixed using χPT based formaluae to fit our data for $f_{\rm PS}$ and $m_{\rm PS}$ using the physical value of f_π and m_π as input. The corresponding lattice spacings are $a_{\beta=3.8} \approx 0.1$ fm, $a_{\beta=3.9} \approx 0.079$ fm,$a_{\beta=4.05} \approx 0.063$ fm and $a_{\beta=4.2} \approx 0.051$ fm.

For each values of β, we have several values of the bare twisted quark mass $a\mu_q$. They have been chosen such that they cover a range of pseudoscalar mass between 280 MeV and 650 MeV.

The physical box length L in most of the simulation is $\sim$ 2fm. For all the runs we impose the inequality

$$m_{\rm PS} L \gtrsim 3 \tag{4.22}$$

This guarantees in principle that the volume effects are under control. Note that we use the mass of the charged pseudoscalar meson to fulfill this criterium. As we will see latter, at finite lattice spacing, the mass of the neutral pseudoscalar meson is substantially lower and condition Eq. (4.22) is far from being fulfilled. Taking as a reference $m^{\pm}_{\rm PS}$ is however justified by the fact that the splitting is a large $\mathcal{O}(a^2)$ effect and by checking for anomalous volume effects in various observables. So far, no large finite size effects have been observed. The box size in fermi together with the $m_{\rm PS}L$ value for our runs are shown in Table 4.1.

4.4.2 Main results

Until now we have explained how to compute physical observables on a lattice. However, in order to make reliable and quantitative predictions, a careful study of systematic errors is mandatory. One of the important systematic effects that we will be concerned in all this work are the lattice discretization effects.

To this aim one needs to compare lattice data obtained at several β values. This cannot be done without defining a system of units. Let us consider for instance a hadron mass measured in lattice units. We denote it by aM. As we explained in chapter 1 the continuum limit is obtained for $aM \to 0$, a regime in which the typical correlation length (or Compton wavelength) becomes large compared to the lattice spacing. To define the continuum limit of the theory we need to construct a finite non vanishing quantity in the limit $a \to 0$. In principle this can be achieved, by choosing any QCD dimensionfull observable, denoted by Λ. If we assume that Λ has the dimension of a length, then by computing, Λ/a one the lattice on can express at finite lattice in units of Λ any other observable :

$$\Lambda M = \frac{\Lambda}{a} aM \tag{4.23}$$

ΛM is a measurement of the mass "in units of Λ". For instance Λ can be the Compton wavelength of the pseudoscalar meson. All observables will be in this case expressed relatively to the pion wavelength, or equivalently relatively to the pion mass.

It is important to understand that the theory predicts only dimensionless quantities and that system of units are a convenient way to compare observables with the real world. Such a system of units does not need to be in GeV. Units are only references to compare quantities, and they are not contained in the model. To use the standard system of units we need to match as many observables as parameters to find the conversion factors between the system of units. These two

Ensemble	$(L/a)^3 \times T/a$	β	$a\mu_q$	$\kappa_{\rm crit}$	$\tau_{\rm int}(P)$	$\tau_{\rm int}(am_{\rm PS})$	τ
A_1	$24^3 \times 48$	3.8	0.0060	0.164111	190(44)	8(2)	1.0
A_2			0.0080		172(80)	10(2)	1.0
A_3			0.0110		130(50)	6(1)	1.0
A_4			0.0165		40(12)	6(1)	1.0
A_5	$20^3 \times 48$		0.0060		250(100)	5(1)	1.0
B_1	$24^3 \times 48$	3.9	0.0040	0.160856	47(15)	7(1)	0.5
B_2			0.0064		23(7)	17(4)	0.5
B_3			0.0085		13(3)	10(2)	0.5
B_4			0.0100		15(4)	7(2)	0.5
B_5			0.0150		30(8)	20(6)	0.5
B_6	$32^3 \times 64$		0.0040		37(11)	2.8(3)	0.5
B_7			0.0030		51(19)	7(1)	1.0
C_1	$32^3 \times 64$	4.05	0.0030	0.157010	18(4)	7(1)	0.5
C_2			0.0060		10(2)	9(2)	0.5
C_3			0.0080		13(3)	7(1)	0.5
C_4			0.0120		5(1)	4.8(6)	0.5
C_5	$24^3 \times 48$		0.0060		12(2)	11(1)	1.0
C_6	$20^3 \times 48$		0.0060		10(2)	7(1)	1.0
D_1	$48^3 \times 96$	4.2	0.0020	0.154073	13(2)	≤ 8	1.0
D_2	$32^3 \times 64$		0.0065		6(1)	≤ 8	1.0

Table 4.1: Summary of (20) ensembles generated by ETMC. We give the lattice volume $L^3 \times T$ and the values of β, the twisted mass parameter $a\mu_q$, the critical hopping parameter $\kappa_{\rm crit}$ as determined at $\mu_{q,\rm min}$ and the trajectory length τ. The values of the lattice spacing that correspond to the four values of β are $a \approx 0.1\,$fm ($\beta = 3.8$), $a \approx 0.079\,$fm ($\beta = 3.9$), $a \approx 0.063\,$fm ($\beta = 4.05$) and $a \approx 0.051\,$fm ($\beta = 4.2$). In addition we provide values for the integrated autocorrelation time of two typical quantities, the plaquette P and the pseudo scalar mass $am_{\rm PS}$, in units of $\tau = 0.5$. We refer to ref. [80] for details on the determination of the autocorrelation time.

steps are often merged in one by choosing for instance Λ to be the inverse nucleon mass m_N in GeV^{-1}, and thus by fixing directly the lattice spacing.

A good system of units is defined through an observable that can be computed on the lattice with a good precision.

The Sommer parameter r_0, first introduced in [82], satisfies this last criterium and will be extensively used in this work as a system of units convenient to compare lattice simulations. The quantity r_0/a is defined via the force between static quarks and is extracted from a purely gluonic correlation function. It has the advantage of being accurately determined in lattice QCD simulations. However the value of r_0 in physical units ($r_0 \approx 0.45$fm) is not well known.

The Sommer scale will be used in practice to study the continuum limit presented in chapter 6 and 7. We thus briefly discuss here its measurement, for a more detailed explanation see [80]. We show in Fig. 4.12 r_0/a as a function of $(a\mu_q)^2$ for $\beta = 3.9$ (a) and $\beta = 4.05$ (b). The mass dependence is rather weak and consistent with a linear fit. Note that this small dependence makes the extrapolation to the chiral limit ($\mu_q = 0$) reliable and explains why r_0/a defines a convenient system of units. A precise study of the extrapolation procedure of r_0/a leads to the r_0^χ/a values shown in Table 4.2 together with its systematical errors.

As explained in chapter 2, our strategy to reach maximal twist for $N_f = 2$ simulations, is to tune am_0, for the lowest bare twisted quark mass $a\mu_q$ such that $m_{\rm PCAC}$ defined in Eq. (2.24)

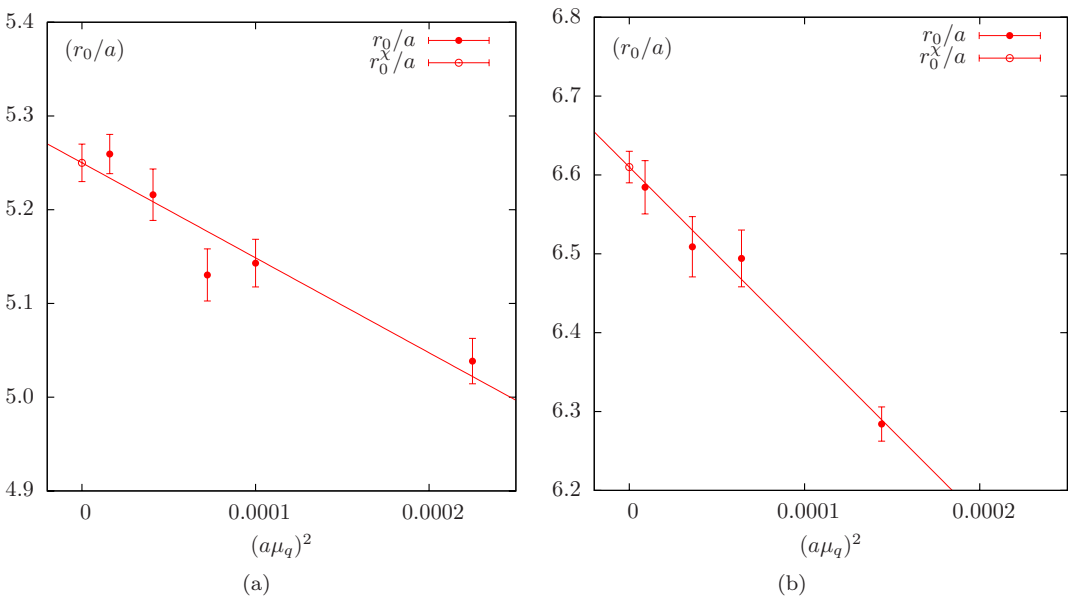

Figure 4.12: r_0/a as a function of $(a\mu_q)^2$ for (a) $\beta = 3.9$ and (b) $\beta = 4.05$. The lines represent a linear extrapolation in $(a\mu_q)^2$ to the chiral limit. Note that we have always used the largest available volume for a given value of $a\mu_q$, see table 4.1.

β	r_0^χ/a
3.8	4.462(45)
3.9	5.631(39)
4.05	6.727(48)
4..2	8.358(63)

Table 4.2: r_0^χ/a extrapolate using a quadratic fit. The errors are statistical and systematical added in quadrature. Results taken from [81].

vanishes. More precisely we demand to fulfill the condition[2]

$$|Z_A a m_{\mathrm{PCAC}}/a\mu_q| \leq 0.1 \tag{4.24}$$

with an error satisfying

$$\Delta(|Z_A a m_{\mathrm{PCAC}}/a\mu_q|) \leq 0.1 \tag{4.25}$$

Another condition is that the value of $a\mu_q$ chosen to make the tuning correspond to a pseudoscalar mass of ≈ 300 MeV for all values of β. We recall that the pertinence of this criteria, which guarantees automatic $\mathcal{O}(a)$ improvement, is discussed in [80].

We show in Fig. 4.13 our measurement of $Z_A a m_{\mathrm{PCAC}}/a\mu_q$ as a function of $(r_0\mu_R)^2$ for our gauge ensembles tuned to maximal twist. The value of the renormalized quark mass for which the runs have been tuned is indicated by an arrow. Note that, in this region of pseudoscalar mass and for the three largest β values, the measurements are compatible within the error. At

[2]Note that here we use the renormalized version of the criterium Eq. (4.21). This is possible since renormalization constant have been determined. The tuning has however been done without the knowledge of the renormalization factors.

$\beta = 3.8$, large autocorrelation times were observed at the lowest quark mass. We include in Fig. 4.13 only the ensembles for which a reliable estimation of $m_{\rm PCAC}$ was possible.

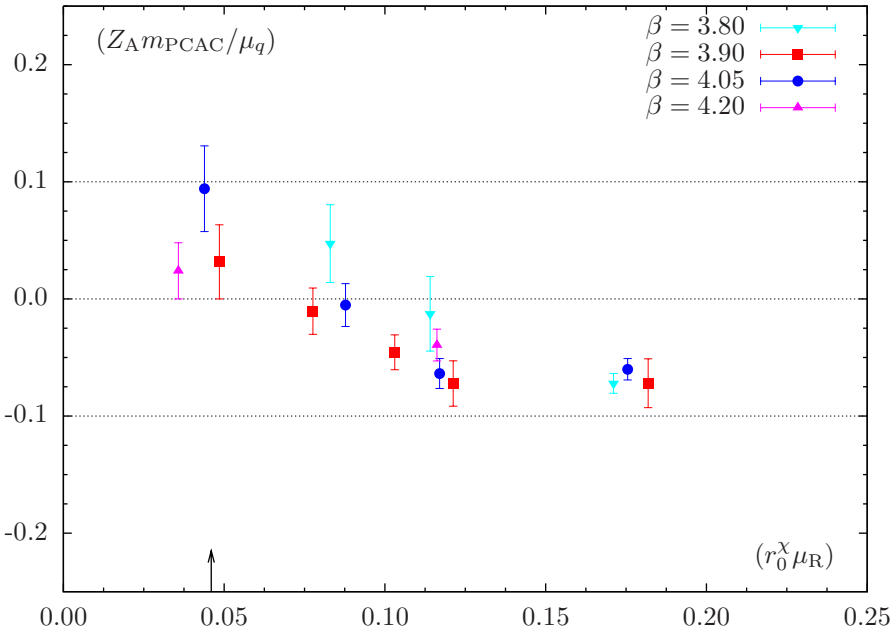

Figure 4.13: Renormalised ratio of the PCAC quark mass over the twisted mass against the renormalised twisted mass $\mu_{\rm R} = \mu_q/Z_{\rm P}$ at the four values of β. The statistical uncertainties on $Z_{\rm P}$ and $Z_{\rm A}$ are not included. The data at $\beta = 4.2$ have been included by estimating the renormalisation constants as described in the text. At $\beta = 3.8$, the data for the lightest quark mass has not been included for the reasons explained in the text. The band indicates our condition for tuning to maximal twist, which is clearly achieved to a good precision. The arrow indicates the value of $r_0^\chi \mu_{\rm R}$ where we tuned the PCAC mass to zero.

In order to compare the data of the pseudoscalar decay constant at $\beta = 3.9$, $\beta = 4.05$ and $\beta = 4.2$, three values of reference pseudoscalar mass have been chosen: $r_0^\chi m_{\rm PS} = 0.614$ (which correspond to the lightest pseudoscalar mass of the $\beta = 4.2$ ensemble), $r_0^\chi m_{\rm PS} = 0.900$ and $r_0^\chi m_{\rm PS} = 1.100$. The corresponding values of $f_{\rm PS}$ are obtained by (small) interpolation. The data are also extrapolated using χPT to the same volume of reference $r_0^\chi L = 5.0$.

We show in Fig. 4.14(a) the scaling of the pseudoscalar decay constant $f_{\rm PS}$ in finite volume, for a fixed pseudoscalar mass $r_0^\chi m_{\rm PS}$, as a function of $(a/r_0)^2$. When possible, data points obtained for $\beta = 3.8$ are shown but not included in the linear continuum extrapolation. They are in good agreement with the fit obtained using $\beta = 3.9$, $\beta = 4.05$ and $\beta = 4.2$. The slope of the curve is very small, indicating small lattice artefacts.

In Fig. 4.14(b) we show $(r_0^\chi m_{\rm PS})^2$ as a function of $(a/r_0)^2$ for three values of the renormalized quark mass. The data obtained with our smallest lattice spacing were not included because the renormalization constant Z_P is missing. The continuum extrapolation is flat, and proves that twisted fermions offers a good approach to the continuum with small $\mathcal{O}(a^2)$ artefacts, at least for the charged pseudoscalar decay constant and mass.

As explained in the chapter 2, the twisted mass approach has the drawback of breaking isospin symmetry at finite lattice spacing. The main consequence is that large cutoff effects are observed in the difference between the neutral ($m_{\rm PS}^0$) and charged ($m_{\rm PS}^\pm$) pseudoscalar masses. Note that, in view of Eq. (3.28), the evaluation the two-point correlation function of neutral mesons involves the computation of disconnected diagrams making difficult a precise estimation

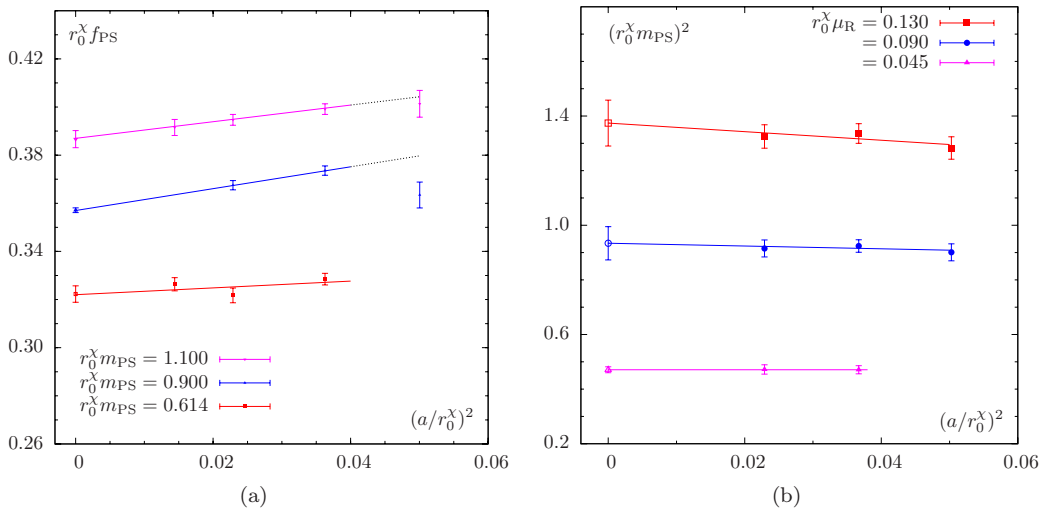

Figure 4.14: Scaling in finite, fixed volume for $r_0^\chi f_{\rm PS}$ at fixed values of $r_0^\chi m_{\rm PS}$ (a) and for $(r_0^\chi m_{\rm PS})^2$ at fixed values of $r_0^\chi \mu_R$ (b). In (b) we cannot include data at $\beta = 4.2$ due to the missing value of the renormalisation factor $Z_{\rm P}$.

of its mass. Using stochastic techniques, disconnected contribution are nevertheless evaluated with a reasonable precision.

We show in Fig. 4.15 the mass splitting between the charged and neutral pseudo scalar mesons as a function of $(a/r_0)^2$ for two different masses of $m_{\rm PS}^{\pm}$. We observe that $m_{\rm PS}^0$ is contaminated with large $\mathcal{O}(a^2)$ effects since $m_{\rm PS}^{\pm}$ has a flat continuum scaling (Fig. 4.14(b)). Note that $(r_0^\chi m_{\rm PS})^2 \sim 0.5$ for $\beta = 3.9$ and $a\mu_q = 0.004$, we thus have an isospin breaking $\sim 35\%$ in our $N_f = 2$ simulations. Note that curiously, in dynamical simulations the neutral pseudoscalar mass is smaller than the charged one, unlike in the quenched approximation [83].

β	$a^{f_{\rm PS}}$ (fm)
3.8	0.0998(19)
3.9	0.079(2)(2)
4.05	0.063(1)(2)
4..2	0.05142(83)

Table 4.3: Lattice spacing fixed using $f_{\rm PS}$, statistical and systematical error estimations are discussed in [81]. Data at $\beta = 3.8$ are used only for cross check and therefore systematic errors are not estimated. Systematic errors at $\beta = 4.2$ are not estimated at the time of the writing because of the unknown value of $Z_P(\beta = 4.2)$.

4.5 $N_f = 2+1+1$ simulations

The ETM Collaboration stopped to produce $N_f = 2$ configurations, and all the computational efforts are now devoted to $N_f = 2+1+1$. As explained in chapter 2, our strategy to tune to maximal twist is to impose simultaneously $m_{\rm PCAC} = 0$ with $m_{0,l} = m_{0,h}$ and with an accuracy $m_{\rm PCAC}/\mu_l < 0.1$. As explained in [84], the tuning of the PCAC mass is performed independently for each value of μ_l. It guarantees automatic $\mathcal{O}(a)$ improvement. Two additional parameters

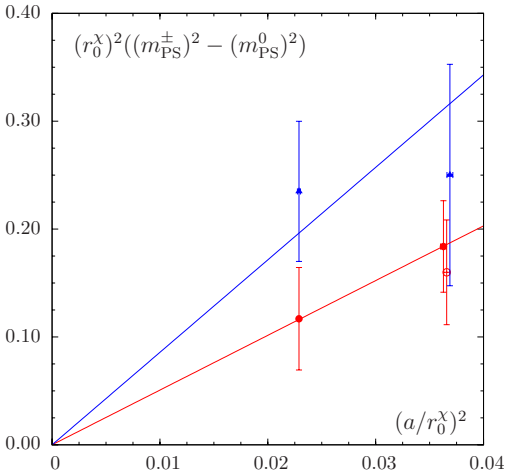

Figure 4.15: The difference of the squared charged and neutral pseudo scalar masses as a function of a^2 in the $N_f = 2$ twisted mass formulation of lattice QCD at two different values of the charged pseudo scalar mass. A significant $O(a^2)$ lattice artefact is observed. The circles (triangles) correspond to a value of the charged pion mass of about 330 (430) MeV. The open circle is a larger physical volume. The lines are only to guide the eye and some points are slightly horizontally displaced for better visibility. Note that $r_0^\chi m_{\rm PS}^\pm$ was not held fixed for this plot, however, due to the large uncertainties on $m_{\rm PS}^0$ the picture should not significantly depend on this approximation.

that control the strange and the charm quark mass are needed compared to the $N_f = 2$ case. These parameters require additional tuning. Let us recall the relation between the renormalized strange (m_s) and charm quark mass (m_c) and the bare parameters μ_σ and μ_δ:

$$(m_{s,c})_{,R} = \frac{1}{Z_P}(\mu_\sigma \mp \frac{Z_P}{Z_S}\mu_\delta) \tag{4.26}$$

Because of the flavour mixing, the tuning of the renormalized strange (respectively charm) quark mass cannot be done independently of the renormalized charm (respectively strange) quark mass. In practice we fix the couple (μ_σ, μ_δ) to their matching value $(\mu_\sigma^{\rm matching}, \mu_\delta^{\rm matching})$ by requiring the following condition:

$$\begin{aligned} m_K^{\rm phys} &= m_K^{\rm lat}(m_\pi, \mu_\sigma^{\rm matching}, \mu_\delta^{\rm matching}) \\ m_D^{\rm phys} &= m_D^{\rm lat}(m_\pi, \mu_\sigma^{\rm matching}, \mu_\delta^{\rm matching}) \end{aligned} \tag{4.27}$$

where $m_{K,D}^{\rm lat}(m_{\rm PS}, \mu_\sigma, \mu_\delta)$ is computed for several values of the parameters μ_l, μ_σ and μ_δ and then extrapolated to $m_{\rm PS} = m_\pi$ using χPT.

Compared to $N_F = 2$ simulations, we use the Iwasaki action for the gluon instead of the tree level Symanzik one as explained in chapter 2. With this gauge action we observe a smoother dependence of quantities sensitive to possible phase transition. The change of gauge action explains why the β values are quite different (β roughly divided by a factor 2 for the same lattice spacing).

In Table 4.4 we summarize the $N_f = 2 + 1 + 1$ runs generated by the ETM collaboration. Each run in the table has $\sim$ 5000 thermalized trajectories. In order to convince ourself that simulations were under control, our first goal was to study the systematic effects and to compare

our results with our well established $N_F = 2$ case. That is why we have generated ensembles for two values of the lattice spacing corresponding to $\beta = 1.90$ and to $\beta = 1.95$. To study the finite volume dependence we also simulate three volumes at $\beta = 1.90$ at a pseudoscalar mass of ~ 300 MeV corresponding to a bare light quark mass of $\mu_l = 0.004$. Two runs have been dedicated to the tuning of strange and charm quark masses. Note that simulations on a two smaller lattice spacings corresponding to $\beta = 2.0$ and $\beta = 2.1$ and smaller quark mass are running on the supercomputers.

Label	β	κ	$a\mu_l$	$a\mu_\sigma$	$a\mu_\delta$	L/a	T/a	$m_\pi L$	$\lvert\epsilon/\mu_l\rvert$
$A40.20$	1.90	0.1632700	0.0040	0.150	0.190	20	48	3.0	0.14(14)
$A40.24$	1.90	0.1632700	0.0040	0.150	0.190	24	48	3.5	0.07(14)
$A60.24$	1.90	0.1632650	0.0060	0.150	0.190	24	48	4.1	0.03(3)
$A80.24$	1.90	0.1632600	0.0080	0.150	0.190	24	48	4.8	0.02(2)
$A100.24$	1.90	0.1632550	0.0100	0.150	0.190	24	48	5.3	0.02(2)
$A100.24s$	1.90	0.1632550	0.0100	0.150	0.197	24	48	5.3	0.35(1)
$A30.32$	1.90	0.1632720	0.0030	0.150	0.190	32	64	4.0	0.08(7)
$A40.32$	1.90	0.1632700	0.0040	0.150	0.190	32	64	4.5	0.04(5)
$A50.32$	1.90	0.1632670	0.0050	0.150	0.190	32	64	5.0	0.05(2)
$B25.32$	1.95	0.1612400	0.0025	0.135	0.170	32	64	3.4	0.06(6)
$B35.32$	1.95	0.1612400	0.0035	0.135	0.170	32	64	4.0	0.02(2)
$B55.32$	1.95	0.1612360	0.0055	0.135	0.170	32	64	5.0	0.08(1)
$B75.32$	1.95	0.1612320	0.0075	0.135	0.170	32	64	5.8	0.05(1)
$B85.24$	1.95	0.1612312	0.0085	0.135	0.170	24	48	4.6	0.01(2)

Table 4.4: Input parameters, $m_\pi L$ and $|\epsilon/\mu_l|$ for all ensembles used in this paper. Every ensemble has ~ 5000 thermalized trajectories of length $\tau = 1$. We have two main ensemble sets: A and B, at $\beta = 1.90$ and $\beta = 1.95$ respectively.

4.5.1 Selected non baryonic results

Our first attempt to fix the scale was done using the Sommer parameter r_0/a. It has the advantage to be a pure gauge quantity and can be accurately computed.

We show in Fig. 4.16, the variation of r_0/a as a function of $(a\mu_l)^2$ the bare light quark mass squared. We compare one $N_f = 2$ run at $\beta = 3.9$ and a $N_f = 2+1+1$ run at $\beta = 1.95$ normalized at the lightest quark mass. The first observation is that the μ_l dependence is more pronounced in the $N_f = 2+1+1$ case than in the $N_f = 2$ one. Since $r0/a$ is very sensitive to κ in the vicinity of $\kappa_{\rm crit}$, the fact that we now tune to maximal twist at every value of $a\mu_l$, might, provide an explanation for the observed change of slope. These differences tend to diminish when increasing the value of β.

Using a quadratic fit of the form

$$\frac{r_0}{a} = \frac{r_0^\chi}{a} + \alpha a^2 \mu_l^2 \tag{4.28}$$

one can extrapolate to the chiral limit r_0^χ/a. Our first estimates of this important quantity is then summarized in Table 4.5 which includes only statistical errors. We would like to emphasize that despite the smallness of the statistical error in Table 4.5, our estimation of the Sommer parameter is much weaker than in the $N_f = 2$ case. This is due to our present lack of control on systematic errors.

β	r_0^χ/a
1.90	5.24(2)
1.95	5.71(4)

Table 4.5: r_0^χ/a extrapolate using a quadratic fit. Only statistical errors are shown.

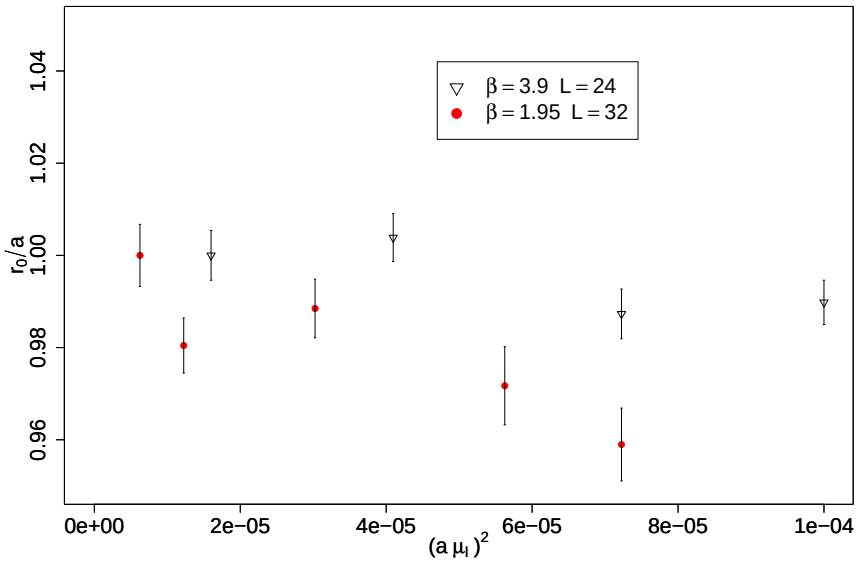

Figure 4.16: Comparison between $N_f = 2$ and $N_f = 2 + 1 + 1$ of the variation of r_0/a as a function of $(a\mu_l)^2$ the bare light quark mass squared. Data have been normalized at the smallest value of the light quark mass.

As we explained previously in this chapter, $am_{\rm PS}$ and $af_{\rm PS}$ can be determined during the run using the online measurements. In order to improve the error bars, offline measurements are performed that allow to extract them with smaller statistical error bars. We plot in Fig. 4.17 $r_0^\chi f_{\rm PS}$ as a function of $(r_0^\chi m_{\rm PS})^2$, for the $\beta = 1.95$ run and for several $N_f = 2$ runs. The data does not include volume corrections.

In order to extract the lattice spacing from our data sets, we perform a next to leading order $SU(2)$ chiral perturbation theory fit of the computed $m_{\rm PS}$ and $f_{\rm PS}$. We use continuum formulae and correct for finite size effects both à la Gasser and Leutwyler [85], or with two additional low energy constant $\bar{l}_1$ and $\bar{l}_2$, as described in [86]. The results are listed in table 4.6. We have performed these fits for the ensembles A and B separately, and also by combining them in a single fit. In table 4.6, we include a systematic error, estimated at $2 - 5\%$, coming from the dispersion between NLO and NNLO fits.

Note that since the quark mass enters in the χPT expression, combining the two sets at different lattice spacings requires the knowledge of the quark mass renormalization factor $Z_\mu = 1/Z_P$ which is not yet available. To overcome this difficulty we consider the ratio of Z_P at two β values as additional parameters of the fit. We use as inputs the physical f_π and m_π, and extract f_0, $\bar{l}_3$ and $\bar{l}_4$. A complete analysis (analogous to [87]) of the systematic effects is in progress.

The isospin breaking in the light pseudoscalar mesons sector has been estimated by Carsten

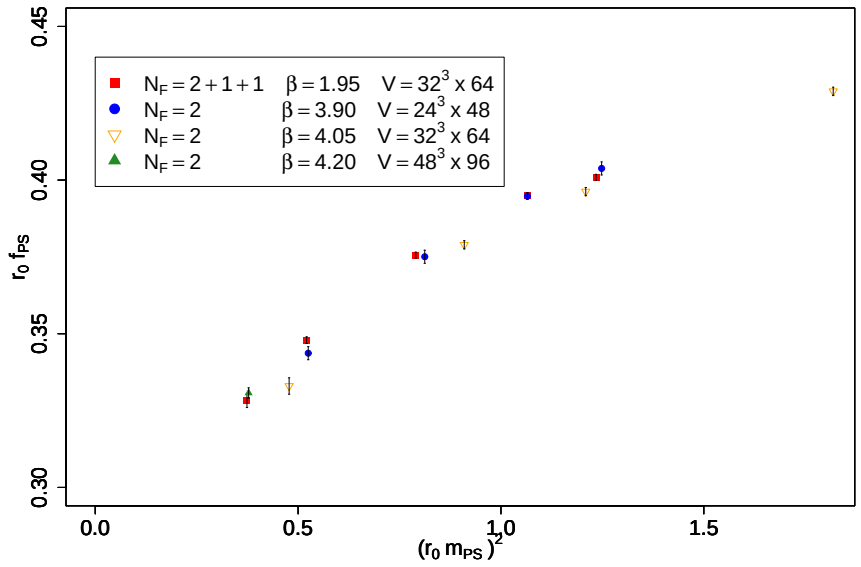

Figure 4.17: Comparison between $N_f = 2$ and $N_f = 2+1+1$ of the variation of $r_0 f_{\rm PS}$ as a function of $(r_0 m_{\rm PS})^2$.

set	pts	f_0(MeV)	l_3	l_4	$a_{\beta=1.90}$(fm)	$a_{\beta=1.95}$(fm)
$\mathcal{A}$ & $\mathcal{B}$	11	121(4)	3.5(2)	4.7(2)	0.086(6)	0.078(6)
$\mathcal{A}$	6	121(4)	3.4(2)	4.8(2)	0.086(7)	
$\mathcal{B}$	5	121(4)	3.7(2)	4.7(2)		0.078(7)

Table 4.6: Results from the NLO $SU(2)$ χPT fits for combined, only set A and only set B respectively. Errors are dominated by a systematic error of $2-5\%$ due to performing an NLO fit. The column "pts" refers to the number of ensembles used in that fit.

Urbach for *two* gauge ensembles. We show in Fig. 4.18 the relative difference between the neutral and charge pseudoscalar states as a function of $(a/r_0^\chi)^2$. In order to compare with our $N_f = 2$ data. we show, with empty triangle and for a fixed pseudoscalar reference mass, the corresponding results. The isospin breaking is dramatically large in $N_f = 2+1+1$ simulations, with for instance a neutral pseudoscalar meson mass of about $\sim 50\%$ of the charged one at $\beta = 1.90$. This led us to the conclusion that we have to decrease the lattice spacing in order to be in the same setup than in our well understood $N_f = 2$ simulations. This explain our actual strategy which consists to run with $\beta = 2.0$ and $\beta = 2.1$. Note that the isospin breaking at $\beta = 1.95$ is already comparable to the $N_f = 2$ case. Details concerning the analysis in the light sector can be found in [88]. A paper concerning the analysis in the heavy sector is already submitted [89].

We will come back to the isospin breaking issue in the baryon sector in chapters 6 and 7.

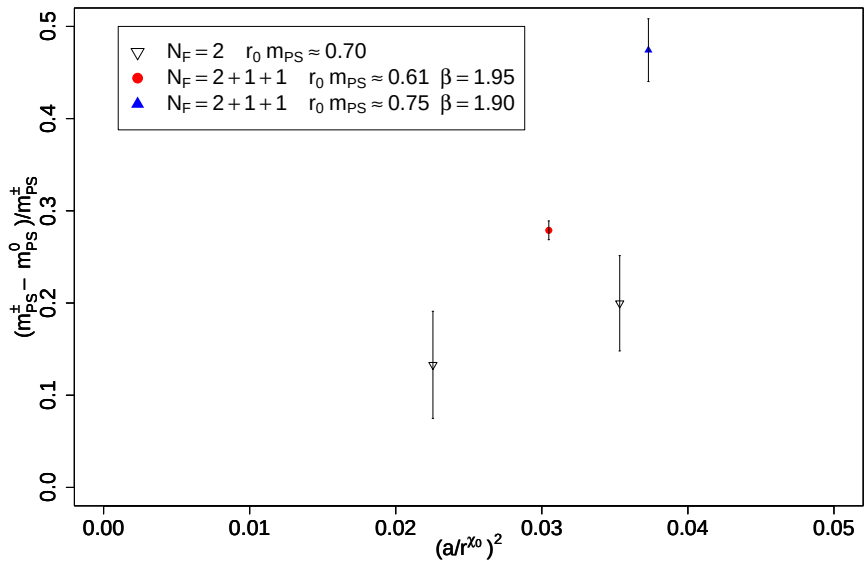

Figure 4.18: Relative mass splitting between the neutral and charged pseudoscalar obtained for $N_f = 2+1+1$ as a function of $(a/r_0)^2$, for two β values. The reference pion mass are not the same. In order to compare with $N_f = 2$ the same observable is shown for a reference pseudoscalar mass of $r_0 m_{\rm PS} = 0.7$.

	L/a	r_0/a	$am^{\pm}_{\rm PS}$	$am^{0}_{\rm PS}$	$af_{\rm PS}$	am_K	am_D
$A40.24$	24	5.178(44)	0.14527(39)	0.0762(49)	0.06541(33)	0.25779(43)	0.9400(107)
$A40.60$	24	5.209(58)	0.17261(44)	0.107(7)	0.07169(23)	0.26695(51)	0.9298(117)
$A40.80$	24	4.989(40)	0.19858(41)	0.131(9)	0.07623(22)	0.27706(60)	0.9319(93)
$A100.24$	24	4.864(21)	0.22276(41)	-	0.07924(19)	0.28807(33)	0.9426(99)
$A30.30$	32	5.217(30)	0.12358(48)	-	0.06483(40)	-	-
$A40.32$	32	5.179(49)	0.14141(40)	-	0.06767(26)	-	-
$A50.32$	32	5.081(45)	0.15720(42)	-	0.07108(27)	-	-
$B25.32$	32	5.728(35)	0.10679(58)	-	0.05714(34)	0.21239(49)	0.8354(68)
$B35.32$	32	5.616(31)	0.12621(45)	0.077(1)	0.06052(24)	0.21835(28)	0.8286(84)
$B55.32$	32	5.662(33)	0.15503(26)	-	0.06590(17)	-	-
$B75.32$	32	5.566(44)	0.18044(24)	-	0.06902(12)	0.23753(33)	0.8361(126)
$B25.24$	24	5.493(41)	0.1937(6)	-	0.0700(3)	0.24476(44)	0.8650(76)

Table 4.7: Selected observables in the non baryonic sector for $N_f = 2+1+1$ simulations.

Chapter 5

Relevant Aspects of Chiral Perturbation theory

Contents

Effective theories are a powerful tool to analyze lattice results. We have already mentionned that the effective action *à la Symanzik*, permits to improve our understanding on the way that the continuum limit is reached. Another interesting effective field theory, is the so-called *chiral perturbation theory* (χPT) which was introduced by Weinberg [90–92] and systematically developed by Gasser and Leutwyler [93, 94]. A large part of the following discussion is based on lectures of [95] [96] [97] or Ph.D [98].

5.1 Chiral Symmetry in QCD

Let us consider the two degenerate flavour QCD Lagrangian. We saw in section 1.2 that it is symmetric under $\mathrm{SU}(2)_V \times \mathrm{SU}(2)_A \times \mathrm{U}(1)_\mathrm{V}$ in the limit of vanishing quark masses. Nature should be approximately described in this limit. We expect that hadrons can be classified into degenerate multiplets, labelled by the irreducible representation of the symmetry group. However, assuming that the vaccuum state of QCD is invariant under vector and axial transformation leads to a phenomenological contradiction. Indeed in this hypothesis, it can be shown that the vector and axial conserved charged operator have opposite parity. As a consequence any state of positive parity should have a degenerate negative parity partner. This is not observed in Nature. For instance the $J^P = 1/2^-$ baryon octet is $\approx 50\%$ heavier than the $J^P = 1/2^+$ one. Moreover it was shown in [99] that in the chiral limit the vaccuum is necessarily invariant under $\mathrm{SU}(2)_V \times \mathrm{U}(1)_\mathrm{V}$.

The way to solve this puzzle, is to assume that the vacuum is not invariant under axial transformations. This spontaneous symmetry breaking gives rise to the appearance of massless particles, the so-called *Goldstone bosons* due to *Golstone's theorem* [100–103]. The numbers of Goldstone bosons is equal to the dimension of the spontaneously broken group, so in the particular case of two flavour it is equal to three. These bosons are identified with the three pion states which are significantly lighter than any other particle of the QCD spectrum. Their small masses are due to the fact that in practice $\mathrm{SU}(2)_A$ is explicitly broken (softly) by the non vanishing u and d quark masses. Anticipating on chiral perturbation theory results, we can already guess that pion mass will vanish when the quark masses are sent to zero (chiral limit). Note also that a non-vanishing scalar quark condensate in the chiral limit is a sufficient (but not a necessary) condition for a spontaneous symmetry breaking in massless QCD.

Transformation properties of the Goldstone bosons field U can be worked out to obtain an effective theory describing its dynamics. The result is the chiral Lagrangian.

In the two flavour case, let us define

$$U(x) = \exp\left(i\frac{\phi(x)}{F_0}\right) \tag{5.1}$$

with

$$\phi = \sum_{i=1}^{3} \phi_i \tau_i = \begin{pmatrix} \pi^0 & \sqrt{2}\pi^+ \\ \sqrt{2}\pi^- & -\pi^0 \end{pmatrix}. \tag{5.2}$$

We will sometimes denote

$$\vec{\phi} = \begin{pmatrix} \phi_1 \\ \phi_2 \\ \phi_3 \end{pmatrix} \tag{5.3}$$

The most general chirally invariant lowest order effective Lagrangian density reads

$$\mathcal{L}_\pi = \frac{F_0^2}{4}\mathrm{Tr}\left\{\partial_\mu U \partial^\mu U^\dagger\right\} \tag{5.4}$$

where $F_0 \approx 132$ MeV is the *pion decay constant*. One can then compute observables perturbatively, and obtain in this way the so-called *chiral perturbation theory* (χPT). It can be shown that this Lagrangian is completely invariant under chiral rotations. The quark masses that explicitly break chiral symmetry can however be taken into account in this formalism using the following term :

$$\mathcal{L}_m = \frac{F_0^2 B_0}{2} \mathrm{Tr}\left\{\mathcal{M}U^\dagger + U\mathcal{M}^\dagger\right\} \tag{5.5}$$

where $\mathcal{M}$ is the mass matrix :

$$\mathcal{M} = \mathrm{diag}\ (\mathrm{m_u}, \mathrm{m_d}) \tag{5.6}$$

and an effective coupling constant B_0. The precise definition and properties of Pauli matrices τ_i are given in Appendix A.1.

Computing the self energy of the pion provides a relation between the quark and pseudoscalar mass. One obtain the following result, historically first derived using current algebra:

$$m_{\mathrm{PS}}^2 = 2B_0(m_u + m_d) \tag{5.7}$$

One can generalize this approach systematically including higher orders terms and obtain a more accurate expansion around vanishing pion mass. It can be shown that this non renormalizable effective theory is valid in the limit of small momentum. However in practice its precise validity range has to be determined using non perturbative ab initio calculation. Chiral perturbation theory allows to compute order by order the dependence of selected observables, like pion scattering length [104] or decay constant, as a function of the pion or quark masses. Note that effective chiral perturbation theory can also be generalized to describe finite size or finite lattice spacing effects. Given our present range of simulated pion masses, χPT is an unavoidable tool to interpret the dependence of the results on the quark masses and extrapolate to them to the physical point. Conversely, once the improvement of algorithm and computers will allow us to reach the physical point, we will dispose of a non perturbative determination of the validity range of the chiral expansion.

5.2 Baryonic chiral perturbation theory.

In this thesis, we will focus on the baryonic sector. An extension of the preceding chiral expansion taking into account the baryon degrees of freedom was first developed in [105]. However the power counting of the corresponding Lagrangian was ill defined. [1] The solution was provided by the so-called *heavy-baryon chiral perturbation theory* (HBχPT), introduced in [106,107], which is not only an expansion in terms of small pion masses and momenta but also in the inverse nucleon mass $1/M_N$.

We will follow here the first approach of [105], which gives at one loop, the same result as HBχPT. In this section, ψ denotes the nucleon doublet under $SU(2)_V$. They consider the lowest order Lagrangian

$$\mathcal{L}_{\pi N}^{(1)} = \overline{\psi}\Big(i\not{D} - m + \frac{g_A}{2}\gamma^\mu\gamma_5 u_\mu\Big)\psi \tag{5.8}$$

where

$$u_\mu = i\Big[u^\dagger\partial_\mu u - u\partial_\mu u^\dagger\Big], \tag{5.9}$$

is the so-called *vielbein*, and

$$u^2(x) = U(x) = \exp\left(\frac{i}{F_0}\begin{pmatrix}\pi^0 & \sqrt{2}\pi^+\\ \sqrt{2}\pi^- & \pi^0\end{pmatrix}\right) \tag{5.10}$$

[1] in practice , it is impossible to define what are the relevant terms at a given order in perturbation theory.

contains the pion field.

The covariant derivative is defined in the following way :

$$D_\mu \psi = (\partial_\mu + \Gamma_\mu)\psi, \tag{5.11}$$

where the so-called *connection* is given by

$$\Gamma_\mu = \frac{1}{2}\Big[u^\dagger \partial_\mu u + u \partial_\mu u^\dagger\Big]. \tag{5.12}$$

The parameters m and g_A are respectively the nucleon mass and the axial coupling constant in the chiral limit. Quark masses are included using the next-to-leading order πN Lagrangian $\mathcal{L}^{(2)}_{\pi N}$:

$$\mathcal{L}^{(2)}_{\pi N} = c_1 \mathrm{Tr}\left\{\chi U^\dagger + U\chi^\dagger\right\} \tag{5.13}$$

where

$$\chi = 2F_0\mathcal{M} \tag{5.14}$$

and c_1 is a new low energy constant, related to the sigma term of the nucleon. The computation of the nucleon self energy is done using the following effective Lagrangian

$$\mathcal{L}_{\text{eff}} = \mathcal{L}_\pi + \mathcal{L}^{(1)}_{\pi N} + \mathcal{L}^{(2)}_{\pi N} \tag{5.15}$$

Expanding the U field, and keeping only terms with one and two pion fields, we get the following effective Lagrangian:

$$\mathcal{L}_{\text{eff}} = \mathcal{L}_{\text{free}} + \mathcal{L}_{\text{int}} + \mathcal{O}(\phi^3) \tag{5.16}$$

with

$$\mathcal{L}_{\text{free}} = \frac{1}{2}\phi_i(\Box + M^2)\phi_i + \overline{\psi}(i\partial\!\!\!/ - m)\psi \tag{5.17}$$

and

$$\mathcal{L}_{\text{int}} = -\frac{g_A}{2}\frac{1}{F_0}\overline{\psi}\gamma^\mu\gamma_5\partial_\mu\phi(x)\psi - \frac{1}{4F_0^2}\overline{\psi}\gamma_\mu\vec{\phi}(x)\wedge\partial_\mu\vec{\phi}(x)\cdot\vec{\tau}\psi \tag{5.18}$$

The mass term $M^2 = 2B_0(m_u + m_d)$ is the lowest order expression for the squared pion mass in terms of the low energy coupling constant B_0 and the quark masses.

Defining the Fourier transform as

$$\phi(x) = \int \frac{d^4p}{(2\pi)^4} e^{-ipx}\phi(p) \tag{5.19}$$

the Feynman rules in momentum space can be derived [2] and are:

[2] multiplying by i and replacing derivative by $-ip_\mu$

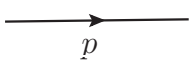

$$\frac{i}{\not p - m}, \tag{5.20}$$

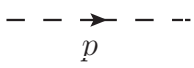

$$\frac{i}{p^2 - M^2}. \tag{5.21}$$

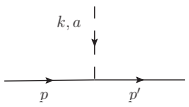

$$-\frac{g_A}{2F_0}\not k\gamma_5\tau^a. \tag{5.22}$$

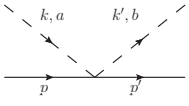

$$\frac{1}{4F_0^2}(\not k + \not k')\epsilon_{abc}\tau_c. \tag{5.23}$$

At this order the proton propagator can be written as

$$S_p(p) = \frac{i}{\not p - m} + \frac{i}{\not p - m}[-i\Sigma(p^2)]\frac{i}{\not p - m} + \cdots = \frac{i}{\not p - m - \Sigma(p^2)} \tag{5.24}$$

where the self energy is defined as the sum over the one particle irreducible (1 PI) Feynman diagrams.

The nucleon mass is then given by the pole of the propagator i.e :

$$m_N - m - \Sigma(m_N) = 0 \tag{5.25}$$

The next-to-leading order πN Lagrangian $\mathcal{L}^{(2)}_{\pi N}$ yields the constant contribution

$$\Sigma^{\text{tree}} = -4c_1 M^2 \tag{5.26}$$

The one loop diagrams that contribute to the self energy of the nucleon are given in Fig. 5.1. The first diagram gives a non zero contribution. The second one vanishes because of the Feynman rule Eq. (5.23) that imposes different pion isospin components due to the presence of the completely antisymmetric tensor.

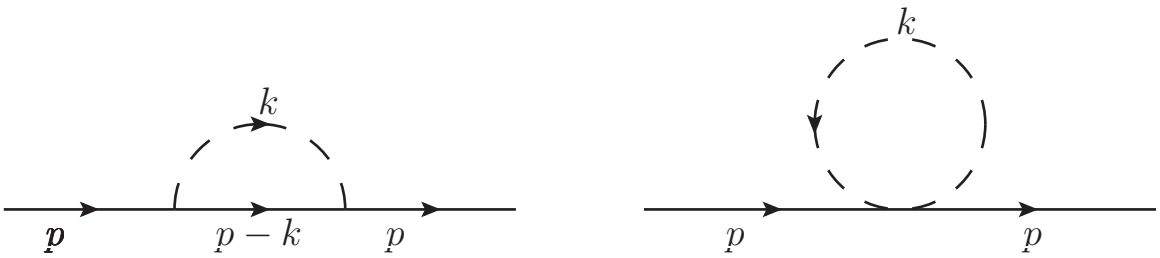

Figure 5.1: One-loop contributions to the nucleon self energy.

Using dimensional regularization, the one-loop contribution to the nucleon self energy reads:

$$-i\Sigma^{1-\text{loop}}(p) = \frac{3g_A^2}{4F_0^2}\mu^{4-d}\int\frac{d^dk}{(2\pi)^d}\not k\frac{\not p - \not k - m}{(p-k)^2 - m^2}\not k\mathbb{1}_2\frac{1}{k^2 - M^2} \tag{5.27}$$

One can perform a convenient reduction of this integral to a sum of scalar loop integrals, and get :

$$\begin{aligned}\Sigma^{1-\text{loop}}(\not p) &= \frac{3g_A^2}{4F_0^2}\left\{-(\not p+m)\mu^{4-d}i\int\frac{\mathrm{d}^dk}{(2\pi)^d}\frac{1}{(p-k)^2-m^2+i\varepsilon}\right.\\ &-(\not p+m)M^2\mu^{4-d}i\int\frac{\mathrm{d}^dk}{(2\pi)^d}\frac{1}{(k^2-M^2+i\varepsilon)[(p-k)^2-m^2+i\varepsilon]}\\ &+(p^2-m^2)\mu^{4-d}i\int\frac{\mathrm{d}^dk}{(2\pi)^d}\frac{\not k}{(k^2-M^2+i\varepsilon)((p-k)^2-m^2+i\varepsilon)}\\ &\left.-\mu^{4-d}i\int\frac{\mathrm{d}^dk}{(2\pi)^d}\frac{\not k}{k^2-M^2+i\varepsilon}\right\}. \end{aligned} \tag{5.28}$$

The last term of this equation vanishes since the integrand is odd in k. The others are well known one-loop scalar integral. Using the notation introduce in Appendix D, one can rewrite the regularized self energy as:

$$\begin{aligned}\Sigma^{1-\text{loop}}(\not p) &= \frac{3g_A^2}{4F_0^2}\frac{1}{16\pi^2}\left\{(\not p+m)A_0(m)+(\not p+m)M^2B_0(-p,M,m)\right.\\ &\left.-(p^2-m^2)\not pB_1(-p,M,m)\right\}. \end{aligned} \tag{5.29}$$

In the modified minimal substraction scheme $\widetilde{\overline{\text{MS}}}$ all the terms proportional to

$$R_{\widetilde{\overline{\text{MS}}}} = R_{\overline{\text{MS}}} + 1 = \frac{2}{4-d} - \gamma_E + \log 4\pi + 1 \tag{5.30}$$

diverge when $d \to 4$ and are absorbed in the definition of the renormalized coupling constants. For the sake of simplicity we choose the renormalization scale $\mu = m$. In what follows, we will implicitly renormalize the coupling constants g_A, c_1 and m (the bare mass). A precise definition of the infinite renormalization shift is given in [108]. We are left with the following expression for the renormalized self energy :

$$\Sigma_r^{1-\text{loop}}(\not p) = \frac{3g_A^2}{4F_0^2}\frac{1}{16\pi^2}\left\{(\not p+m)M^2B_0^r(-p,M,m)-(p^2-m^2)\not pB_1^r(-p,M,m)\right\}. \tag{5.31}$$

where the superscript r on the integrals means that the terms proportional to R have been substracted. To solve Eq. (5.25), we have to evaluate the self energy arround the nucleon mass, such that the difference $m_N - m = \mathcal{O}(p^2)$. One finally obtains :

$$m_N = m - 4c_1M^2 + \frac{3g_A^2}{32\pi^2F_0^2}mM^2B_0^r(-m_N,M,m) \tag{5.32}$$

Expanding around $M \sim 0$ and $m_N \sim m$ using Eq. (D.15) we get :

$$m_N = m - 4c_1M^2 + \frac{3g_A^2}{32\pi^2F_0^2}mM^2 - \frac{3g_A^2}{32\pi F_0^2}M^3 \tag{5.33}$$

The fact that the third term of the right hand side is quadratic in the pion mass (*i.e* linear in the quark mass) is a manifestation of the power counting problem that we have mentioned

in the introduction. It can be solved formally performing another finite renormalization and we finally obtain an expression for the nucleon mass at $\mathcal{O}(p^3)$ which reads

$$m_N = m - 4c_1 M^2 - \frac{3\mathrm{g}_A^2}{32\pi F_0^2} M^3 \tag{5.34}$$

This results was first obtained in [105]. Note that a systematic solution of the power counting problem was found in [106]. The idea was to perform a $1/m$ expansion of the Lagrangian Eq. (5.15). This approach is thus named *heavy baryon chiral perturbation theory* (HBχPT) . To the order $\mathcal{O}(p^3)$, the results for the nucleon mass given in Eq. (5.34) is unchanged.

The relation between the sigma term defined in 3.7 and the low energy constants is given at $\mathcal{O}(p^3)$ by the formula:

$$\sigma_N = m_q \frac{dm_N}{dm_q} \approx m_\pi^2 \frac{dm_N}{dm_\pi^2} = -4c_1 m_\pi^2 - \frac{9\mathrm{g}_A^2}{32\pi f_\pi^2} m_\pi^4 \tag{5.35}$$

5.3 SU(2) Heavy baryon chiral perturbation theory.

In this section we review the theoritical results that will be used in chapters 6 and 7 to analyze lattice data. The previous section has already shown the philosophy and computation techniques of baryonic chiral perturbation theory. We will focus here on the final results and on their physical interpretation. All the chiral expansions given in this section have been obtained using $SU(2)$ HBχPT in the continuum [109].

5.3.1 Nucleon

Nucleon (N) mass is known to higher order within several expansion schemes. In each of them, the N-Δ coupling $g_{N\Delta}$ appears at the level of the Lagrangian. Let us begin with a generic parametrization of the nucleon mass :

$$m_N = m_N^{(0)} + m_N^{(2)} + m_N^{(3)}(\Delta, \mu) + m_N^{(4)}(\Delta, \mu) + \dots \tag{5.36}$$

The parameter Δ is the Δ-N mass difference. It will be fixed to its physical value. The dependence of Δ as a function the quark mass contributes to higher order terms. The terms $m_N^{(n)}$ are of order m_π^n in the limit of vanishing Δ. The leading contribution $m_N^{(0)}$ is the nucleon mass in the chiral limit.

The leading order of the expansion is given by

$$m_N^{LO}(m_\pi) = m_N^{(0)} - 4c_N^{(1)}\, m_\pi^2 \tag{5.37}$$

with two fit-parameters, the baryon mass in the chiral limit $m_N^{(0)}$ and the quadratic coefficient $c_N^{(1)}$.

We will also consider a cubic expansion of the following form

$$m_N(m_\pi) = m_N^{(0)} - 4c_N^{(1)} m_\pi^2 + c_N^{(2)} m_\pi^3 \tag{5.38}$$

treating $c_N^{(2)}$ as an additional fit parameter.

As already mentioned, the $\mathcal{O}(p^3)$ is given by

$$m_N(m_\pi) = m_N^{(0)} - 4c_N^{(1)}\, m_\pi^2 - \frac{3g_A^2}{16\pi f_\pi^2}\, m_\pi^3 \tag{5.39}$$

To this order, the parameters are $m_N^{(0)}$, $c_N^{(1)}$, g_A and f_π. In practice, given our present accuracy, it is difficult to determine the coefficient of the cubic term from our present lattice results. The g_A and f_π values will be taken from experiment in our fits.

The next to leading order SU(2) HBχPT result [109] is given by

$$m_N^{NLO}(m_\pi) = m_N^{LO}(m_\pi) - \frac{3g_A^2}{16\pi f_\pi^2} m_\pi^3 - \frac{8g_{N\Delta}^2}{3(4\pi f_\pi)^2}\ \mathcal{F}(m_\pi, \Delta_{\Delta N}, \lambda) \tag{5.40}$$

with the non analytic function [110]

$$\mathcal{F}(m,\Delta,\lambda) = (\Delta^2 - m^2 + i\epsilon)^{3/2}\ \log\left(\frac{\Delta + \sqrt{\Delta^2 - m^2 + i\epsilon}}{\Delta - \sqrt{\Delta^2 - m^2 + i\epsilon}}\right) - \frac{3}{2}\Delta m^2 \log\left(\frac{m^2}{\lambda^2}\right) - \Delta^3 \log\left(\frac{4\Delta^2}{m^2}\right) \tag{5.41}$$

depending on the threshold parameter $\Delta_{XY} = m_Y^{(0)} - m_X^{(0)}$. This function is defined with a branch cut on the real positive axe. Note the appearance of the coupling constant $g_{\Delta N}$ between the nucleon, the Δ and the pion.

The next to next to leading order (NNLO) expression is

$$\begin{aligned} m_N^{NNLO}(m_\pi) &= m_N^{NLO}(m_\pi) + m_\pi^4 \left[\beta_N + \frac{16 g_{\Delta N}^2 c_N^{(1)}}{(4\pi f_\pi)^2} - \frac{9 g_{\Delta N}^2}{4 m_N^{(0)} (4\pi f_\pi)^2} - \frac{45 g_A^2}{324 m_N^{(0)} (4\pi f_\pi)^2}\right] \\ &+ \frac{16 g_{\Delta N}^2 c_N^{(1)}}{(4\pi f_\pi)^2} m_\pi^2\ \mathcal{J}(m_\pi, \Delta, \lambda) \\ &+ \frac{m_\pi^4}{(4\pi f_\pi)^2} \log\left(\frac{m_\pi^2}{\lambda^2}\right)\left[12 c_N^{(1)} - \frac{3\alpha_N}{4\pi f_\pi} - \frac{27 g_A^2}{16 m_N^{(0)}} - \frac{5 g_{\Delta N}}{2 m_N(0)}\right] \end{aligned} \tag{5.42}$$

where

$$\mathcal{J}(m,\Delta,\lambda) = 2\Delta\sqrt{\Delta^2 - m^2 + i\epsilon}\ \log\left(\frac{\Delta - \sqrt{\Delta^2 - m^2 + i\epsilon}}{\Delta + \sqrt{\Delta^2 - m^2 + i\epsilon}}\right) + 2\Delta^2 \log\left(\frac{4\Delta^2}{m^2}\right) + m^4 \log\left(\frac{m^2}{\lambda^2}\right) \quad . \tag{5.43}$$

5.3.2 Baryon loops and the $\mathcal{F}$ function.

It is worthwhile to note that the $\mathcal{F}$ function appears at NLO when taking into account the $N - \pi - \Delta$ vertex. Anticipating on the strange baryons, we can already mention that $\mathcal{F}$ will appear at NLO when a pion is coupled to two different baryonic states $X - \pi - Y \neq X$. A diagram corresponding to this contribution is shown in Fig. 5.2. A baryon X with a mass m_X coupled to a baryon $Y \neq X$ with a mass $m_Y = m_X + \Delta_{XY}$ via a pion-baryon axial coupling, contributes to the mass of X as:

$$M_X = \cdots + \frac{g_{XY}^2}{16\pi^2 f_\pi^2} \mathcal{F}(m_\pi, \Delta_{XY}, \mu) \tag{5.44}$$

One can show that for $\Delta > 0$, $\mathcal{F}(m,\Delta,\mu)$ is real and can be directly computed from Eq. (5.41) and satisfies the following properties :

$$\mathcal{F}(m,-\Delta,\mu) = \begin{cases} -\mathcal{F}(m,\Delta,\mu) + 2i\pi(\Delta^2 - m^2)^{\frac{3}{2}} & m < \Delta \\ -\mathcal{F}(m,\Delta,\mu) + 2\pi\left(m^2 - \Delta^2\right)^{\frac{3}{2}} & m > \Delta \end{cases} \tag{5.45}$$

which corrects a typo in the sign of the second term in Ref. [111]. Notice that $\mathcal{F}(m,-\Delta,\mu)$ has an imaginary contribution below the threshold $m < \Delta$, which correspond to the $X \to Y\pi$ decay.

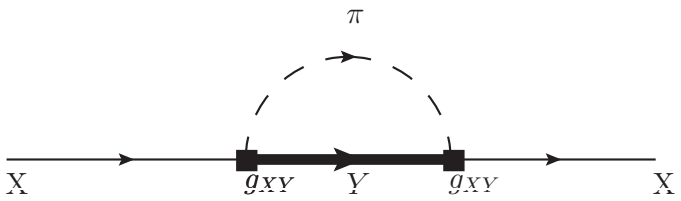

Figure 5.2: General diagram generating the $\mathcal{F}$ functions. A state X is coupled to a state Y via a pion-baryon axial coupling.

It is also straightforward to show that

$$\lim_{\Delta \to 0^{\pm}} \mathcal{F}(m_\pi, \Delta, \mu) = \pm \pi m_\pi^3 \tag{5.46}$$

for an arbitrary $m > 0$.

When analyzing the baryon masses with HBχPT expansion three different situations occur: $\Delta > 0$, $0 < \Delta << m$ and $\Delta < 0$. They are shown in Figs. 5.3 5.4 5.5 for $\Delta = 0.3, 0.1$ and -0.3 GeV respectively. The scale μ has been fixed to 1 GeV in all this work, but, in this section, we show a gray band to indicate the envelop of the curve for $\mu \in [0.9, 1.1]$ GeV.

In Fig. 5.3, $\mathcal{F}$ is compared to the limiting case $\Delta \to 0$ given by Eq. (5.46). As expected their difference becomes larger when the pion mass is increased.

On the contrary, we see in Fig. 5.4, corresponding to a smaller threshold $\Delta = 0.1$ GeV, that $\mathcal{F}$ is very well approximated by πm_π^3 in the pion mass region where the cubic term is relevant ($m > 0.2$). Note however that for very small pion masses, well below the physical point, $\mathcal{F}$ tend to zero slower than m_π^3 and their ratio diverges.

The last important case, corresponding to $\Delta = -0.3$ GeV, is shown in Fig. 5.5. They describe the – real and imaginary – self energy contribution for a resonant baryon which decays into a pion plus a lighter baryon. This will be the case for decuplet baryons, namely $\Delta \to \pi N$, $\Sigma^* \to \pi\Sigma$, and $\Xi^* \to \pi\Xi$. Since $\Delta < 0$, $\mathcal{F}$ becomes complex below the threshold $m < |\Delta|$. It can be shown using the optical theorem [112, 113] that the imaginary part of the self energy is related to the partial width $\Gamma_{X \to \pi Y}$ of the baryon[3]

[3]I thank J. Debove to point out this fact.

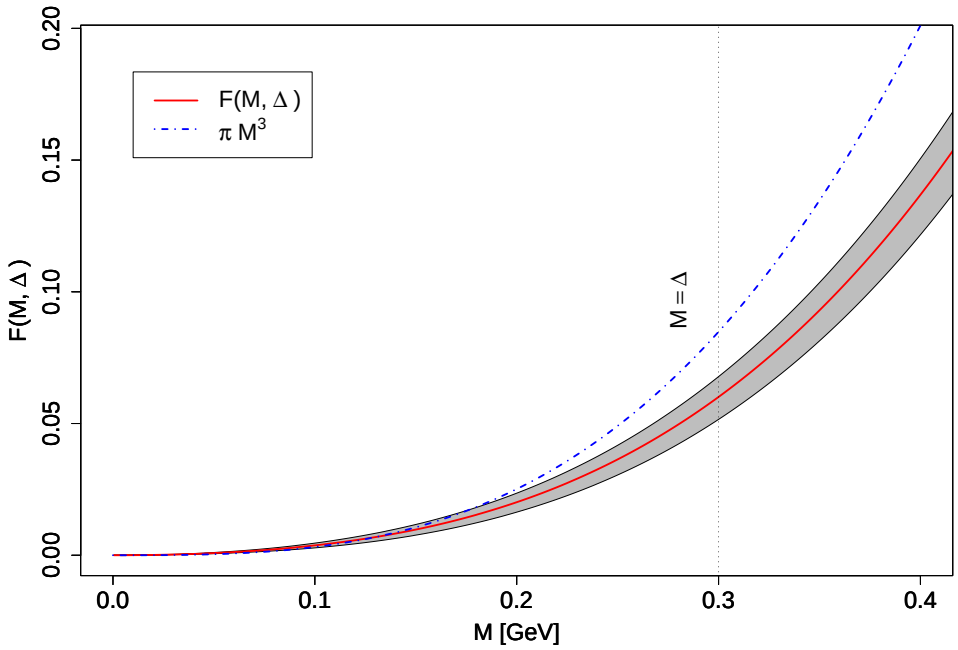

Figure 5.3: The $\mathcal{F}$ function for a fixed value of $\Delta = 0.3$ GeV as a function of M. The grey zone is obtained varying the renormalization scale in the range $[0.9, 1.1]$ GeV.

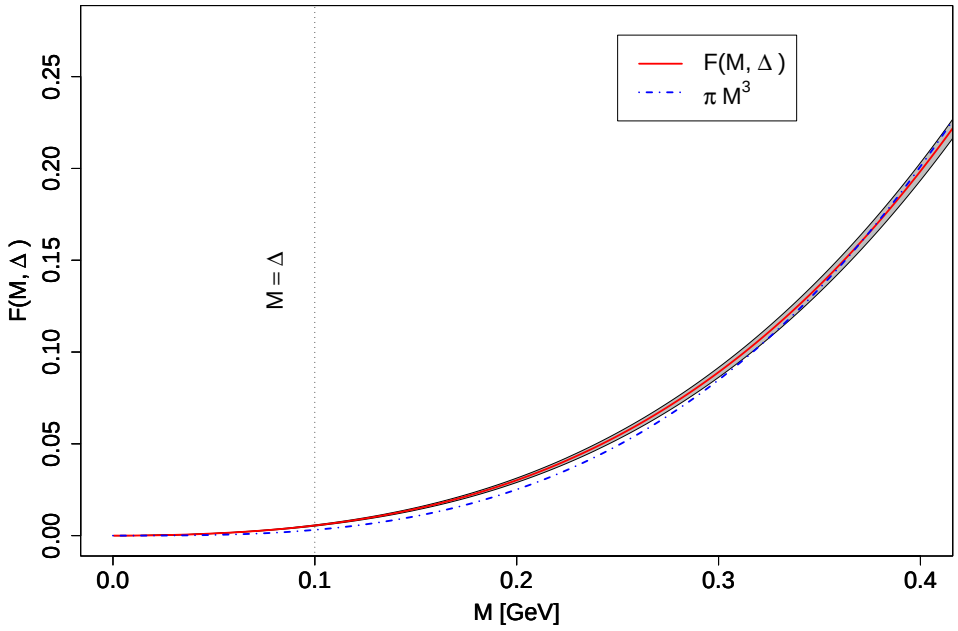

Figure 5.4: The $\mathcal{F}$ function for a fixed value of $\Delta = 0.1$ GeV as a function of M. The grey zone is obtained varying the renormalization scale in the range $[0.9, 1.1]$ GeV.

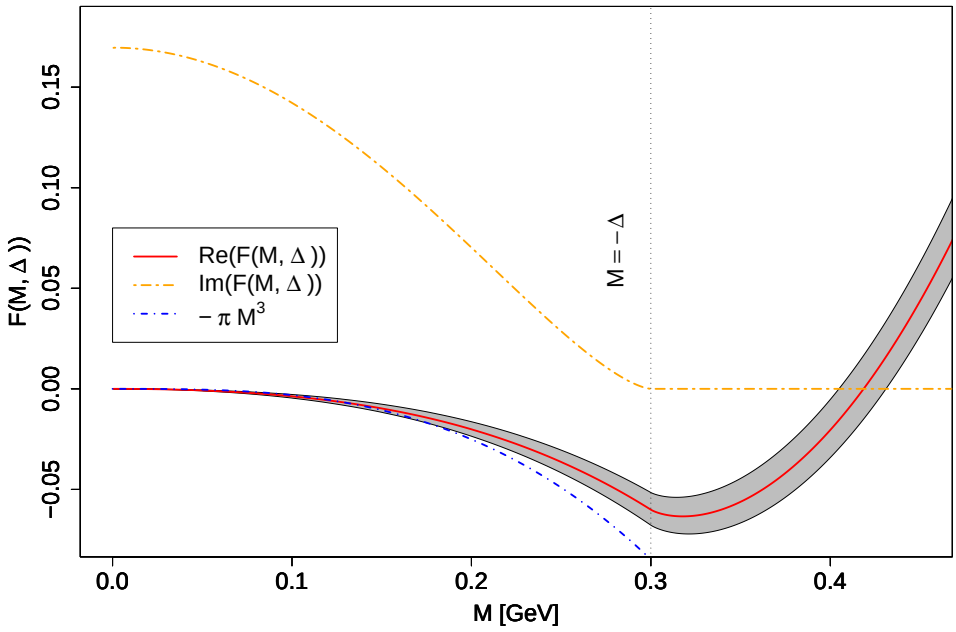

Figure 5.5: Real and imaginary part of $\mathcal{F}$ for a fixed value of $\Delta = -0.3$ GeV as a function of M. The grey zone is obtained varying the renormalization scale in the range $[0.9, 1.1]$ GeV. The imaginary part is scale independent.

5.3.3 Convergence of chiral corrections

To estimate the contributions to the nucleon mass coming from the different terms in HBχPT expansion, we have fixed the two parameters $m_N^{(0)}$ and c_1 from a fit, and keep the remaining coupling constants from Eq. (5.58). We choose in this analysis $m_N^{(0)} = 0.880$ GeV and $4c_1 = -4.81$ GeV^{-1} taken from Table 6.10 which correspond to a $\mathcal{O}(p^3)$ fit giving a satisfactory descriptions of the lattice data as well as the physical point.

Following the notations of eq. 5.36 we have at $\mathcal{O}(p^3)$

$$m_N^{(2)}(m_\pi, \Delta, \mu) = m_{\text{tree}}(m_\pi) \tag{5.47}$$

$$m_N^{(3)}(m_\pi, \Delta, \mu) = m_{N\pi-\text{loop}}(m_\pi) \tag{5.48}$$

with

$$m_{\text{tree}}(m_\pi) = -4c_N^{(1)} m_\pi^2 \tag{5.49}$$

$$m_{N\pi-\text{loop}}(m_\pi) = -\frac{3g_A^2}{16\pi f_\pi^2} m_\pi^3 \tag{5.50}$$

Going to NLO, will require an additional contribution to $m_N^{(3)}(m_\pi, \Delta, \mu)$ which reads:

$$m_{\Delta\pi-\text{loop}}(m_\pi) = -\frac{8g_{N\Delta}^2}{3(4\pi f_\pi)^2}\, \mathcal{F}(m_\pi, \Delta_{\Delta N}, \mu) \tag{5.51}$$

We will first consider an $\mathcal{O}(p^3)$ fit. The various contribution divided by the nucleon mass at the same order are separately plotted in Fig. 5.6. As can be seen the quadratic term (m_{tree} in red) gives a positive contribution increasing with the pion mass. The loop contributions (N-loop in orange) is negative and decrease the pion mass dependence of the correction, as shown by the complete $\mathcal{O}(p^3)$ chiral corrections indicated by the blue curve. We would like to stress that at this level of approximation all the contributions are monotonous in the pion mass range of interest (below 500 MeV). The relative contribution of the constant term decreases and the chiral corrections increases and reach $\approx 30\%$ for $m_{\text{PS}} = 0.4$ GeV.

The corresponding NLO results are displayed in Fig. 5.7. The additional contribution coming from Δ loop is indicated by a dotted magenta line. It is negative and very close to the N loop indicating that a precise determination of the $g_{N\Delta}$ coupling would be very difficult even at low pion mass. When including this term one finds a total NLO chiral corrections (shown in green) which is non-monotonous and nearly constant. As a consequence, the relative constant contribution (in black) start to increase above 350 MeV. The relative difference between the solid curves indicates a poor convergence of the chiral expansion for pion mass > 200 MeV.

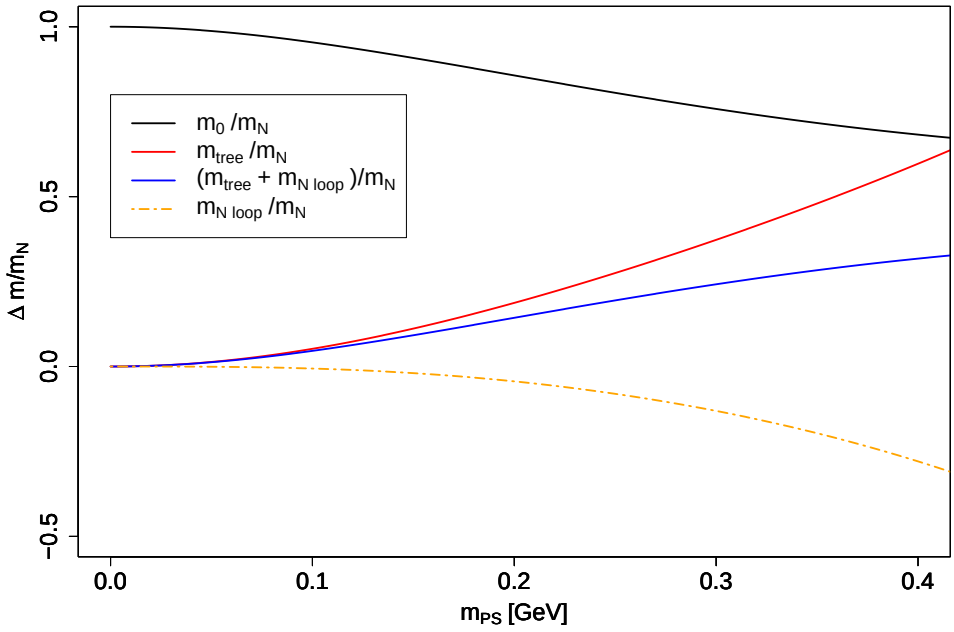

Figure 5.6: Pion mass dependence of the relative contribution to the $\mathcal{O}(p^3)$ nucleon mass

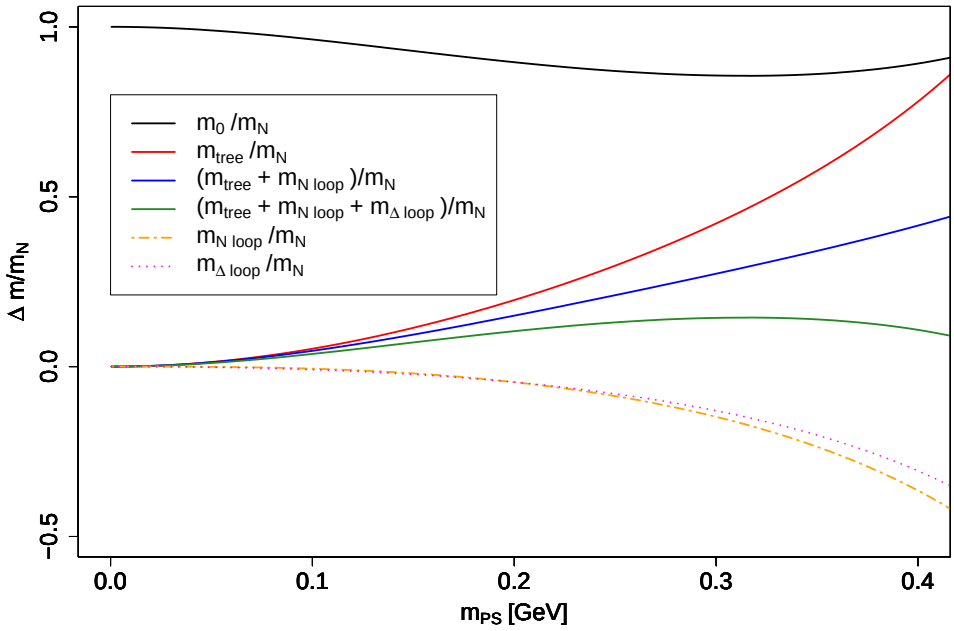

Figure 5.7: Pion mass dependence of the relative contribution to the NLO nucleon mass

5.3.4 Octet and Decuplet baryons

The preceding heavy baryon chiral perturbation (HBχPT) equations discussed in details in the nucleon case can be extended to the octet and decuplet.

The leading order $SU(2)$ results are given by

$$m_X^{\rm LO}(m_\pi) = m_X^{(0)} - 4c_X^{(1)} m_\pi^2 \,, \tag{5.52}$$

with two fit-parameters, the baryon mass in the chiral limit $m_X^{(0)}$ and $c_X^{(1)}$, which gives the leading contribution to the σ_X-term.

A natural generalization of the $\mathcal{O}(p^3)$ results for the nucleon and Δ to the rest of the octet and decuplet baryons [114, 115] is given by

$$\begin{aligned}
m_N(m_\pi) &= m_N^{(0)} - 4c_N^{(1)}\, m_\pi^2 - \frac{3g_A^2}{16\pi f_\pi^2}\, m_\pi^3 && \text{(5.53a)}\\
m_\Lambda(m_\pi) &= m_\Lambda^{(0)} - 4c_\Lambda^{(1)}\, m_\pi^2 - \frac{g_{\Lambda\Sigma}^2}{16\pi f_\pi^2}\, m_\pi^3 && \text{(5.53b)}\\
m_\Sigma(m_\pi) &= m_\Sigma^{(0)} - 4c_\Sigma^{(1)} m_\pi^2 - \frac{2g_{\Sigma\Sigma}^2 + g_{\Lambda\Sigma}^2/3}{16\pi f_\pi^2}\, m_\pi^3 && \text{(5.53c)}\\
m_\Xi(m_\pi) &= m_\Xi^{(0)} - 4c_\Xi^{(1)} m_\pi^2 - \frac{3g_{\Xi\Xi}^2}{16\pi f_\pi^2}\, m_\pi^3 \quad , && \text{(5.53d)}
\end{aligned}$$

for the octet baryons and

$$\begin{aligned}
m_\Delta(m_\pi) &= m_\Delta^{(0)} - 4c_\Delta^{(1)}\, m_\pi^2 - \frac{25}{27}\frac{g_{\Delta\Delta}^2}{16\pi f_\pi^2}\, m_\pi^3\\
m_{\Sigma^*}(m_\pi) &= m_{\Sigma^*}^{(0)} - 4c_{\Sigma^*}^{(1)} m_\pi^2 - \frac{10}{9}\frac{g_{\Sigma^*\Sigma^*}^2}{16\pi f_\pi^2}\, m_\pi^3\\
m_{\Xi^*}(m_\pi) &= m_{\Xi^*}^{(0)} - 4c_{\Xi^*}^{(1)} m_\pi^2 - \frac{5}{3}\frac{g_{\Xi^*\Xi^*}^2}{16\pi f_\pi^2}\, m_\pi^3\\
m_\Omega(m_\pi) &= m_\Omega^{(0)} - 4c_\Omega^{(1)} m_\pi^2 \,, && \text{(5.54)}
\end{aligned}$$

for the decuplet baryons.

In addition we consider what we call the cubic fit

$$m_X(m_\pi) = m_X^{(0)} - 4c_X^{(1)} m_\pi^2 + c_X^{(2)} m_\pi^3 \tag{5.55}$$

treating $c_X^{(2)}$ as an additional fit parameter.

The next to leading order SU(2) χPT results [109] for the octet are given by

$$\begin{aligned}
m_N^{NLO}(m_\pi) &= m_N^{LO}(m_\pi) - \frac{3g_A^2}{16\pi f_\pi^2}\, m_\pi^3 - \frac{8g_{N\Delta}^2}{3(4\pi f_\pi)^2}\, \mathcal{F}(m_\pi, \Delta_{N\Delta}, \mu)\\
m_\Lambda^{NLO}(m_\pi) &= m_\Lambda^{LO}(m_\pi) - \frac{g_{\Lambda\Sigma}^2}{(4\pi f_\pi)^2}\, \mathcal{F}(m_\pi, \Delta_{\Lambda\Sigma}, \mu) - \frac{4g_{\Lambda\Sigma^*}^2}{(4\pi f_\pi)^2}\, \mathcal{F}(m_\pi, \Delta_{\Lambda\Sigma^*}, \mu)\\
m_\Sigma^{NLO}(m_\pi) &= m_\Sigma^{LO}(m_\pi) - \frac{2g_{\Sigma\Sigma}^2}{16\pi f_\pi^2}\, m_\pi^3 - \frac{g_{\Lambda\Sigma}^2}{3(4\pi f_\pi)^2}\, \mathcal{F}(m_\pi, -\Delta_{\Lambda\Sigma}, \mu) - \frac{4g_{\Lambda\Sigma^*}^2}{3(4\pi f_\pi)^2}\, \mathcal{F}(m_\pi, \Delta_{\Sigma\Sigma^*}, \mu)\\
m_\Xi^{NLO}(m_\pi) &= m_\Xi^{LO}(m_\pi) - \frac{3g_{\Xi\Xi}^2}{16\pi f_\pi^2}\, m_\pi^3 - \frac{2g_{\Xi^*\Xi}^2}{(4\pi f_\pi)^2}\, \mathcal{F}(m_\pi, \Delta_{\Xi\Xi^*}, \mu) && \text{(5.56)}
\end{aligned}$$

and for the decuplet baryons:

$$\begin{aligned}
m_\Delta^{NLO}(m_\pi) &= m_\Delta^{LO}(m_\pi) - \frac{25}{27}\frac{g_{\Delta\Delta}^2}{16\pi f_\pi^2}\, m_\pi^3 - \frac{2g_{\Delta N}^2}{3(4\pi f_\pi)^2})\, \mathcal{F}(m_\pi, -\Delta_{N\Delta}, \mu) \\
m_{\Sigma^*}^{NLO}(m_\pi) &= m_{\Sigma^*}^{LO}(m_\pi) - \frac{10}{9}\frac{g_{\Sigma^*\Sigma^*}^2}{16\pi f_\pi^2}\, m_\pi^3 - \frac{2}{3(4\pi f_\pi)^2}\left[g_{\Sigma^*\Sigma}^2\, \mathcal{F}(m_\pi, -\Delta_{\Sigma\Sigma^*}, \mu) + g_{\Lambda\Sigma^*}^2\, \mathcal{F}(m_\pi, -\Delta_{\Lambda\Sigma^*}, \mu)\right] \\
m_{\Xi^*}^{NLO}(m_\pi) &= m_{\Xi^*}^{LO}(m_\pi) - \frac{5}{3}\frac{g_{\Xi^*\Xi^*}^2}{16\pi f_\pi^2}\, m_\pi^3 - \frac{g_{\Xi^*\Xi}^2}{(4\pi f_\pi)^2}\, \mathcal{F}(m_\pi, -\Delta_{\Xi\Xi^*}, \mu) \\
m_\Omega^{NLO}(m_\pi) &= m_\Omega^{LO}(m_\pi)
\end{aligned} \tag{5.57}$$

depending on the threshold parameter $\Delta_{XY} = m_Y^{(0)} - m_X^{(0)}$ and on the scale μ of chiral perturbation theory, fixed to $\mu = 1$ GeV

In our fits, the nucleon axial charge g_A and pion decay constant f_π are fixed to their experimental values (we use the convention such that $f_\pi = 130.70$ MeV). The remaining pion-baryon axial coupling constants are taken from SU(3) relations [109]:

Octet :	$g_A = D + F$,	$g_{\Sigma\Sigma} = 2F$,	$g_{\Xi\Xi} = D - F$,	$g_{\Lambda\Sigma} = 2D$
Decuplet :	$g_{\Delta\Delta} = \mathcal{H}$,	$g_{\Sigma^*\Sigma^*} = \frac{2}{3}\mathcal{H}$,	$g_{\Xi^*\Xi^*} = \frac{1}{3}\mathcal{H}$	
Transition :	$g_{\Delta N} = \mathcal{C}$,	$g_{\Sigma^*\Sigma} = \frac{1}{\sqrt{3}}\mathcal{C}$,	$g_{\Xi^*\Xi} = \frac{1}{\sqrt{3}}\mathcal{C}$,	$g_{\Lambda\Sigma^*} = -\frac{1}{\sqrt{2}}\mathcal{C}$

(5.58)

As can be seen, in the octet case, and once g_A is fixed, the axial coupling constants depend on the single parameter written as $\alpha = \frac{D}{D+F}$. Its value is poorly known. It can be taken either from the quark model ($\alpha = 3/5$), from the phenomenology of semi-leptonic decays or from hyperon-nucleon scattering. Note that its various determination are not compatible within errors. We take the "educated guess" of Ref. [109] namely $2D = 1.47$ or $\alpha = 0.58$. The decuplet coupling constants depend on a single parameter for which we again take the value $\mathcal{H} = 2.2$ from Ref. [109]. This value is not far from that predicted by SU(6) symmetry, $\mathcal{H} = \frac{9}{5}g_A = 2.29$ used in our previous work [116] resulting in the same cubic term for the nucleon and Δ. For fixing the octet-decuplet transition couplings we take the value $\mathcal{C} = 1.48$ from Ref. [110] . This choice neglects large systematic uncertainties, and an attempt to circumvent will be follow at the very end of this work. (see section 7.7).

With the coupling constants fixed in this way, the LO, the $\mathcal{O}(p^3)$ as well as the NLO fits are left with the two independent fit parameters $m_X^{(0)}$ and $c_X^{(1)}$. All mass parameters $m_X^{(0)}$ are treated independently unlike what is done in Ref. [109] where a universal mass parameter was used for all baryons with the same strangeness.

A noticeable result of this expansion is the absence of a cubic term in the expression for the Λ and Ω masses given in Eqs. (5.56) and (5.57). In the case of Ω, it follows from the absence of light valence quarks. However the absence of a cubic term in the NLO expression of Λ, although a consequence of χPT, is nevertheless a questionable result, since it relies on the assumption that $m_\pi \ll M_\Sigma - M_\Lambda$. In the limit $\Delta \to 0^+$ the non analytic function $\mathcal{F}$ becomes

$$\mathcal{F}(m_\pi, \Delta \to 0, \lambda) = \pi m_\pi^3 \tag{5.59}$$

which generates a cubic term for the Λ and slightly modifies the one for Σ. The corresponding expressions are given by

$$\begin{aligned}
m_\Lambda(m_\pi) &= m_\Lambda^{(0)} - 4c_\Lambda^{(1)}\, m_\pi^2 - \frac{g_{\Lambda\Sigma}^2}{16\pi f_\pi^2}\, m_\pi^3\,, \\
m_\Sigma(m_\pi) &= m_\Sigma^{(0)} - 4c_\Sigma^{(1)} m_\pi^2 - \frac{2g_{\Sigma\Sigma}^2 + g_{\Lambda\Sigma}^2/3}{16\pi f_\pi^2}\, m_\pi^3\,,
\end{aligned} \tag{5.60}$$

in agreement with the results of Eq. (5.53).

The expressions for the strange baryon masses to NNLO in χPT given in Ref. [109] involve in general more unknown low energy constants, but we found no advantage to use extrapolations to such order.

Chapter 6

Nucleon and Δ analysis

Contents

We come now to the analysis of the Nucleon and the Δ. This chapter has two parts, first we will focus on results obtained with $N_f = 2$ simulations. The goal will be here to show how to analyze systematic effects and how to use HBχPT to perform predictions. These results have been published in the following references [117] and [116]. The second part is devoted to the analysis of the first $N_f = 2 + 1 + 1$ results. The issues raised here is somehow different from the $N_f = 2$ case since we are mostly interested to prove that simulations are reliable, and do not introduce large systematic effects in the baryon masses. A part of this work is already published in two proceedings [84] [118] and will be soon available in a forthcoming paper [119].

6.1 Light baryon masses with $N_f = 2$ dynamical twisted fermions

6.1.1 Tuning of the smearing parameters

As described in 3.4 we combine APE smearing of the gauge links with Gaussian smearing of the quark operator in order to have interpolating fields with a larger overlap with the ground state. Defining the root mean square radius (r.m.s) introduced in [120] by

$$r^2 = \Big\langle \frac{\sum_{\vec{x}} \vec{x}^2 J_P(\vec{x},t_0) J_P^\dagger(\vec{x},t_0)}{\sum_{\vec{x}} J_P(\vec{x},t_0) J_P^\dagger(\vec{x},t_0)} \Big\rangle \tag{6.1}$$

the parameters α and n are varied so that the root mean square (r.m.s) radius r obtained using the proton interpolating field (J_P) is in the range of $0.3 - 0.4$fm. The tuning has been performed on a $24^3 \times 48$ lattice at $\beta = 3.9$ and $\mu = 0.0085$. In order to have a root mean square constant for the various β values, we readjust the values n. The final smearing parameters use in this work are summarized in Table 6.1.

In Fig. 6.1, we show the local-local (LL) and the smeared-smeared (SS) nucleon effective mass on a $24^3 \times 48$ lattice at $\beta = 3.9$ and $\mu = 0.0085$. The statistic is, both for LL and SS, of the order of 300 configurations. The excited states contribution are clearly suppressed by the smearing procedure and lead to a plateau some time slices earlier. As seen in this plot, for a particular choice of parameters, the local-local and smeared-smeared results have always been found in agreement within the error bars.

We will use hereafter, without mentioning it, smeared-smeared correlators to extract baryon masses.

Other methods exist that allow to improve the plateau determination. A promising new one is for instance, the *distillation* [121,122]. However a complete investigation of what would be the best strategy for a fixed computational time to extract nucleon mass is still missing.

β	N_{Gaussian}	α_{Gaussian}	N_{APE}	α_{APE}
3.8	30	4.0	20	0.5
3.9	50	4.0	20	0.5
4.05	70	4.0	20	0.5
4.2	90	4.0	20	0.5

Table 6.1: Smearing parameters for our $N_f = 2$ runs

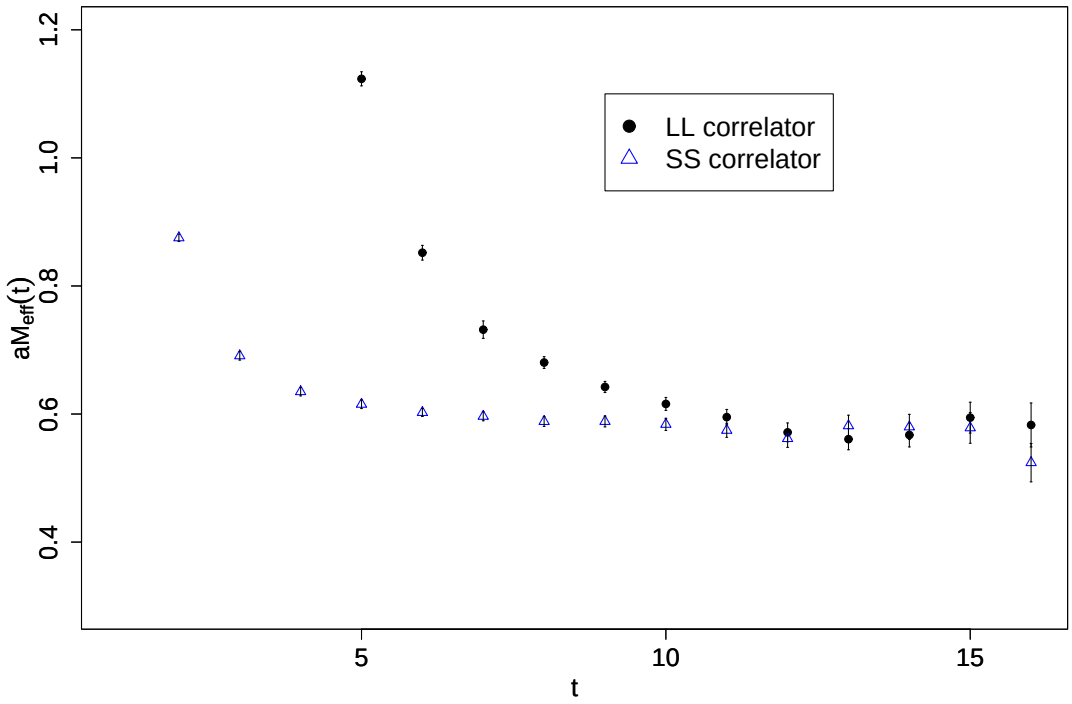

Figure 6.1: Nucleon effective mass for LL and SS correlators on a $24^3 \times 48$ lattice with $\beta = 3.9$ $\mu = 0.0085$ as a function of the time in lattice unit.

6.1.2 Effective masses

Using the smearing parameters determined in the previous section, we draw in Fig. 6.2 the nucleon effective mass obtained on a $48^3 \times 96$ lattice at $\beta = 4.2$, $\mu = 0.002$. The number of configurations used for this measurement is ~ 250. Fortunately, such statistics are sufficient to measure the nucleon mass with an accuracy of $\sim 1\%$. Statistical errors are determined using the Jackknife method. We observe that the signal oscillate for $t/a \geq 20$, a phenomenon which is common to most of measurement performed with smeared smeared correlators.

The Δ effective masses on the same ensemble are shown in Fig. 6.3. They have been obtained by averaging the correlators of the degenerate pairs Δ^{++}/Δ^{-} and Δ^{+}/Δ^{0}.

As can be seen the quality of the plateau is worse than in the nucleon case. This is a general fact for all our ensembles, and is responsible for larger error bar on the Δ mass. Is it possible to relate the large statistical fluctuations of the Δ mass to some physical properties ? The most natural could be its broad width, which should manifest itself for sufficiently light pion mass in lattice QCD simulations. However, as far as I know, no theoritical statement based on models or on QCD exist, quantifying this behaviour.

Effective masses of the nucleon and Δ have been computed on all available gauge ensembles presented in Table 4.1. The plateau is chosen according to the method describe in 3.4, namely imposing that the derivative of the measured mass with respect to the starting point t_1 of the fit is compatible with zero.

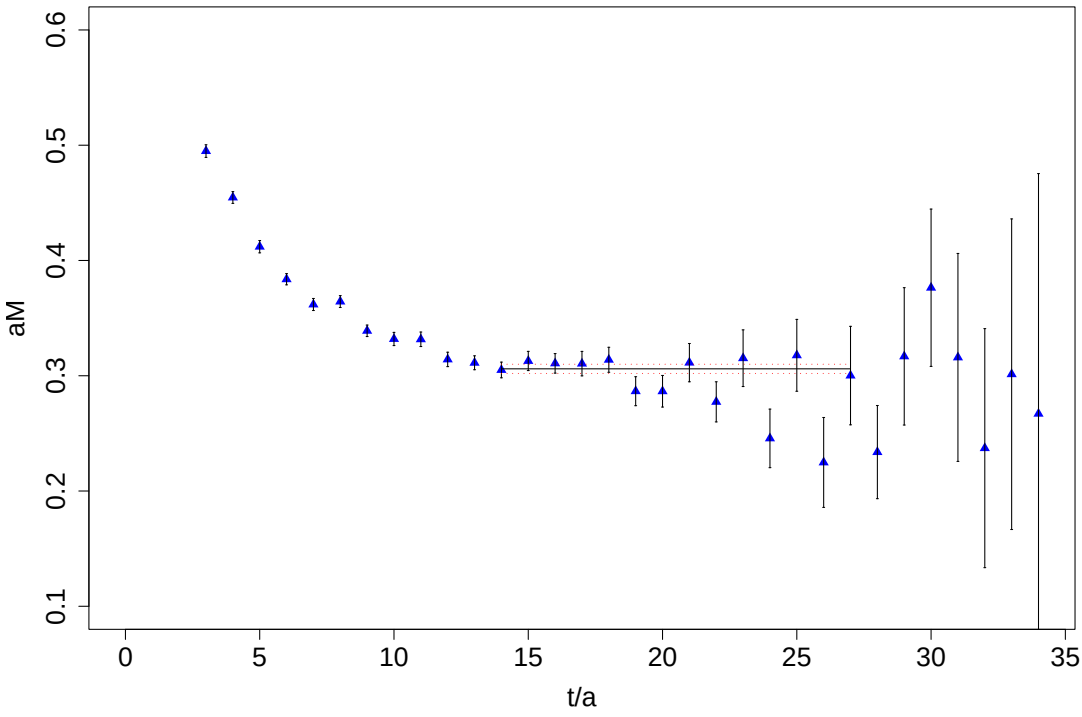

Figure 6.2: Nucleon effective mass on a $48^3 \times 96$ lattice with $\beta = 4.2$ $\mu = 0.002$ as a function of the time in lattice unit

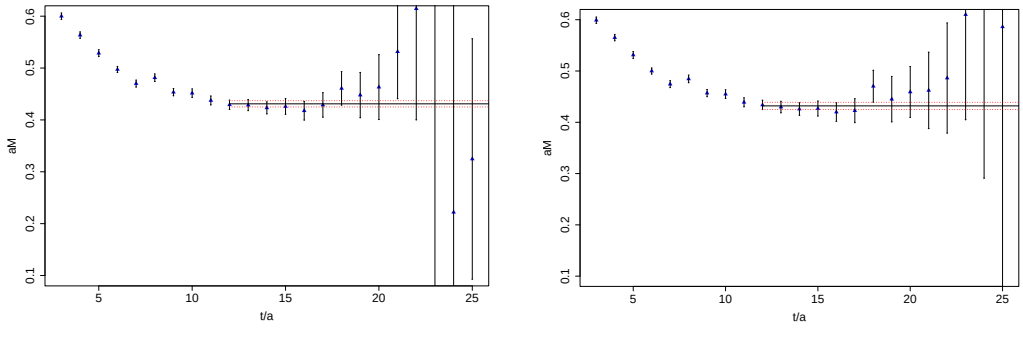

(a) (b)

Figure 6.3: Δ^{++}, Δ^{-} (a) and Δ^{+}, Δ^{0} (b) effective masses on a $48^3 \times 96$ lattice with $\beta = 4.2$ $\mu = 0.002$ as a function of the time in lattice unit

6.1.3 Dispersion Relation

To study baryon spectroscopy, it is sufficient to extract masses using correlator at 0 momentum. However nothing prevents us from using any non vanishing momenta authorized by the discretization. It is not very interesting from point of view of QCD predictions, since the statistical noise increases with momenta, but it is a good check of the analysis and gives some hints on the

size of discretization effects. This is also of crucial importance for matrix element analysis. On the lattice, one expects to recover the relativistic dispersion relation up to $\mathcal{O}(a^2)$:

$$E(\vec{p}) = \sqrt{\vec{p}^2 + M^2} + \mathcal{O}(a^2) \tag{6.2}$$

where $E(\vec{p})$ is the energy of the state with a 3−momentum $\vec{p}$ and M the rest mass of the particle.

Following the strategy defined for the analysis at 0 momentum, we analyze the energy dependence of the nucleon for the first non vanishing lattice momenta. To convert energy and momenta to physical units we use here the lattice spacing determined in [81] (see Table 4.3) using f_π. Note that the smallest momentum on $\beta = 3.9$ lattice is already quite large (~ 500 MeV), that is not always suitable to extract physically interesting observables. Indeed, some quantities cannot be computed at $\vec{p} = 0$, and the only way to access them is by extrapolating data obtained at non vanishing momentum. This is for instance the case for the proton magnetic moment. In order to diminish the error due to the extrapolation to 0-momentum one can use twisted boundary conditions of the fermion fields. The reader interested in the method is referred to the paper [123–125]. The idea is to impose generalized boundary conditions such that:

$$\psi(x + L[\mu]) = \begin{cases} \psi(x) \text{ for } \mu = 0 \\ e^{i\theta_i}\psi(x) \text{ for } \mu = i \in \{1, 2, 3\} \end{cases} \tag{6.3}$$

where $\vec{\theta}$ is an arbitrary vector angle. The dispersion relation energy Eq. (6.2) becomes :

$$E(\vec{p}_{n,\theta}, \vec{\theta}) = \sqrt{\vec{p}^2_{n,\theta} + m^2} + \mathcal{O}(a^2) \tag{6.4}$$

where

$$\vec{p}_{n,\theta} = \frac{2\pi}{L}\vec{n} + 3\vec{\theta} \tag{6.5}$$

The angles $\vec{\theta}$ can be chosen as small as needed. It can be shown that to implement the twisted boundary conditions is equivalent to perform the inversion of an effective Dirac operator :

$$D(x, y)_{\vec{\theta}} = U(\theta, x)D(x, y)\mathcal{U}^{-1}(\theta, y) \tag{6.6}$$

where $U(\theta, x) = e^{i\vec{\theta}\cdot\vec{x}}$.

We have measured such correlators on a $24^3 \times 48$ lattice at $\beta = 3.9$, $\mu = 0.01$ and results are displayed in Fig. 6.4. Blue points show the nucleon energy for the first lattice momenta. Triangles represent nucleon energy obtained using twisted boundary conditions with various twist angles. The red curve shows the continuum dispersion relation and it turns to be in complete agreement with the lattice results for $|p|^2 \lesssim 3$ GeV^2.

6.1.4 Overall raw results

Before studying quantitatively systematic effects, we compiled in Figs. 6.5 and 6.6, the representative measurements of the nucleon and Δ mass. In order to compare results corresponding to different lattice spacing, baryon masses are converted in r_0 units and plotted as a function of $(r_0 m_{PS})^2$. We excluded from this plot measurements done on lattices with $m_{\rm PS}L \lesssim 3.0$. Such small lattices are reserved to study finite volume dependence. We also excluded from this plot results obtained at $\beta = 3.8$. Indeed as explained in Chapter 4 long autocorrelation of the PCAC masses are responsible for underestimated errors and it is thus questionable that we effectively tune our simulations at maximal twist. In all the baryon spectroscopy analysis we only use $\beta = 3.8$ as a cross check for discretization errors.

The nucleon as well as the Δ masses obtained at several lattice spacing with various volumes agree nicely indicating that lattice artefacts are small. There is however one dramatic exception:

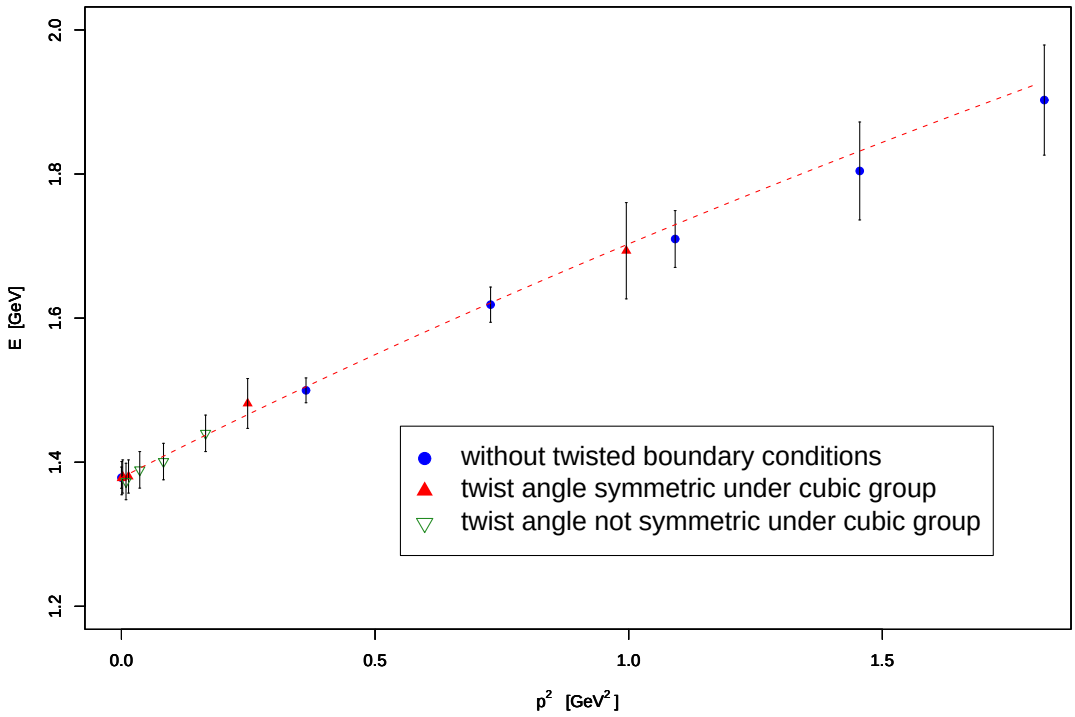

Figure 6.4: Dispersion relation of the nucleon computed on a $24^3 \times 48$ lattice at $\beta = 3.9$ and $\mu = 0.01$. The points using twisted boundary conditions have been computed on ~ 300 configurations. The points obtained without twisted boundary conditions are measured on ~ 500 configurations. The red dashed curve show the continuum dispersion relation.

the Δ mass at $\beta = 4.2$ on a $48^3 \times 96$ lattice, which appears anomalously heavy. This behavior is not due to excited states contamination since this result does not depend on the choice of the fit starting point. Given that $m_{\rm PS}L \sim 3.5$ we are also not expecting large volume effect (see the following section). Furthermore with such a β value which correspond to a lattice spacing of ~ 0.053fm, discretization effects should also be small. It turns out that the point that was supposed to be the best looks crazy. This puzzle is not yet solved. Could it be related to the nature of Δ which is a πN resonance ? Let us consider the Δ decay into πN, which according to parity and angular momentum conservation occurs in a P-wave. On the lattice one thus expect that the decay is allowed if the kinematical condition

$$m_\Delta \geq \sqrt{\left(\frac{2\pi}{L}\right)^2 + m_N^2} + \sqrt{\left(\frac{2\pi}{L}\right)^2 + m_\pi^2} \tag{6.7}$$

is fulfilled. Since the first lattice momenta $(2\pi/L)$ available is rather high this criteria is not fulfilled by our simulated point. However we cannot exclude the existence of parity breaking effects due to the twisted mass formulation. In this case the kinematical threshold condition turns into

$$m_\Delta - m_N \geq m_{\rm PS} \tag{6.8}$$

which is satisfied only for this $\beta = 4.2$, $L = 48$ simulation.

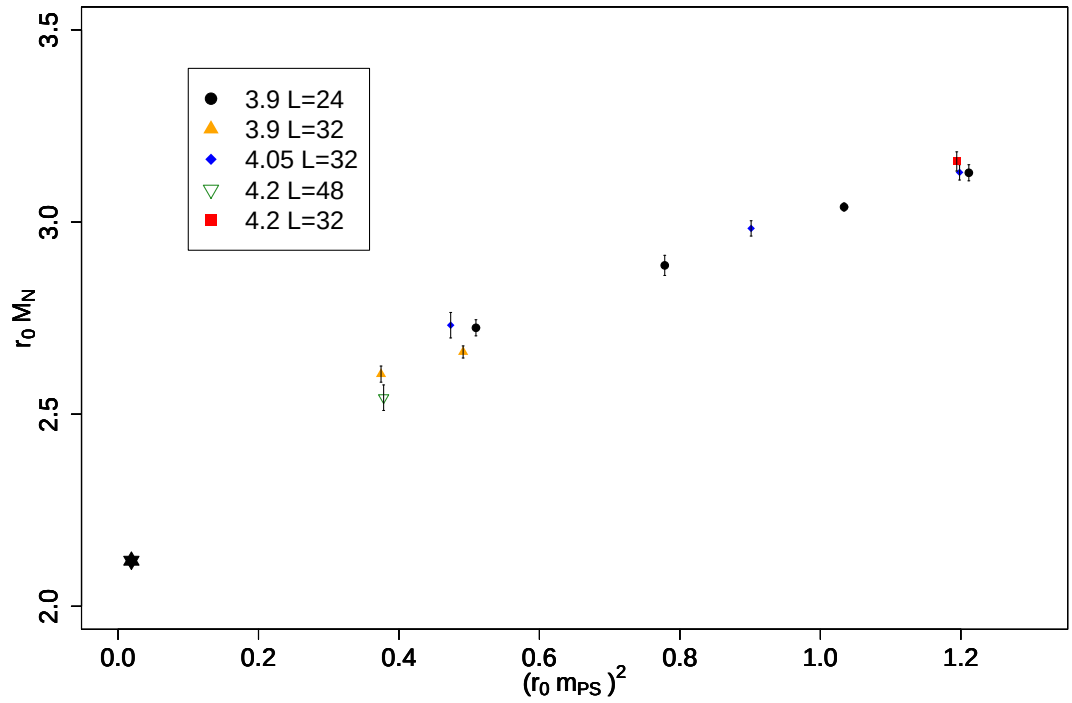

Figure 6.5: Nucleon mass measurement in units of r_0 as a function of $(r_0 m_{\rm PS})^2$. The experimental point is fixed using the value of $r_0 = 0.420(9)(11)$ fm obtain in the mesonic sector in [81].

6.1.5 Finite Volume Effects

Finite volume corrections to the nucleon mass in $N_f = 2$ lattice QCD have been studied in Ref. [126] within the p-expansion which assumes that finite size effects originate from pions propagating around the spatial box. Using relativistic $SU(2)$ baryon chiral perturbation theory [127] the finite volume corrections to the nucleon mass to $\mathcal{O}(p^4)$ take the form:

$$m_N(\infty) = m_N(L) - \delta m_a(L) - \delta m_b(L) \tag{6.9}$$

where

$$\begin{aligned} \delta m_a(L) &= \frac{3 g_A^2 m_N^0 m_\pi^2}{8\pi^2 f_\pi^2} \int_0^\infty dx \sum_{\mathbf{n}}{}' K_0\left(L|\mathbf{n}|\sqrt{(m_N^0)^2 x^2 + m_\pi^2(1-x)}\right) \\ \delta m_b(L) &= \frac{3 m_\pi^4}{2\pi^2 f_\pi^2} \sum_{\mathbf{n}}{}' \left[(2c_1 - c_3)\frac{K_1\left(L|\mathbf{n}|m_\pi\right)}{L|\mathbf{n}|m_\pi} + c_2 \frac{K_2\left(L|\mathbf{n}|m_\pi\right)}{\left(L|\mathbf{n}|m_\pi\right)^2}\right] \quad . \end{aligned} \tag{6.10}$$

$K_\nu(x)$ is the modified Bessel function and the sum is over all integer vectors $\mathbf{n}$ excluding $\mathbf{n} = \mathbf{0}$. The parameters m_N^0 and c_1 are determined by fitting first the nucleon mass to the same order which is given by [128–130]

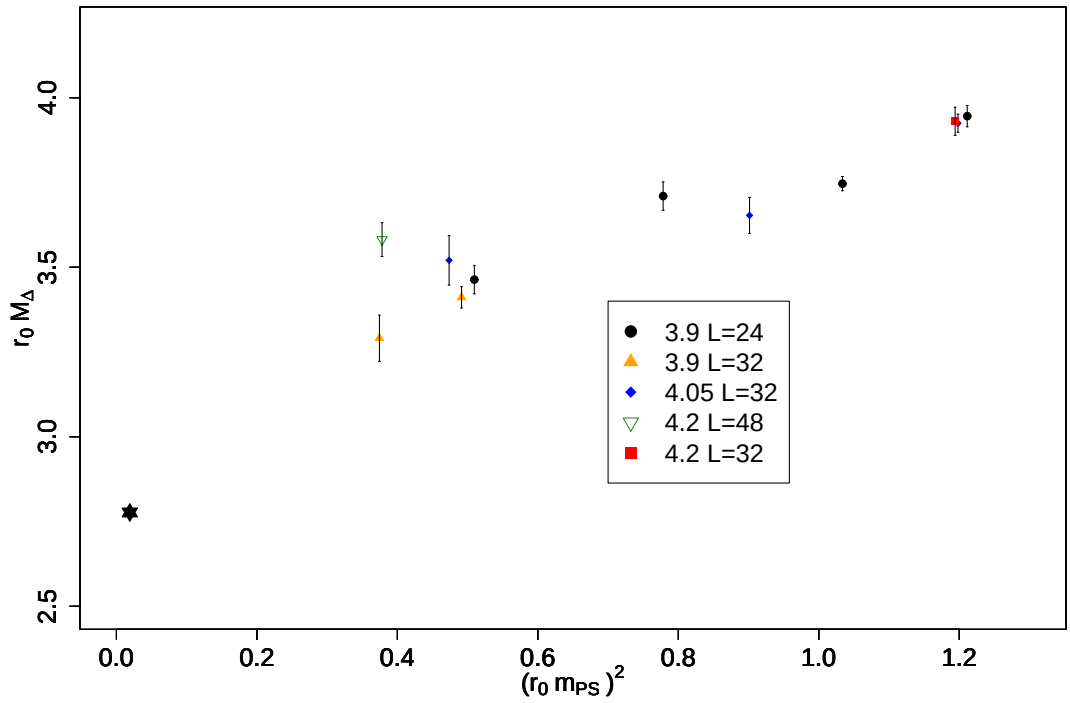

Figure 6.6: Δ mass measurement in units of r_0 as a function of $(r_0 m_{\rm PS})^2$. The experimental point is fixed using the value of r_0 obtain in the mesonic sector.

$$\begin{aligned} m_N &= m_N^0 - 4c_1 m_\pi^2 - \frac{3g_A^2}{16\pi f_\pi^2} m_\pi^3 - 4E_1(\lambda) m_\pi^4 \\ &+ \frac{3m_\pi^4}{16\pi^2 f_\pi^2}\left[\frac{1}{4}\left(c_2 - \frac{2g_A^2}{m_N^0}\right) - \left(c_2 - 8c_1 + 4c_3 + \frac{g_A^2}{m_N^0}\right)\log\left(\frac{m_\pi}{\lambda}\right)\right] \end{aligned} \tag{6.11}$$

We take the cut-off scale $\lambda = 1$ GeV, $f_\pi = 130.70$ MeV and fix the low energy constants $c_2 = 3.2$ GeV^{-1} [131] and $c_3 = -3.45$ GeV^{-1} [129,132], values consistent with empirical nucleon-nucleon phase shifts [133,134]. The fit parameters of Eq. (6.10) – m_N^0, c_1 and the counter-term E_1 – are used to estimate the volume corrections in Eq. (6.10). The results are listed in Table 6.2. As can be seen the corrections for our lattices are, in all cases except one, smaller than the statistical errors. Concerning the Δ a recent analysis using SU(3) heavy baryon chiral perturbation theory has shown that the volume corrections are smaller than for the nucleon [135].

Given the uncertainties both from the theoritical and fitting procedure associated with Eq. (6.10), we have developed an independent and purely phenomenological approach to estimate finite volume correction. We represent in Fig. 6.7 the nucleon and the Δ masses as a function of $m_{\rm PS}L$ obtained using four volumes at $\beta = 3.9$ and $a\mu = 0.004$.

We clearly see that for $m_{\rm PS}L < 3$ result are contaminated by finite volume effects. In order to guide the eyes and to have a quantitative behavior we perform a fit of the form

$$M(m_\pi L) = M_\infty + A\frac{e^{-Bm_\pi L}}{m_\pi L} \tag{6.12}$$

am_π	$am_N(L)$	$a\delta_a(L) + a\delta_b(L)$
$\beta = 3.9$ $24^3 \times 48$		
0.1362	0.5111(58)	0.0068
0.1684	0.5514(49)	0.0046
0.1940	0.5786(67)	0.0026
0.2100	0.5973(43)	0.0021
$\beta = 3.9$ $32^3 \times 64$		
0.1168	0.4958(34)	0.0014
0.1338	0.5126(46)	0.0011
$\beta = 4.05$ $32^3 \times 64$		
0.1038	0.4091(60)	0.0035
0.1432	0.4444(47)	0.0018
0.1651	0.4714(31)	0.0012

Table 6.2: Volume correction to the nucleon mass.

where M_∞ is the mass in infinite volume and A and B characterize the volume dependence. This parameter together with the finite volume correction are summarized in Table 6.3. For the nucleon as well as for the Δ, the parameter B is of order one, indicating that the behaviour of the masses are, as expected, control by the lightest state namely the pion.

state	aM_∞	A	B	$aM_{max} - aM_\infty$
N	0.503	2.36	1.13	0.010
Δ	0.641	1.46	0.848	0.010

Table 6.3: Best fit values of the volume dependence of the octet and decuplet masses.

The finite volume corrections using our phenomenological approach are systematically larger than those given by χPT. Moreover, the Δ correction are sizeable and comparable to the nucleon ones, contrary to the statement of [135]. The fits displayed in Fig. 6.7 suggest that volume effects are under control. A larger volume would be interesting to check that fit coefficient does not change.

6.1.6 Isospin breaking

One important issue of twisted mass formulation of lattice QCD is the isospin symmetry breaking at finite lattice spacing. In the baryonic sector, as already mentioned, the proton and the neutron are degenerate in infinite statistics limit. The same property holds for the Δ^{++}/Δ^- and for Δ^+/Δ^0 independently. However the splitting between Δ^{++}/Δ^- and Δ^+/Δ^0 is a lattice artefact. The relative mass difference defined as

$$\frac{\Delta M_\Delta}{M_\Delta} = 2\frac{M_\Delta^{++/-} - M_\Delta^{+/0}}{M_\Delta^{++/-} + M_\Delta^{+/0}} \tag{6.13}$$

is shown in Fig. 6.8 for all the measurements performed at $\beta = 3.9$, $\beta = 4.05$ and $\beta = 4.2$. As can be seen, the splitting is $\leq 2\%$ and compatible with zero due to the large error bar for most of our ensembles indicating that isospin breaking in the Δ system is at least one order of magnitude smaller than for the pseudoscalar mesons. The only exception to this statement is the ensemble corresponding to $\beta = 3.9$ and $a\mu = 0.003$. One reason could be that this run has been generated keeping the κ_c of $a\mu = 0.004$ which does not insure maximal twist.

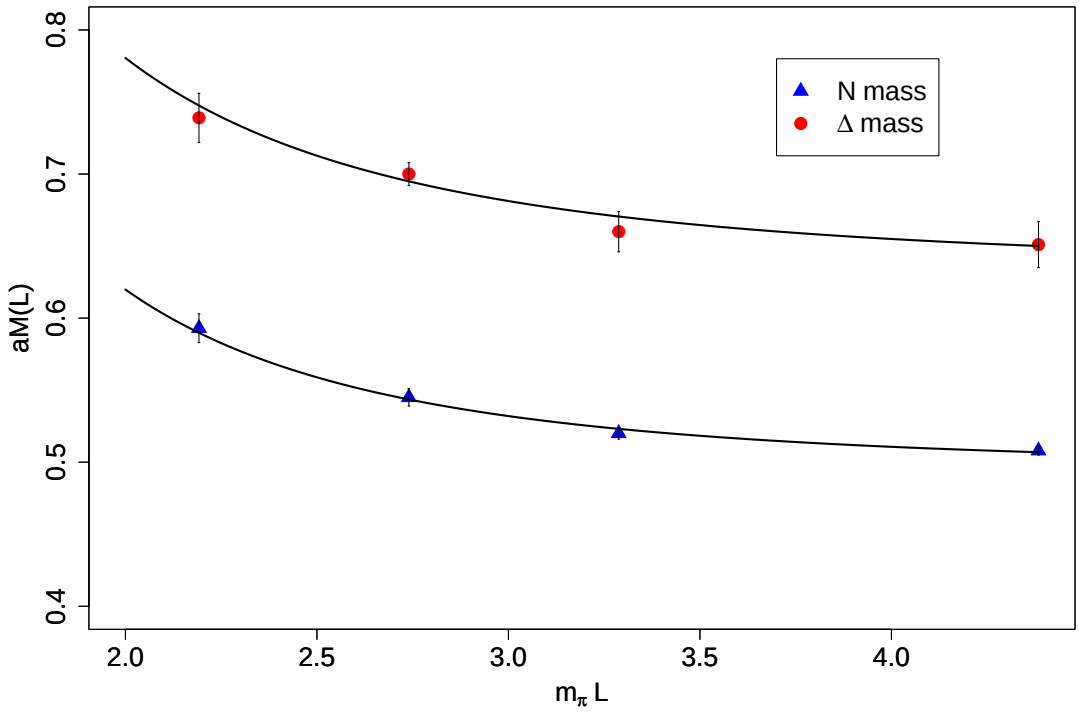

Figure 6.7: Nucleon and Δ^{++}/Δ^{-} mass as a function of $m_\pi L$. The measurements are performed on gauge ensemble generated at $\beta = 3.9$,$\mu = 0.004$ and $L/a = 16, 20, 24, 32$. The dependence as been fitted by $M = M_\infty + +A\frac{e^{-Bm_\pi L}}{m_\pi L}$, to guide the eyes.

In our preceding publications [116], the Δ isospin breaking was always found compatible with zero within errors. The difference with respect to this new analysis is due the significant increases of the statistic which gives a non zero result for $\beta = 3.9$ $L = 24$ ensembles. For instance, for $a\mu = 0.0085$ we have averaged on 2000 measurements instead of 300 in the previous work. This computational effort allows us to better quantify the effect.

6.1.7 Continuum extrapolation

In order to assess cut-off effects we use results at $\beta = 3.9$, $\beta = 4.05$ and $\beta = 4.2$. They are first converted to units of the Sommer scale r_0, and interpolated to the same pion mass for each β value. Interpolating linearly or with one-loop order chiral perturbation theory gives values consistent within error bars.

The continuum extrapolation of the nucleon and Δ are shown in Fig. 6.9 and 6.10. The figures also include results at $\beta = 3.8$ for consistency check. As one can see, the a^2 dependence of the nucleon mass is consistent with a constant behaviour, verifying that for lattice spacings below 0.1 fm, the discretization effects are small.

For the Δ the situation is less clear. The $\beta = 3.8$ results are not confirming small lattice spacing effects. But the results obtained at $\beta = 3.9$ and 4.05 still agree within the error bars. This is also true for the measurement performed at $\beta = 4.2$ but only for the largest pseudoscalar mass. The anomalous result at $\beta = 4.2$ and $r_0^\chi m_{\rm PS} = 0.61$, has already been discussed in Fig. 6.6. Since its validity is doubtful we decide to exclude it from the continuum extrapolation.With this caveat and within statistical errors, cut-off effects seem under control. They will be used to

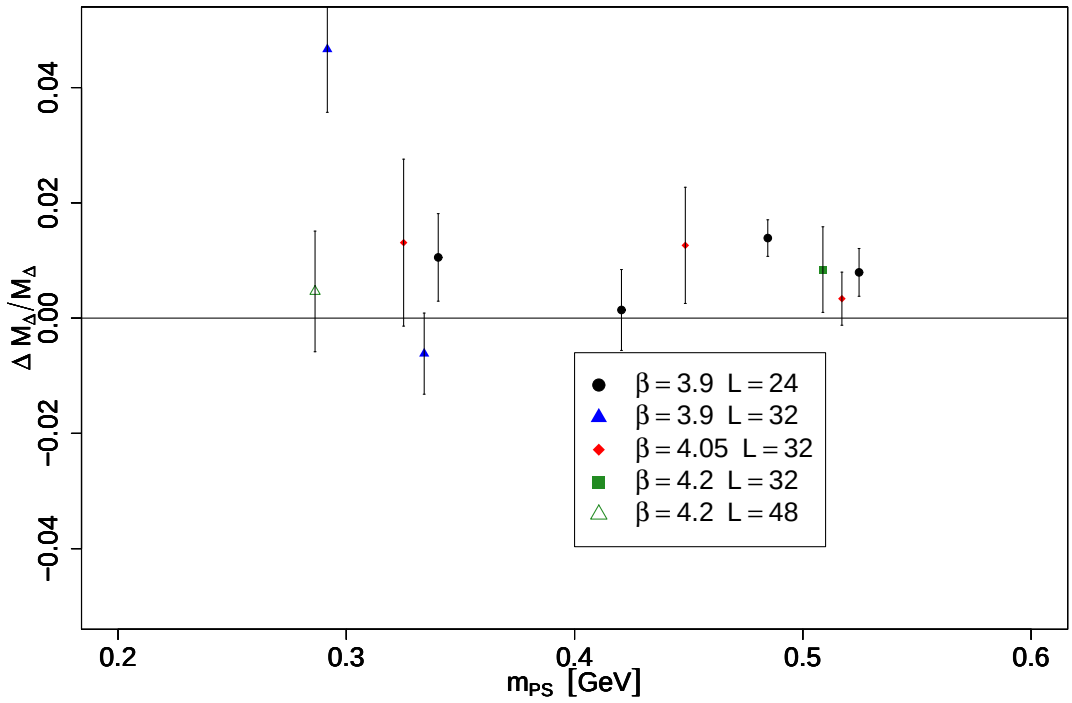

Figure 6.8: The mass splitting between $\Delta^{++,-}$ and $\Delta^{+,0}$ normalized with mean value of their mass as a function of m_{PS}. The lattice spacing used to set the scale is the one compute from f_π.

extrapolate N and Δ masses to the continuum by a constant fit. Our final continuum results at six values of $r_0^\chi m_{\rm PS}$ are given in Table 6.4.

$r_0^\chi m_{\rm PS}$	$r_0^\chi M_N$	$r_0^\chi M_\Delta$
0.61	2.608(31)	3.401(84)
0.70	2.713(17)	3.504(42)
0.80	2.820(14)	3.573(17)
0.90	2.929(7)	3.658(14)
1.00	3.0430(2)	3.774(20)
1.09	3.150(5)	3.927(02)

Table 6.4: Continuum extrapolation of the nucleon and Δ masses at fixed reference pion mass in unit of r_0

6.1.8 Fixing the lattice spacing with the nucleon mass

The lattice spacing can be fixed following different procedures. In principle any dimensional quantity can be used for setting the scale.

As mentioned in 4.4.2, the Sommer scale r_0 has the advantage of being well determined on the lattice. Furthermore its chiral limit, although not totally straightforward, appears linear in our lattice simulations. However its value does not correspond to any measured experimental quantity.

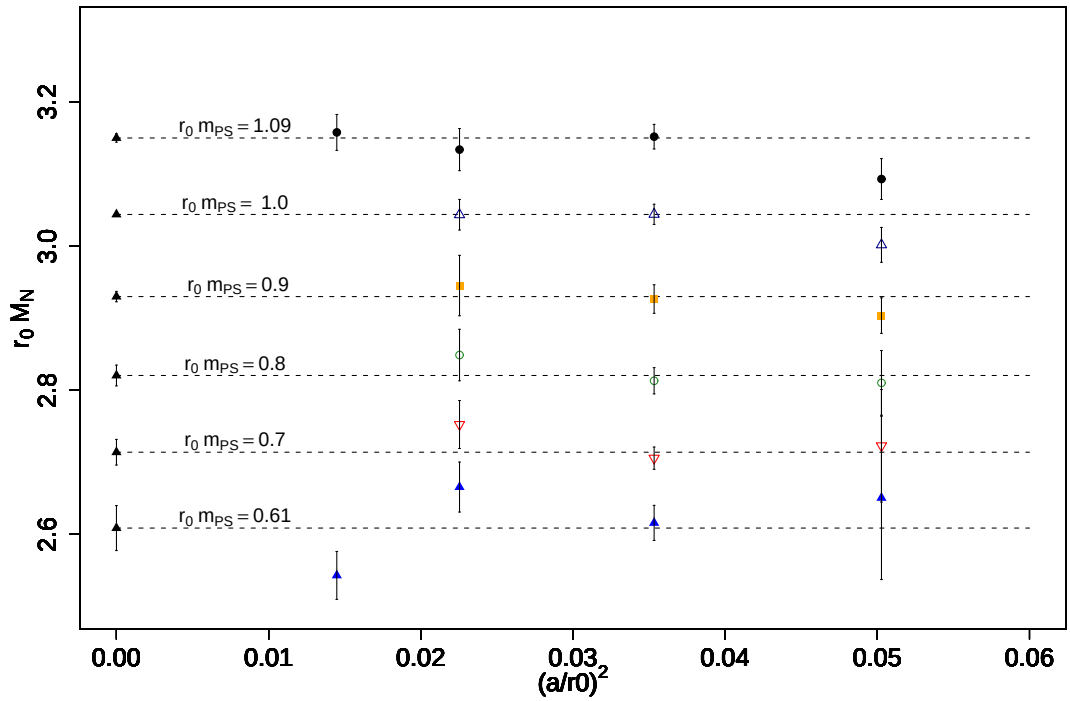

Figure 6.9: Constant extrapolation to the continuum limit for the nucleon. The data at $\beta = 3.8$ which correspond to the larger lattice spacing are not include in the fit. Data at $\beta = 4.2$ are included in the extrapolation. The interpolation is done using a $\mathcal{O}(p^3)$ fit of the data.

The problem is somehow the opposite for all the experimentally well known physical quantities. Indeed, we expect, for most of the observables, a large dependence on the pion mass and the lattice spacing determination has therefore to rely on χPT extrapolations. This procedure sullies the lattice spacing with a large systematic errors, not always under control. Hopefully, in the next few years simulation at the physical point would greatly improve the quality of the scale determination.

In the mesonic sector the scale has been determined using r_0 or $f_{\rm PS}$, and the two determination agree with each other. This result give us confidence in our understanding of the scale determination.

As a further check, and given the quality of the continuum extrapolation, it is tempting to use the nucleon to set the scale.

Two strategies will be followed. The first one consists in directly determining the lattice spacing for each β value. We will be confronted with the fact that at $\beta = 4.2$ only two light quark masses are available, and that the chiral extrapolation is not possible. The lattice spacing extracted according to this method will be denoted by a^N_β.

The second strategy is to fix r_0 before trying to estimate the lattice spacing. It presents the advantage that we can determine this quantity directly in the continuum. One can moreover determine r_0 choosing various subsets of data and thus estimate a systematic error on r_0. We will denote r_0^N the value of the Sommer parameter determined in the nucleon sector. This notation will be used all along this work. Once r_0 fixed, one can then determine the lattice spacing for the various ensembles by using the value r_0^χ/a measured by the collaboration [81] and summarized in Table 4.2.

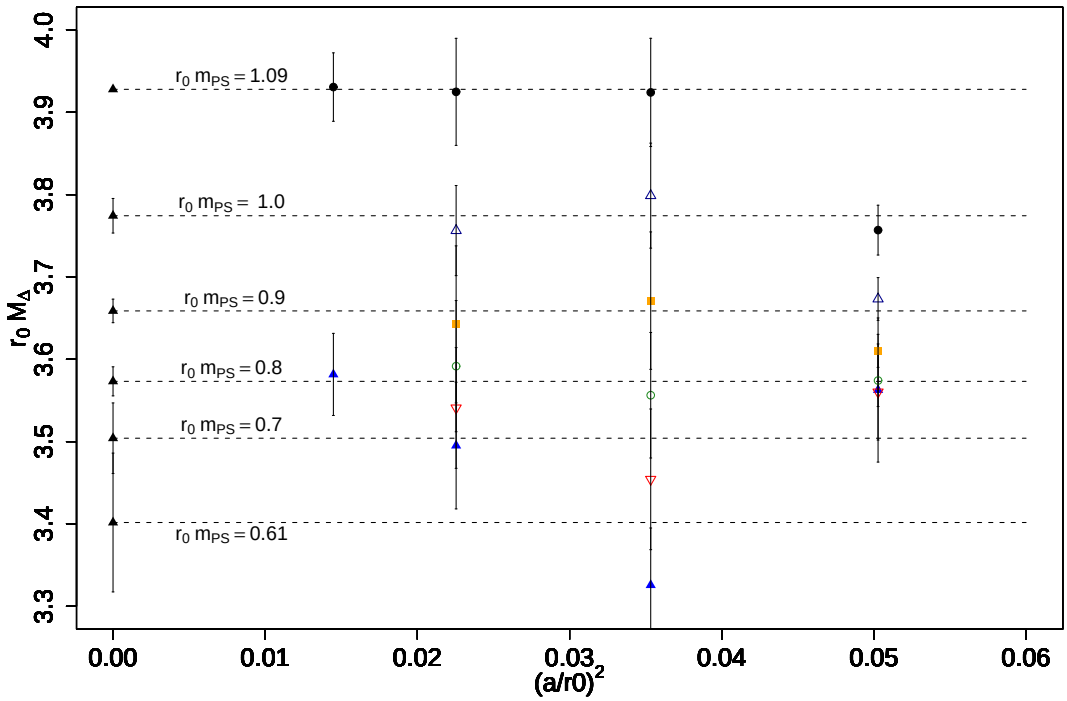

Figure 6.10: Constant extrapolation to the continuum limit for the Δ^{++}/Δ^{-}. The data at $\beta = 3.8$ which correspond to the larger lattice spacing are not include in the fit. Data at $\beta = 4.2$ are not included in the extrapolation for $r_0 m_{PS} = 0.61$. The interpolation is done using a $\mathcal{O}(p^3)$ fit of the data.

Let us define the following quantity

$$\frac{\Delta m_N}{m_N}(a) = \left| \frac{m_N^{\text{phys}} - a^{-1}\left(a m_N^{\text{latt}}(m_\pi)\right)}{m_N^{\text{phys}}} \right| \tag{6.14}$$

where m_N^{phys} is the physical nucleon mass in GeV and $m_N^{\text{latt}}(m_\pi)$ its extrapolated value at the physical point. We determine the lattice spacing by minimizing Eq. (6.14) with respect to a. We plot in Fig. 6.11 $\frac{\Delta m_N}{m_N}$ as a function of a for data at $\beta = 3.9$. The extrapolation to the physical point is performed using the $\mathcal{O}(p^3)$ HBχPT fit. The vertical red dotted line show the value of the lattice spacing obtained. The error on the fit parameters is translated into an error on a and represented by the two vertical black dotted lines. The same procedure can be repeated at $\beta = 4.05$ and the results are summarized in Table 6.5. Even if the systematic errors are large, we observe that the lattice spacing seems to be larger than the one estimated using f_π in Table 4.3.

Following our second strategy, we introduce the equivalent of Eq. (6.14) for the Sommer parameter r_0:

$$\frac{\Delta m_N}{m_N}(r_0) = \left| \frac{r_0 m_N^{\text{phys}} - \left(r_0 m_N^{\text{latt}}(m_\pi)\right)}{m_N^{\text{phys}}} \right| \tag{6.15}$$

We show in Fig. 6.12 its variation with respect to r_0. The extrapolation to the physical point is obtained with $\mathcal{O}(p^3)$ HBχPT fit in the continuum. Note that this extrapolation depends on r_0 through the dimensionful cubic term. A vertical red dotted line indicates the minimum

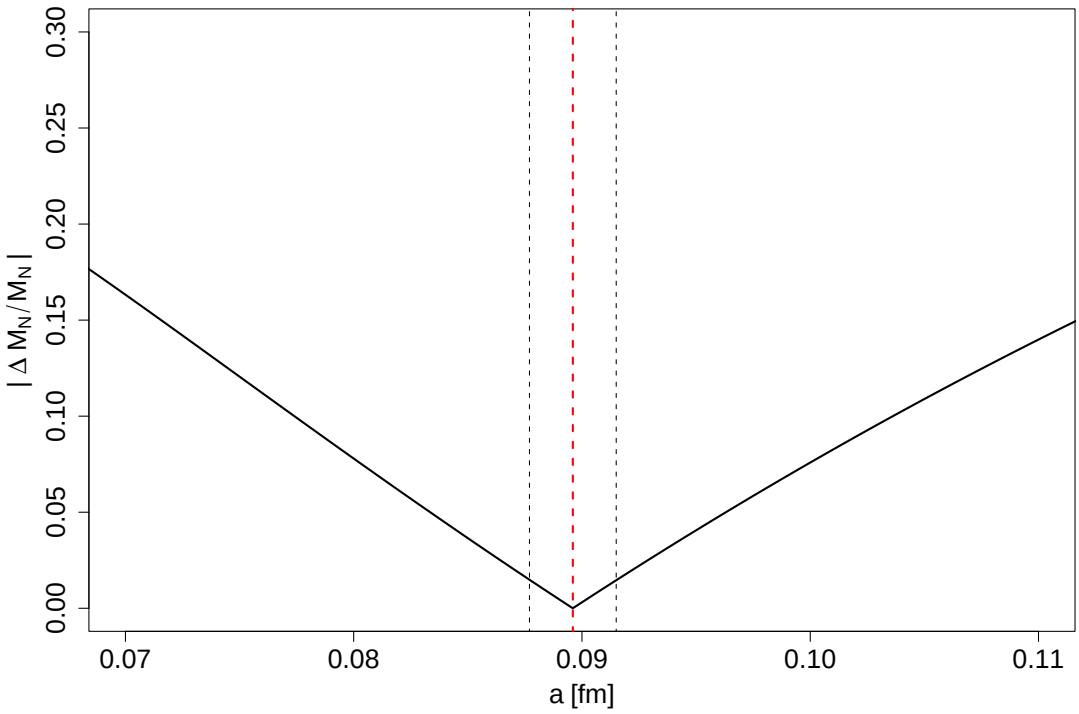

Figure 6.11: Determination of the lattice spacing at $\beta = 3.9$ using $\mathcal{O}(p^3)$ HBχPT fit. We show the quantity define in Eq. (6.14) as a function of a. The optimal value is indicated by a vertical red dotted line. We obtain $a = 0.0896(19)$fm

β	a^N_β (fm)
3.9	0.0896(19)
4.05	0.0737(47)
4.2	?

Table 6.5: Lattice spacing values using $\mathcal{O}(p^3)$ HBχPT fit at fixed lattice spacing. Only two ensembles are available at $\beta = 4.2$, the fit cannot be performed and no estimation of the lattice spacing can be provided using this method.

and two black dotted lines indicates the error on the fit parameter. We show in Fig. 6.13 the corresponding extrapolation of the continuum nucleon mass in r_0 units as a function of $(r_0 m_{\rm PS})^2$. The physical point is fixed using the optimal r_0 obtained in Fig. 6.12.

In order to estimate a systematic error on r_0 we perform the same fit on various ensembles. The value of r_0 obtained are summarized in Table 6.6. All the values are compatible between errors. This is due to the small discretization effects in our simulations. It seems reasonable to choose as a central value r_0 extracted in the continuum and estimate the systematic error by averaging its distance to the other central values. We find this way what will be refered as $r_0^N = 0.460(15)(20)$ fm.

This value has to be compared with the result published in [81] and extracted from the mesonic sector $r_0 = 0.420(9)(11)$ fm. These two independent estimates of r_0 are compatible within errors despite the fact that the central values are quite different. Note that the uncertainty due to the

chiral extrapolation of the nucleon mass, in particular its dependence on g_A, are not estimated and probably explain this tension. Nevertheless we will use r_0^N in the following analysis.

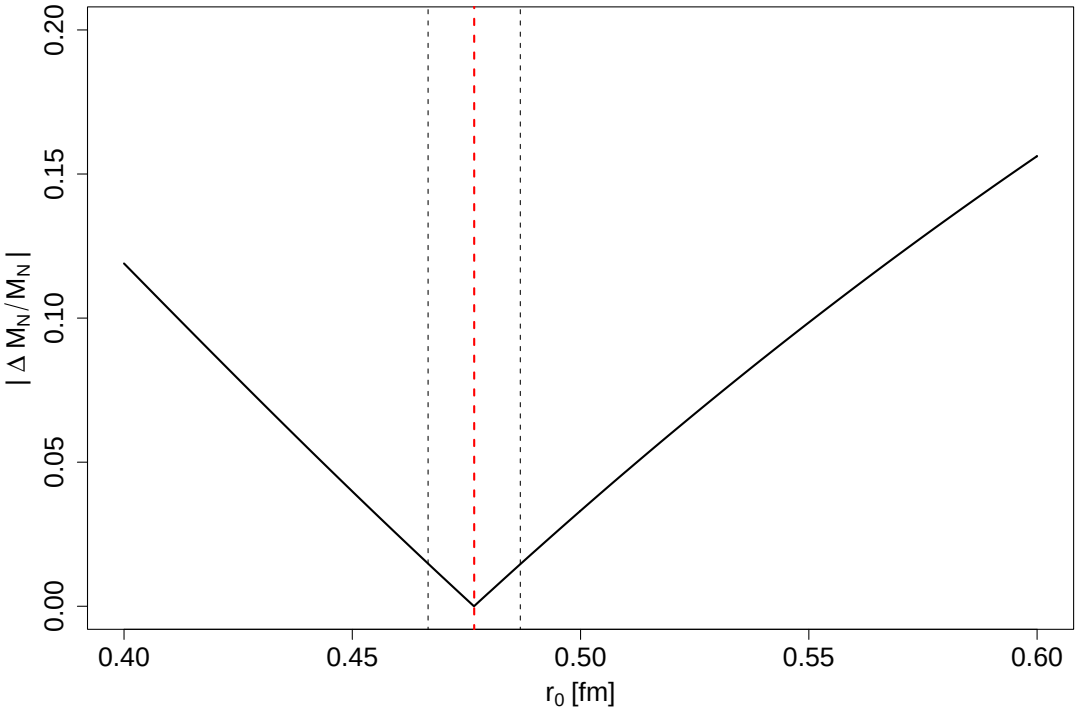

Figure 6.12: Determination of the Sommer scale r_0 at $\beta = 3.9$ using $\mathcal{O}(p^3)$ HBχPT fit. We show the quantity defined in Eq. (6.15) as a function of r_0. The optimal value is indicated by a vertical red dotted line. We obtain $r_0 = 0.4767(101)$fm.

Ensembles	r_0 (fm)
3.9	0.476(10)
4.05	0.491(30)
3.9&4.05	0.478(07)
3.9&4.05&4.2	0.475(06)
continuum	0.460(15)

Table 6.6: r_0 values using $\mathcal{O}(p^3)$ HBχPT fit for various ensemble.

6.1.9 Chiral extrapolation of the nucleon mass

Given that cutoff effects are not sizeable, we have chosen to use the continuum HBχPT even at finite lattice spacing. In particular, we will use SU(2) HBχPT [109] for two reasons: the first one is that our simulations are done for a mass-degenerate dynamical quarks doublet and the second one because there is strong evidence that SU(3) χPT fails to describe lattice data [135].

For easy reading, we recall here the various expression given in chapter 5. We will use the

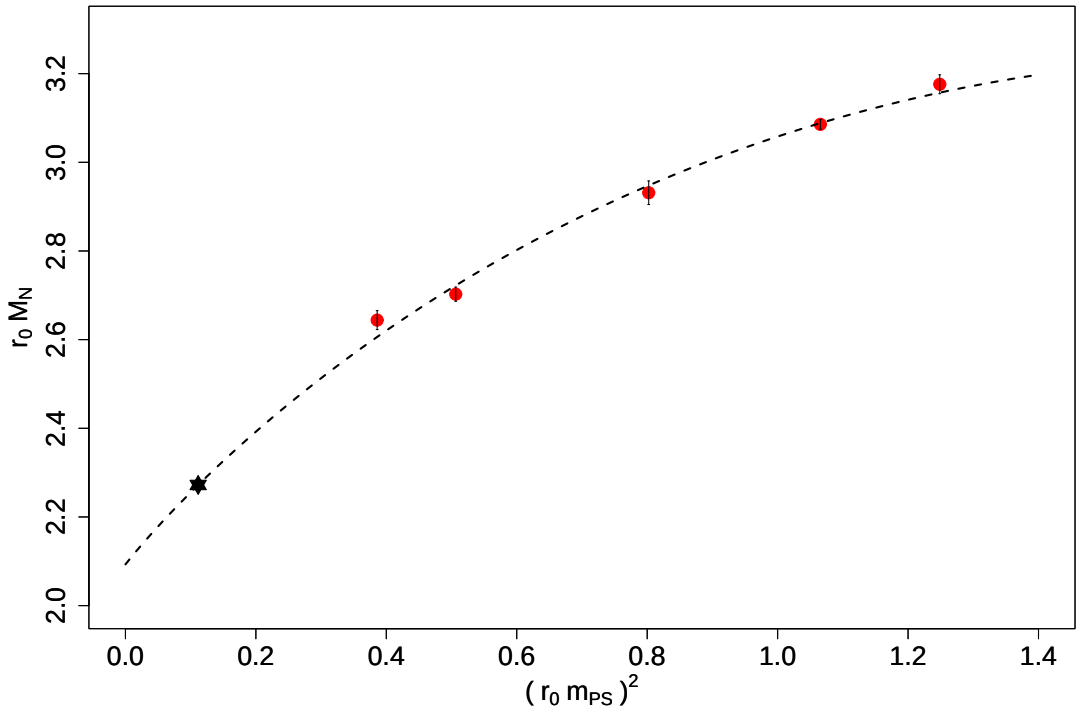

Figure 6.13: The $\mathcal{O}(p^3)$ HBχPT fit which correspond to the optimal value of r_0 determined in Fig. 6.12, namely $r_0 = 0.4767(101)$fm.

LO Eq. (5.37) extrapolation :

$$m_N^{\mathrm{LO}}(m_\pi) = m_N^{(0)} - 4c_N^{(1)} m_\pi^2 \,, \tag{6.16}$$

which involve two parameters $m_N^{(0)}$ and $c_N^{(1)}$.

The $\mathcal{O}(p^3)$ HBχPT inspired fit (Eq. (5.53a))

$$m_N(m_\pi) = m_N^{(0)} - 4c_N^{(1)}\, m_\pi^2 - \frac{3g_A^2}{16\pi f_\pi^2}\, m_\pi^3 \tag{6.17}$$

which depends on the same two parameter as far as we take the experimental values of g_A and f_π. This fit will be always accompanied by a 1σ confidence level band.

The cubic fit Eq. (5.55)

$$m_N(m_\pi) = m_N^{(0)} - 4c_N^{(1)} m_\pi^2 + c_N^{(2)} m_\pi^3 \tag{6.18}$$

which considers the coefficient of m_π^3 as additional fit parameter.

We begin by studying the chiral behavior at $\beta = 3.9$. The lattice data have been converted in physical units multiplying first by r_0^χ/a and dividing by r_0 taken from the meson sector [81]. The results are displayed in Fig. 6.14. The LO fit describes well the lattice results but leads to extrapolated values inconsistent with experiment The same happens using the cubic fit. The $\mathcal{O}(p^3)$ fit gives a behavior more compatible with the experiment although the nucleon mass is overestimated by 80 MeV. The best fit value are summarized in Table 6.7. Note that the large uncertainty on the fitted cubic coefficient is a strong indication that we are not seeing the curvature in our data and that smaller pion masses are needed to be able to produce reliable results.

fit	$m_N(m_\pi)$ (GeV)	$c_N^{(1)}$ (GeV^{-1})	$c_N^{(2)}$ (GeV^{-2})	χ^2/ndof
LO	1.144(11)	1.389(51)	-	0.995
$\mathcal{O}(p^3)$	1.020(21)	4.889(95)	-	3.369
cubic	1.112(44)	2.305(899)	−1.47(1.44)	0.982

Table 6.7: Best fit parameters and statistical error obtained at $\beta = 3.9$. The scale has been fixed in the mesonic sector using $r_0 = 0.420(9)(110)$ fm. The corresponding plot is Fig. 6.14

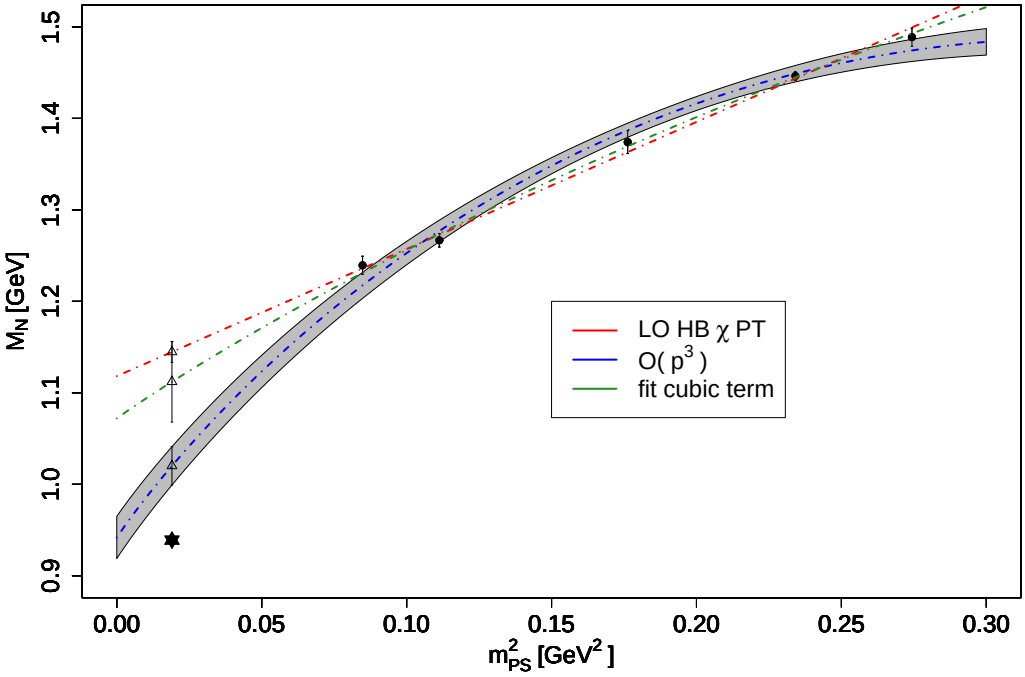

Figure 6.14: Chiral fit at finite lattice spacing with $\beta = 3.9$ ensembles . The corresponding best fit parameters are given in Table 6.8. A one sigma confidence band is shown for the $\mathcal{O}(p^3)$ fit. The scale is set in the meson sector with $r_0 = 0.420(9)(110)$ fm

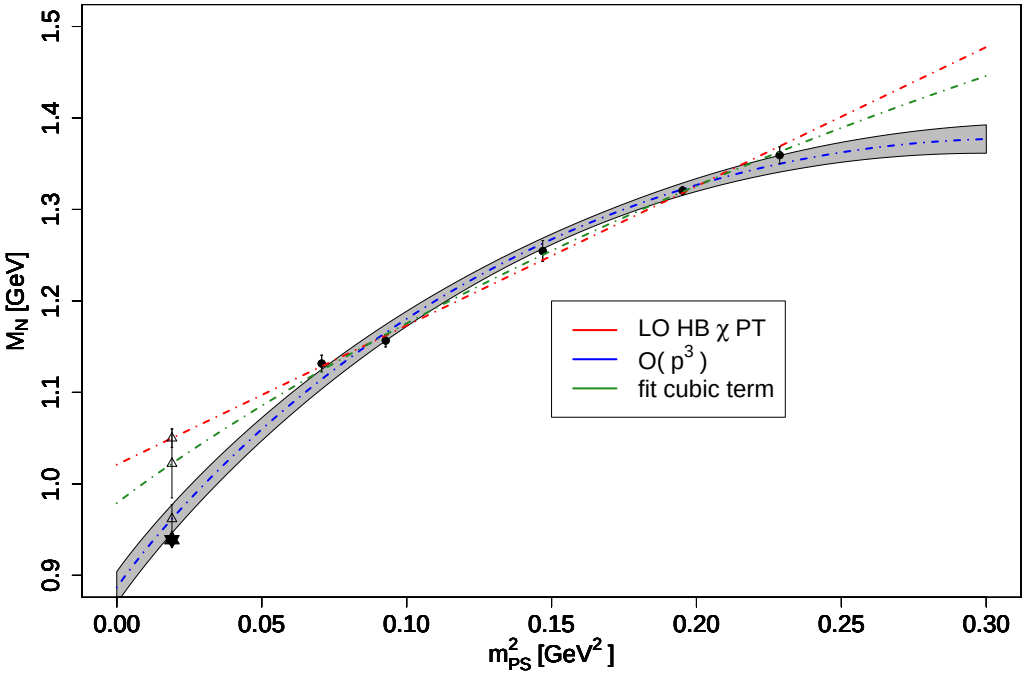

Figure 6.15: Chiral fit at finite lattice spacing with $\beta = 3.9$ ensembles . The corresponding best fit parameters are given in Table 6.8. A one sigma confidence band is shown for the $\mathcal{O}(p^3)$ fit. The scale is set in the nucleon sector with $r_0^N = 0.460(15)(20)$ fm

The same study is shown in Fig. 6.15 using the r_0^N value to fix the scale. Since r_0^N is fixed in the continuum with the nucleon mass the three fits get closer to the physical point. The fit $\mathcal{O}(p^3)$ is even nearly compatible with the experimental value and with our first estimation of the nucleon mass [116]. This is the confirmation that lattice spacing effects are small in our data. Best fit values are summarized in Table 6.8.

fit	$m_N(m_\pi)$ (GeV)	$c_N^{(1)}$ (GeV^{-1})	$c_N^{(2)}$ (GeV^{-2})	χ^2/ndof
LO	1.049(10)	1.521(57)	-	0.995
$\mathcal{O}(p^3)$	0.961(15)	4.717(86)	-	2.284
cubic	1.022(38)	2.524(985)	−1.76(1.73)	1.965

Table 6.8: Best fit parameters and statistical error obtained at $\beta = 3.9$. The scale has been fixed in the nucleon sector using $r_0^N = 0.460(15)(20)$ fm. The corresponding plot is Fig. 6.15

Since we are able to perform the continuum extrapolation of the nucleon data, it is better to use them to study the chiral limit of the nucleon mass. We show in Fig. 6.16 the chiral extrapolation of the nucleon using the value of r_0 obtained in the mesonic sector. Best fit values are summarized in Table 6.9. The results are very similar to those of Fig. 6.14 corresponding to $\beta = 3.9$. The same kind of disagreement with respect to the experimental point is observed, due to the incompatibility between the r_0 fixed in the meson sector and the nucleon data.

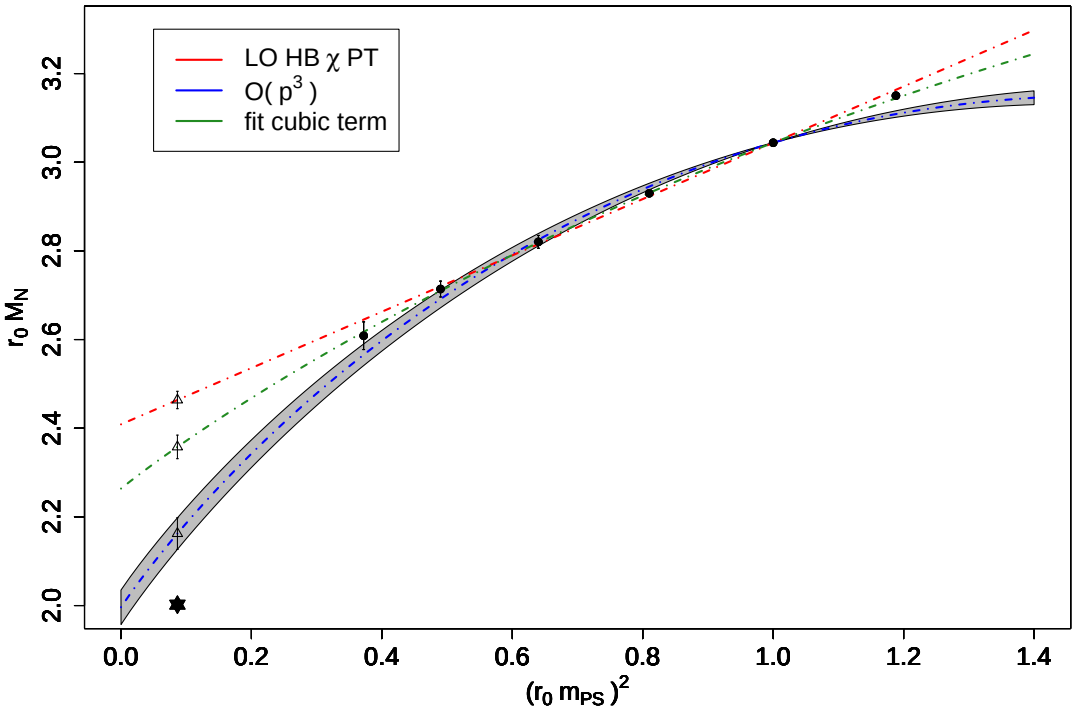

Figure 6.16: Chiral fit of the nucleon in the continuum. The corresponding best fit parameters are given in Table 6.9. The scale is set in the meson sector with $r_0 = 0.420(9)(110)$ fm. The 6 data points are included in the fit.

We finally show in Fig. 6.17 what are the prediction of the LO and cubic fits in the case where

fit	$r_0 m_N(m_\pi)$	$c_N^{(1)}/r_0$	$c_N^{(2)}/r_0^2$	χ^2/ndof
LO	2.482(22)	0.614(20)	-	1.561
$\mathcal{O}(p^3)$	2.103(58)	2.351(55)	-	11.06
cubic	2.381(17)	1.080(63)	−0.332(44)	0.107

Table 6.9: Best fit parameters and statistical error obtained in the continuun. The scale has been fixed in the mesonic sector using $r_0 = 0.420(9)(110)$ fm. The corresponding plot is Fig. 6.16.

we fix r_0^N using the $\mathcal{O}(p^3)$ fit. The main conclusion is that our lattice data miss completely any behavior different from the linear one. Best fit values are summarized in Table 6.10. The only way to describe the physical nucleon mass is by fixing the coefficient of the cubic term to its experimental value and by adjusting the scale.

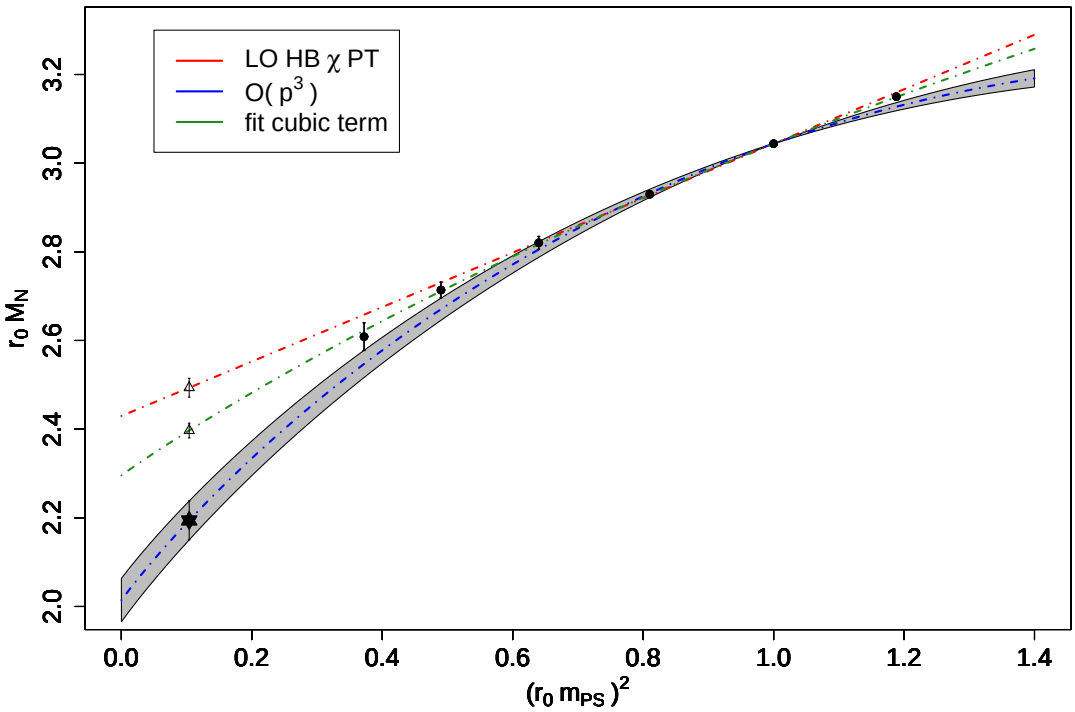

Figure 6.17: The same as Fig. 6.16 except that the scale has been fixed in the nucleon sector using $r_0^N = 0.460(15)(20)$ fm.

fit	$r_0 m_N(m_\pi)$	$c_N^{(1)}/r_0$	$c_N^{(2)}/r_0^2$	χ^2/ndof
LO	2.494(21)	0.614(21)	-	1.561
$\mathcal{O}(p^3)$	2.194(44)	2.060(42)	-	6.610
cubic	2.396(17)	1.080(63)	−0.333(45)	0.107

Table 6.10: Best fit parameters and statistical error corresponding to Fig. 6.17. The scale is fixed using $r_0^N = 0.460(15)(20)$ fm.

6.1.10 Chiral extrapolation for the Δ

The extrapolation of the Δ is a more delicate issue for several reasons. First the chiral perturbation theory is more questionable, due to the fact that this particle is a ~ 120 MeV broad πN resonance. Moreover the cubic term is not fixed by SU(2) HBχPT and can only be related to the nucleon one by $SU(6)$ symmetry.

We show in Fig. 6.18 the chiral extrapolation of the continuum Δ mass in physical units as a function of $m_{\rm PS}^2$. The dimensionless lattice data have been converted using r_0^N since it gives our best results in the nucleon case. The physical point is shown by a black star.

As in the nucleon case the LO fit describes the data well but is far away from the physical point. The cubic fit is even not stable. The $\mathcal{O}(p^3)$ suffers from a large uncertainty but give a satisfactory result, inside the Δ width. The fit parameter are given in Table 6.11.

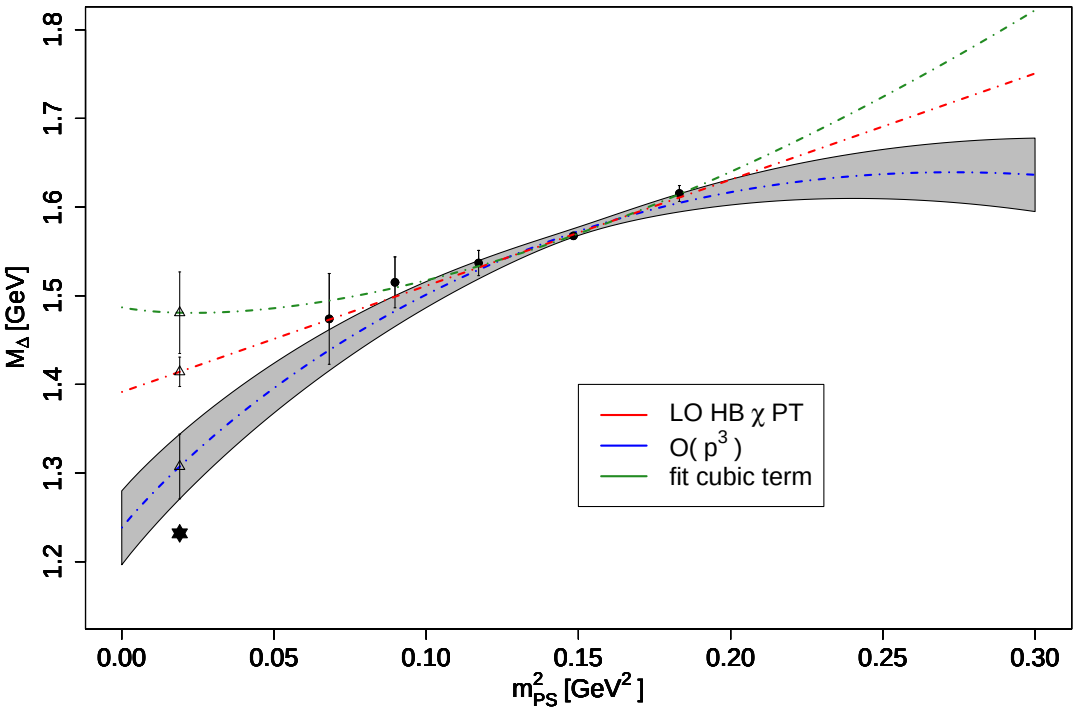

Figure 6.18: Chiral fit of the Δ mass in the continuum. The scale has been fixed using $r_0^N = 0.460(15)(20)$ fm. 5 points are included in the fit. A one sigma confidence band is shown for the $\mathcal{O}(p^3)$ fit. Corresponding parameters are given in Table 6.11

fit	$m_N(m_\pi)$ (GeV)	$c_N^{(1)}$ (GeV^{-}1)	$c_N^{(2)}$ (GeV^{-2})	χ^2/ndof
LO	1.414(17)	1.197(105)	-	0.285
$\mathcal{O}(p3)$	1.307(36)	4.410(230)	-	1.380
cubic	1.481(46)	−0.8(1.7)	3.51(1.76)	0.143

Table 6.11: The best fit parameters for the various chiral fit corresponding to Fig. 6.18.

6.2 Light baryon masses with $N_f = 2 + 1 + 1$ dynamical twisted fermions

Our aim in this section is to investigate whether or not , from the nucleon and Δ spectroscopy side, $N_f = 2+1+1$ simulations are under control. We mean by that to examine if this observable manifest large lattice artefacts due for instance to the charm quark in the sea with a mass very close to the cutoff. We also want to study finite size effects. Indeed we recall that the neutral-charged pseudoscalar splitting is $\sim 50\%$ at $\beta = 1.90$, and with such a light π^0 state it is reasonable to be afraid of potentially large volume effects.

The smearing parameters are the ones of $N_f = 2$, for the equivalent lattice spacing. They are listed in Table 6.12. All the masses are extracted from smeared-smeared correlators. The data used in this section are summarized in Tables F.8 and F.9

β	N_{Gaussian}	α_{Gaussian}	N_{APE}	α_{APE}
1.90	50	4.0	20	0.5
1.95	70	4.0	20	0.5

Table 6.12: Smearing parameters for our $N_f = 2 + 1 + 1$ runs

We will first examine the raw N and Δ results and devote the following sections to a separate study of the various systematic effects.

We plot in Fig. 6.19 the nucleon mass as a function of $(r_0 m_{\text{PS}})^2$. We use the value r_0^χ/a of Table 4.5 in order to compare ensembles different lattice spacing. Note first that the results obtained at $\beta = 1.90$ $\mu_l = 0.004$ on the $32^3 \times 64$ and on the $24^3 \times 48$ lattice agree, indicating a small volume effects. A systematic difference is observed between $\beta = 1.95$ and $\beta = 1.90$, which, as we mentioned in chapter 4, can be due to the strong instability of the $\beta = 1.90$ runs.

We plot in Fig. 6.20 the $\Delta^{++/-}$ mass in units of the Sommer parameter r_0 as a function of $(r_0 m_{\text{PS}})^2$. As in the $N_f = 2$ simulations, the statistical error bars are large. At first glance the situation seems more chaotic than for the nucleon. The results at $\beta = 1.90$ are not compatible with those obtained at $\beta = 1.95$. And on top of that, the Δ exhibit a strong volume dependence. None of these facts were present in $N_f = 2$ simulations. We will see at the end of the section all these anomalies are associated with the $\beta = 1.90$ ensembles.

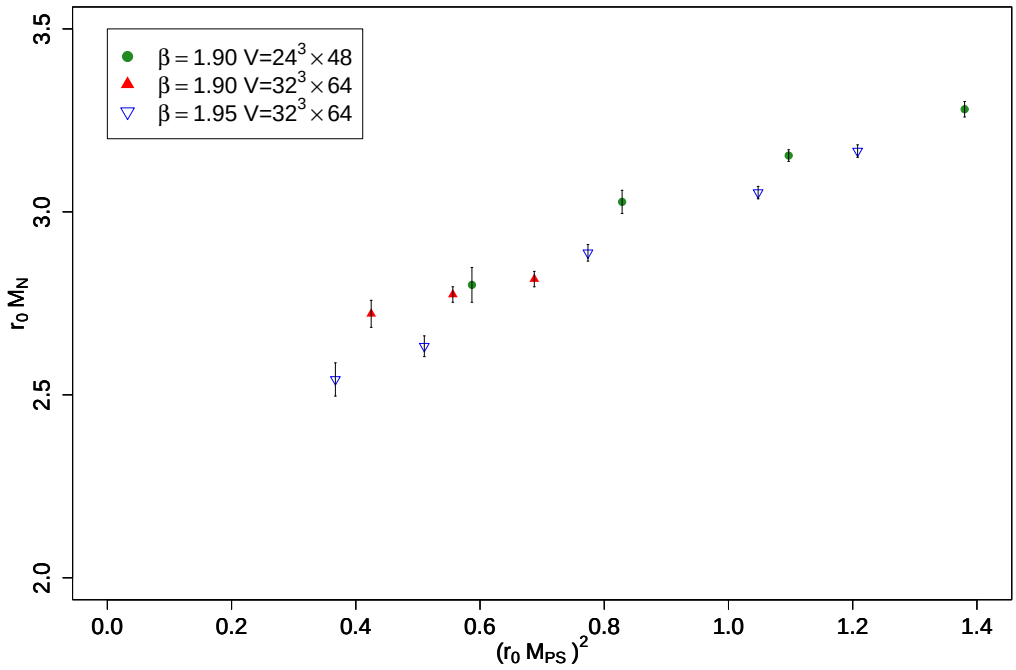

Figure 6.19: Nucleon mass in r_0 units for all ensembles with $N_f = 2 + 1 + 1$

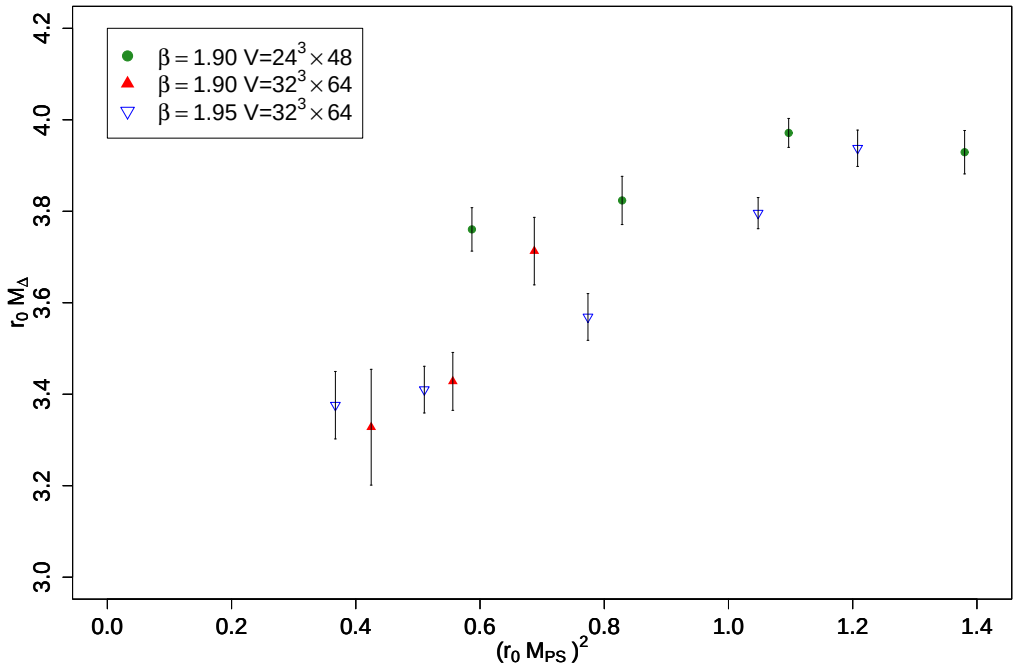

Figure 6.20: Δ mass in r_0 units for all ensembles with $N_f = 2 + 1 + 1$

6.2.1 Finite Volume Effect

At $\beta = 1.90$ three volumes are available for $\mu_l = 0.004$. We can thus compare these results with the detailed volume study obtained in the section 6.1.5 with $N_f = 2$. Note that the charged pseudoscalar masses are of the same order for the $N_f = 2$ and $N_f = 2+1+1$ runs.

We show in Fig. 6.21 the volume dependence of $r_0 m_N$ and $r_0 m_\Delta$. The $N_f = 2+1+1+$ data have been normalized on the $N_f = 2$ parametrization at the largest volume point in order to facilitate the comparison.

In the nucleon case the two larger volumes are in agreements with $N_f = 2$, while the smaller one is not reliable. It correspond to a $20^3 \times 48$ lattice, with a poor signal and with a statistical error which is probably underestimated.

Concerning the Δ, we observe that the intermediate volume shows a large deviation from the expected behavior, which indicates that the volume effects for $N_f = 2+1+1$ are more sizeable than for $N_f = 2$ simulations. However, given the instability of $\beta = 1.90$ runs, it is difficult to state a definitive conclusion. To claim that finite volume effects are under control it would be necessary to generates runs on several volumes at $\beta = 1.95$.

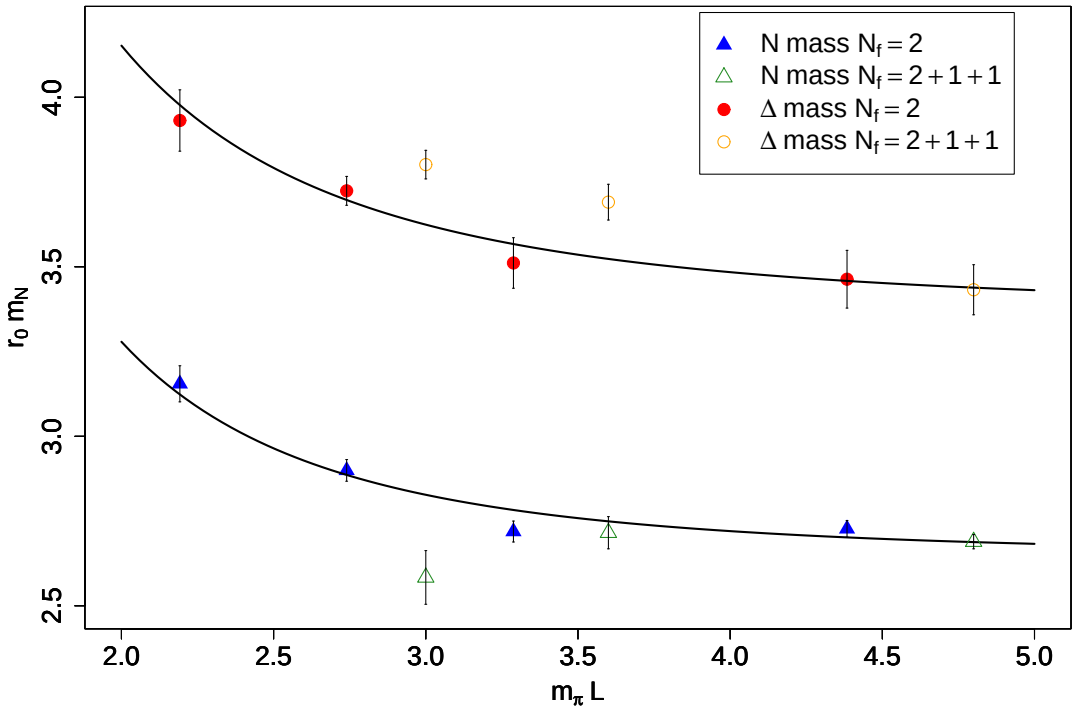

Figure 6.21: Finite volume dependence N and Δ in unit of r_0. Comparison between $N_f = 2$ and $N_f = 2+1+1$. The data $N_f = 2+1+1$ have been shifted such that our larger volume match the $N_f = 2$ results. The black curve is a fit of $N_f = 2$ and is here to guide the eyes.

6.2.2 Isospin breaking

The presence of heavy flavours in the sea generates an unexpectedly large isospin breaking in pseudoscalar meson sector. We showed in section 6.1.6 that in the $N_f = 2$ case most of our Δ ensembles were characterized, by a relative mass difference among the isospin components smaller than 2%.

We show in Fig. 6.22, the relative mass difference defined in Eq. (6.13) as a function of the pseudoscalar mass. We observe that the Δ isospin breaking is comparable to the $N_f = 2$ case.

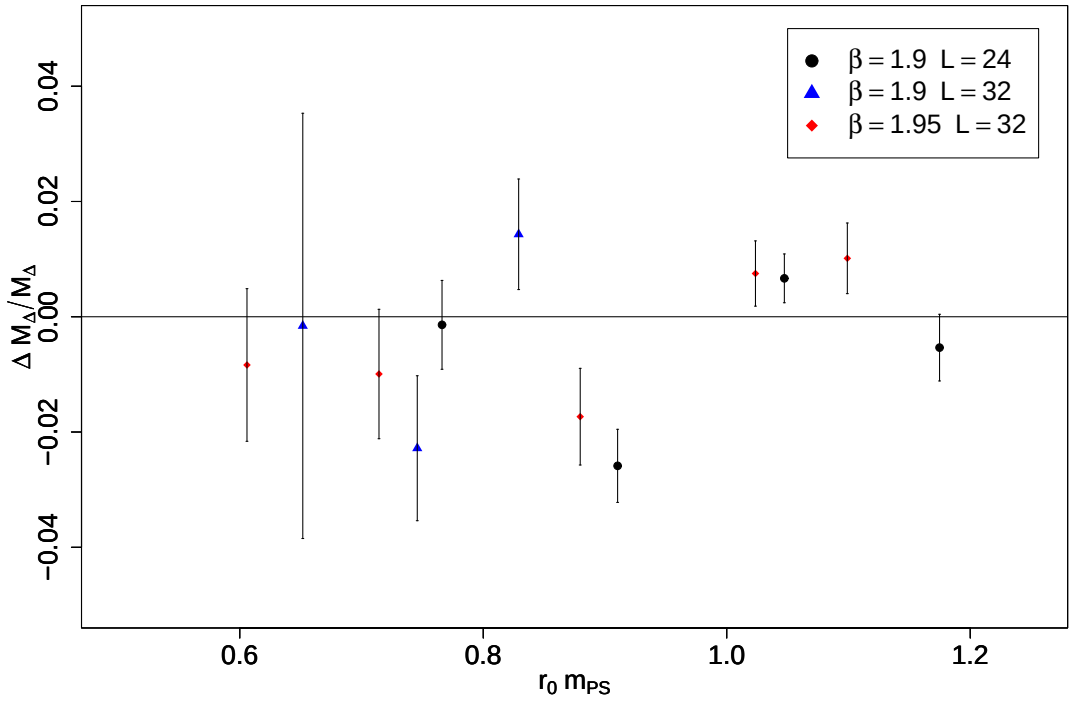

Figure 6.22: The mass splitting between $\Delta^{++,-}$ and $\Delta^{+,0}$ normalized with mean value of their mass as a function of $r_0 m_{\rm PS}$ for $N_f = 2 + 1 + 1$ ensemble

6.2.3 Lattice artefacts

Since we have at our disposal results at two β values, we could in principle study, as in the $N_f = 2$ case, the scaling of the nucleon mass. However with our serious doubts concerning $\beta = 1.90$ ensembles the conclusion will remain preliminary. Any attempt to perform a continuum extrapolation for $N_f = 2 + 1 + 1$ seems to us premature.

Despite this reservation, we think that in the nucleon case, the following exercise could have some interest. We show in Fig. 6.23 for six reference pion masses, the nucleon scaling in r_0 units. The interpolation is performed using a $\mathcal{O}(p^3)$ HBχPT fit, but does not depend on it. Interpolating linearly in $(r0m_{\rm PS})^2$ would have provided similar results. Note that, as expected from the raw nucleon data in Fig. 6.19, the results obtained at $\beta = 1.90$ are systematically heavier than those obtained at $\beta = 1.95$. A constant extrapolation is shown, in order to compare with the continuum values obtained for $N_f = 2$ indicated by dark blue points on the left. As can be seen we observe quite a good agreement between the two independent predictions. Taking into

account that we are comparing with different number of flavours, different lattice spacing and for broad range of pion masses, this consistency is quite impressive, at least strongly encouraging. We summarize the extrapolated value in Table 6.13.

$r_0^X m_{\rm PS}$	$r_0^X M_N$
0.61	2.567(51)
0.70	2.676(51)
0.80	2.806(49)
0.90	2.942(36)
1.00	3.068(38)
1.09	3.178(23)

Table 6.13: Continuum extrapolation of the nucleon mass at fixed reference pion mass in unit of r_0. This values correspond to the extrapolation shown in Fig. 6.23

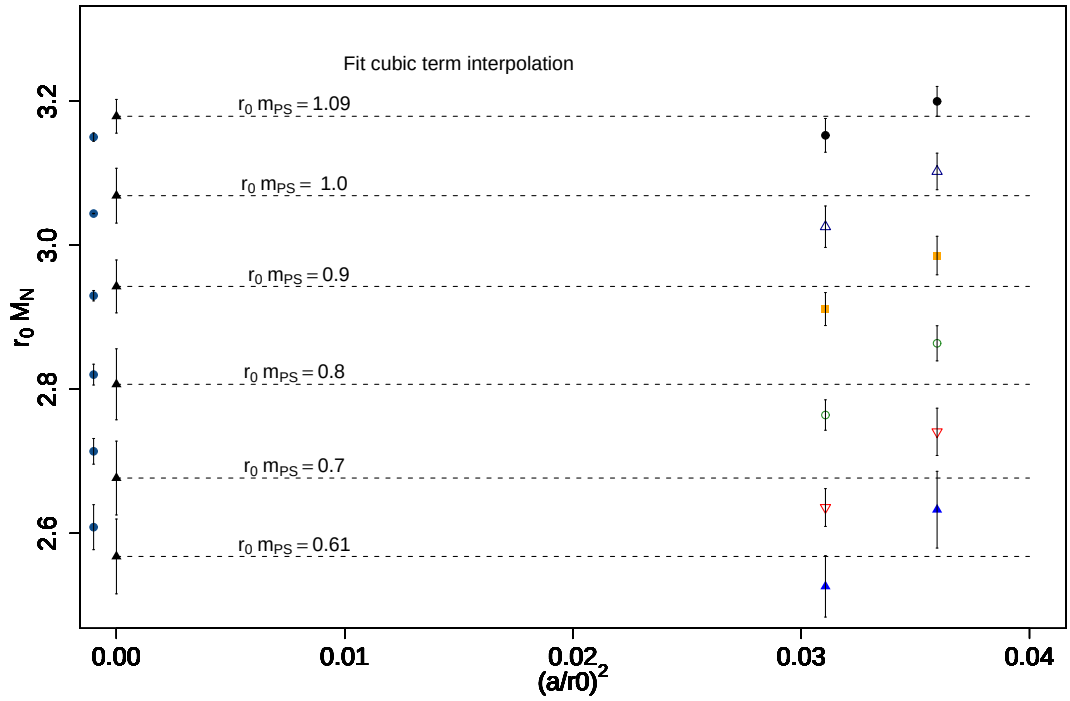

Figure 6.23: Scaling nucleon on $N_f = 2+1+1$ ensembles : constant extrapolation for several reference $r_0 m_{ps}$. The $N_f = 2$ continuum results are shown by blue point. They have been shifted for clarity. Corresponding fitted values are summarized in Table 6.13

6.2.4 Fixing the scale

Several attempts to set the scale for $Nf = 2+1+1$ runs have been performed in the meson sector and these first estimations of the lattice spacing are summarized in Table 4.6. As we did in section 6.1.8 for $N_f = 2$, we have chosen to estimate the lattice spacing or/and the Sommer

scale with the nucleon mass. In order to know the sensitivity of the result to the functional form of the chiral fit, we have tried the several choices listed below:

- Fit A : $\mathcal{O}(p^3)$
- Fit B : $\mathcal{O}(p^3)$ overestimating of 10% the cubic term
- Fit C : $\mathcal{O}(p^3)$ underestimating of 10% the cubic term
- Fit D : cubic fit

The value of r_0 minimizing Eq. (6.15) are summarized in Table 6.14, independently for the two gauge ensembles. As expected, the cubic fit D gives anomalously large results, due to the m_π^2 linear behaviour of the data. The value obtained with the fit A are in agreement within the errors for the two β values. A variation of 10% of the cubic term is responsible for a $< 4\%$ variation of the Sommer scale. To have an idea of the corresponding lattice spacing we choose to average the r_0 value obtained at $\beta = 1.90$ and $\beta = 1.95$ with the fit A. We thus obtain $r_0 \sim 0.44$ fm, which correspond respectively to $a_{\beta=1.90} \sim 0.084$ fm and $a_{\beta=1.95} \sim 0.077$ fm in good agreement with results obtained in the meson sector.

Ensembles	r_0 (fm) (A)	r_0 (fm) (B)	r_0 (fm) (C)	r_0 (fm) (D)
1.90	0.457(26)	0.466(22)	0.445(32)	0.509(6)
1.95	0.436(19)	0.446(14)	0.424(25)	0.475(30)

Table 6.14: Sommer scale values using $\mathcal{O}(p^3)$ HBχPT fit for various ensemble and for the fits A,B,C and D.

These results are confirmed by a direct determination of the lattice spacing, independent of r_0^χ/a. Minimizing Eq. (6.14) for the chiral extrapolation A B C or D gives the results summarized in Table 4.6. The value obtained with an $\mathcal{O}(p^3)$ does not show any tension with the previous result and with the meson analysis.

Ensembles	a (fm) (A)	a (fm) (B)	a (fm) (C)	a (fm) (D)
1.90	0.087(5)	0.089(6)	0.085(7)	0.097(11)
1.95	0.076(4)	0.078(4)	0.074(6)	0.083(5)

Table 6.15: Lattice spacing values using $\mathcal{O}(p^3)$ HBχPT fit for various ensemble and for the fits A,B,C and D.

6.3 Final remarks

As a conclusion of this chapter, we would like to point out that, disregarding the $\beta = 1.90$ ensemble, the $N_f = 2 + 1 + 1$ nucleon and Δ results are in very nice agreement with $N_f = 2$ continuum ones.

This is illustrated in Figs. 6.24 and 6.25, displaying the $\beta = 1.95$ nucleon and Δ data in r_0 units as a function of $(r_0 m_{\rm PS})^2$ together with the $N_f = 2$ continuum extrapolated values. The agreement is striking, and promises nice perspectives for the three nearly finished runs at $\beta = 2.1$ on $48^3 \times 96$ lattices, with pion masses below 300 MeV.

It is also worth noticing that we present here for the first time lattice QCD dynamical simulations which incorporate, on top of the light sector, the strange and charm quark virtual effects.

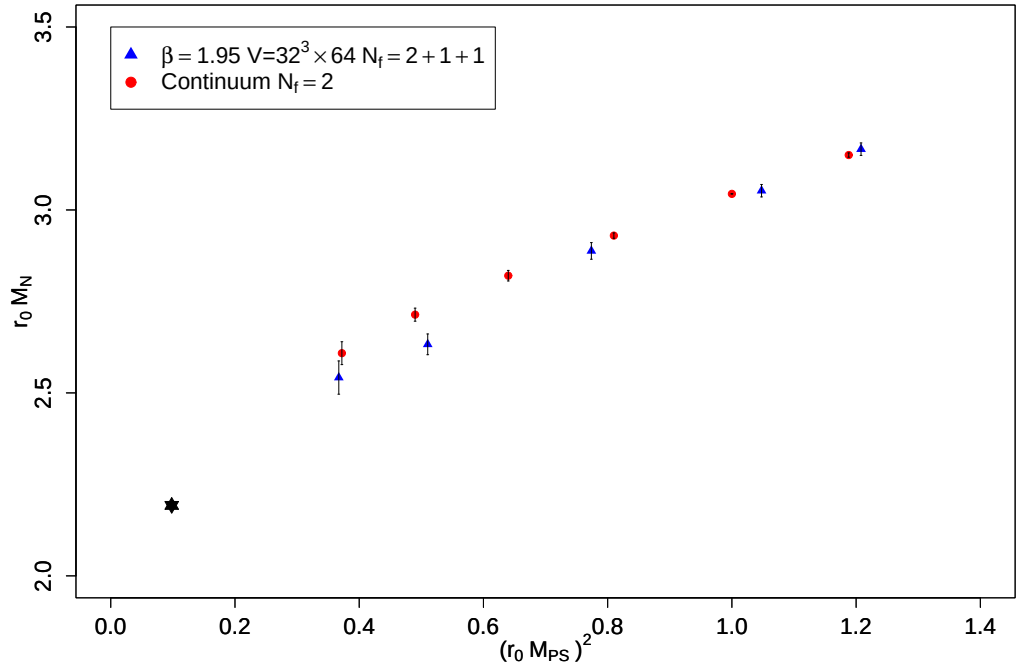

Figure 6.24: Comparison of the continuum $N_f = 2$ results and of the finite lattice spacing data obtained at $\beta = 1.95$ for $N_f = 2+1+1$ for the nucleon mass. The physical point is set with r_0^N obtained with $N_f = 2$

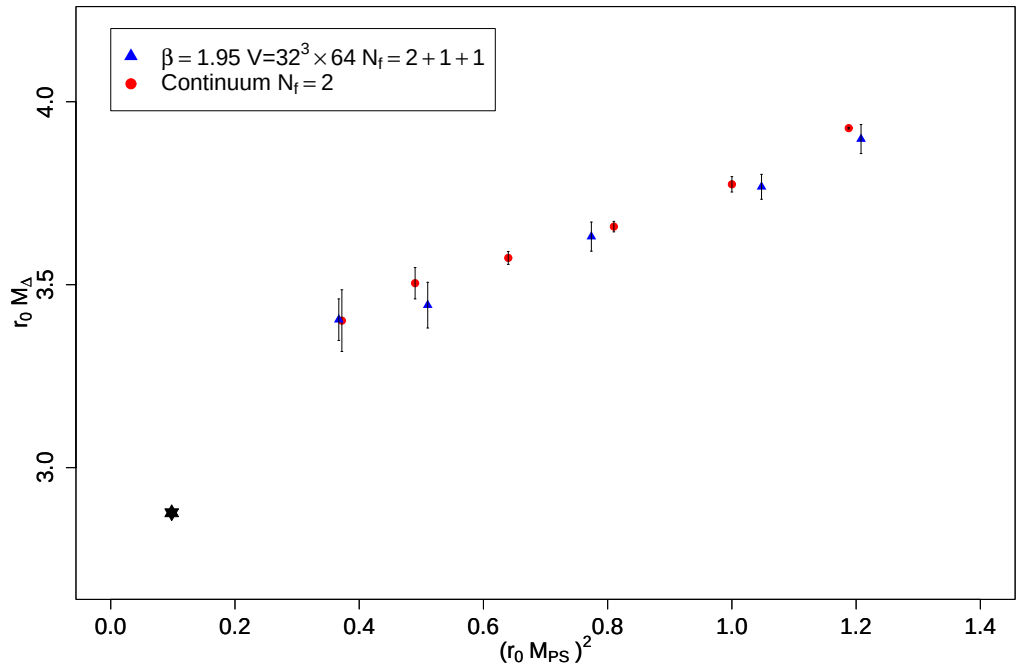

Figure 6.25: The same plot than in Fig. 6.24 for the Δ. The physical point is set with r_0^N obtained with $N_f = 2$

Chapter 7

Strange Baryons Analysis

Contents

The previous study devoted to the analysis of the non strange baryons using twisted mass fermions has been extended to ground state baryons containing strange quarks.

This analysis has been performed only in the framework of two dynamical degenerate flavours, neglecting the strange loop contribution to baryon masses. This is the so-called partially quenched approximation. We consider an Osterwalder-Seiler strange quark following the approach employed in the study of the pseudoscalar meson constants [136, 137]. Extension of this analysis using mixed action strategy as well as unitary setup are in progress on the $N_f = 2+1+1$ ETMC configurations.

Most of the material present in this chapter is published in [138, 139].

Other works of particular relevance are the calculations of the low-lying baryon spectrum using two degenerate flavours ($N_f = 2$) of light dynamical quarks by the MILC collaboration [140,141] using Kogut-Susskind fermions. There are also calculations using two degenerate flavours of light quarks and a strange quark with mass tuned to its physical value ($N_f = 2 + 1$) mainly using clover improved Wilson fermions with different levels of smearing applied by the QCDSF-UKQCD collaboration [126] for the nucleon mass, and the PACS-CS [75] and BMW [76] collaborations for the octet and decuplet spectrum. The LHPC computed the octet and decuplet spectrum using a hybrid action with domain wall valence fermions on Kogut-Susskind sea quarks [111]. Preliminary results on the nucleon mass are also computed using $N_f = 2+1$ domain wall fermions by the RBC-UKQCD collaboration [142, 143].

7.1 Lattice setup

We use in this study all the techniques introduced for the nucleon and Δ. The details of the analysis are given in chapter 3. The interpolating fields are listed in Table 3.2 and Table 3.3. The Osterwalder-Seiler action [144] use to simulate the strange quark in the valence sector reads:

$$S_s = a^4 \sum_x \overline{\chi}_s(x) \left(D_W[U] + m_0 + i\mu_s\gamma_5\right) \chi_s(x) \tag{7.1}$$

This is naturally implemented in the twisted mass approach by introducing an additional doublet of strange quark and keeping only the positive diagonal component τ_3. The m_0 value is taken to be equal to the critical mass determined in the light sector, thus guaranteeing the $\mathcal{O}(a)$ improvement in all observables. The reader interested in the advantage of this mixed action in the mesonic sector is referred to [136, 137, 145–147]. All the data used in this chapter are summarized in Tables F.1–F.6

7.2 Strange mass determination

In a previous paper of the ETM collaboration [136], pseudoscalar meson masses have been computed for different values of the sea and valence quark at $\beta = 3.9$. Using the experimental value of the the kaon to pion mass ratio m_K/m_π, the bare strange quark can be determined. We will use all along this chapter $a\mu_s = 0.0217$ at $\beta = 3.9$ taken from Table 2 of Ref. [136].

In a more recent study of the kaon and D-mesons pseudoscalar decay constants [137], the computation was extended to $\beta = 3.8$ and $\beta = 4.05$. However, no value of the bare strange quark mass was published and an accurate extraction of it is still in progress. One can obtain an estimate of the bare strange quark mass at a given value of β taking the results at $\beta = 3.9$ as a reference and using the scaling relation:

$$a\mu_s(\beta) = \frac{Z_p(\beta)}{Z_p(\beta = 3.9)} \frac{a(\beta)}{a(\beta = 3.9)} a\mu_s(\beta = 3.9) \; . \tag{7.2}$$

The values we use for $\beta = 3.8$ and $\beta = 4.05$ given in Table 7.1. are obtained by applying Eq. (7.2) [148]. We use the value of the renormalization constant $Z_p(\beta)$ found in the preliminary analysis of Ref. [149] within the RI' scheme.

	$\beta = 3.8$	$\beta = 3.9$	$\beta = 4.05$
$a\mu_s$	0.0208(15)(48)	0.0217(22)	0.0166(18)(29)

Table 7.1: Bare strange quark mass used in the valence sector for different β values.

7.3 Effective masses

In Figs. 7.1 and 7.2 we show the baryon effective masses of the octet and decuplet representation respectively. As can be seen a plateau region can be identified for all baryons. They have been obtained using smeared-smeared correlation functions. Although local correlators are expected to have the same value in the large time limit, smearing suppresses excited state contributions yielding a plateau at earlier time separations and a better accuracy in the mass extraction. Note that the Δ signal remains the worst even with a very large statistic.

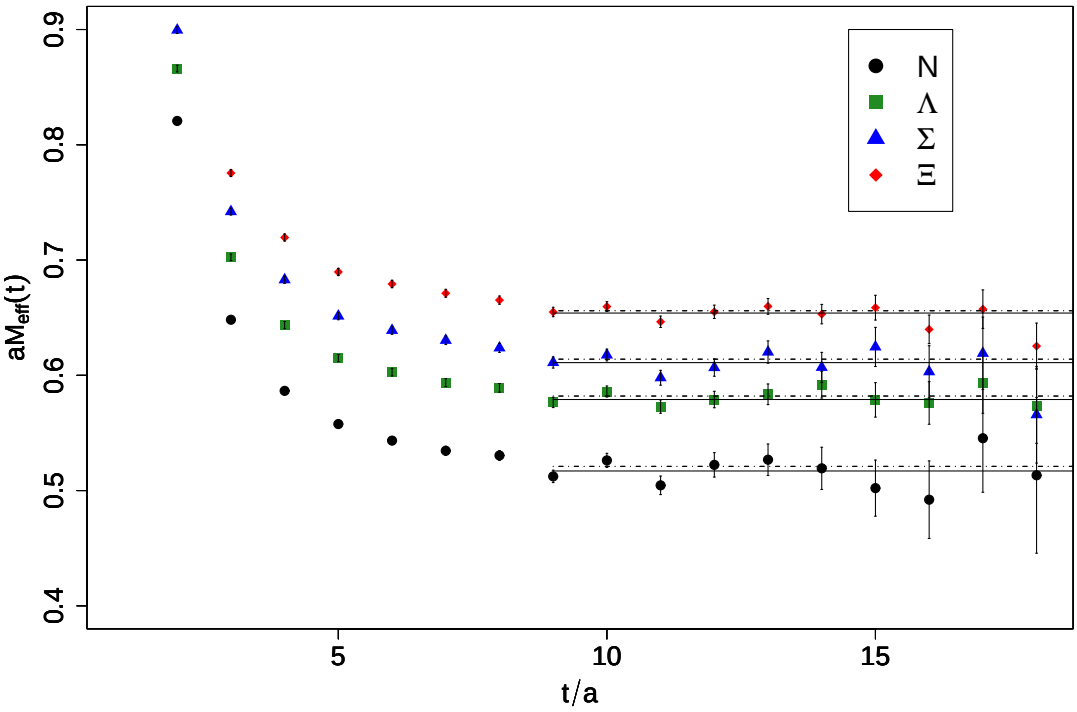

Figure 7.1: Effective masses of the octet states for $\beta = 3.9$ $a\mu = 0.004$ on a $24^3 \times 48$ lattice using 2987 configurations

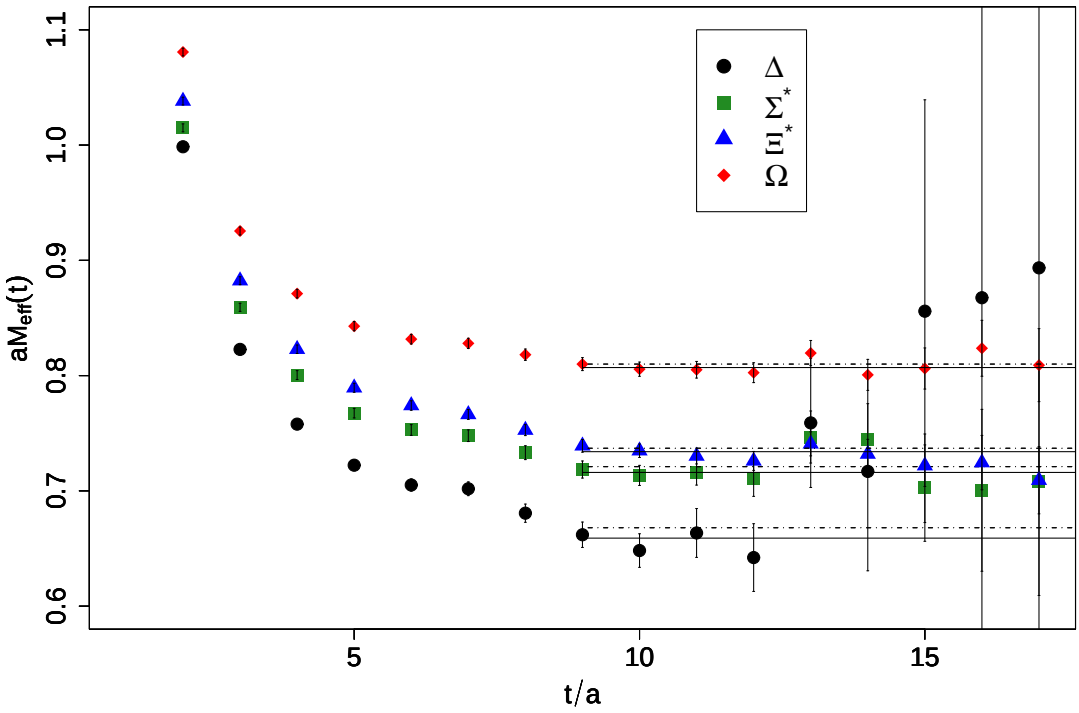

Figure 7.2: Effective masses of the decuplet states for $\beta = 3.9$ $a\mu = 0.004$ on a $24^3 \times 48$ lattice using 2987 configurations

7.3.1 Strange quark mass dependence

The dependence of the masses of strange baryons on the bare strange quark mass has been investigated at $\beta = 3.9$ for $a\mu = 0.004$. The results are displayed in Figs. 7.3 and 7.4. Corresponding data are summarized in Table F.1 and F.2 The vertical dotted lines indicate the value of the tuned bare strange quark mass as taken from Table 7.1. The SU(3) symmetric point $\mu_s = \mu_l$ is given by the nucleon and Δ masses for the octet and decuplet, respectively.

As can be seen in the SU(3) limit all the octet and decuplet masses converge to a single point. Cutoff effects can account for the small deviations. For clarity we only show in Fig. 7.3 the mass of the Λ, $\Sigma^{\rm av}$ and $\Xi^{\rm av}$. They should be degenerate with the nucleon in the limit of $\mu_s = \mu_l$. Indeed, if one computes the nucleon mass with the same statistics as the one used for $\Sigma^{\rm av}$ and $\Xi^{\rm av}$, one finds them to be degenerate within the errors as can be seen in Fig. 7.3 .

The corresponding results for the decuplet baryons are displayed in Fig. 7.4. As can be seen, also in the case of the decuplet masses there is convergence to the Δ mass as predicted in the exact SU(3) limit $\mu_s = \mu_l$.

The μ_s dependence of the strange baryon masses provides an estimate of systematic errors due to the uncertainty on the bare strange quark mass. As already explained, the kaon mass at the physical point is used to fix μ_s. This gives $a\mu_s = 0.0217(22)$. The 10% uncertainty leads to a corresponding error on the strange baryon. It can be estimated by the performing a linear regression of the form

$$M_X = A_X + B_X a\mu_s \tag{7.3}$$

in the vicinity of $a\mu_s = 0.0217$.

Denoting δ_A and δ_B the error on the fit paramters, and $\delta\mu_s$ the error on the bare strange quark mass the systematical error reads

$$\delta M = \sqrt{A^2\delta\mu_s^2 + \mu_s^2\delta_A^2 + \delta_B^2} \tag{7.4}$$

We summarize in Table 7.2 the best fit values for the ground state strange baryons, together with their associated systematic error δM. One can see from this table that these errors range from 17 to 41 MeV depending on strangeness content of the states. This is a direct consequence of the slopes observed in figure 7.3 and 7.4 which are roughly proportional to the number of strange quark.

It is worth noticing that when the statistical errors are given on the final spectrum one must bear in mind that there is a systematic error of about the same magnitude due to the strange quark mass determination.

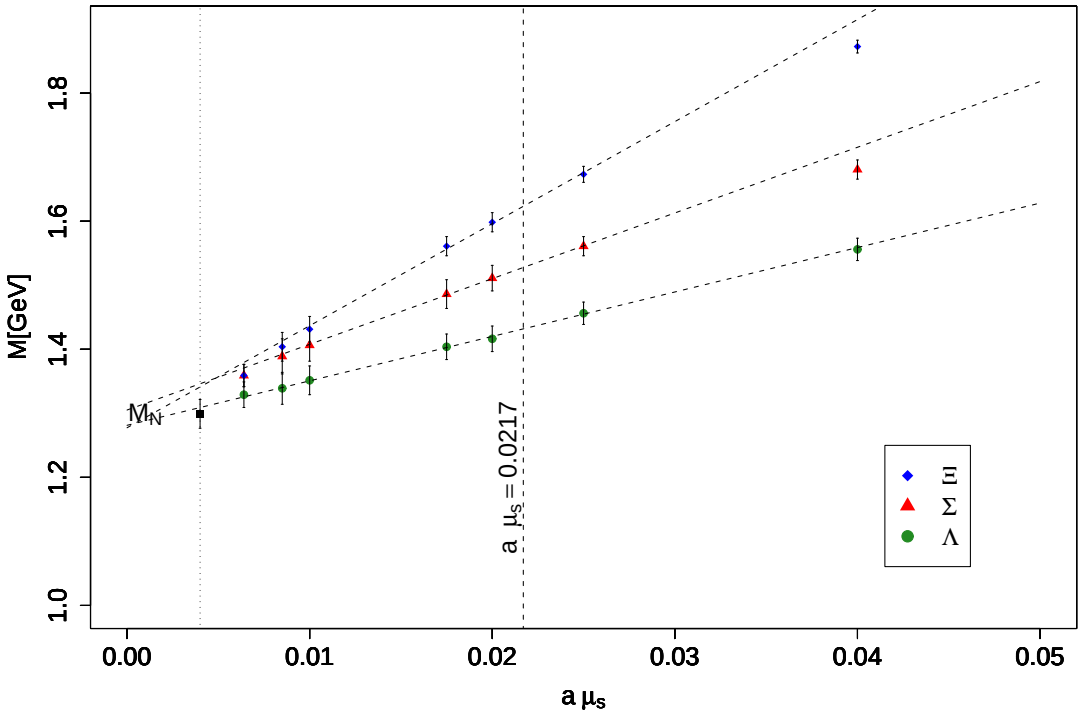

Figure 7.3: Masses for octet baryons at $\beta = 3.9$ and $a\mu = 0.004$ on a lattice of size $24^3 \times 48$ as a function of $a\mu_s$. The vertical dashed line indicates the value of the tuned bare strange quark mass. The dotted lines are to guide the eye.

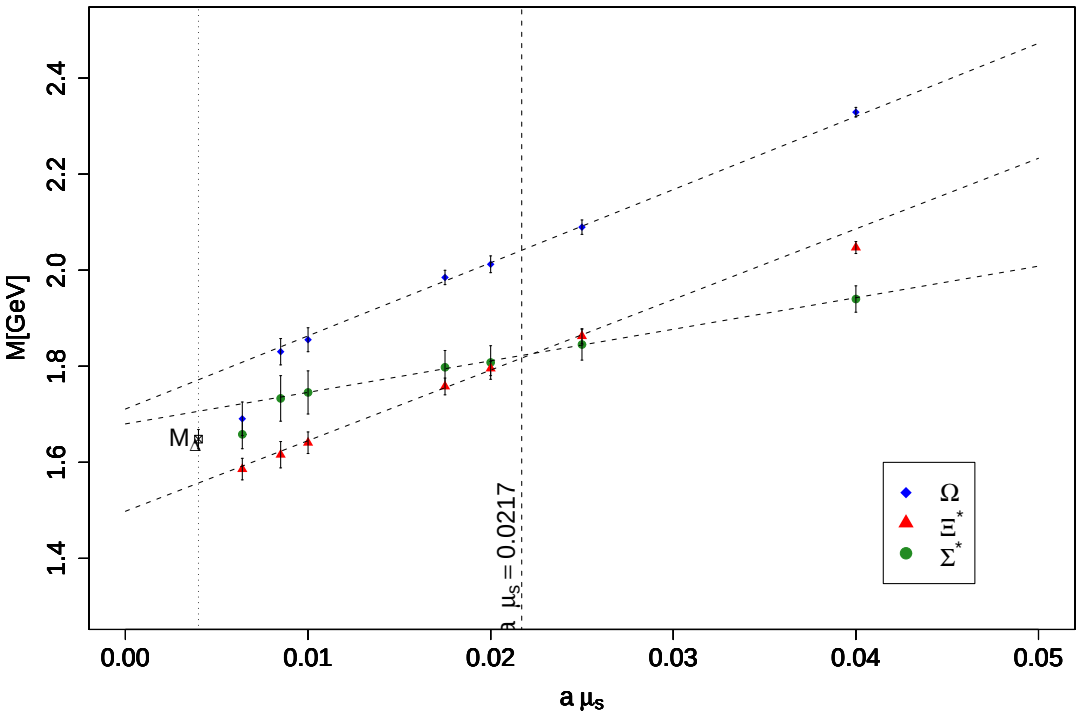

Figure 7.4: The same as for Fig. 7.3 but for the decuplet baryons.

state	A(GeV)	B(GeV)	δM(GeV)
Λ	6.9(3)	1.281(6)	0.017
Σ	10.3(1)	1.305(3)	0.023
Ξ	15.9(5)	1.277(11)	0.038
Σ^*	6.6(3)	1.680(7)	0.018
Ξ^*	14.7(5)	1.165(9)	0.035
Ω	15.2(8)	1.711(17)	0.041

Table 7.2: Linear fits (Eq. (7.3)) of figure 7.3 and 7.4 in the vicinity of $a\mu_s = \{0.0100, 0.0175, 0.0200, 0.0250\}$ and corresponding error obtained by (7.4),

7.4 Lattice Artefacts

7.4.1 Finite Volume Effects

Following the strategy of chapter 6, to study the finite volume effects on the nucleon mass, we parametrize as in Eq. (6.12) the mass dependence of the baryons as a function of $m_{\rm PS}L$. Results are shown in Figs. 7.5 and 7.6 and fit parameters summarized in Table 7.3. The description of the baryon masses is very good with the exception of Ξ^* and Ω where the fits do not converge. This is due to the $L = 20$ results which is not compatible with a monotonic function.

The finite volume effects for strange baryons are found to be smaller than for the nucleon. The only exception is the Σ^* but it is accompanied by large uncertainties in the fit and they remain compatible with statistical errors above $m_{\rm PS}L \geq 3.3$. In the Ξ^* and Ω cases, where the fit is not possible, the two larger volumes give results which are compatible each other.

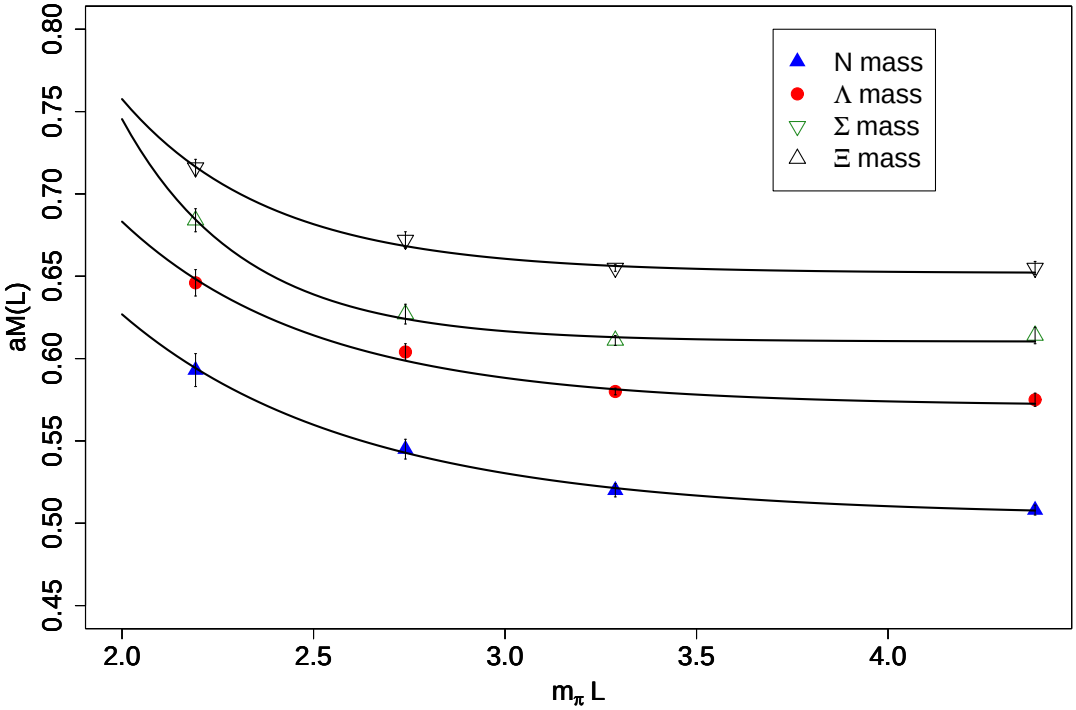

Figure 7.5: Mass of the octet as a function of $m_\pi L$. The measurements are performed on gauge ensemble generated at $\beta = 3.9$,$\mu = 0.004$ and $L/a = 16, 20, 24, 32$ The dependence as been fitted by $M = M_\infty + +A\frac{e^{-Bm_\pi L}}{m_\pi L}$, to guide the eyes.

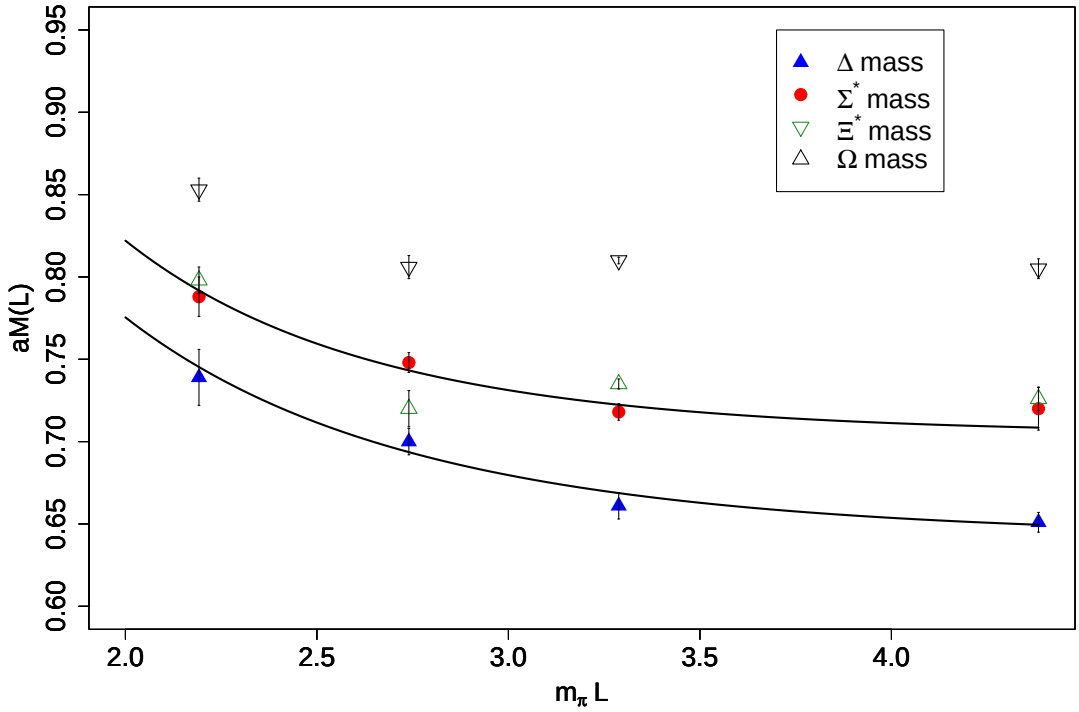

Figure 7.6: Mass of the decuplet as a function of $m_\pi L$. The measurements are performed on gauge ensemble generated at $\beta = 3.9$,$\mu = 0.004$ and $L/a = 16, 20, 24, 32$ The dependence as been fitted by $M = M_\infty + +A\frac{e^{-Bm_\pi L}}{m_\pi L}$, to guide the eyes.

state	aM_∞	B	C	$aM_{max} - aM_\infty$
N	0.503	2.36	1.13	0.010
Λ	0.570	4.20	1.46	0.005
Σ	0.610	54.5	2.65	0.004
Ξ	0.651	13.80	2.096	0.004
Δ	0.641	1.46	0.848	0.010
Σ^*	0.704	1.99	1.069	0.016
Ξ^*	-	-	-	-
Ω	-	-	-	-

Table 7.3: Best fit values of the volume dependence of the octet and decuplet masses.

7.4.2 Isospin breaking

The twisted mass action breaks isospin explicitly to $\mathcal{O}(a^2)$. How large this breaking is depends on the size of the $\mathcal{O}(a^2)$ terms in each particular observables. It was shown that this cut-off effect is enhanced for the neutral pion [150] compared to other quantities. We here address this issue for the octet and decuplet baryons. We already found in section 6.1.6 that for the Δ case the relative mass differences was smaller than 2%. The same quantity is shown in Figs. 7.7, 7.8 7.10 7.9 for the Σ, Ξ, Σ^* and Ξ^* charge multiplets as a function of the pion mass at two values of β.

In the octet case, one sees a non vanishing isospin breaking both for Σ and Ξ. Its relative value with respect to the corresponding averaged mass is $\approx 5\%$. For the Ξ, the mass splitting decreases with the lattice spacing, while for Σ the a^2 dependence is not sizeable.

In the decuplet case, at $\beta = 3.9$, the splitting of the Ξ^* is $\approx 2\%$ while it is compatible with zero for the Σ^*. When decreasing the lattice spacing ($\beta = 4.05$), one observes that the mass splitting of the Ξ^* decreases and becomes also compatible with 0.

Taking into account the results obtained with the smaller lattice spacing, we can conclude that the octet manifests an isospin breaking of $\approx 3\%$ while the decuplet results are compatible with zero.

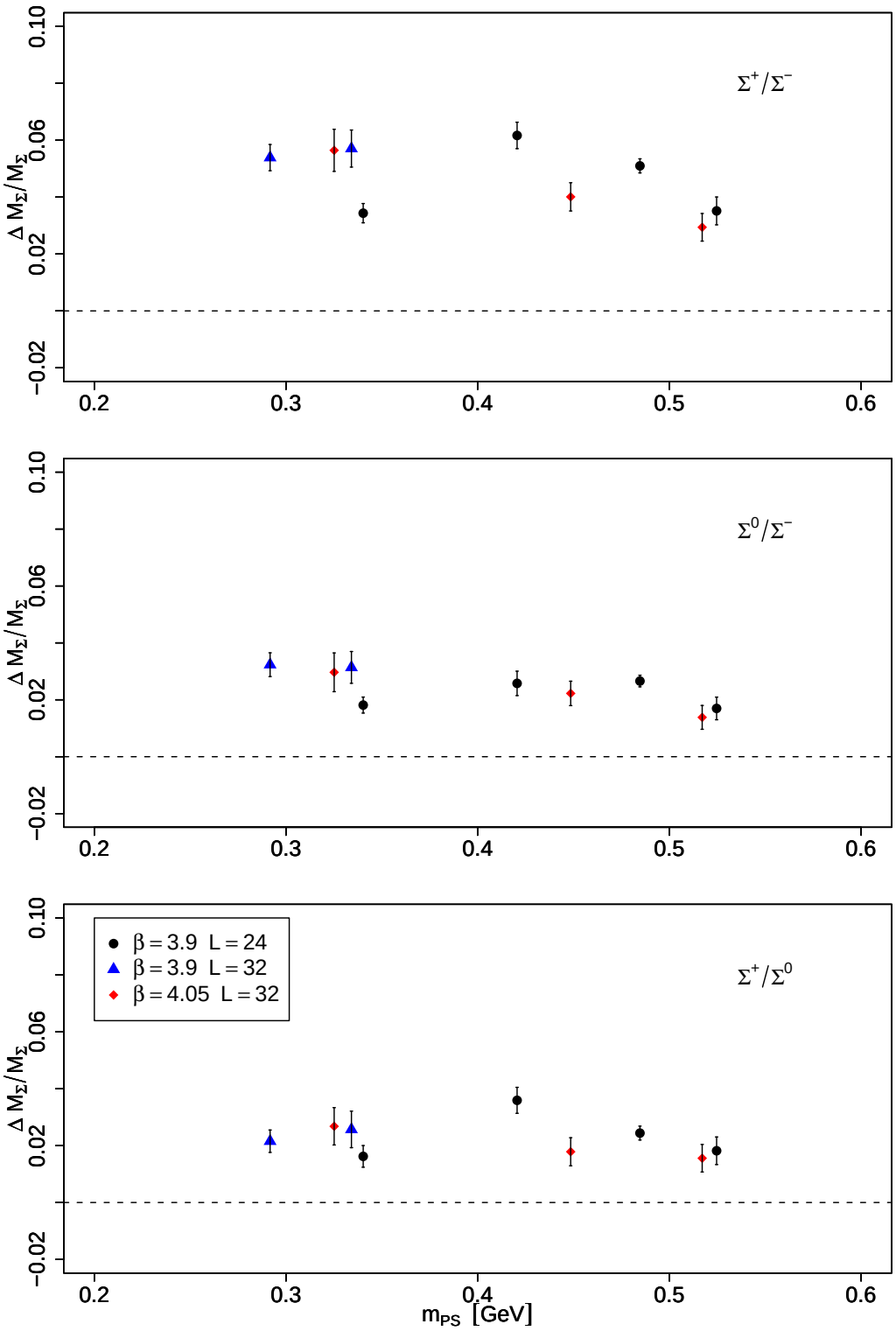

Figure 7.7: The mass splitting between in the Σ^+ and Σ^- normalized with mean value of their mass as a function of $m_{\rm PS}$.

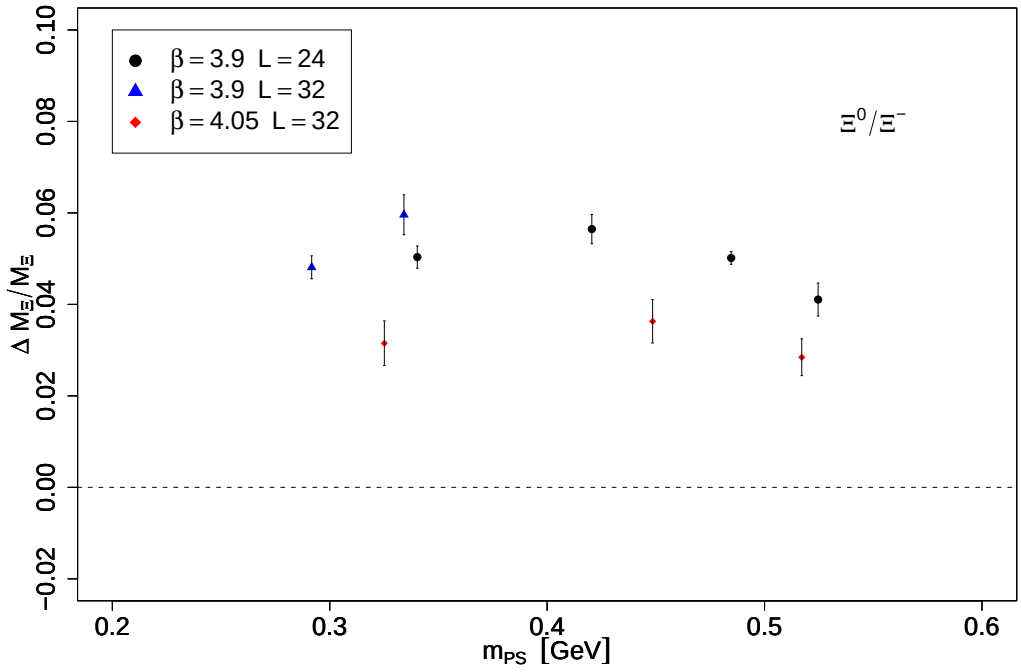

Figure 7.8: The mass splitting between in the Ξ^0 and Ξ^- normalized with mean value of their mass as a function of m_{PS}.

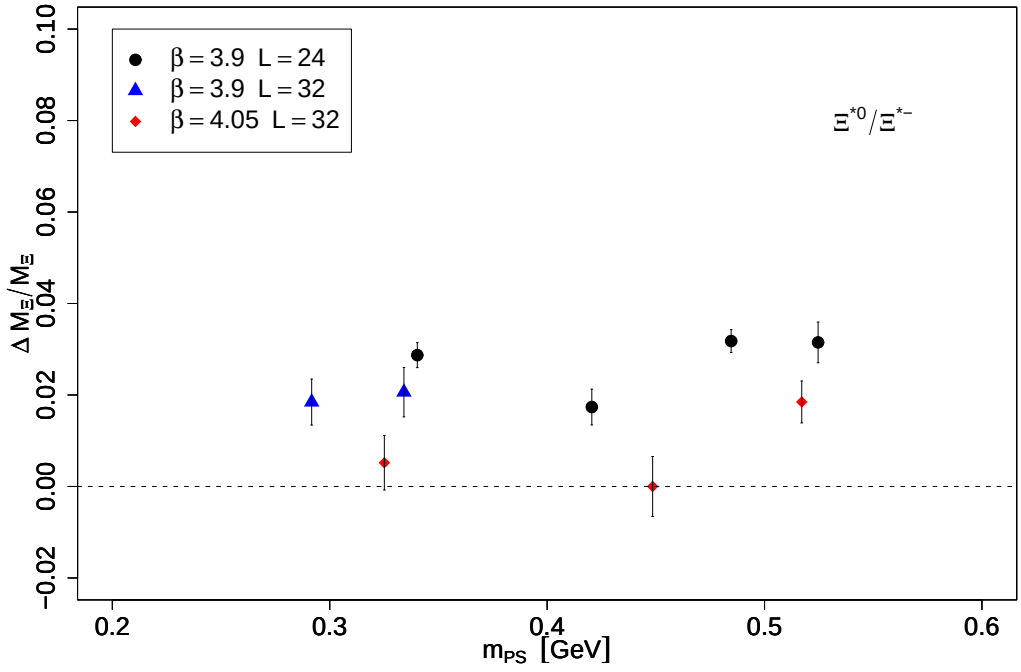

Figure 7.9: The mass splitting between in the Ξ^{*0} and Ξ^{*-} normalized with mean value of their mass as a function of m_{PS}.

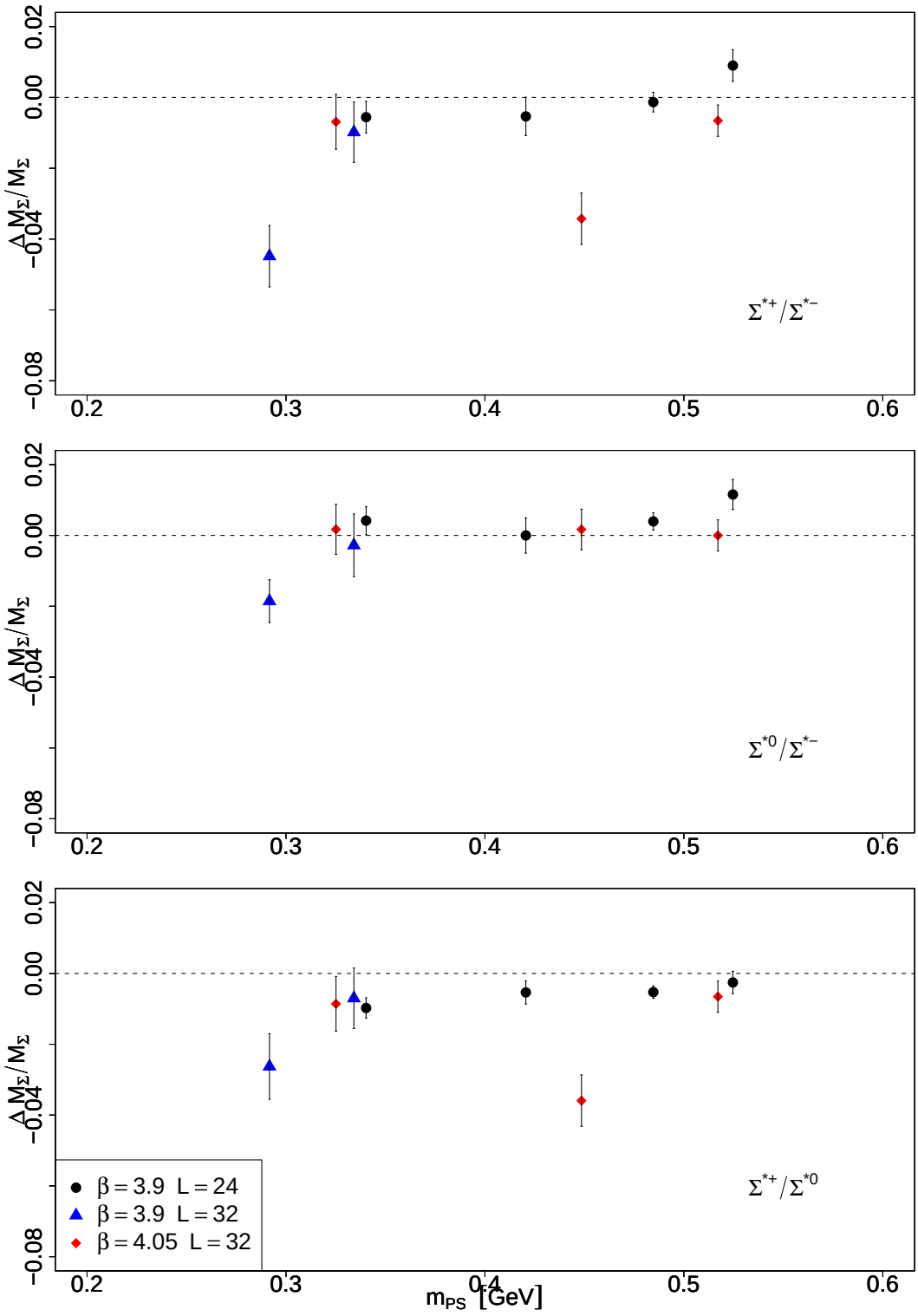

Figure 7.10: The mass splitting between in the Σ^{*+} and Σ^{*-} normalized with mean value of their mass as a function of $m_{\rm PS}$.

7.4.3 Continuum Extrapolation

In order to assess cut-off effects we use results at $\beta = 3.9$ and $\beta = 4.05$. The lattice masses, expressed in units of the Sommer scale r_0, are interpolated to fixed $r_0 m_{\rm PS}$ for each β-value. Interpolating linearly or with one-loop chiral perturbation theory gives values consistent within error bars. Given the size of these cut-off effects a weighted average of the baryon masses between these two β values gives an estimate of their continuum limit. It must be stressed that estimating the strange quark mass at $\beta = 4.05$ using Eq. (7.2) may cause residual cut-off effects on the few percent level that are not taken into account.

The results obtained from the weighted averaging of data at $\beta = 3.9$ and $\beta = 4.05$ are listed in Table 7.4 and are plotted in Figs. 7.11, 7.4.3, 7.4.3 7.15 7.13 and 7.16. In the figures we also include results at $\beta = 3.8$. If cut-off effects are small for all β-values then results at $\beta = 3.8$ should fall on the same line. As can be seen the situation is less clear than in the nucleon case Fig. 6.9. For the Λ mass results at $\beta = 3.8, 3.9$ and $\beta = 4.05$ are consistent with a constant. This holds approximately also for the other baryons. A precise estimation of the cutoff effects would require to interpolate at the same kaon mass of reference $r_0 m_K$, and thus to have several bare strange quark mass for each μ_l and β value. These inversions are not available and one has to live with that.

Within the statistical errors one can therefore concludes that cut-off effects are under control at least in the octet and for lattice spacing below 1 fm.

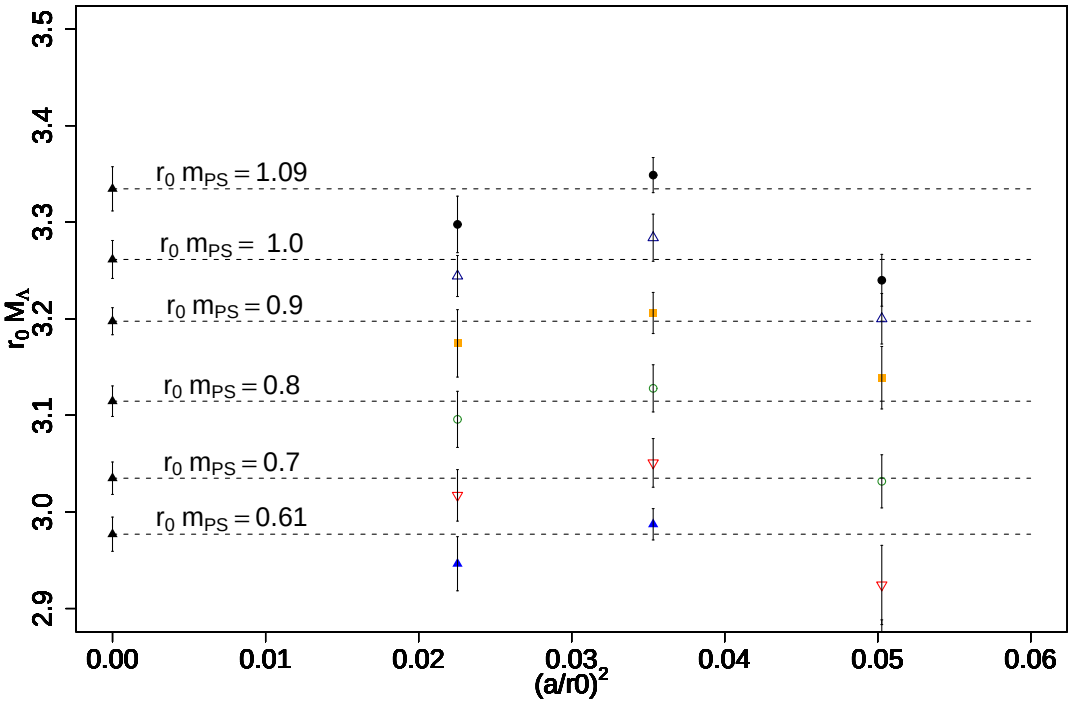

Figure 7.11: Constant extrapolation to the continuum limit for the Λ. The data at $\beta = 3.8$ which correspond to the larger lattice spacing are not include in the fit. The interpolation is done using a $\mathcal{O}(p^3)$ fit of the data.

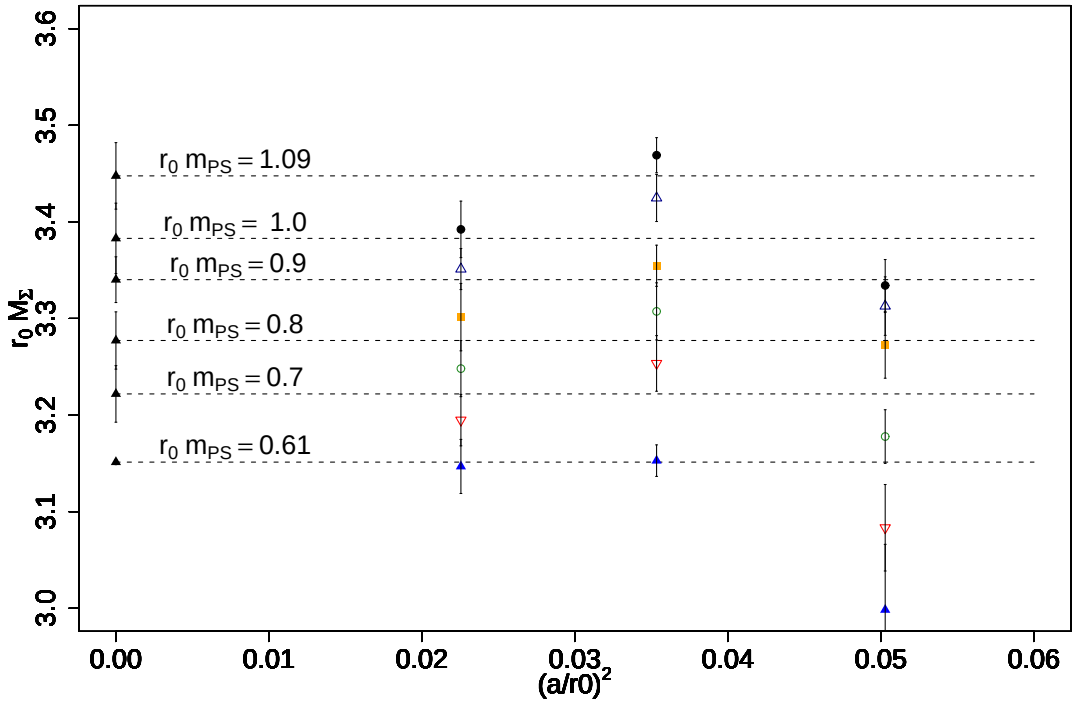

Figure 7.12: Scaling of the Σ. The notation are the same than in Fig. 7.11.

$r_0^\chi m_{\rm PS}$	$r_0^\chi M_\Lambda$	$r_0^\chi M_\Sigma$	$r_0^\chi M_\Xi$	$r_0^\chi M_{\Sigma^*}$	$r_0^\chi M_{\Xi^*}$	$r_0^\chi M_\Omega$
0.61	2.976(14)	3.151(14)	3.404(09)	3.771(23)	3.774(23)	4.231(14)
0.70	3.034(18)	3.221(19)	3.428(14)	3.862(34)	3.852(27)	4.250(23)
0.80	3.114(18)	3.277(20)	3.476(16)	3.902(37)	3.890(27)	4.269(25)
0.90	3.197(18)	3.340(18)	3.553(13)	3.960(30)	3.957(23)	4.301(25)
1.00	3.261(16)	3.382(16)	3.555(14)	3.995(26)	3.949(23)	4.295(22)
1.09	3.334(15)	3.447(15)	3.591(15)	4.104(21)	4.021(24)	4.370(18)

Table 7.4: Continuum extrapolation of the octet and decuplet masses at fixed reference pion mass in unit of r_0. Results obtained from Figs. 7.11, 7.4.3, 7.4.3, 7.15, 7.13, 7.16

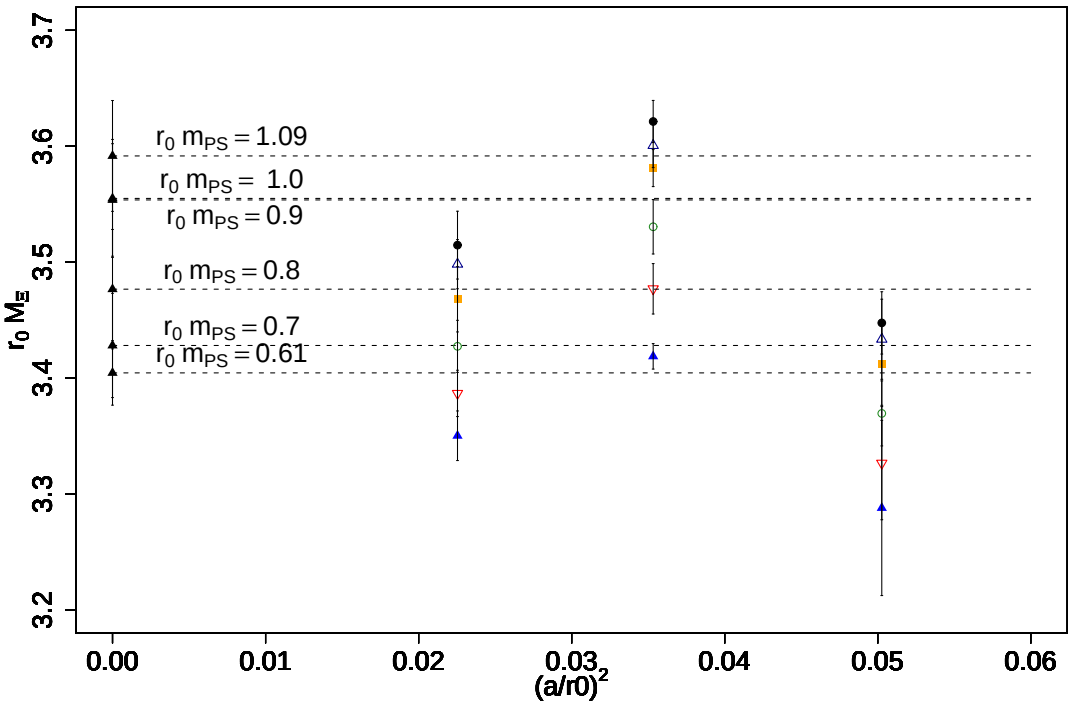

Figure 7.13: Scaling of the Ξ. The notation are the same than in Fig. 7.11.

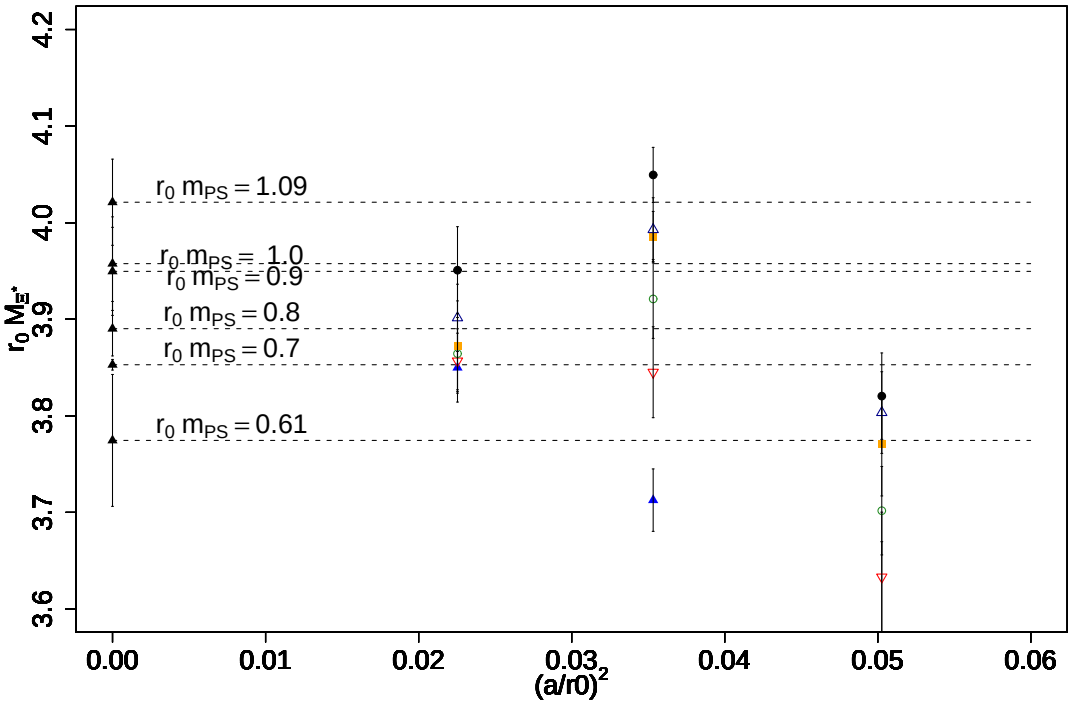

Figure 7.14: Scaling of the Ξ^*. The notation are the same than in Fig. 7.11.

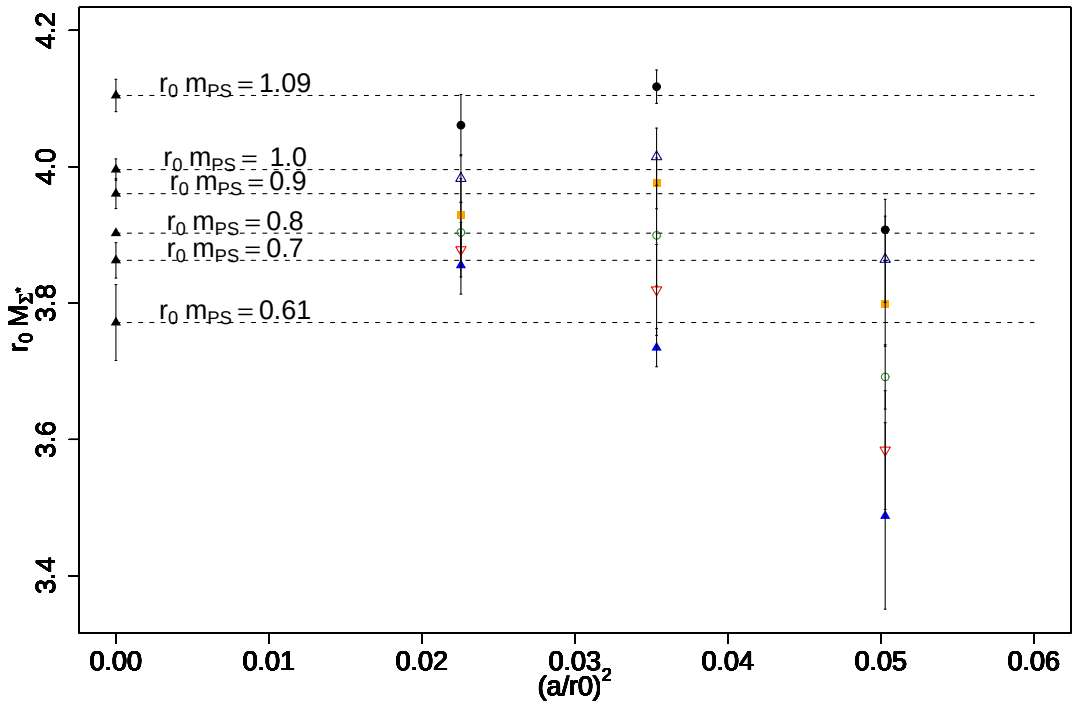

Figure 7.15: Scaling of the Σ^*. The notation are the same than in Fig. 7.11.

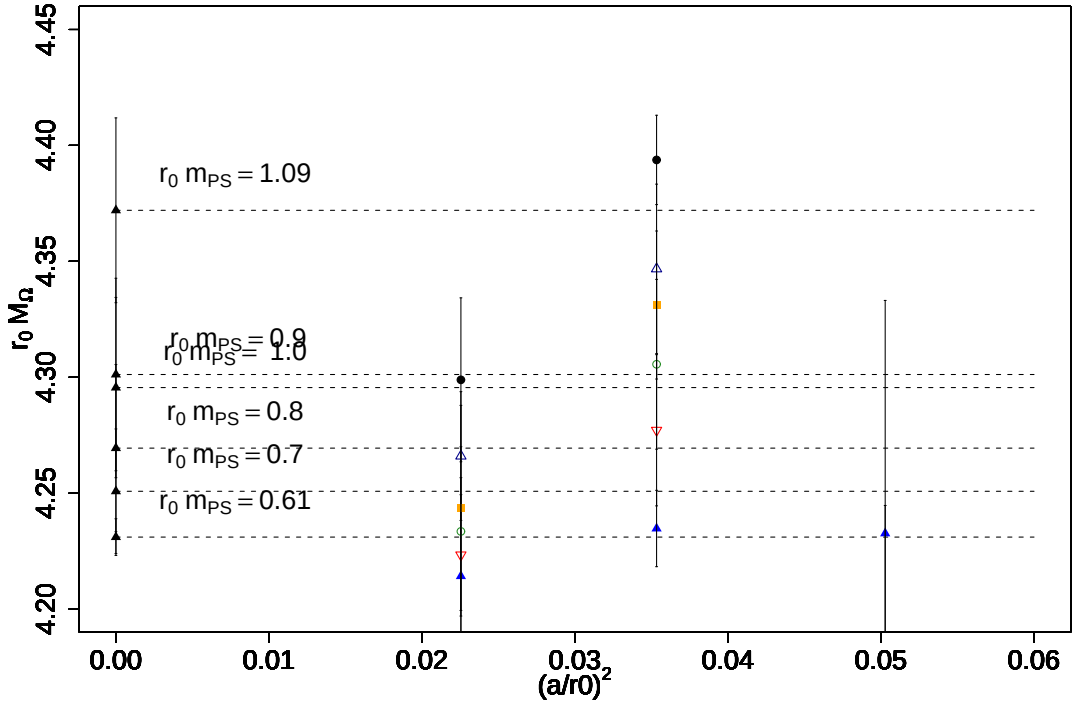

Figure 7.16: Scaling of the Ω. The notation are the same than in Fig. 7.11.

7.5 Gell-Mann Okubo relation

We examine in this section the Gell-Mann-Okubo (GMO) relations presented in Chapter 1 and based on flavour SU(3) symmetry [12] using lattice results. We use continuum results in all the figures.

For the $J^\pi = 1/2^+$ octet the GMO relation reads:

$$\frac{M_\Xi + M_N}{2} = \frac{3M_\Lambda + M_\Sigma}{4} \tag{7.5}$$

The results are displayed in Fig. 7.17 where the left and right hand side terms of the equality (7.5) are separately plotted as a function of m_π^2. Their differences are compatible with zero at any pion masss. The experimental values are respectively 254 MeV and 248 MeV (up and down empty triangles). These results are similar to those presented in [151] using dynamical mixed action - domain wall on rooted staggered - quarks.

For the $J^\pi = 3/2^+$ decuplet, the Gell-Mann Okubo relations results into an equal mass difference among two consecutive ($\Delta S = 1$) isospin multiplets

$$M_{\Sigma^*} - M_\Delta = M_{\Xi^*} - M_{\Sigma^*} = M_\Omega - M_{\Xi^*} \tag{7.6}$$

Corresponding results are displayed in Figure 7.18. As one can see, the GMO relation is quite strongly violated; the three differences involved in (7.6) are spread over 200 MeV for the range of pion masses that have been computed. The main anomaly comes from the Σ^*/Ξ^* pair which, except maybe for the lowest m_π value, appears in a reversed order. The experimental values $153 - 149 - 139$ MeV are indicated with empty symbols. Notice that the differences not involving the Σ^*/Ξ^* pair seems to join it at the physical point (vertical dotted line).

A third relation exists, mixing the $J^\pi = 1/2^+$ octet and $J^\pi = 3/2^+$ decuplet masses

$$3M_\Lambda - M_\Sigma - 2M_N = 2(M_{\Sigma^*} - M_\Delta) \tag{7.7}$$

Experimentaly it is fullfilled at 10% level (276 MeV and 305 MeV). The corresponding lattice results are shown in Fig. 7.19. One can see that, as in the Octet case, the relation is satisfied ($D_8 = D_{10}$) at each pion mass and that the chiral limit is already reached at its lower value $m_\pi = 313$ MeV.

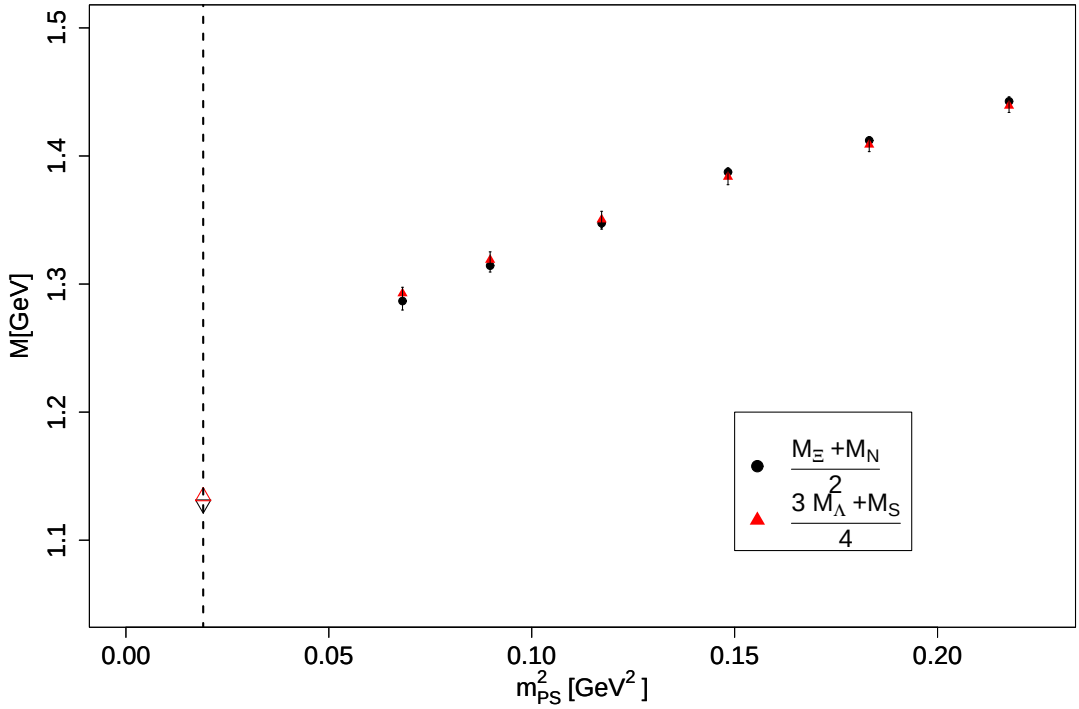

Figure 7.17: Gell Mann Okubo relation for the octet (Eq. (7.5)) as a function of $m^2_{\rm PS}$. Continuum data are used.

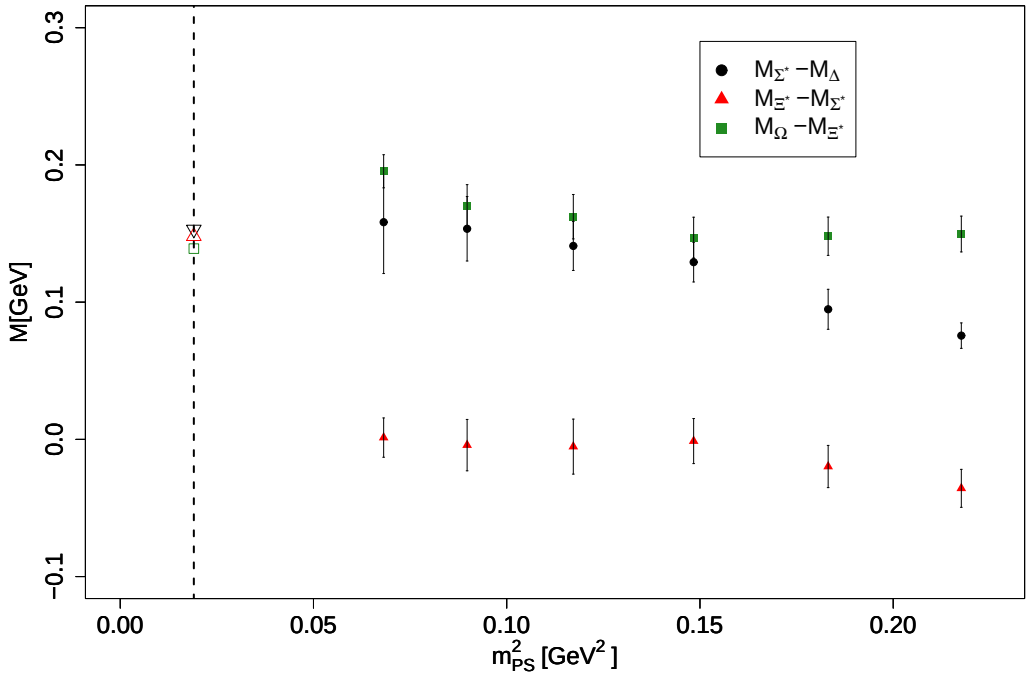

Figure 7.18: Gell Mann Okubo relation for the decuplet (Eq. (7.6)) as a function of $m^2_{\rm PS}$. Continuum data are used.

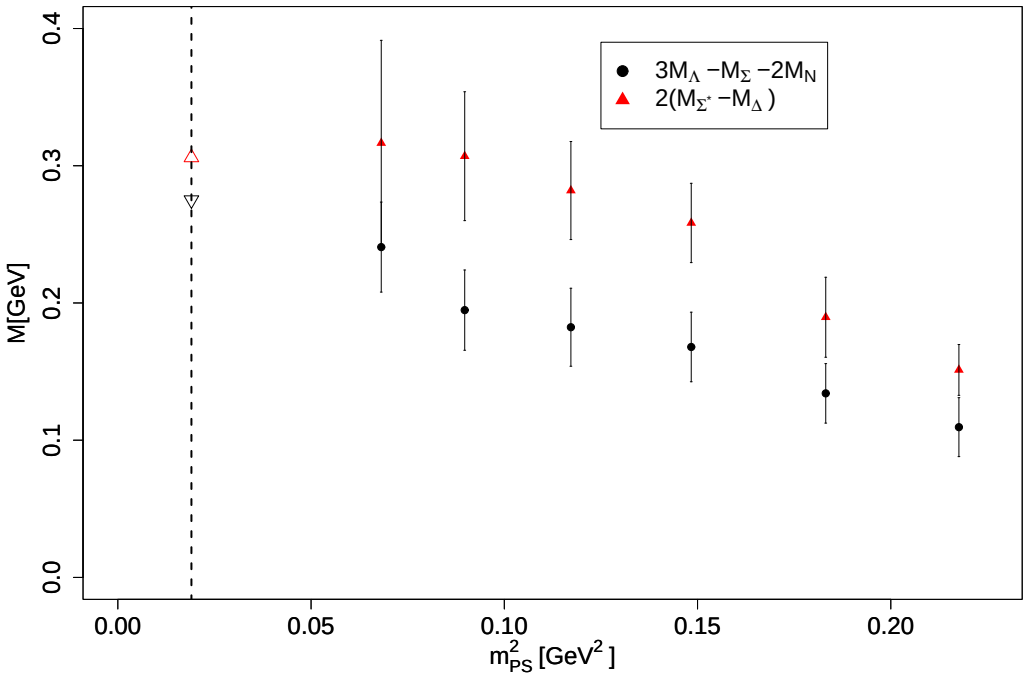

Figure 7.19: Mixed octet-decuplet Gell Mann Okubo relation (Eq. (7.7)) as a function of $m^2_{\rm PS}$. Continuum data are used.

In summary the Octet and mixed Octet-Decuplet GMO equalities are satisfied at any pion mass, although in general with values which, notwithstanding equal, are far from the ones expected in the chiral limit and which interpolate well. The Decuplet rule is violated due to inversion of the Σ^*/Ξ^* states but seems to agree at the physical point.

It is worth noticing that all these GMO relations must be exact in the SU(3) limit which can be reached with $m_u = m_d = m_s$. In our simulation this corresponds to $am_u = am_d = am_s = 0.0217$ which in terms of pion mass is $m^2_\pi \approx 0.50$ GeV^2 This means that the differents quantities plotted in Figs. 7.18 and 7.19 must tends to zero at the limit $m^2_\pi \to 0.50$ GeV^2.

7.6 Chiral Extrapolation

We show in Figs. 7.20 7.21, 7.22, the chiral extrapolations for the octet baryon masses and in Figs. 7.23, 7.24, 7.25 the corresponding fits for the decuplet given in physical units. We emphasize that the physical point is not included in these fits.

The LO expression describes well the lattice results but leads to extrapolated values inconsistent with the experimental point. The $\mathcal{O}(p^3)$ $HB\chi PT$ expansion given in Eqs. (**??**) and (**??**) with two fit parameters $m^{(0)}$ and $c^{(1)}$ provides a good description of lattice data but, apart from the nucleon and Δ, fails to describe the experimental point. The NLO leads to a clear improvement in the case of the Λ and Σ masses, whereas for the rest of the baryons the improvement is marginal. Apart from the preceding remarks, there is no clear advantage in using higher order fits, especially NNLO, which even turns out to be numerically unstable for the case of the Δ and Ω masses. Therefore our main conclusion is that the $\mathcal{O}(p^3)$ HBχPT provides a reasonable description for the nucleon and Δ masses whereas NLO $SU(2)$ for the strange baryon masses, yielding values at the physical point in agreement with experiment except for Ξ, Σ^* and Ω.

The discrepancies with respect to the paper [139] are due to differences in the analysis. In [139] the chiral extrapolation was done using a combined fit of the data at several β values. In this work we have first extrapolated to the continuum, despite of the fact that the behaviour of the masses are not completely under control, and then perform chiral fits. Note also that the values of r_0/a change $\approx 2\%$ with respect to the value used in [139]. The best value of the fit parameters are summarized in Tables 7.6, 7.7, 7.8 and 7.9. The uncertainties on the scale determination, have been added on the fit parameters shown in the tables. The larger source of systematic uncertainty are due to the chiral extrapolation.

Using $m_\pi^2 \sim \mu$ the σ-term of the octet and decuplet baryons can be estimated using that

$$\sigma_X = m_\pi^2 \frac{dM_X}{dm_\pi^2} \tag{7.8}$$

We list in Table 7.5 the values we obtain using the nucleon mass to set the scale. As can be seen, the value extracted depends on the fitting Ansatz. In the most interesting case of the nucleon the result of $\mathcal{O}(p^3)$ changes by two standard deviations if the coefficient of the cubic term in m_π is fitted, indicating that fit coefficient are very sensitive to the functional form of the fit. In the case of the Λ fitting the cubic term gives the same value as that obtained to $\mathcal{O}(p^3)$, compatible to that of the nucleon. This is another indication of the argument presented above in favor of the presence of a cubic term in m_π of comparable size as that of the nucleon. In fact the main conclusion of this exercise is that by determining the coefficient of the cubic term from the data one obtains a σ-term that for all baryons except the Ω is comparable within errors to the value of nucleon σ-term. Comparing to the results of NLO we can see that for the nucleon this fit produces too much curvature as already observed for instance in Ref. [111]. For the other baryons a reasonable value is obtained depending on the quality of the fits as seen in the figures.

	σ_N	σ_Λ	$\sigma_{\Sigma^{\rm Av.}}$	$\sigma_{\Xi_{\rm Av.}}$	$\sigma_{\Delta^{\rm Av.}}$	$\sigma_{\Sigma^{*\rm Av.}}$	$\sigma_{\Xi^{*\rm Av.}}$	σ_Ω
$\mathcal{O}(p^3)$	67(1)(3)	35.7(4)(1.5)	37.6(3)(1.8)	13.1(1.7)(5)	59(3)(3)	32(1)(1)	19.0(2.5)(7)	5.1(9)(1)
cubic	45(5)(9)	35(9)(9)	40(7)(15)	27(30)(9)	16(19)(5)	48(19)(21)	55(21)(28)	17(10)(8)
NLO	95(2)(5)	51(1)(3)	53.1(9)(2.8)	17.8(1.6)(8)	74(4)(3)	45.6(8)(1.7)	29(1)(1)	-

Table 7.5: σ-term in MeV using the fit parameters determined from $\mathcal{O}(p^3)$ χPT (Eqs. (5.53) and 5.54), using a cubic fit (Eq. (5.55)) and NLO (Eqs. (5.56) and 5.57). We used the scale from the nucleon mass to convert to physical units.

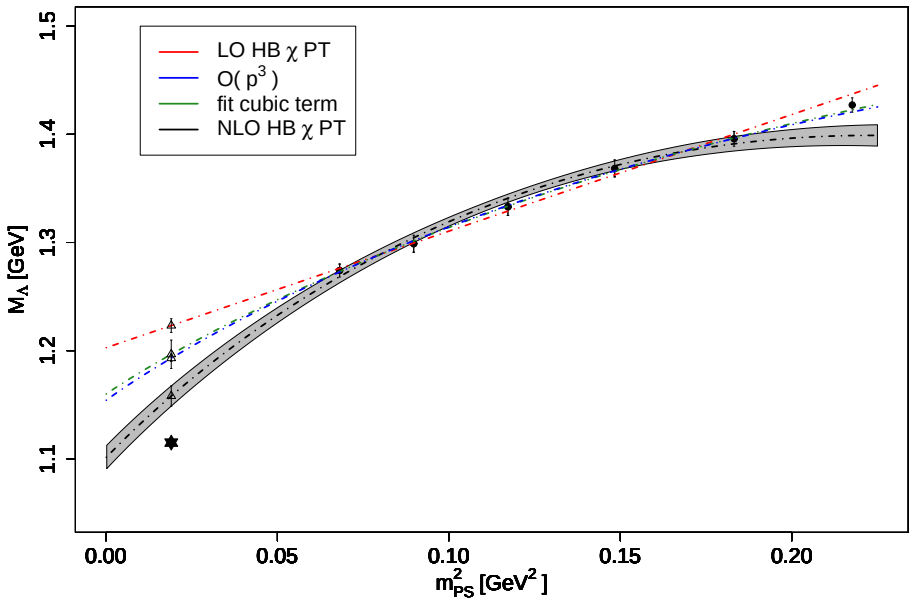

Figure 7.20: Chiral extrapolation of the Λ mass in physical units with continuum data. We show chiral extrapolation linear in $m_{\rm PS}^2$, the $\mathcal{O}(p^3)$ and NLO SU(2) chiral perturbation theory given in Eqs. (**??**). For clarity, we include an error band only for $\mathcal{O}(p^3)$ fit. The physical point is shown by a star. It has been fixed using r_0^N

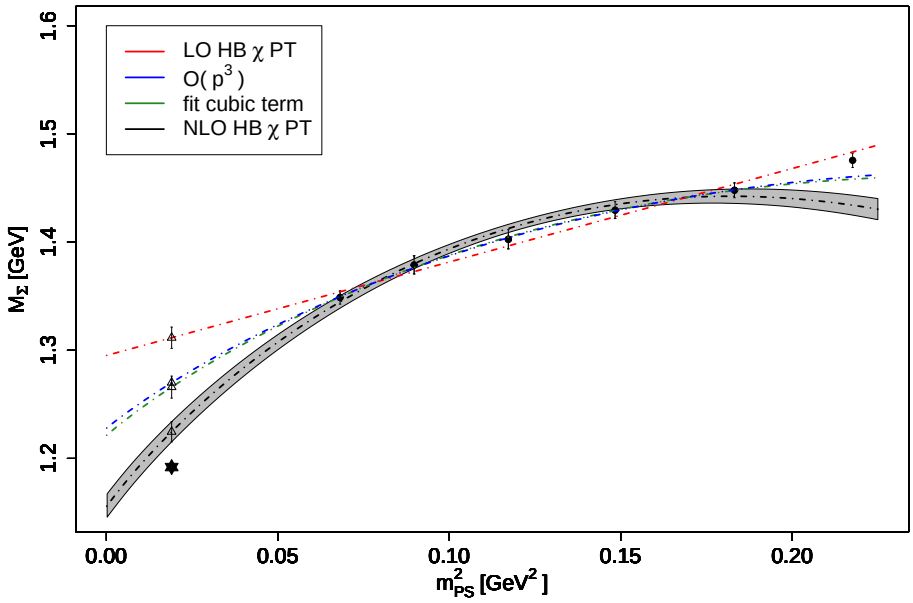

Figure 7.21: Chiral extrapolation of the Σ mass in physical units with continuum data. The rest of the notation is the same as that in Fig. 7.20

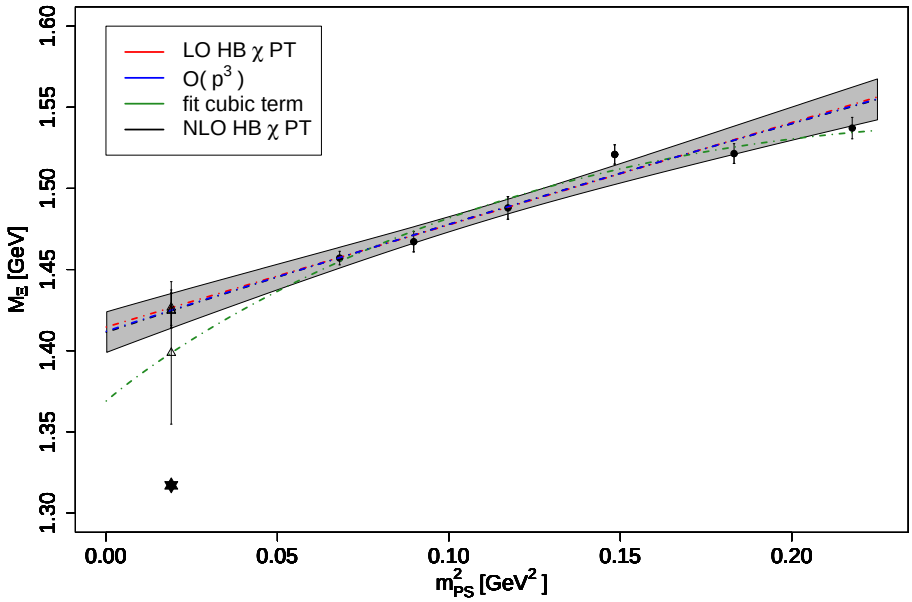

Figure 7.22: Chiral extrapolation of the Ξ mass in physical units with continuum data. The rest of the notation is the same as that in Fig. 7.20

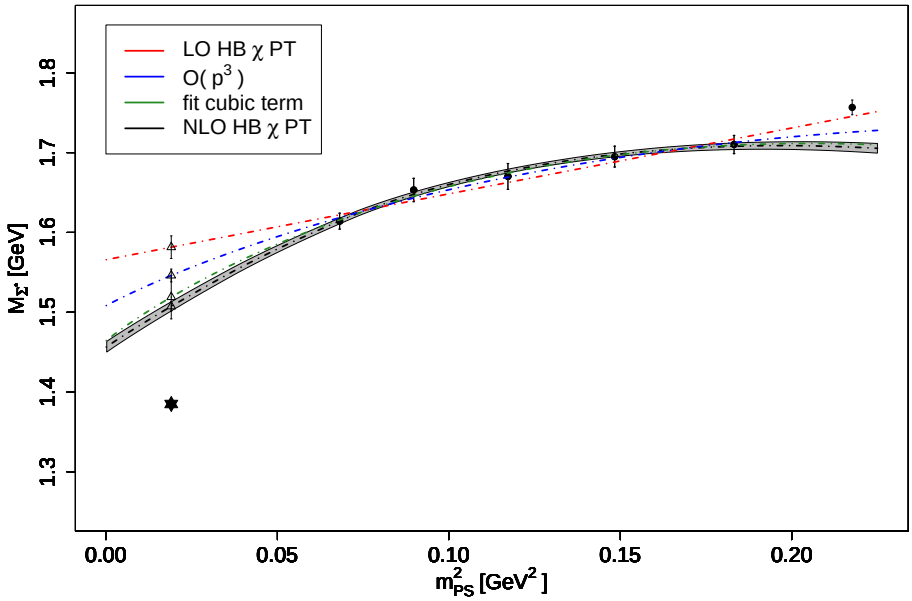

Figure 7.23: Chiral extrapolation of the Σ^* mass in physical units with continuum data. The rest of the notation is the same as that in Fig. 7.20

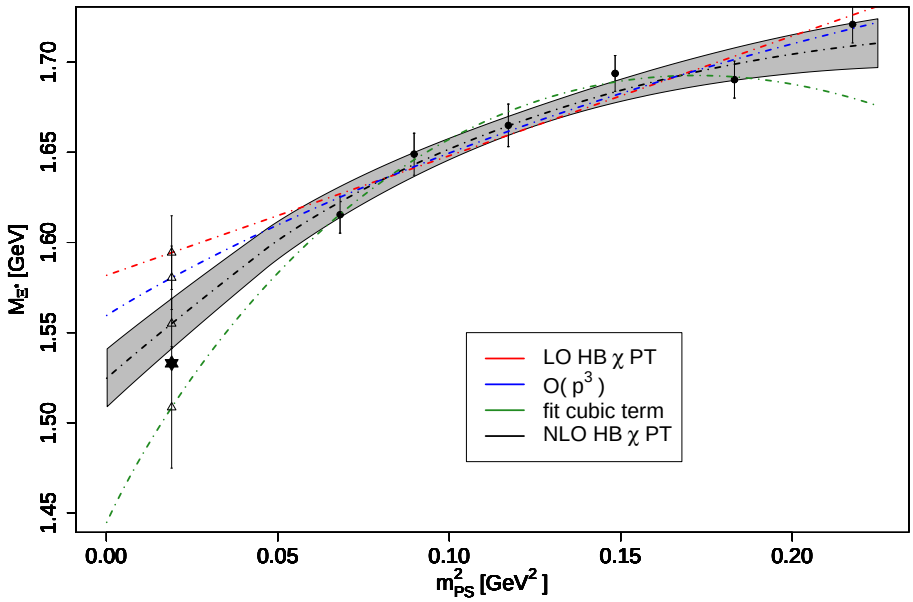

Figure 7.24: Chiral extrapolation of the Ξ^* mass in physical units with continuum data. The rest of the notation is the same as that in Fig. 7.20

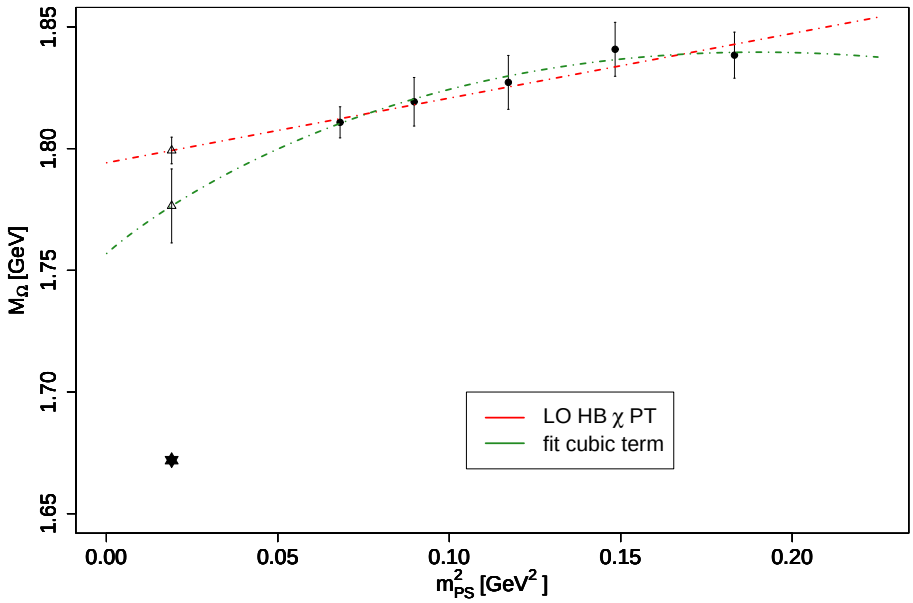

Figure 7.25: Chiral extrapolation of the Ω mass in physical units with continuum data. The plot show the LO and the cubic fit. The rest of the notation is the same as that in Fig. 7.20

	LO		
	M_X	c_X^1	χ^2
Λ	1.223(6)(42)	1.077(49)(37)	1.32
Σ	1.312(10)(45)	0.865(75)(30)	3.11
Ξ	1.427(11)(49)	0.631(89)(22)	2.35
Σ^*	1.582(14)(55)	0.825(108)(29)	0.76
Ξ^*	1.594(20)(55)	0.664(152)(23)	1.79
Ω	1.799(5)(62)	0.266(46)(9)	0.25

Table 7.6: Summary of the LO fit results corresponding to the figures. The first error is statistical, the second come from the error on the scale.

	$\mathcal{O}(p^3)$		
	M_X	c_X^1	χ^2
Λ	1.193(3)(41)	2.400(23)(83)	0.29
Σ	1.270(2)(44)	2.700(18)(93)	0.18
Ξ	1.425(11)(49)	0.704(87)(24)	6.8
Σ^*	1.546(8)(53)	2.407(61)(83)	0.74
Ξ^*	1.580(18)(55)	1.260(130)(44)	3.99

Table 7.7: Summary of the $\mathcal{O}(p^3)$ fit results. The first error is statistical, the second come from the error on the scale.

	NLO		
	M_X	c_X^1	χ^2
Λ	1.158(9)(40)	4.265(72)(147)	2.89
Σ	1.224(9)(42)	4.932(71)(170)	2.79
Ξ	1.425(11)(49)	0.724(87)(99)	6.78
Σ^*	1.507(6)(52)	2.871(44)(99)	0.38
Ξ^*	1.555(14)(54)	1.600(103)(55)	2.48

Table 7.8: Summary of the NLO fit results. The first error is statistical, the second come from the error on the scale.

	cubic fit			
	M_X	c_X^1	c_X^2	χ^2
Λ	1.196(13)(41)	2.24(42)(8)	−2.22(79)(15)	0.27
Σ	1.266(10)(44)	2.88(33)(100)	−3.84(62)(27)	0.15
Ξ	1.398(44)(48)	1.90(1.45)(7)	−2.45(2.79)(17)	5.09
Σ^*	1.519(27)(52)	3.61(89)(12)	−5.32(1.68)(37)	0.38
Ξ^*	1.508(34)(52)	4.33(1.04)(15)	−6.96(1.96)(48)	0.74
Ω^*	1.776(15)(61)	1.308(506)(45)	−1.99(97)(14)	0.24

Table 7.9: Summary of the cubic fit results. The first error is statistical, the second come from the error on the scale.

7.7 Fixing the SU(3) coupling constants from lattice data using HBχPT

Until now, our lattice data have been used to predict the particle spectrum through HBχPT extrapolation to the physical point. As explained in the previous section, in practice this has been possible only by assigning some values to the meson-baryon coupling constants. Our assumptions relied on SU(3) flavor and $SU(6)$ spin-flavor symmetry. The experimental values were thus not considered as an input and from this point of view the obtained results can be considered as a check of low energy QCD.

A different way to make use of our results is to assume first that QCD describes effectively the baryon spectrum and that our lattice data including the extrapolation procedure are a good approximation of QCD. In this case we can force our fits to pass through the experimental value and obtain as a result the meson-baryon coupling constants. These constants are in general poorly known and our work constitutes a first attempt to determine them from lattice data.

We will consider in this section the second approach only on the assumptions of $\mathcal{O}(p^3)$. The nucleon is used to set the scale. Physical units are thus obtained using r_0^N which assumes the value $g_A = 1.269$.

The octet case involve, apart from g_A, three coupling constants: $g_{\Sigma\Sigma}, g_{\Xi\Xi}$ and $g_{\Lambda\Sigma}$ and the $\mathcal{O}(p^3)$ fits are enough to determine them. The results are given in Fig. 7.26 and Table 7.10. As one can see, the octet is very well describe by this approach, but the fitted meson-baryon couplings are much larger than the $SU(3)$ one, specially for Ξ which is one order of magnitude greater. These results are stables within errors when adding or retrieving one point in the fit.

The decuplet $\mathcal{O}(p^3)$ fits involve three coupling constants: $g_{\Delta\Delta}, g_{\Sigma^*\Sigma^*}, g_{\Xi^*\Xi^*}$ and the corresponding results are given in Fig. 7.27 and Table 7.10. Apart from $g_{\Delta\Delta}$, which is in reasonable agreement, the fitted meson-baryon couplings are two times larger than the $SU(6)$ prediction.

The preceding results inspire us the following alternative. If $\mathcal{O}(p^3)$ give a valid description of baryon masses in our pion mass range, as we assumed for the nucleon and Δ, then $SU(3)$ and $SU(6)$ are badly broken. In the opposite case, one can expect large contributions due to the higher order corrections. They will effectively modify the $SU(3)$ coupling constant by the NLO terms. For instance in the case of the Λ expression, and by approximating $\mathcal{F} \approx \pi m_\pi^3$ one obtains

$$g_{\Lambda\Sigma}^2(fit) = g_{\Lambda\Sigma}^2 + 4g_{\Lambda\Sigma^*}^2 \tag{7.9}$$

Assuming $g_{\Lambda\Sigma^*} \sim 1$, one obtains $g_{\Lambda\Sigma} \sim 1.8$ which much closer to the $SU(3)$ predictions. The same exercise with the Ξ will also decrease our estimation of $g_{\xi\xi}$ but will remain nevertheless times larger than the $SU(3)$ values.

	$g_{\Lambda\Sigma}$	$g_{\Sigma\Sigma}$	$g_{\Xi\Xi}$	$g_{\Delta\Delta}$	$g_{\Sigma^*\Sigma^*}$	$g_{\Xi^*\Xi^*}$
fit $\mathcal{O}(p^3)$	2.69(18)(9)	1.70(13)(27)	1.61(12)(6)	2.92(26)(10)	3.49(21)(12)	1.63(9)(6)
$SU(3) - SU(6)$	1.47	1.05	0.21	2.2	1.46	0.73

Table 7.10: coupling constant appearing in the $\mathcal{O}(p^3)$ expression. The value fitted on our data with an $\mathcal{O}(p^3)$ fit and the theoritical one from $SU(6)$ symmetry of the coupling constant are shown

Our attempts to determine the coupling constant using NLO expansion failed. The fits were satisfactory but lead to separate contributions of the cubic and non analytic terms which tend to compensate each other and were meaningless.

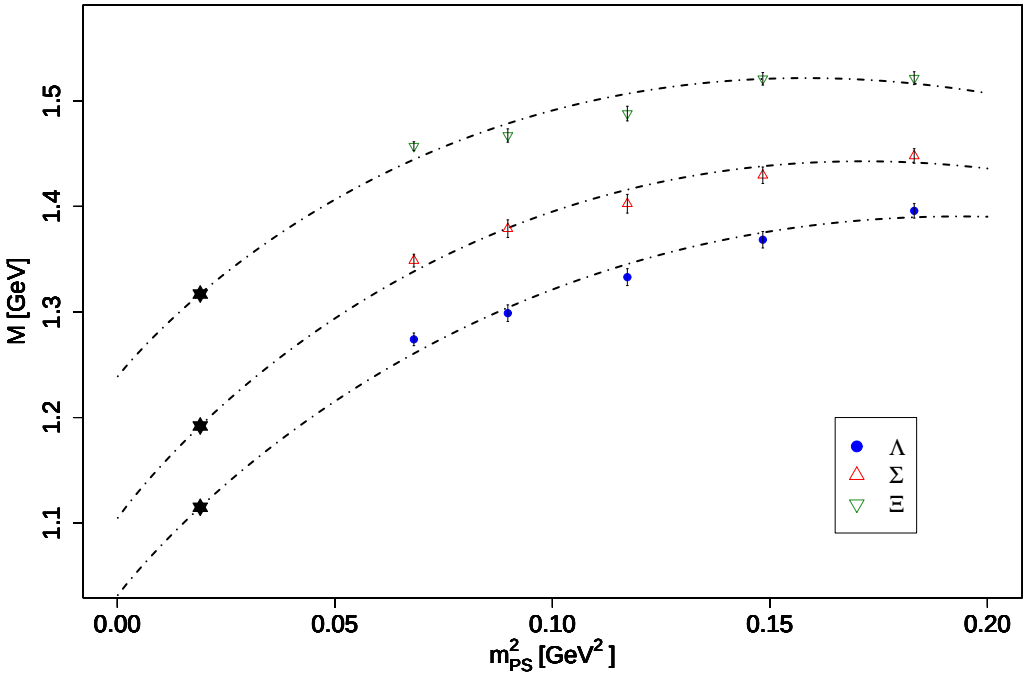

Figure 7.26: $\mathcal{O}(p^3)$ HBχPT fit including the physical point for the octet. The scale r_0^N is used.

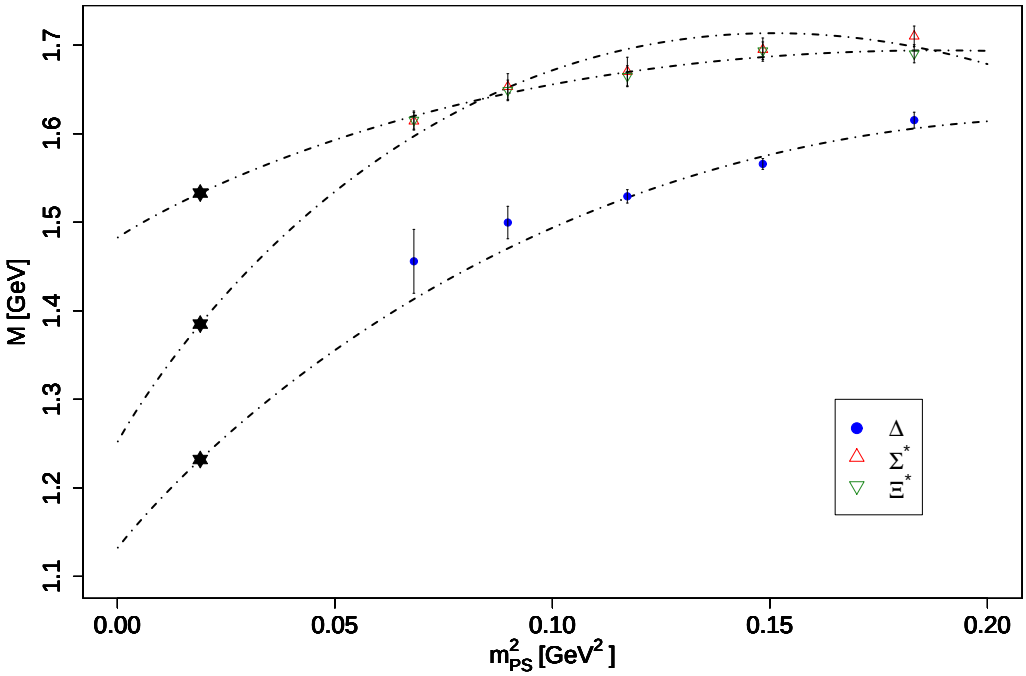

Figure 7.27: $\mathcal{O}(p^3)$ HBχPT fit including the physical point for the decuplet. The scale r_0^N is used.

7.8 Final remarks

The aim of this chapter is the computation of the low-lying strange baryon masses using twisted mass fermions at maximal twist. It is in line with ongoing efforts by other lattice collaborations worldwide to predict the baryon spectrum from first principles. Comparison of lattice results with experiment is regarded as an important benchmark for lattice QCD and justifies the use of different lattice actions, each with different systematic errors. For example, the twisted mass action with only one parameter to be tuned, provides automatic $\mathcal{O}(a)$ improvement. However isospin symmetry is restored in the continuum limit. We have examined the consequences of isospin breaking on the baryon masses and found them to be either under control or compatible with zero. On our finer lattice at $\beta = 4.05$ the maximal isospin violation is obtained in the octet only in the case of the Cascade where we find that $m_{\Xi^0} - m_{\Xi^-} \sim 50$ MeV.

An investigation of the Gell-Mann-Okubo relations has been carried out. For the octet baryon masses we find that these relations are satisfied at all pion masses. For the decuplet baryon masses we see deviations and it will be interesting to study these relations at smaller quark masses.

The final continuum results at the physical limit shown in Fig. 7.28 are in satisfying agreement with experiment in view of the largest uncertainty coming fron the chiral extrapolation, which are not estimated, and from systematic errors in setting the scale, which are an order of magnitude larger than statistical errors.

Besides the masses we have extracted from the various fits the σ-term. As expected, for strange baryon they are systematically smaller than the nucleon one, even if they suffer from large uncertainties.

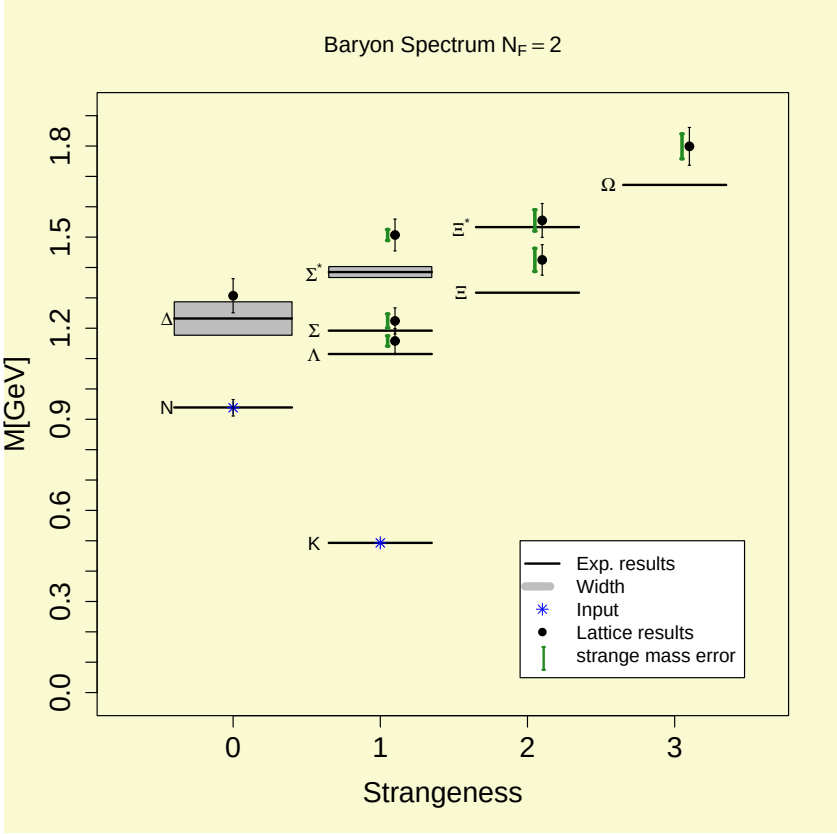

Figure 7.28: Octet and decuplet spectrum. The values shown are obtained after continuum and chiral extrapolation. Systematical errors due to the scale have been added. For the nucleon and Δ we used $\mathcal{O}(p^3)$ fit while we use NLO SU(2) HBχPT for strange baryons.

Chapter 8

Conclusion

After a brief historical introduction of the particle physics evolution through strong interaction phenomenology, we have presented the basis of the Quantum Field Theory formalism. We have shown that Quantum Chromodynamics is expected to have a variety of mechanisms and phenomena that have still to be understood. So far, a large class of issues raised by QCD have been addressed pertubatively and have shown the validity of this theory at high energy. At low energy, the perturbative expansion breaks down and other methods are needed.

Lattice QCD is the only quantitative method which allows the computation of low energy observables and, in the infinite volume and continuum limits, is supposed to reproduce experiment. Twisted mass fermions are one possible way to discretize the theory on a lattice. They have the advantage of being automatically $\mathcal{O}(a)$ improved when they are tuned to maximal twist, thus providing good scaling properties. They constitute a good compromise between Wilson-Clover and the expensive chiral fermions. The price to pay is the breaking of isospin, flavour and parity symmetries.

The European Twisted Mass Collaboration (ETMC) has made a large effort to produce dynamical twisted mass configurations with degenerate and non degenerate quarks. It provides thus an ideal context to compute a large variety of observables to accurately test low energy QCD. As a consequence, these results will bring us constraints on new physics and improve our knowledge on non-perturbative phenomena which could have an important impact on the future of particle physics.

In particular spectroscopy studies are not only related to the original question raised by the quark model, but they are also a reliable way to obtain new predictions for exotic baryons or glueballs. Furthermore, spectroscopy studies constitute an important benchmark for lattice simulations. To reach a competitive level of prediction a large number of steps have to be performed from configuration generation on supercomputers to the calculation of correlators and their analysis. This work address all the aspects in which I have been involved during my Ph.D, from the theoritical as well as from the numerical point of view.

To achieve this aim several steps have been necessary. The first advance was the formal developments needed to obtain a general formula which allow the evaluation of generic baryonic correlators. The Eq. (3.31) fulfilled this role, and has even been generalized to the evaluation of an arbitrary three point functions. An efficient implementation in parallel codes has then been realized and is now actively used to produce all the corresponding correlators. This has been done taking into account the important computational resources needed to produce results on for instance $48^3 \times 96$ lattices which have to be done with parallel code. We have also improved the overlap between the interpolating field and the ground state using smearing techniques and developed an efficient analysis code. More recently a large amount of time has been spent to

obtain theoritical understanding of Heavy Baryon Chiral perturbation theory expansion, which was a key step to interpret our lattice data.

The numerical lattice results concerning baryon masses, both in the $N_f = 2$ and $N_f = 2+1+1$ case, are respectively presented and analyzed in the last two chapters.

In the $N_f = 2$ case, we insist on the study of finite size and lattice spacing effects which can be particularly well understood with the variety of volume and lattice spacings produced by the collaboration. The results concerning the nucleon (summarized in Fig. 6.5 and Fig. 6.9) show a nice coherence even when taking into account such a variety of ensembles.

This coherence is lost when considering the other baryons for which we are unable to claim that lattice artefacts are smaller than statistical errors. We think for instance to the Δ mass (summarized in Fig. 6.10) which shows a large dispersion (summarized in Fig. 6.6) and an erratic scaling behaviour even with a third lattice spacing. No explanations have been found to clarify this point and further studies are needed.

Concerning the strange baryon, an important source of uncertainty comes from the large error ($\sim 10\%$) in the bare strange quark mass. This spoiled our approach to the continuum (Figs. 7.11-7.16) which moreover suffers from having only two reliable lattice spacings.

Despite that, an important conclusion of our study was that, the additional artefact due to the breaking of isospin symmetry is shown to be under control both in the light (Δ) and strange sector.

These remarks concern only the systematic effects inherent to the lattice data without any reference to the experimental point. This issue is related to the chiral extrapolation which was addressed in chapters 5, 6 and 7.

Our first remark is that without an underlying effective theory (here HBχPT) we cannot draw any conclusion from our data. Actually they can be found compatible with a linear behaviour in m_π, even with a quadratic one or with any other exotic analytic form. Secondly, once having choose a precise version of χPT, our results are very sensitive to the order of the expansion, which indicates that the convergence of such expansion is doubtful at least in our range of masses.

At a given order, we are still not able to determine the parameters and to be in agreement with the experimental point. Some of them have to be fixed by some assumption ($SU(3) - SU(6)$ and phenomenology of hyperon-nucleon interaction).

By doing so we were able to found reasonable parametrization of the results that are compatible with the experimental points. It is thus impossible to have any serious doubt about the fact that QCD correctly describe baryon spectroscopy.

A key point of this success, is the scale determination (either r_0 or a). During the last three years, the $\beta = 3.9$ value of a determined from mesonic sector and in the same collaboration , has changed from $a = 0.087(1)$ to $0.079(2)$ fm. This large uncertainty of 10%, lead us to determine ourselves the scale, using the nucleon as a reference, and found $a_{\beta=3.9} \sim 0.089(2)$ fm. We would like to stress that the significant disagreement between the estimation of the lattice spacing obtained in the meson and baryon sector is a direct consequence of the chiral behaviour uncertainties. In fact, the scale extracted from the nucleon mass data depends on the order of the expansion and on the value assumed for the low energy constants. To circumvent this caveat, one clearly needs to compute the spectrum at the physical pion mass. This will be hopefully available soon.

Another important restriction of the strange baryons results is the quenching of the strange quark. The systematic effect introduced by this approximation are not controlled even if in the past one has never observed a sizeable effect due to quenching in the masses.

This last point, introduce us to the second part of this work which is the $N_f = 2 + 1 + 1$ calculations. Indeed, during my PhD, the collective decision was taken, to go one step further and

to start the ambitious project of producing for the first time configurations which, in addition to the light quarks, take into account the strange and charm degrees of freedom. I have contributed to this project by generating configurations on supercomputer like BlueGene and by performing all the necessary control steps in the algorithm and by producing the first two-point correlators calculation. The nucleon and Δ analysis were performed and showed to be compatible with the $N_f = 2$ results (Figs. 6.24 and 6.25). We have also demonstrated that the isospin breaking was not amplified, compared to the $N_f = 2$ case, and that the scaling properties were not modified by the introduction of the strange and charm quark masses.

This work paves the way to several improvements and offers new perspectives in lattice QCD.

First, the analysis of the $N_f = 2$ strange baryon is being currently updated by using the new lattice spacing ensembles at $\beta = 4.2$ ($a \sim 0.053$ fm) and by properly studying the strange quark mass dependence. Together with the two existing β values, this will allow to control finite lattice spacing artefacts.

Second, the analysis of strange baryon with $N_f = 2 + 1 + 1$ remains to be done, following the so-called unitary and mixed action approaches. Of particular interest is the case of Ω which is surprisingly heavy in our actual results and could be an alternative to fix the bare strange quark mass and/or the lattice spacing.

A third interesting issue, is the optimization of the ground state overlap with the interpolating field. This can be studied using correlation matrices and eventually other smearing techniques. This would be a first step before addressing the question of excited states. In view of the problems encountered in this work, a particular care should be taken to improve the Δ mass extraction.

An almost unexplored issue would be to extend this work to the charm and strange charmed baryons, some of them not being measured experimentally. In this case the problem of chiral extrapolation should be less severe, while discretization effects are expected to be larger.

The $2 + 1 + 1$ configurations open other doors to compute interesting quantities, such that the strange quark mass dependence of the nucleon mass. More generally measurement of the strange content of the nucleon would join effort made by experimentalist to reveal the structure of the baryons.

Conclusion

Après une brève introduction historique de l'évolution de la physique des particule à travers la phénoménologie de l'interaction forte, nous avons présenté les bases du formalisme de la théorie quantique des champs. Nous avons montré en quoi la chromodynamique quantique présente une grande variété de mécanismes et de phénomènes qui restent à comprendre. Jusqu'à présent, seul le régime perturbatif de la théorie a été validé à haute énergie. À basse énergie, la théorie des perturbations au voisinage de $\alpha_s = 0$ ne converge pas et d'autres méthodes sont nécessaires.

La QCD sur réseau est la seule méthode quantitative qui permet de faire des calculs d'observables à basse énergie en contrôlant les effets systématiques de volume et de maille finis. Les fermions twistés sont un choix possible de discrétisation. Ils ont l'avantage d'être automatiquement améliorés d'ordre a lorsqu'ils sont simulés à angle de twist maximal. Ils constituent un bon compromis entre les fermions Wilson-Clover et les coûteux fermions chiraux. Le prix à payer est la brisure de la symétrie d'isospin,ainsi que celles de parité et de saveur (lorsque l'on considère le secteur lourd).

La European Twisted Mass Collaboration (ETMC) a realisé un effort important pour produire des configurations dynamiques $N_F = 2$ ou $N_F = 2 + 1 + 1$. Ces ensembles fournissent le cadre idéal au calcul d'un large spectre d'observables afin de tester précisement la QCD à basse énergie. Idéalement, ces connaissances sur les phénomènes non perturbatifs fourniront des contraintes sur la nouvelle physique et auront ainsi un impact important sur la communauté des physiciens des particules.

À ce titre, l'étude de la spectroscopie n'est pas seulement reliée à la question originelle soulevée par le modèle des quarks, mais offre aussi une façon fiable d'obtenir des prédictions concernant les baryons exotiques ou les "glueballs". Par ailleurs, elle sert de point de repère pour le calcul d'autres observables. Afin d'atteindre ces objectifs, un grand nombre d'étapes doivent être réalisées depuis la génération des configurations de jauges jusqu'au calcul des corrélateurs et leur analyse. Ce travail soulève tous les aspects dans lesquels j ai été impliqué au cours de ma thèse, autant du point de théorique que numérique.

Pour atteindre ce but, plusieurs étapes ont été nécessaires. La première avancée a été le developpement d'une formule générale permettant de calculer un corrélateur baryonique générique. L'équation 3.31 remplit ce rôle et a même été généralisée au calcul d'une fonction à trois points arbitraire. Une implémentation efficace dans un code parallèle a ensuite été réalisée et est maintenant activement utilisée pour produire les corrélateurs correspondants. Cette avancée a été effectuée en tenant compte des importants moyens de calcul nécessaires pour produire des résultats sur des réseau $48^3 \times 96$ qui ne peuvent être traités qu'en parallèle. Nous avons également amélioré le recouvrement des opérateurs baryoniques avec les états fondamentaux en construisant des opérateurs effectifs "étalés". Un code d'analyse performant a aussi été construit afin d'analyser efficacement l'ensemble des informations disponibles. Plus récemment un temps important a été consacré à l'obtention d'une compréhension théorique de la théorie des pertubations chirales des baryons lourds, qui est un outil essentiel pour interprêter les résultats bruts.

Les résultats numériques concernant les masses des baryons, dans le cas $N_f = 2$ et $N_f = 2 + 1 + 1$ sont présentés et analysés dans les deux derniers chapitres.

Dans le cas $N_f = 2$, on insiste sur l'étude des effets de taille finis et de discrétisation qui peuvent être particulièrement bien compris en utilisant la grande variété de volumes et de mailles produite par la collaboration. Les résultats concernants le nucléon (résumé en Fig. 6.5 et Fig. 6.9) montrent au premier coup d'oeil une belle cohérence, et ce, même lorsque l'on considère une telle variété d'ensembles.

Cette cohérence est perdue dès lors que l'on considère les autres baryons, pour lesquels nous n'avons pu démontrer que les artefacts réseau étaient plus petits que les erreurs statistiques. Nous pensons par exemple au cas de la masse du Δ résumé en Fig. 6.10) qui montre une grande dispersion (résumé en Fig. 6.6) et un comportement ératique en fonction de la maille. Aucune explication pour clarifier ce point n'a été obtenue, et une étude plus approndie se révèle être nécessaire.

Concernant les baryons étranges, une source d'erreurs systématiques importante vient de l'incertitude sur la masse du quark étrange nue. Cette incertitude rend le contrôle de la limite du continu (Figs. 7.11-7.16) difficile, d'autant plus que seules deux mailles fiables sont utilisables pour cette analyse.

Malgré ceci, une conclusion importante de notre étude est que l'artefact additionnel dû à la brisure de la symétrie d'isospin est sous contrôle dans le secteur léger et étrange.

Ces remarques concernent uniquement les effets systématiques inhérents aux données réseau et ne font aucunement référence aux point expérimentaux. La question de l'extrapolation chirale est traitée dans les chapitres 5, 6 et 7.

La première conclusion importante est que sans une théorie effective (ici HBχPT), il est impossible de tirer des conclusions à partir de nos données. En fait, celles-ci sont compatibles avec un comportement linéaire ou quadratique en m_π, ou bien encore avec d'autres formes analytiques exotiques. Même une fois choisie une version précise de perturbations chirales, les résultats sont extrêmement sensibles à l'ordre auquel l'éxpansion est tronquée, ce qui indique que la convergence d'une telle série est douteuse au moins dans le régime dans lequel nous avons des données.

À un ordre de perturbation fixé, on reste incapable de déterminer tous les paramètres et d'être en accord avec le point expérimental. Certains paramètres sont donc fixés en faisant des hypothèses basées sur la phénomologie (symétrie $SU(3) - SU(6)$ et interactions hypérons-nucléon).

En procédant ainsi, nous obtenons une paramétrisation raisonnable des résultats qui est compatible avec les points expérimentaux. En tout cas, les résultats ne suggèrent pas de sérieux doutes quant à la validité de QCD pour décrire la spectroscopie des états fondamentaux de baryons.

Il est intéressant de noter qu'un point essentiel de ce succès est la détermination de l'échelle (que ce soit la maille a ou le paramètre de Sommer r_0). Durant ces trois dernières années, l'estimation de la maille à $\beta = 3.9$ déterminée dans le secteur des mésons et dans la même collaboration est passée de $a = 0.087(1)$ à $0.079(2)$ fm. Cette incertitude de 10% nous a conduit à déterminer nous même l'échelle en utilisant la masse du nucléon comme référence. Nous trouvons alors $a_{\beta=3.9} \sim 0.089(2)$ fm. Il est important de souligner ici que le désaccord significatif entre l'estimation de la maille obtenue dans le secteur des mésons et des baryons est une conséquence directe de l'incertitude sur le comportement chiral des quantités utilisées pour fixer la maille. En fait, l'échelle extraite de la masse du nucléon dépend de l'ordre auquel l'expansion chirale est tronquée et de la valeur des constantes de basses énergie utilisées. Pour éviter ce problème il est nécessaire de parvenir à calculer le spectre à des masses de pion plus proches de la masse du pion physique. On a de bonne raison d'espérer que celles ci devraient être disponible bientôt, certaines collaborations étant déjà parvenues à réaliser cet exploit.

Une autre restricition important concernant les résultats sur les baryons étranges est l'approximation de "quenching" du quark étrange. Cet effet systématique introduit une approximation non contrôlée. Même si aucun groupe n'a observé d'effets signficatifs lorsque le quark étrange est traité dans cette approximation, il est important de s'affranchir d'une telle hypothèse.

Ce dernier point nous conduit naturellement à la deuxième partie de ce travail : les simulations $N_f = 2 + 1 + 1$. En effet, durant ma thèse, la décision collective a été prise de faire un pas supplémentaire et de commencer le projet ambitieux de produire pour la première fois des configurations qui prennent en compte les quarks étranges et le quark charmés en plus des quarks légers. J'ai contribué à la génération de telles configurations sur des supercalculateurs comme la Blue Gene/P et réalisé les étapes de contrôles nécessaires de l'algorithme et de la production des premiers corrélateurs à deux points. Les analyses du nucléon et du Δ ont également été menées à bien et se révèlent être compatible avec l'analyse des résultats obtenus dans le cas $N_f = 2$ (voir Figs. 6.24 et 6.25). Nous avons également montré que la brisure d'isospin n'était pas amplifiée, comparativement au cas $N_f = 2$, et que le comportement en fonction de a^2 etait compatible avec les résultats $N_f = 2$ malgré l'introduction des quarks charmés et étranges.

Ce travail ouvre de nouvelles perspectives en QCD sur réseau.

Tout d'abord, l'analyse des baryons étranges dans le cas $N_f = 2$ est actuellement complétée à $\beta = 4.2$ tout en étudiant prudemment la dépendence en la masse du quark étrange. En utilisation conjointe avec les résultats existants aux deux autres mailles, nous pourrons contrôler les effets de discrétisation.

L'analyse des baryons étranges sur les configurations $N_f = 2 + 1 + 1$ reste à faire et deux approches peuvent alors être suivies ("unitaire" ou "mixte"). Il serait particulièrement intéressant d'étudier le Ω qui jusqu'à présent apparaît comme etonnament lourd dans nos résultats et qui pourrait être une alternative judicieuse pour fixer la masse du quark étrange ou la maille.

Une troisième question intéressante est l'optimisation du recouvrement entre les champs interpolants et les états fondamentaux du spectre baryonique. Ceci peut être étudié en utilisant des matrices de corrélations et éventuellement d'autres techniques de smearing. Cela serait sans doute la première étape avant s'intéresser à la question des états excités. Au vue des problèmes rencontrés dans ce travail, il semble nécessaire d'apporter un soin particulier à l'amélioration de l'extraction de la masse du Δ.

On pourrait par ailleurs étendre ce travail aux baryons charmés et charmés étranges, certains d'entre eux n'ayant pas été mesurés expérimentalement. Ceci donnerait accès à un secteur quasiment non exploré en QCD sur réseau. Dans ce cas, le problème de l'extrapolation chirale devrait être moins sévère contrairement à celui dû aux effets de discrétisation.

Les configurations $2 + 1 + 1$ ouvrent les portes pour calculer d'autres quantités intéressantes comme la masse du nucléon en fonction de la masse du quark étrange. De manière plus générale la mesure du contenu étrange du nucléon rejoindrait les efforts des expérimentateurs pour réveler la structure des baryons.

Appendix A

Conventions

A.1 Pauli Matrices

The Pauli matrices are defined by

$$\sigma_1 = \begin{pmatrix} 0 & 1 \\ 1 & 0 \end{pmatrix}, \qquad \sigma_2 = \begin{pmatrix} 0 & -i \\ i & 0 \end{pmatrix}, \qquad \sigma_3 = \begin{pmatrix} 1 & 0 \\ 0 & -1 \end{pmatrix}.$$

They are a basis of the Lie algebra of the $SU(2)$ group. They satisfy the following relations

$$\begin{aligned} [\sigma_a, \sigma_b] &= 2i\varepsilon_{abc}\,\sigma_c \\ \{\sigma_a, \sigma_b\} &= 2\delta_{ab}\cdot I \end{aligned} \tag{A.1}$$

and

$$\sigma_a\sigma_b = \delta_{ab}\cdot \mathbb{1} + i\varepsilon_{abc}\sigma_c\,. \tag{A.2}$$

The Baker-Campbell-Hausdorff formula is :

$$e^{\hat{A}}\hat{B}e^{-\hat{A}} = \hat{B} + [\hat{A},\hat{B}] + \frac{1}{2!}[\hat{A},[\hat{A},\hat{B}]] + \frac{1}{3!}[\hat{A},[\hat{A},[\hat{A},\hat{B}]]] + \cdots \tag{A.3}$$

A.2 Dirac Matrices

We use the following convention :

$$\gamma_0 = \begin{pmatrix} 0 & 0 & -1 & 0 \\ 0 & 0 & 0 & -1 \\ -1 & 0 & 0 & 0 \\ 0 & -1 & 0 & 0 \end{pmatrix}, \quad \gamma_1 = \begin{pmatrix} 0 & 0 & 0 & -i \\ 0 & 0 & -i & 0 \\ 0 & i & 0 & 0 \\ i & 0 & 0 & 0 \end{pmatrix}, \quad \gamma_2 = \begin{pmatrix} 0 & 0 & 0 & -1 \\ 0 & 0 & 1 & 0 \\ 0 & 1 & 0 & 0 \\ -1 & 0 & 0 & 0 \end{pmatrix} \tag{A.4}$$

$$\gamma_3 = \begin{pmatrix} 0 & 0 & -i & 0 \\ 0 & 0 & 0 & i \\ i & 0 & 0 & 0 \\ 0 & -i & 0 & 0 \end{pmatrix}, \quad \gamma_5 = \begin{pmatrix} 1 & 0 & 0 & 0 \\ 0 & 1 & 0 & 0 \\ 0 & 0 & -1 & 0 \\ 0 & 0 & 0 & -1 \end{pmatrix} \tag{A.5}$$

They satisfy

$$\{\gamma_\mu, \gamma_\nu\} = 2\delta_{\mu\nu} \tag{A.6}$$

$$\gamma_\mu^\dagger = \gamma_\mu \tag{A.7}$$

$$\gamma_5^\dagger = \gamma_5 \tag{A.8}$$

We define $\sigma_{\mu\nu} = i\left[\gamma_\mu, \gamma_\nu\right]/2$.
We define the charge conjugation matrix C as :

$$C = i\gamma_0\gamma_2 = \begin{pmatrix} 0 & -i & 0 & 0 \\ i & 0 & 0 & 0 \\ 0 & 0 & 0 & i \\ 0 & 0 & -i & 0 \end{pmatrix} \tag{A.9}$$

which satisfy the following relation:

$$C\gamma_\mu C^{-1} = -\gamma_\mu^T \tag{A.10}$$

$$C = \gamma_0\gamma_2, \quad C^T = -C = C^{-1} = C^\dagger \tag{A.11}$$

$$\{\gamma_0, C\} = 0 \tag{A.12}$$

$$\left(C\gamma_\mu\right)^T = C\gamma_\mu \tag{A.13}$$

A.3 $SU(3)$ group

A representation of the Lie algebra associated to $\mathrm{SU(3)_c}$ is given by 3×3 antihermitean and traceless matrices. Meaning that

$$X^\dagger = -X, \quad \text{and } \mathrm{Tr}\left\{X\right\} = 0 \tag{A.14}$$

This is a $N^2 - 1 = 9$ dimensional algebra. A basis T^a that satify

$$\mathrm{Tr}\left\{T^a T^b\right\} = \frac{1}{2}\delta^{ab} \tag{A.15}$$

can be defined. A standard basis is defined from the Gell-Mann matrices λ^a by :

$$t^a = \frac{\lambda^a}{2i} \tag{A.16}$$

where

$$\begin{aligned} \lambda^{1,2,3} &= \begin{pmatrix} \sigma^{1,2,3} & 0 \\ 0 & 0 \end{pmatrix} \quad , \qquad \lambda^4 = \begin{pmatrix} 0 & 0 & 1 \\ 0 & 0 & 0 \\ 1 & 0 & 0 \end{pmatrix} \\ \lambda^5 &= \begin{pmatrix} 0 & 0 & -i \\ 0 & 0 & 0 \\ i & 0 & 0 \end{pmatrix} \quad , \qquad \lambda^6 = \begin{pmatrix} 0 & 0 & 0 \\ 0 & 0 & 1 \\ 0 & 1 & 0 \end{pmatrix} \\ \lambda^7 &= \begin{pmatrix} 0 & 0 & 0 \\ 0 & 0 & -i \\ 0 & i & 0 \end{pmatrix} \quad , \qquad \lambda^8 = \frac{1}{\sqrt{3}} \begin{pmatrix} 1 & 0 & 0 \\ 0 & 1 & 0 \\ 0 & 0 & -2 \end{pmatrix} \end{aligned} \tag{A.17}$$

With this convention the structure constant f^{abc} defined by

$$[t^a, t^b] = i f^{abc} t^c \tag{A.18}$$

are real and antisymmetric.

Appendix B

Bilinear operators dictionnary

Let χ denote a doublet of two degenerate light quarks in twisted mass QCD at maximal twist, and ψ thee corresponding field in the physical base.

$$\mathcal{O}^a_{\mathrm{S}} = \overline{\chi}\tau^a\chi = \begin{cases} \overline{\psi}\tau^a\psi, & a = 1,2 \\ -i\overline{\psi}\gamma_5\mathbb{1}\psi, & a = 3 \end{cases} \tag{B.1}$$

$$\mathcal{O}^a_{\mathrm{P}} = \overline{\chi}\gamma_5\tau^a\chi = \begin{cases} \overline{\psi}\gamma_5\tau^a\psi, & a = 1,2 \\ -i\overline{\psi}\mathbb{1}\psi, & a = 3 \end{cases} \tag{B.2}$$

$$\mathcal{O}^a_{\mathrm{V}} = \overline{\chi}\gamma_\mu\tau^a\chi = \begin{cases} \overline{\psi}\gamma_5\gamma_\mu\tau^2\psi, & a = 1 \\ -\overline{\psi}\gamma_5\gamma_\mu\tau^1\psi, & a = 2 \\ \overline{\psi}\gamma_\mu\tau^3\psi, & a = 3 \end{cases} \tag{B.3}$$

$$\mathcal{O}^a_{\mathrm{A}} = \overline{\chi}\gamma_5\gamma_\mu\tau^a\chi = \begin{cases} \overline{\psi}\gamma_\mu\tau^2\psi, & a = 1 \\ -\overline{\psi}\gamma_\mu\tau^1\psi, & a = 2 \\ \overline{\psi}\gamma_5\gamma_\mu\tau^3\psi, & a = 3 \end{cases} \tag{B.4}$$

$$\mathcal{O}^a_{\mathrm{T}} = \overline{\chi}\sigma_{\mu\nu}\tau^a\chi = \begin{cases} \overline{\psi}\sigma_{\mu\nu}\tau^a\psi, & a = 1,2 \\ -i\overline{\psi}\gamma_5\sigma_{\mu\nu}\tau^3\psi, & a = 3 \end{cases} \tag{B.5}$$

Appendix C

Symmetries

C.1 Wilson fermions

The parity symmetry transformation for Wilson fermions is given by

$$\mathcal{P}\colon \begin{cases} U(x_0,\mathbf{x};0) \to U(x_0,-\mathbf{x};0), \quad U(x_0,\mathbf{x};k) \to U^{-1}(x_0,-\mathbf{x}-a\hat{k};k), \quad k=1,\,2,\,3 \\ \chi(x_0,\mathbf{x}) \to \gamma_0\chi(x_0,-\mathbf{x}) \\ \overline{\chi}(x_0,\mathbf{x}) \to \overline{\chi}(x_0,-\mathbf{x})\gamma_0 \end{cases} \tag{C.1}$$

ordinary time-reversal is

$$\mathcal{T}\colon \begin{cases} U(x_0,\mathbf{x};0) \to U^{-1}(-x_0-a,\mathbf{x};0), \quad U(x_0,\mathbf{x};k) \to U(-x_0,\mathbf{x};k), \quad k=1,\,2,\,3 \\ \chi(x_0,\mathbf{x}) \to i\gamma_0\gamma_5\chi(-x_0,\mathbf{x}) \\ \overline{\chi}(x_0,\mathbf{x}) \to -\overline{\chi}(-x_0,\mathbf{x})i\gamma_5\gamma_0 \end{cases} \tag{C.2}$$

And charge conjugation is

$$\mathcal{C}\colon \begin{cases} U(x;\mu) \longrightarrow U(x;\mu)^* \\ \chi(x) \longrightarrow C^{-1}\overline{\chi}(x)^T \\ \overline{\chi}(x) \longrightarrow -\chi(x)^T C \end{cases} \tag{C.3}$$

where $C = i\gamma_0\gamma_2$.

C.2 twisted mass fermions

We list here the form of the symmetries of the twisted mass action for an arbitrary value of the twist angle ω. The $SU(2)$ axial and vector transformation read:

$$SU_{\mathrm{V}}(2)_\omega\colon \begin{cases} \chi(x) \longrightarrow \exp(-i\frac{\omega}{2}\gamma_5\tau^3)\exp(i\frac{\alpha_V^a}{2}\tau^a)\exp(i\frac{\omega}{2}\gamma_5\tau^3)\chi(x), \\ \overline{\chi}(x) \longrightarrow \overline{\chi}(x)\exp(i\frac{\omega}{2}\gamma_5\tau^3)\exp(-i\frac{\alpha_V^a}{2}\tau^a)\exp(-i\frac{\omega}{2}\gamma_5\tau^3). \end{cases} \tag{C.4}$$

$$SU_{\mathrm{A}}(2)_\omega\colon \begin{cases} \chi(x) \longrightarrow \exp(-i\frac{\omega}{2}\gamma_5\tau^3)\exp(i\frac{\alpha_A^a}{2}\gamma_5\tau^a)\exp(i\frac{\omega}{2}\gamma_5\tau^3)\chi(x), \\ \overline{\chi}(x) \longrightarrow \overline{\chi}(x)\exp(i\frac{\omega}{2}\gamma_5\tau^3)\exp(i\frac{\alpha_A^a}{2}\gamma_5\tau^a)\exp(-i\frac{\omega}{2}\gamma_5\tau^3). \end{cases} \tag{C.5}$$

The discrete symmetries are

$$\mathcal{P}_\omega\colon \begin{cases} U(x_0,\mathbf{x};0) \longrightarrow U(x_0,-\mathbf{x};0), \quad U(x_0,\mathbf{x};k) \longrightarrow U^{-1}(x_0,-\mathbf{x}-a\hat{k};k), \quad k=1,2,3 \\ \chi(x_0,\mathbf{x}) \longrightarrow \gamma_0 \exp(i\omega\gamma_5\tau^3)\chi(x_0,-\mathbf{x}), \\ \overline{\chi}(x_0,\mathbf{x}) \longrightarrow \overline{\chi}(x_0,-\mathbf{x}) \exp(i\omega\gamma_5\tau^3)\gamma_0, \end{cases} \tag{C.6}$$

$$\mathcal{T}_\omega\colon \begin{cases} U(x_0,\mathbf{x};0) \longrightarrow U^{-1}(-x_0-a,\mathbf{x};0), \quad U(x_0,\mathbf{x};k) \longrightarrow U(-x_0,\mathbf{x};k), \quad k=1,2,3 \\ \chi(x_0,\mathbf{x}) \longrightarrow i\gamma_0\gamma_5 \exp(i\omega\gamma_5\tau^3)\chi(-x_0,\mathbf{x}), \\ \overline{\chi}(x_0,\mathbf{x}) \longrightarrow -i\overline{\chi}(-x_0,\mathbf{x}) \exp(i\omega\gamma_5\tau^3)\gamma_5\gamma_0. \end{cases} \tag{C.7}$$

Note that charge conjugation takes a form that is invariant under the rotation to the physical basis.

Appendix D

One-loop integrals

D.1 Definitions

We define the one-loop tensor integral, as in [152], to be :

$$T^N_{\mu_1\dots\mu_P}(p_1,\dots,p_{N-1},m_0,\dots,m_{N-1}) = \frac{(2\pi\mu)^{4-D}}{i\pi^2}\int d^Dq \frac{q_{\mu_1}\cdots q_{\mu_P}}{D_0D_1\cdots D_{N-1}} \tag{D.1}$$

with the denominator factors

$$D_0 = q^2 - m_0^2 + i\varepsilon, \qquad D_i = (q+p_i)^2 - m_i^2 + i\varepsilon, \qquad i = 1,\dots,N-1, \tag{D.2}$$

Conventionally T^N is denoted by the Nth character of the alphabet, *i.e* $T^1 = A$, $T^2 = B$,... and the scalar integrals carry an index 0.

Lorentz covariance of the integrals allows to decompose tensor integrals into a sum of scalar integral. Let us consider as an example a case useful in chapter 5. We have

$$B_\mu(p_1,m_0,m_1) = p_{1\mu}B_1(p_1,m_0,m_1) = \frac{(2\pi\mu)^{4-D}}{i\pi^2}\int d^Dq \frac{q_\mu}{D_0D_1}, \tag{D.3}$$

and $B_1(p_1,m_0,m_1)$ can be expressed in terms of scalar one loop integral as :

$$p^2B_1(p_1,m_0,m_1) = \frac{1}{2}\left(A_0(m_0) - A_0(m_1) - f_1B_0(p_1,m_0,m_1)\right) \tag{D.4}$$

with $f_1 = p_1^2 - m_1^2 + m_0^2$.

D.2 Scalar one-point function

The scalar one-point function reads in $\overline{\text{MS}}$

$$A_0(m) = -m^2\left(\frac{m^2}{4\pi\mu^2}\right)^{\frac{D-4}{2}}\Gamma(1-\frac{D}{2}) = m^2(R_{\overline{\text{MS}}} - \log\frac{m^2}{\mu^2} + 1) + O(D-4), \tag{D.5}$$

with the UV-divergence contained in

$$R_{\overline{\text{MS}}} = \frac{2}{4-D} - \gamma_E + \log 4\pi \tag{D.6}$$

or in $\widetilde{\rm MS}$

$$A_0(m) = -m^2(\frac{m^2}{4\pi\mu^2})^{\frac{D-4}{2}}\Gamma(1-\frac{D}{2}) = m^2(R - \log\frac{m^2}{\mu^2}) + O(D-4), \tag{D.7}$$

$$R_{\widetilde{\rm MS}} = R_{\overline{\rm MS}} + 1 = \frac{2}{4-D} - \gamma_E + \log 4\pi + 1 \tag{D.8}$$

and γ_E is Euler's constant. The terms of order $O(D-4)$ are only relevant for two- or higher-loop calculations.

D.3 Scalar two-point function

The two-point function is given in $\widetilde{\rm MS}$ by

$$B_0(p_{10}, m_0, m_1) = R_{\widetilde{\rm MS}} - 1 - \int_0^1 dx \log\frac{[p_{10}^2x^2 - x(p_{10}^2 - m_0^2 + m_1^2) + m_1^2 - i\varepsilon]}{\mu^2} + O(D-4) \tag{D.9}$$

$$= R_{\widetilde{\rm MS}} + 1 - \log\frac{m_0m_1}{\mu^2} + \frac{m_0^2 - m_1^2}{p_{10}^2}\log\frac{m_1}{m_0} - \frac{m_0m_1}{p_{10}^2}(\frac{1}{r} - r)\log r \tag{D.10}$$

$$+O(D-4), \tag{D.11}$$

where r and $\frac{1}{r}$ are determined from

$$x^2 + \frac{m_0^2 + m_1^2 - p_{10}^2 - i\varepsilon}{m_0m_1}\,x + 1 = (x+r)(x+\frac{1}{r}). \tag{D.12}$$

The variable r never crosses the negative real axis even for complex physical masses . For $r < 0$ the $i\varepsilon$ prescription yields $\Im{\rm m}\, r = \varepsilon\,{\rm sgn}(r - \frac{1}{r})$. Consequently the result (D.11) is valid for arbitrary physical parameters.

D.4 More on the B_0 function

Let us derive some properties of the B_0 function, in order to relate baryon chiral perturbation and heavy baryon chiral perturbation theory.

To solve the equation D.12, let

$$\Omega = \frac{m_0^2 + m_1^2 - p_{10}^2 - i\varepsilon}{2m_0m_1} \tag{D.13}$$

we obtain :

$$r = \Omega + \sqrt{\Omega^2 - 1}, \text{and } \frac{1}{r} = \Omega - \sqrt{\Omega^2 - 1} \tag{D.14}$$

An interesting limit is the case where $m_0 << m_1$ and $p = -m_1$. Some complex analysis show that :

$$B_0(-m_1, m_0, m_1) = R_{\widetilde{\rm MS}} + 1 - \pi\frac{m_0}{m_1} + \mathcal{O}(m_0^2) \tag{D.15}$$

Another important properties gives the relation with the heavy baryon chiral perturbation results. For future purpose let us introduce

$$\Delta = m_x - m_1 \tag{D.16}$$

where m_x is typically the mass of an other state coupled to the particle of mass m_1. We want to compute $B_0(-m_1, m_0, m_x)$, in the large m_1 limit,

we have

$$\Omega \xrightarrow[m_1 \to \infty]{} \frac{\Delta}{m_0} - i\varepsilon \tag{D.17}$$

Using that

$$\log \frac{a + \sqrt{a^2 - c^2}}{c} = \frac{1}{2} \log \frac{a + \sqrt{a^2 - c^2}}{a - \sqrt{a^2 - c^2}}. \tag{D.18}$$

Then one obtain for $m_1 \to +\infty$

$$B_0(-m_1, m_0, m_x) = \frac{1}{m_0} \sqrt{(\Delta - i\varepsilon)^2 - m_0^2} \log \frac{\Delta - i\varepsilon - \sqrt{(\Delta + i\varepsilon)^2 - m_0^2}}{\Delta - i\varepsilon + \sqrt{(\Delta + i\varepsilon)^2 - m_0^2}} \tag{D.19}$$

Note the similiraty with the $\mathcal{F}$ function define in ....

Appendix E

SuperComputers

The recent installation of the BlueGene/P machine in the computation center of IDRIS have improve considerably the computation power in France. This machine has been used extensively during the three years of Ph.D. After describing basic notions of scalability, this Appendix describes what are the main advantages of this architecture.

E.1 Scalability

The scalability of a code measure its ability to be executed efficiently on an increasing number of process. It is a characteristic of the implementation of the code, on the way the process are disstributed on the machine and on the architecture of the machine.
There is two common way of measuring it. The first one is called *strong scaling* and consist to measure the time needed to solve a problem of fixed size while the number of CPU used increases. The second one is the *weak scaling* which consists to keep the size of the problem fixed on each CPU (in the case of lattice QCD, the local volume) and to increase the number of CPU.

Given a reference number of processors n_{ref} and the computation time $T_{ref} = T(n_{ref})$ to realize one task on n_{ref} CPU. For strong scaling test one define the acceleration A and the efficiency E as follow :

$$A(n) = \frac{T_{ref}}{T(n)} \tag{E.1}$$

$$E(n) = A(n)\frac{n_{ref}}{n} \tag{E.2}$$

For a weak scaling test reads the definition are

$$A(n) = \frac{n}{n_{ref}}\frac{T_{ref}}{T(n)} \tag{E.3}$$

$$E(n) = \frac{T_{ref}}{T(n)} \tag{E.4}$$

Another way to measure characterize a code is to compute the total sustained power counting the number of floatting operation by seconds in flops.

Weak scaling test are particularly important for Lattice QCD computations. Indeed, to study of systematic effects one need to decrease or the lattice spacing keeping the physical volume fixed or to increase the physical volume keeping fixed the lattice spacing. In both case, the number of lattice points increases and a larger number of CPU has to be used. The BlueGene/P architecture allow to have a linear acceleration up to the use of the whole machine without any problems. This

have even been checked on the Juelich machine which is composed of 72 racks of BlueGene/P (294912 core!) as shown in Fig. E.1.

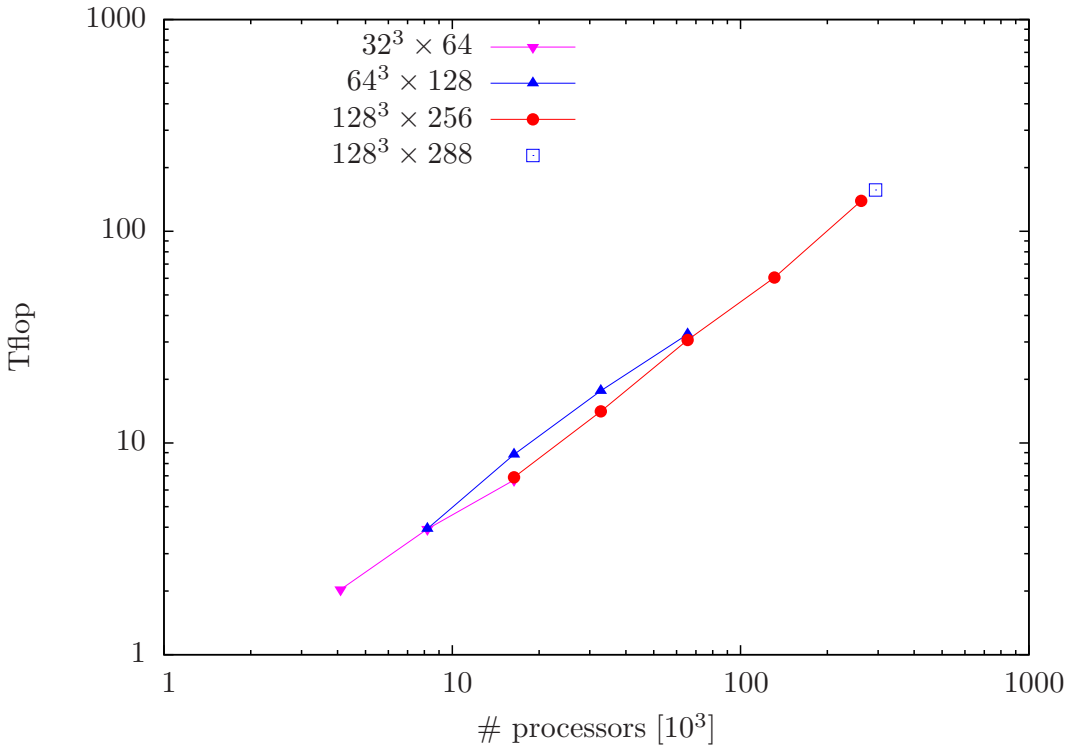

Figure E.1: Scaling of the production code on the Blue Gene/P in Juelich

E.2 IBM Blue Gene/P "Babel"

The Blue Gene project is a familly of supercomputer produced by IBM designed to deliver high parallel performance, and to have economical power and cooling consumption. One of the goal of these machines was to study protein. It is worthwhile to note that the architectur choice has been dictated by computer like QCDSP and QCDOC which have been conceived by physicist to perform lattice QCD simulations. A lot of information on architecture and on designed application development can be found in [153].

E.2.1 Architecture

The frontend is composed of 16 Power5+ at 1850 MHz with 64 Go of memory. The frontend is used to compile code and submit jobs. Babel used a GPFS filesystem shared with the cluster Vargas and the WORKDIR is of 350 To. The maximum transfert rate is of 8 Go/s.

The computation nodes are composed of :

- 10 racks of Blue Gene/P
- Each rack is composed of 32 node cards
- Each rack is divided in 2 midplanes

- Each node card has 32 computation nodes
- Each node has 4 core

The characteristic of each nodes is summarized in Table E.1.

Core	Power PC 450 32 bit
Number of core by nodes	4
CPU frequency	850 MHz
Memory	2 Go
Power (peak)	13.6 Gflop/s
Memory bandwifth	12.7 Go/s
Electric power	30 W

Table E.1: Characteristic of the Blue Gene/P nodes

The complete configuration summarized in Fig. E.2 (10 240 nodes, 40 960 core) has thus a power peak of 139 Tflop/s and 20 To of memory. One important feature is that every 2 node cards (every 64 core), there is one input-output nodes which manage all the I/O of the 64 nodes. It explains why every job have to be executed on on a multiple of 64 nodes. This particularity has been fully exploited, thanks to two collaborators (A. Deuzeman and S. Reker). They have re-implemented the LIME functionality using MPI IO. The performance gains is huge (up to ~ 200) . We show some the general performance of the LEMON library in Table E.2. In practice the time the time to write a gauge configuration on large lattices is shown in Fig. E.3. This benefits is even more appreciable when reading or writting propagators since they are in general bigger files (4.5 larger for 12 sources or even 18 larger for propagators in the heavy sector).

BG/P	Read	Write
LIME	$\sim 80MB/s$	$40MB/s$
LEMON	up to $17GB/s$	up $8GB/s$

Table E.2: Comparison of LIME and LEMON I/O performance

conf write time	$V = 48^3 \times 96$	$V = 64^3 \times 128$
LIME	150 s	480 s
LEMON	~ 1 s	~ 3 s

Table E.3: Comparison of LIME and LEMON to write configuration on the BG/P

A BG/P core is relatively slow (only 850 MHz), this main feature allow to redude the electric consumption of each core. In counter part the number of core is very large. The performances of the BG/P system come thus of a huge number of core with low performances and a low consumption. As a consequence, to take benefits of such an massivelly parallel architecture (this kind of architecture is refered as Massive parallel processing (MPP)) it is mandatory to have application that can be executed with a very high level of parallelism. The tmLQCD freely available software suite fill this aim [154], a lot of detail on the code can be found in [155].

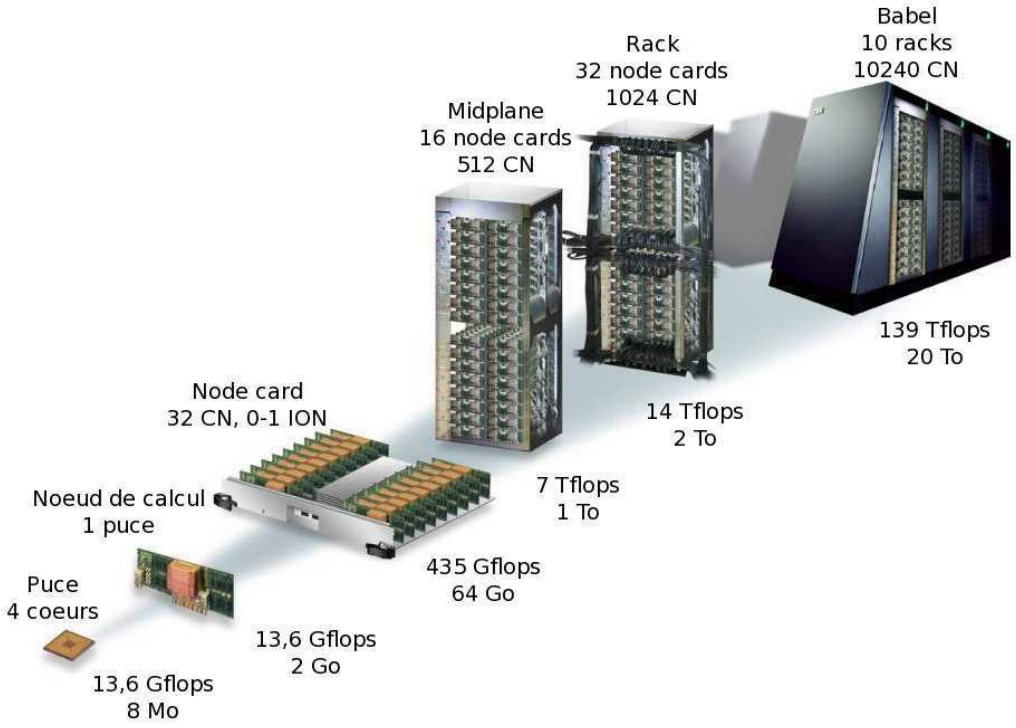

Figure E.2: BlueGene/P Idris

E.2.2 Network

Blue Gene have a very powerful network that allow to have exceptional perfomances for MPI communication. The nodes are connected by a low-latency 3D torus network. The communication between the four core of each nodes can be thought as a fourth dimension to the network. This feature is particularly usefull for lattice QCD computations, since one can then match our four dimensional periodic physic lattice on a network that can be thougth as a four dimensional torus.

As an example of partition used in practice during the gauge configuration production, we give some order of magnitude in Table E.4. The placement of process on each core is very important to guarantee efficiency of the code. The ideal is to choose a parallelisation that make neighboor in the four dimensional lattice also neighboor on the machine.

Volume	# of racks	$N_x \times N_y \times N_z \times N_t$	Local Volume	$\sim$ T/traj. (s)
$32^3 \times 64$	1	$8 \times 8 \times 4 \times 16$	$4 \times 4 \times 8 \times 4$	850
$48^3 \times 96$	2	$16 \times 8 \times 4 \times 16$	$3 \times 6 \times 12 \times 6$	2900
$64^3 \times 128$	4	$16 \times 8 \times 8 \times 16$	$4 \times 8 \times 8 \times 8$	6000

Table E.4: Parallelisation used in production and order of magnitude. The time by trajectory is a rough estimate obtained for $N_f = 2 + 1 + 1$ runs using the tmLQCD package with $\sim 80\%$ acceptance and with a pion mass ~ 300 MeV.

Appendix F

Data

$a\mu_s$	stat.	am_Λ	$am_{\Sigma^{\mathrm{Av}}}$	am_{Σ^+}	am_{Σ^0}	am_{Σ^-}	$am_{\Xi^{\mathrm{Av}}}$	am_{Ξ^0}	am_{Ξ^-}
$24^3 \times 48$									
0.0064	597	0.533(8)	0.545(7)	0.549(12)	0.563(5)	0.537(6)	0.545(7)	0.560(11)	0.530(6)
0.0085	316	0.537(10)	0.557(11)	0.559(19)	0.557(12)	0.554(8)	0.563(9)	0.585(14)	0.549(8)
0.0100	316	0.542(9)	0.564(10)	0.567(18)	0.564(11)	0.561(7)	0.574(8)	0.597(13)	0.560(7)
0.0175	315	0.563(8)	0.596(9)	0.600(14)	0.593(9)	0.593(7)	0.626(6)	0.644(8)	0.610(6)
0.0200	308	0.568(8)	0.606(8)	0.609(13)	0.602(9)	0.603(6)	0.641(6)	0.660(8)	0.625(5)
0.0250	311	0.584(7)	0.626(6)	0.627(12)	0.619(8)	0.620(6)	0.671(5)	0.688(7)	0.656(5)
0.0400	316	0.624(7)	0.674(6)	0.676(10)	0.667(7)	0.672(6)	0.751(4)	0.764(5)	0.738(4)
0.0800	314	0.718(7)	0.780(5)	0.787(7)	0.772(7)	0.776(7)	0.935(3)	0.945(4)	0.926(3)

Table F.1: Octet masses for $\beta = 3.9$, $a\mu = 0.004$ on a $24^3 \times 48$ lattice as a function of $a\mu_s$.

$a\mu_s$	stat.	$am_{\Sigma^{*\mathrm{Av}}}$	$am_{\Sigma^{*+}}$	$am_{\Sigma^{*0}}$	$am_{\Sigma^{*-}}$	$am_{\Xi^{*\mathrm{Av}}}$	$am_{\Xi^{*0}}$	$am_{\Xi^{*-}}$	am_Ω
$24^3 \times 48$									
0.0064	597	0.665(12)	0.658(18)	0.669(14)	0.669(14)	0.636(9)	0.645(12)	0.628(9)	0.678(14)
0.0085	316	0.695(19)	0.719(13)	0.713(16)	0.733(9)	0.648(11)	0.670(15)	0.624(10)	0.734(11)
0.0100	316	0.700(18)	0.722(12)	0.715(15)	0.697(22)	0.658(9)	0.680(13)	0.636(9)	0.744(10)
0.0175	315	0.721(14)	0.729(14)	0.736(12)	0.718(19)	0.705(7)	0.722(8)	0.690(7)	0.796(6)
0.0200	308	0.725(14)	0.734(13)	0.741(11)	0.718(17)	0.720(6)	0.734(7)	0.704(7)	0.807(7)
0.0250	311	0.740(13)	0.735(16)	0.753(11)	0.740(17)	0.747(6)	0.759(6)	0.733(6)	0.838(6)
0.0400	316	0.778(11)	0.770(13)	0.788(9)	0.778(15)	0.821(5)	0.831(5)	0.811(5)	0.934(4)
0.0800	314	0.864(7)	0.854(11)	0.870(8)	0.865(9)	0.993(4)	0.996(5)	0.987(4)	1.169(3)

Table F.2: Decuplet masses for $\beta = 3.9$, $a\mu = 0.004$ on a $24^3 \times 48$ lattice as a function of $a\mu_s$

$a\mu$	stat.	am_N	am_Λ	$am_{\Sigma^{\mathrm{Av}}}$	am_{Σ^+}	am_{Σ^0}	am_{Σ^-}	$am_{\Xi^{\mathrm{Av}}}$	am_{Ξ^0}	am_{Ξ^-}
					$16^3 \times 32$					
0.0040	636	0.593(10)	0.646(8)	0.684(7)	0.711(9)	0.684(7)	0.647(9)	0.716(5)	0.737(7)	0.695(5)
					$20^3 \times 40$					
0.0040	526	0.545(6)	0.604(5)	0.627(6)	0.657(6)	0.633(7)	0.602(7)	0.672(5)	0.690(7)	0.652(4)
					$24^3 \times 48$					
0.0040	4115	0.520(4)	0.580(2)	0.611(3)	0.622(4)	0.612(3)	0.601(2)	0.655(2)	0.672(3)	0.639(2)
0.0064	545	0.551(5)	0.602(4)	0.630(4)	0.652(5)	0.629(4)	0.613(4)	0.673(3)	0.694(4)	0.654(3)
0.0085	1817	0.580(2)	0.622(2)	0.648(2)	0.664(3)	0.648(2)	0.631(2)	0.678(2)	0.695(2)	0.661(1)
0.0100	477	0.597(4)	0.633(4)	0.654(4)	0.666(6)	0.654(4)	0.643(4)	0.682(4)	0.696(5)	0.668(3)
					$32^3 \times 64$					
0.0030	652	0.497(4)	0.563(3)	0.595(3)	0.610(4)	0.597(3)	0.578(4)	0.644(2)	0.660(3)	0.629(2)
0.0040	232 (1071)	0.508(3)	0.575(4)	0.614(5)	0.631(7)	0.615(5)	0.596(5)	0.655(4)	0.674(5)	0.635(4)

Table F.3: Baryon masses in the octet representation at $\beta = 3.9$ in lattice units. Note that for the nucleon on $32^3 \times 64$ lattices at $\beta = 3.9$,$\mu = 0.004$ the statistic is of 1071 measurements.

$a\mu$	stat.	$am_{\Delta^{++,-}}$	$am_{\Delta^{+,0}}$	$am_{\Sigma^{*\mathrm{Av}}}$	$am_{\Sigma^{*+}}$	$am_{\Sigma^{*0}}$	$am_{\Sigma^{*-}}$	$am_{\Xi^{*\mathrm{Av}}}$	$am_{\Xi^{*0}}$	$am_{\Xi^{*-}}$	am_Ω
						$16^3 \times 32$					
0.0040	636	0.739(17)	0.779(13)	0.788(12)	0.781(14)	0.796(13)	0.786(13)	0.798(8)	0.801(9)	0.794(8)	0.853(7)
						$20^3 \times 40$					
0.0040	526	0.700(8)	0.714(9)	0.748(6)	0.743(7)	0.754(7)	0.731(11)	0.720(11)	0.719(16)	0.734(8)	0.806(7)
						$24^3 \times 48$					
0.0040	782	0.661(8)	0.668(8)	0.718(5)	0.714(6)	0.721(5)	0.718(5)	0.735(3)	0.742(3)	0.721(4)	0.810(2)
0.0064	545	0.708(8)	0.709(9)	0.747(7)	0.744(8)	0.748(7)	0.748(7)	0.749(5)	0.755(6)	0.742(5)	0.814(6)
0.0085	348	0.715(4)	0.725(4)	0.757(3)	0.755(4)	0.759(3)	0.756(4)	0.751(4)	0.767(3)	0.743(4)	0.818(3)
0.0100	477	0.753(6)	0.759(6)	0.782(5)	0.781(6)	0.783(5)	0.774(8)	0.766(5)	0.774(6)	0.750(7)	0.831(4)
						$32^3 \times 64$					
0.0030	659	0.628(13)	0.658(7)	0.704(5)	0.676(12)	0.694(8)	0.707(6)	0.701(6)	0.711(6)	0.698(6)	0.797(3)
0.004	232 (1071)	0.651(6)	0.647(8)	0.720(13)	0.710(10)	0.715(11)	0.717(11)	0.726(7)	0.735(8)	0.720(6)	0.805(6)

Table F.4: Baryon masses in the decuplet representation at $\beta = 3.9$ in lattice units.Note that for the Δ on $32^3 \times 64$ lattices at $\beta = 3.9$,$\mu = 0.004$ the statistic is of 1071 measurements.

$a\mu$	stat.	am_N	am_Λ	$am_{\Sigma^{av}}$	$am_{\Sigma+}$	am_{Σ^0}	$am_{\Sigma-}$	$am_{\Xi^{av}}$	am_{Ξ^0}	$am_{\Xi-}$
$32^3 \times 64$										
0.0030	269	0.412(5)	0.452(4)	0.479(4)	0.492(5)	0.479(4)	0.465(5)	0.508(3)	0.516(4)	0.500(3)
0.0060	253	0.450(3)	0.483(3)	0.500(3)	0.509(4)	0.500(3)	0.489(3)	0.524(3)	0.533(4)	0.514(3)
’ 0.0080	410	0.472(3)	0.496(3)	0.510(3)	0.518(4)	0.510(3)	0.503(3)	0.528(3)	0.535(3)	0.520(3)

Table F.5: Baryon masses in the octet representation at $\beta = 4.05$ in lattice units.

$a\mu$	stat.	$am_{\Delta++,-}$	$am_{\Delta+,0}$	$am_{\Sigma^{*av}}$	$am_{\Sigma^{*}+}$	$am_{\Sigma^{*}0}$	$am_{\Sigma^{*}-}$	$am_{\Xi^{*av}}$	$am_{\Xi^{*}0}$	$am_{\Xi^{*}-}$	am_Ω
$32^3 \times 64$											
0.0030	269	0.531(11)	0.538(11)	0.582(6)	0.579(7)	0.584(6)	0.583(6)	0.579(5)	0.580(5)	0.577(5)	0.634(5)
0.0060	253	0.551(8)	0.558(8)	0.592(5)	0.574(7)	0.595(5)	0.594(5)	0.582(5)	0.581(6)	0.581(5)	0.638(4)
0.0080	410	0.592(4)	0.594(4)	0.611(4)	0.608(4)	0.612(4)	0.612(4)	0.594(4)	0.601(4)	0.590(4)	0.646(3)

Table F.6: Baryon masses in the decuplet representation at $\beta = 4.05$ in lattice units.

$a\mu$	stat.	am_N	$am_{\Delta++,-}$	$am_{\Delta+,0}$
$32^3 \times 64$				
0.0065	380	0.380(3)	0.473(5)	0.477(5)
$48^3 \times 96$				
0.0020	273	0.306(4)	0.431(6)	0.433(7)

Table F.7: Baryon masses in the light sector for $\beta = 4.2$

$a\mu$	stat.	am_N	$am_{\Delta^{++,-}}$	$am_{\Delta^{+,0}}$
		$20^3 \times 48$		
0.004	610	0.506(15)	0.735(8)	0.740(9)
		$24^3 \times 48$		
0.004	912	0.531(9)	0.714(10)	0.713(9)
0.006	479	0.574(6)	0.744(6)	0.725(10)
0.008	450	0.598(3)	0.748(6)	0.753(6)
0.010	501	0.622(4)	0.749(7)	0.745(9)
		$32^3 \times 64$		
0.003	480	0.516(7)	0.632(44)	0.631(24)
0.004	488	0.526(4)	0.665(14)	0.650(12)
0.005	401	0.534(4)	0.694(8)	0.704(14)

Table F.8: Baryon masses in the light sector for $\beta = 1.90$

$a\mu$	stat.	am_N	$am_{\Delta^{++,-}}$	$am_{\Delta^{+,0}}$
		$24^3 \times 48$		
0.0085	485	0.558(3)	0.687(7)	0.694(7)
		$32^3 \times 64$		
0.0025	925	0.448(8)	0.600(10)	0.595(13)
0.0035	509	0.464(5)	0.607(11)	0.601(9)
0.0055	476	0.509(4)	0.640(7)	0.629(9)
0.0075	524	0.538(3)	0.664(6)	0.669(6)

Table F.9: Baryon masses in the light sector for $\beta = 1.95$

Bibliography

[1] J. Chadwick, "POSSIBLE EXISTENCE OF A NEUTRON," *Nature* **129** (1932) 312.

[2] H. Yukawa, "On the interaction of elementary particles," *Proc. Phys. Math. Soc. Jap.* **17** (1935) 48–57.

[3] L. Leprince-Ringuet, "Photographic Evidence for the Existence of a Very Heavy Meson," *Rev. Mod. Phys.* **21** no. 1, (Jan, 1949) 42–43.

[4] M. Gell-Mann, "Isotopic Spin and New Unstable Particles," *Phys. Rev.* **92** no. 3, (Nov, 1953) 833–834.

[5] T. Nakano and K. Nishijima, "Charge Independence for V-particles," *Prog. Theor. Phys.* **10** (1953) 581–582.

[6] S. Sakata, "On a Composite Model for the New Particles," *Prog. Theor. Phys.* **16** (1956) 686–688.

[7] M. Gell-Mann, "Symmetries of baryons and mesons," *Phys. Rev.* **125** (1962) 1067–1084.

[8] Y. Ne'eman, "Derivation of strong interactions from a gauge invariance," *Nucl. Phys.* **26** (1961) 222–229.

[9] M. Gell-Mann, "A Schematic Model of Baryons and Mesons," *Phys. Lett.* **8** (1964) 214–215.

[10] M. Gell-Mann, "The Eightfold Way: A Theory of strong interaction symmetry,". CTSL-20.

[11] S. Okubo, "Note on unitary symmetry in strong interactions," *Prog. Theor. Phys.* **27** (1962) 949–966.

[12] J. F. Donoghue, E. Golowich, and B. R. Holstein, "Dynamics of the standard model," *Camb. Monogr. Part. Phys. Nucl. Phys. Cosmol.* **2** (1992) 1–540.

[13] C.-N. Yang and R. L. Mills, "Conservation of isotopic spin and isotopic gauge invariance," *Phys. Rev.* **96** (1954) 191–195.

[14] S. Coleman, *Aspects of symmetry : Selected Erice Lectures*. Cambridge University Press, 1985.

[15] R. P. Feynman, "Space-time approach to nonrelativistic quantum mechanics," *Rev. Mod. Phys.* **20** (1948) 367–387.

[16] A. S. Wightman, "Quantum Field Theory in Terms of Vacuum Expectation Values," *Phys. Rev.* **101** (1956) 860–866.

[17] R. F. Streater and A. S. Wightman, "PCT, spin and statistics, and all that,". Redwood City, USA: Addison-Wesley (1989) 207 p. (Advanced book classics).

[18] H. A. Kramers, "," *Nuovo Cim.* **15** (1938) 108.

[19] S. S. Schweber, "QED and the men who made it: Dyson, Feynman, Schwinger, and Tomonaga,". Princeton, USA: Univ. Pr. (1994) 732 p.

[20] G. 't Hooft, "Renormalization of Massless Yang-Mills Fields," *Nucl. Phys.* **B33** (1971) 173–199.

[21] G. 't Hooft, "RENORMALIZABLE LAGRANGIANS FOR MASSIVE YANG-MILLS FIELDS," *Nucl. Phys.* **B35** (1971) 167–188.

[22] G. 't Hooft and M. J. G. Veltman, "Regularization and Renormalization of Gauge Fields," *Nucl. Phys.* **B44** (1972) 189–213.

[23] J. Debove *Private communication* .

[24] H. Lehmann, "On the Properties of propagation functions and renormalization contants of quantized fields," *Nuovo Cim.* **11** (1954) 342–357.

[25] G. Kallen, "QUANTUM ELECTRODYNAMICS. (ENGLISH TRANSLATION),". Springer-verl./new York 1972, 233p.

[26] D. J. Gross and F. Wilczek, "ULTRAVIOLET BEHAVIOR OF NON-ABELIAN GAUGE THEORIES," *Phys. Rev. Lett.* **30** (1973) 1343–1346.

[27] S. Weinberg, "Nonabelian Gauge Theories of the Strong Interactions," *Phys. Rev. Lett.* **31** (1973) 494–497.

[28] D. J. Gross and F. Wilczek, "Asymptotically Free Gauge Theories. 1," *Phys. Rev.* **D8** (1973) 3633–3652.

[29] H. D. Politzer, "RELIABLE PERTURBATIVE RESULTS FOR STRONG INTERACTIONS?," *Phys. Rev. Lett.* **30** (1973) 1346–1349.

[30] H. D. Politzer, "Asymptotic Freedom: An Approach to Strong Interactions," *Phys. Rept.* **14** (1974) 129–180.

[31] E. C. G. Stueckelberg and A. Petermann, "Normalization of constants in the quanta theory," *Helv. Phys. Acta* **26** (1953) 499–520.

[32] M. Gell-Mann and F. E. Low, "Quantum electrodynamics at small distances," *Phys. Rev.* **95** (1954) 1300–1312.

[33] K. Osterwalder and R. Schrader, "AXIOMS FOR EUCLIDEAN GREEN'S FUNCTIONS," *Commun. Math. Phys.* **31** (1973) 83–112.

[34] K. G. Wilson, "CONFINEMENT OF QUARKS," *Phys. Rev.* **D10** (1974) 2445–2459.

[35] I. Montvay and G. Munster, "Quantum fields on a lattice,". Cambridge, UK: Univ. Pr. (1994) 491 p. (Cambridge monographs on mathematical physics).

[36] H. B. Nielsen and M. Ninomiya, "No Go Theorem for Regularizing Chiral Fermions," *Phys. Lett.* **B105** (1981) 219.

[37] H. B. Nielsen and M. Ninomiya, "Absence of Neutrinos on a Lattice. 1. Proof by Homotopy Theory," *Nucl. Phys.* **B185** (1981) 20.

[38] H. B. Nielsen and M. Ninomiya, "Absence of Neutrinos on a Lattice. 2. Intuitive Topological Proof," *Nucl. Phys.* **B193** (1981) 173.

[39] **Particle Data Group** Collaboration, C. Amsler *et al.*, "Review of particle physics," *Phys. Lett.* **B667** (2008) 1.

[40] R. Frezzotti, P. A. Grassi, S. Sint, and P. Weisz, "A local formulation of lattice QCD without unphysical fermion zero modes," *Nucl. Phys. Proc. Suppl.* **83** (2000) 941–946, `arXiv:hep-lat/9909003`.

[41] **Alpha** Collaboration, R. Frezzotti, P. A. Grassi, S. Sint, and P. Weisz, "Lattice QCD with a chirally twisted mass term," *JHEP* **0108** (2001) 058, `hep-lat/0101001`.

[42] R. Frezzotti and G. C. Rossi, "Chirally improving Wilson fermions. I: O(a) improvement," *JHEP* **08** (2004) 007, `arXiv:hep-lat/0306014`.

[43] A. Shindler, "Twisted mass lattice QCD," *Phys. Rept.* **461** (2008) 37–110, `arXiv:0707.4093 [hep-lat]`.

[44] S. Sint, "Lattice QCD with a chiral twist," `arXiv:hep-lat/0702008`.

[45] **XLF** Collaboration, W. Bietenholz *et al.*, "Going chiral: Overlap versus twisted mass fermions," *JHEP* **12** (2004) 044, `arXiv:hep-lat/0411001`.

[46] S. Aoki and O. Bar, "Twisted-mass QCD, O(a) improvement and Wilson chiral perturbation theory," *Phys. Rev.* **D70** (2004) 116011, `arXiv:hep-lat/0409006`.

[47] S. R. Sharpe and J. M. S. Wu, "The phase diagram of twisted mass lattice QCD," *Phys. Rev.* **D70** (2004) 094029, `arXiv:hep-lat/0407025`.

[48] R. Frezzotti, G. Martinelli, M. Papinutto, and G. C. Rossi, "Reducing cutoff effects in maximally twisted lattice QCD close to the chiral limit," *JHEP* **04** (2006) 038, `arXiv:hep-lat/0503034`.

[49] D. H. Weingarten and D. N. Petcher, "Monte Carlo Integration for Lattice Gauge Theories with Fermions," *Phys. Lett.* **B99** (1981) 333.

[50] H. Hamber, E. Marinari, G. Parisi, and C. Rebbi, "SPECTROSCOPY IN A LATTICE GAUGE THEORY," *Phys. Lett.* **B108** (1982) 314.

[51] H. Hamber and G. Parisi, "Numerical Estimates of Hadronic Masses in a Pure SU(3) Gauge Theory," *Phys. Rev. Lett.* **47** (1981) 1792.

[52] E. Marinari, G. Parisi, and C. Rebbi, "Computer Estimates of Meson Masses in SU(2) Lattice Gauge Theory," *Phys. Rev. Lett.* **47** (1981) 1795.

[53] F. Fucito *et al.*, "HADRON SPECTROSCOPY IN LATTICE QCD," *Nucl. Phys.* **B210** (1982) 407.

[54] B. L. Ioffe, "Calculation of Baryon Masses in Quantum Chromodynamics," *Nucl. Phys.* **B188** (1981) 317–341.

[55] D. B. Leinweber, R. M. Woloshyn, and T. Draper, "Electromagnetic structure of octet baryons," *Phys. Rev.* **D43** (1991) 1659–1678.

[56] D. B. Leinweber, T. Draper, and R. M. Woloshyn, "Decuplet baryon structure from lattice QCD," *Phys. Rev.* **D46** (1992) 3067–3085, arXiv:hep-lat/9208025.

[57] Y. Chung, H. G. Dosch, M. Kremer, and D. Schall, "CHIRAL SYMMETRY BREAKING CONDENSATES FOR BARYONIC SUM RULES," *Z. Phys.* **C25** (1984) 151.

[58] H. G. Dosch, M. Jamin, and S. Narison, "BARYON MASSES AND FLAVOR SYMMETRY BREAKING OF CHIRAL CONDENSATES," *Phys. Lett.* **B220** (1989) 251.

[59] R. M. Albuquerque, S. Narison, and M. Nielsen, "SU(3) mass-splittings of the heavy-baryons octet in QCD," *Phys. Lett.* **B684** (2010) 236–245, arXiv:0904.3717 [hep-ph].

[60] **ALPHA** Collaboration, U. Wolff, "Monte Carlo errors with less errors," *Comput. Phys. Commun.* **156** (2004) 143–153, arXiv:hep-lat/0306017.

[61] **UKQCD** Collaboration, M. Foster and C. Michael, "Quark mass dependence of hadron masses from lattice QCD," *Phys. Rev.* **D59** (1999) 074503, hep-lat/9810021.

[62] C. Michael, "LATTICE ACTION SUM RULES," *Nucl. Phys.* **B280** (1987) 13.

[63] **UKQCD** Collaboration, A. C. Irving *et al.*, "Tuning actions and observables in lattice QCD," *Phys. Rev.* **D58** (1998) 114504, arXiv:hep-lat/9807015.

[64] G. S. Bali, C. Schlichter, and K. Schilling, "Exploring correlation methods to determine QCD Beta functions on the lattice," *Phys. Lett.* **B363** (1995) 196–200, arXiv:hep-lat/9508027.

[65] R. P. Feynman, "Forces in Molecules," *Phys. Rev.* **56** (1939) 340–343.

[66] J. R. Ellis, K. A. Olive, and C. Savage, "Hadronic Uncertainties in the Elastic Scattering of Supersymmetric Dark Matter," *Phys. Rev.* **D77** (2008) 065026, arXiv:0801.3656 [hep-ph].

[67] P. Weisz *Nucl. Phys.* **B212** (1983) 1.

[68] Y. Iwasaki, "Renormalization Group Analysis of Lattice Theories and Improved Lattice Action: Two-Dimensional Nonlinear O(N) Sigma Model," *Nucl. Phys.* **B258** (1985) 141–156.

[69] N. Metropolis, A. W. Rosenbluth, M. N. Rosenbluth, A. H. Teller, and E. Teller, "Equation of state calculations by fast computing machines," *J. Chem. Phys.* **21** (1953) 1087–1092.

[70] M. Creutz, "Monte Carlo Study of Quantized SU(2) Gauge Theory," *Phys. Rev.* **D21** (1980) 2308–2315.

[71] J. Kuti, J. Polonyi, and K. Szlachanyi, "Monte Carlo Study of SU(2) Gauge Theory at Finite Temperature," *Phys. Lett.* **B98** (1981) 199.

[72] S. Duane, A. D. Kennedy, B. J. Pendleton, and D. Roweth, "Hybrid Monte Carlo," *Phys. Lett.* **B195** (1987) 216–222.

[73] R. Frezzotti and K. Jansen, "A polynomial hybrid Monte Carlo algorithm," *Phys. Lett.* **B402** (1997) 328–334, arXiv:hep-lat/9702016.

[74] B. Bunk, S. Elser, R. Frezzotti, and K. Jansen, "Ordering monomial factors of polynomials in the product representation," *Comput. Phys. Commun.* **118** (1999) 95–109, arXiv:hep-lat/9805026.

[75] **PACS-CS** Collaboration, S. Aoki *et al.*, "2+1 Flavor Lattice QCD toward the Physical Point," *Phys. Rev. D* **79** (2009) 034503, arXiv:0807.1661 [hep-lat].

[76] S. Durr *et al.*, "Ab Initio Determination of Light Hadron Masses," *Science* **322** (2008) 1224–1227.

[77] J. Foley *et al.*, "Practical all-to-all propagators for lattice QCD," *Comput. Phys. Commun.* **172** (2005) 145–162, arXiv:hep-lat/0505023.

[78] **UKQCD** Collaboration, M. Foster and C. Michael, "Hadrons with a heavy colour-adjoint particle," *Phys. Rev.* **D59** (1999) 094509, arXiv:hep-lat/9811010.

[79] **UKQCD** Collaboration, C. McNeile and C. Michael, "Decay width of light quark hybrid meson from the lattice," *Phys. Rev.* **D73** (2006) 074506, hep-lat/0603007.

[80] **ETM** Collaboration, P. Boucaud *et al.*, "Dynamical Twisted Mass Fermions with Light Quarks: Simulation and Analysis Details," *Comput. Phys. Commun.* **179** (2008) 695–715, arXiv:0803.0224 [hep-lat].

[81] R. Baron *et al.*, "Light Meson Physics from Maximally Twisted Mass Lattice QCD," arXiv:0911.5061 [Unknown].

[82] R. Sommer, "A New way to set the energy scale in lattice gauge theories and its applications to the static force and alpha-s in SU(2) Yang-Mills theory," *Nucl. Phys.* **B411** (1994) 839–854, arXiv:hep-lat/9310022.

[83] **XLF** Collaboration, K. Jansen *et al.*, "Flavour breaking effects of Wilson twisted mass fermions," *Phys. Lett.* **B624** (2005) 334–341, arXiv:hep-lat/0507032.

[84] **ETM** Collaboration, R. Baron *et al.*, "Status of ETMC simulations with $N_f = 2 + 1 + 1$ twisted mass fermions," *PoS* **LATTICE2008** (2008) 094, arXiv:0810.3807 [hep-lat].

[85] J. Gasser and H. Leutwyler, "Spontaneously Broken Symmetries: Eeffective Lagrangians at Finite Volume," *Nucl. Phys.* **B307** (1988) 763.

[86] G. Colangelo, S. Durr, and C. Haefeli, "Finite volume effects for meson masses and decay constants," *Nucl. Phys.* **B721** (2005) 136–174, arXiv:hep-lat/0503014.

[87] P. Dimopoulos *et al.*, "Scaling and ChPT Description of Pions from $N_f = 2$ twisted mass QCD," *PoS* **LAT2009** (2009) 117, arXiv:0912.5198 [Unknown].

[88] R. Baron *et al.*, "Light hadrons from lattice QCD with light (u,d), strange and charm dynamical quarks," *JHEP* **06** (2010) 111, arXiv:1004.5284 [hep-lat].

[89] **European Twisted Mass** Collaboration, R. Baron *et al.*, "Computing K and D meson masses with $N_f = 2 + 1 + 1$ twisted mass lattice QCD," arXiv:1005.2042 [hep-lat].

[90] S. Weinberg, "Precise relations between the spectra of vector and axial vector mesons," *Phys. Rev. Lett.* **18** (1967) 507–509.

[91] S. Weinberg, "Nonlinear realizations of chiral symmetry," *Phys. Rev.* **166** (1968) 1568–1577.

[92] S. Weinberg, "Phenomenological Lagrangians," *Physica* **A96** (1979) 327.

[93] J. Gasser and H. Leutwyler, "ON THE LOW-ENERGY STRUCTURE OF QCD," *Phys. Lett.* **B125** (1983) 321.

[94] J. Gasser and H. Leutwyler, "Chiral Perturbation Theory: Expansions in the Mass of the Strange Quark," *Nucl. Phys.* **B250** (1985) 465.

[95] S. Scherer, "Introduction to chiral perturbation theory," *Adv. Nucl. Phys.* **27** (2003) 277, arXiv:hep-ph/0210398.

[96] S. Scherer, "Effective Field Theory of the Single-Nucleon Sector," *Mod. Phys. Lett.* **A23** (2008) 2289–2292, arXiv:0802.2461 [hep-ph].

[97] M. Golterman, "Applications of chiral perturbation theory to lattice QCD," *Lectures given at Les Houches.* (2009) , arXiv:0912.4042 [Unknown].

[98] A. Walker-Loud, "Topics in effective field theory for lattice QCD," *Ph.D thesis* (2006) , arXiv:0608010 [hep-lat].

[99] C. Vafa and E. Witten, "Restrictions on Symmetry Breaking in Vector-Like Gauge Theories," *Nucl. Phys.* **B234** (1984) 173.

[100] Y. Nambu, "Axial vector current conservation in weak interactions," *Phys. Rev. Lett.* **4** (1960) 380–382.

[101] J. Goldstone, "Field Theories with Superconductor Solutions," *Nuovo Cim.* **19** (1961) 154–164.

[102] Y. Nambu and G. Jona-Lasinio, "Dynamical model of elementary particles based on an analogy with superconductivity. I," *Phys. Rev.* **122** (1961) 345–358.

[103] Y. Nambu and G. Jona-Lasinio, "Dynamical model of elementary particles based on an analogy with superconductivity. II," *Phys. Rev.* **124** (1961) 246–254.

[104] M. I. Buchoff, J.-W. Chen, and A. Walker-Loud, "pi-pi Scattering in Twisted Mass Chiral Perturbation Theory," *Phys.Rev.* **D79** (2009) 074503, arXiv:0810.2464 [hep-lat].

[105] J. Gasser, M. E. Sainio, and A. Svarc, "Nucleons with Chiral Loops," *Nucl. Phys.* **B307** (1988) 779.

[106] E. E. Jenkins and A. V. Manohar, "Baryon chiral perturbation theory using a heavy fermion Lagrangian," *Phys. Lett.* **B255** (1991) 558–562.

[107] V. Bernard, N. Kaiser, J. Kambor, and U. G. Meissner, "Chiral structure of the nucleon," *Nucl. Phys.* **B388** (1992) 315–345.

[108] S. Scherer, "Chiral Perturbation Theory: Introduction and Recent Results in the One-Nucleon Sector," *Prog. Part. Nucl. Phys.* **64** (2010) 1–60, arXiv:0908.3425 [hep-ph].

[109] B. C. Tiburzi and A. Walker-Loud, "Hyperons in Two Flavor Chiral Perturbation Theory," *Phys. Lett.* **B669** (2008) 246–253, arXiv:0808.0482 [nucl-th].

[110] B. C. Tiburzi and A. Walker-Loud, "Strong isospin breaking in the nucleon and Delta masses," *Nucl. Phys.* **A764** (2006) 274–302, arXiv:hep-lat/0501018.

[111] A. Walker-Loud *et al.*, "Light hadron spectroscopy using domain wall valence quarks on an Asqtad sea," *Phys.Rev. D* **79** (2009) , arXiv:0806.4549 [hep-lat].

[112] Lord Rayleigh (1871) .

[113] W. Sellmeier (1871) .

[114] M. M. Nagels *et al.*, "Compilation of Coupling Constants and Low-Energy Parameters. 1978 Edition," *Nucl. Phys.* **B147** (1979) 189–276.

[115] M. M. Nagels, T. A. Rijken, and J. J. de Swart, "Baryon Baryon Scattering in a One Boson Exchange Potential Approach. 3. A Nucleon-Nucleon and Hyperon - Nucleon Analysis Including Contributions of a Nonet of Scalar Mesons," *Phys. Rev.* **D20** (1979) 1633.

[116] **European Twisted Mass** Collaboration, C. Alexandrou *et al.*, "Light baryon masses with dynamical twisted mass fermions," *Phys. Rev.* **D78** (2008) 014509, arXiv:0803.3190 [hep-lat].

[117] **ETM** Collaboration, C. Alexandrou *et al.*, "Baryon masses with dynamical twisted mass fermions," *PoS* **LAT2007** (2007) 087, arXiv:0710.1173 [hep-lat].

[118] R. Baron *et al.*, "First results of ETMC simulations with $N_f = 2 + 1 + 1$ maximally twisted mass fermions," arXiv:0911.5244 [Unknown].

[119] R. Baron *et al.*, "Light hadrons from the lattice with dynamical strange and charm," *to be published* .

[120] C. Alexandrou, S. Gusken, F. Jegerlehner, K. Schilling, and R. Sommer, "The Static approximation of heavy - light quark systems: A Systematic lattice study," *Nucl. Phys.* **B414** (1994) 815–855, hep-lat/9211042.

[121] **Hadron Spectrum** Collaboration, M. Peardon *et al.*, "A novel quark-field creation operator construction for hadronic physics in lattice QCD," *Phys. Rev.* **D80** (2009) 054506, arXiv:0905.2160 [hep-lat].

[122] J. Bulava, K. J. Juge, C. J. Morningstar, M. J. Peardon, and C. H. Wong, "Two-particle Correlation Functions with Distilled Propagators," arXiv:0911.2044 [Unknown].

[123] C. T. Sachrajda and G. Villadoro, "Twisted boundary conditions in lattice simulations," *Phys. Lett.* **B609** (2005) 73–85, arXiv:hep-lat/0411033.

[124] G. M. de Divitiis, R. Petronzio, and N. Tantalo, "On the discretization of physical momenta in lattice QCD," *Phys. Lett.* **B595** (2004) 408–413, arXiv:hep-lat/0405002.

[125] P. F. Bedaque, "Aharonov-Bohm effect and nucleon nucleon phase shifts on the lattice," *Phys. Lett.* **B593** (2004) 82–88, arXiv:nucl-th/0402051.

[126] **QCDSF-UKQCD** Collaboration, A. Ali Khan *et al.*, "The nucleon mass in N(f) = 2 lattice QCD: Finite size effects from chiral perturbation theory," *Nucl. Phys.* **B689** (2004) 175–194, arXiv:hep-lat/0312030.

[127] M. Procura, T. R. Hemmert, and W. Weise, "Nucleon mass, sigma term and lattice QCD," *Phys. Rev.* **D69** (2004) 034505, arXiv:hep-lat/0309020.

[128] S. Steininger, U.-G. Meissner, and N. Fettes *JHEP* **9809** (1998) 008.

[129] V. Bernard, T. Hemmert, and U.-G. Meissner *Nucl. Phys.* **A732** (2004) 149.

[130] V. Bernard, T. Hemmert, and U.-G. Meissner *Phys. Lett.* **B622** (2005) 141.

[131] N. Fettes, U.-G. Meissner, and S. Steininger, "Pion nucleon scattering in chiral perturbation theory. I: Isospin-symmetric case," *Nucl. Phys.* **A640** (1998) 199–234, hep-ph/9803266.

[132] M. Procura *et al. Phys. Rev. D* **73** (2006) 114510.

[133] D. R. Entem and R. Machleidt, "Chiral 2pi exchange at order four and peripheral N N scattering," *Phys. Rev.* **C66** (2002) 014002, nucl-th/0202039.

[134] E. Epelbaum, W. Glockle, and U.-G. Meissner, "The two-nucleon system at next-to-next-to-next-to-leading order," *Nucl. Phys.* **A747** (2005) 362–424, nucl-th/0405048.

[135] **PACS-CS** Collaboration, K. I. Ishikawa *et al.*, "SU(2) and SU(3) chiral perturbation theory analyses on baryon masses in 2+1 flavor lattice QCD," arXiv:0905.0962 [hep-lat].

[136] **European Twisted Mass** Collaboration, B. Blossier *et al.*, "Light quark masses and pseudoscalar decay constants from $N_f = 2$ Lattice QCD with twisted mass fermions," *JHEP* **04** (2008) 020, arXiv:0709.4574 [hep-lat].

[137] B. Blossier *et al.*, "Pseudoscalar decay constants of kaon and D-mesons from $N_f = 2$ twisted mass Lattice QCD," *JHEP* **07** (2009) 043, arXiv:0904.0954 [hep-lat].

[138] V. Drach *et al.*, "Partially quenched study of strange baryon with Nf = 2 twisted mass fermions," *PoS* **LATTICE2008** (2008) 123, arXiv:0905.2894 [hep-lat].

[139] C. Alexandrou *et al.*, "The low-lying baryon spectrum with two dynamical twisted mass fermions," *Phys. Rev.* **D80** (2009) 114503, arXiv:0910.2419 [Unknown].

[140] C. W. Bernard *et al.*, "The QCD spectrum with three quark flavors," *Phys. Rev.* **D64** (2001) 054506, arXiv:hep-lat/0104002.

[141] **MILC** Collaboration, C. Aubin *et al.*, "Light pseudoscalar decay constants, quark masses, and low energy constants from three-flavor lattice QCD," *Phys. Rev.* **D70** (2004) 114501, arXiv:hep-lat/0407028.

[142] **RBC and UKQCD** Collaboration, D. J. Antonio *et al.*, "First results from 2+1-flavor domain wall QCD: Mass spectrum, topology change and chiral symmetry with L(s) = 8," *Phys. Rev.* **D75** (2007) 114501, arXiv:hep-lat/0612005.

[143] **RBC and UKQCD** Collaboration, D. J. Antonio *et al.*, "Baryon spectrum in 2+1 flavour domain wall QCD," *PoS* **LAT2006** (2006) 189.

[144] K. Osterwalder and E. Seiler, "Gauge Field Theories on the Lattice," *Ann. Phys.* **110** (1978) 440.

[145] R. Frezzotti and G. C. Rossi, "Chirally improving Wilson fermions. II: Four-quark operators," *JHEP* **10** (2004) 070, hep-lat/0407002.

[146] A. M. Abdel-Rehim, R. Lewis, R. M. Woloshyn, and J. M. S. Wu, "Strange quarks in quenched twisted mass lattice QCD," *Phys. Rev.* **D74** (2006) 014507, hep-lat/0601036.

[147] A. M. Abdel-Rehim, R. Lewis, R. M. Woloshyn, and J. M. S. Wu, "Lattice QCD with a twisted mass term and a strange quark," *Eur. Phys. J.* **A31** (2007) 773–776, hep-lat/0610090.

[148] V. Lubicz and C. Tarantino. Private communication, 2008.

[149] **ETM Collaboration** Collaboration, P. Dimopoulos, R. Frezzotti, G. Herdoiza, C. Urbach, and U. Wenger, "Scaling and low energy constants in lattice QCD with $N_f = 2$ maximally twisted Wilson quarks," *PoS* **LAT2007** (2007) , arXiv:0710.2498 [hep-lat].

[150] R. Frezzotti and G. Rossi, "$O(a^2)$ cutoff effects in Wilson fermion simulations," *PoS* **LAT2007** (2007) 277, arXiv:0710.2492 [hep-lat].

[151] S. R. Beane, K. Orginos, and M. J. Savage, "The Gell-Mann - Okubo mass relation among baryons from fully-dynamical mixed-action lattice QCD," *Phys. Lett.* **B654** (2007) 20–26, arXiv:hep-lat/0604013.

[152] A. Denner, "Techniques for calculation of electroweak radiative corrections at the one loop level and results for W physics at LEP-200," *Fortschr. Phys.* **41** (1993) 307–420, arXiv:0709.1075 [hep-ph].

[153] IBM, "IBM Redbooks : IBM System Blue Gene Solution: Blue Gene/P Application Development." http://www.redbooks.ibm.com/abstracts/sg247287.html.

[154] C. Urbach, "tmLQCD software." http://www.itkp.uni-bonn.de/~urbach/software.html.

[155] K. Jansen and C. Urbach, "tmLQCD: a program suite to simulate Wilson Twisted mass Lattice QCD," *Comput. Phys. Commun.* **180** (2009) 2717–2738, arXiv:0905.3331 [hep-lat].

Résumé

Ce travail s'intéresse au calcul de la masse des baryons à partir de la théorie décrivant l'interaction forte : la chromodynamique quantique (QCD). Cette théorie régit l'interaction entre les quarks et les gluons et a pu durant ces dernières décennies être vérifiée à haute énergie grâce à l'une de ses propriétés : la liberté asymptotique. Celle-ci prédit que les calculs perturbatifs sont valides à haute énergie car la constante de couplage tend vers zéro. Les quantités physiques régissant la physique à basse énergie nécessitent quant à elles un traitement non pertubatif et font l'objet de ce travail. La seule approche connue permettant de calculer ces observables en contrôlant tous les effets systématiques est la QCD sur réseau, elle consiste à formuler la théorie sur un espace temps Euclidien et à évaluer numériquement les intégrales fonctionnelles qui contiennent l'information concernant ces observables. Le Chapitre 1 est une introduction au formalisme de la QCD et à sa formulation discrétisée. Le second chapitre est dédié à la discrétisation particulière utilisée au sein de la collaboration Europan Twisted Mass (ETM), à savoir celle des fermions twistés. Le Chapitre 3 met en place la technologie nécessaire au calcul des masses des hadrons. L'estimation des intégrales fonctionnelles en utilisant le calcul massivement parallèle sur des Super Calculateurs de type Blue Gene, via des méthodes Monte-Carlo, est décrite dans le Chapitre 4. La production de configurations de jauge sur ce type d'architecture constitue une part importante du travail effectué durant cette thèse. Le Chapitre 5 est dédié à la formulation des théories effectives dites de pertubations chirales, qui permettent d'interpréter et d'extrapoler les résultats actuels dans le régime physique. Les Chapitres 6 et 7 sont consacrés aux baryons légers et étranges. Les effets systématiques ainsi que les extrapolations chirales sont largement discutés.

Mots-clés : Chromodynamique quantique sur réseau. Masse des baryons. Supercalculateurs

Abstract

The aim of this work is an ab initio computation of the baryon masses starting from quantum chromodynamics (QCD). This theory describe the interaction between quarks and gluons and has been established at high energy thanks to one of its fundamental properties : the asymptotic freedom. This property predicts that the running coupling constant tends to zero at high energy and thus that perturbative expansions in the coupling constant are justified in this regime. On the contrary the low energy dynamics can only be understood in terms of a non perturbative approach. To date, the only known method that allows the computation of observables in this regime together with a control of its systematic effects is called lattice QCD. It consists in formulating the theory on an Euclidean space-time and to evaluating numerically suitable functional integrals. First chapter is an introduction to the QCD in the continuum and on a discrete space time. The chapter 2 describes the formalism of maximally twisted fermions used in the European Twisted Mass (ETM) collaboration. The chapter 3 deals with the techniques needed to build hadronic correlator starting from gauge configuration. We then discuss how we determine hadron masses and their statistical errors. The numerical estimation of functional integral is explained in chapter 4 . It is stressed that it requires sophisticated algorithm and massive parallel computating on BlueGene type architecture. Gauge configuration production is an important part of the work realized during my Ph.D. Chapter 5 is a critical review on chiral perturbation theory in the baryon sector. The two last chapter are devoted to the analyze in the light and strange baryon sector. Systematics and chiral extrapolation are extensively discussed.

Keywords: Lattice quantum chromodynamic. Baryon mass calculation. Supercomputer